Schweizerische Eidgenossenschaft
Confédération suisse
Confederazione Svizzera
Confederaziun svizra

Eidgenössisches Departement für Umwelt, Verkehr, Energie und Kommunikation UVEK
Département fédéral de l'environnement, des transport, de l'énergie et de la communication DETEC
Dipartimento federale dell'ambiente, dei trasporti, dell'energia e delle communication DATEC

Bundesamt für Strassen
Office fédéral des routes
Ufficio federale delle Strade

Flow Resistance of Fires in Road Tunnels - Validation

Strömungswiderstand von Bränden in Strassentunneln - Validierung

Résistance à l'écoulement des incendies dans les tunnels routiers - Validation

Ostschweizer Fachhochschule
Markus Friedl
Alexander Weber
Rajdeep Deb

Riess Ingenieur-GmbH
Ingo Riess

Research project BGT_20_00A_01
at the request of the Federal Roads Office FEDRO
March 2026 | 1817

Flow Resistance of Fires in Road Tunnels - Validation

Strömungswiderstand von Bränden in Strassentunneln - Validierung

Résistance à l'écoulement des incendies dans les tunnels routiers - Validation

Ostschweizer Fachhochschule
Markus Friedl
Alexander Weber
Rajdeep Deb

Riess Ingenieur-GmbH
Ingo Riess

Research project BGT_20_00A_01
at the request of the Federal Roads Office FEDRO
March 2026 | 1817

Imprint

Research centre and project team

Project management
Markus Friedl

Members
Alexander Weber
Rajdeep Deb
Ingo Riess

Advisory commission

President
Xavier Guigas

Members
Ernesto Casartelli
Bernard Crausaz
Christian Gammeter
Severin Wälchli
Franz Zumsteg

Applicant

Federal Roads Office FEDRO

Source

The document can be downloaded free of charge from
https://www.mobilityplatform.ch/

March 2026

Table of contents

List of illustrations

List of tables

List of abbreviations

AADT	Annual Average Daily Traffic
CFD	Computational Fluid Dynamics
CO	Carbon Monoxide
DNS	Direct Numerical Simulation
FDS	Fire Dynamic Simulator
HGV	Heavy Goods Vehicle
LES	Large Eddy Simulation, approximation of flow turbulence
DES	Detached Eddy Simulation
ODEM	One-Dimensional Egress Model
RANS	Reynolds Averaged Navier Stokes, approximation of flow turbulence
URANS	Unsteady Reynolds Averaged Navier Stokes
STAR-CCM+	Commercial CFD code
TE1D	1-D model for tunnel fires in longitudinal ventilation
VLES	Very Large Eddy Simulation, approximation of flow turbulence in FDS
1-D	One-dimensional
3-D	Three-dimensional
yPlus	Dimensionless wall distance in CFD

List of Symbols

List of Symbols

Symbol	Unit	Description
A_T	m²	Tunnel cross-section area
B	m⁴/s²	Buoyancy term
B	m	Width, e.g. of the tunnel cross-section
b	m	Radius of the fire source
C_1, C_2 etc.	-	Empirical constants as defined in the report
c_p	J/kgK	Specific heat capacity at constant pressure
D_h	m	Hydraulic diameter
d_w	m	Wall distance
f	Hz	Frequency
g	m/s²	Acceleration of gravity
H_T	m	Height of the tunnel profile
k	-	Factor for momentum transfer in transverse ventilation
k	m²/s²	Turbulent kinetic energy
L	m	Length
p	Pa	Pressure
Δp	Pa	Pressure difference
Q	MW	Heat release rate, nominal fire size
Q_C	MW	Convective heat release rate
Re	-	Reynolds number
T	K	Temperature
T_P	K	Plume temperature at the tunnel ceiling
t	s	Time
U_T	m	Circumference of the tunnel profile
u	m/s	Flow velocity
x, y, z	m	Distance in the spatial reference system
α	W/m²K	Heat transfer coefficient
ε	-	Relative surface roughness
κ	-	Von Karman constant
ρ	kg/m³	Air density
λ	-	Pipe friction coefficient
μ	kg/m s	Dynamic viscosity
ν	m²/s	Kinematic viscosity
ζ	-	Local pressure loss coefficient
ω	1/s	Specific dissipation rate

Summary

Initial Situation

The research project "Flow Resistance of Fires in Road Tunnels" (AGT 2017/005) [14], [15] concluded that current tunnel ventilation systems are undersized for fire situations. Flow resistance would be generally underestimated. The project included a theoretical investigation of flow resistance and its relevance for the design of emergency ventilation. The results of the study can be used to determine flow resistance – for use in the designing of ventilation systems using 1-D calculation programs.

For the flow resistance of a fire in longitudinal airflow, the final report describes a system of equations that quantifies the contributions to the total resistance. The system of equations was derived analytically but also includes a contribution derived empirically from CFD simulations.

The ASTRA 13001 guideline [1] was examined in the research project for inherent safety margins. In [15], the expected airflow resistance of a fire was compared to these safety margins. The analysis concluded that airflow resistance exceeds the safety margins and that ventilation systems should therefore be designed for increased thrust.

The study [15] is based on theoretical approaches and flow simulations, as practically no suitable experimental data are available. Before the results can be applied in practice to the planning and design of ventilation systems, the simulations must be validated using full-scale flow tests. Validation is the verification of a computational model with measurements. Small-scale tests are not as meaningful because scaling effects can lead to misleading results.

This research report documents the measurements and the results of this validation. In addition, further CFD simulations are documented, which were used to extrapolate the measurement results to other tunnel geometries or fire sizes.

Literature Study

In the years following the completion of the study [15], other researchers have investigated the flow resistance of fires in road tunnels. This current literature is summarized and evaluated in Chapter 2.2 of this report. The calculation model from [15] is also summarized again.

The publications have in common that they are based exclusively on theoretical considerations, CFD simulations, and model experiments. No large-scale flow tests were conducted that could be used to validate the study [15].

Fire Tests

Chapter 1 describes in detail the preparation and execution of the fire tests. The fire tests were conducted in the "San Pedro des Anes" test tunnel near Gijon, Spain. The tunnel is particularly suitable for the tests because, with a length of 600 m and a cross-section of 48 m², its dimensions are comparable to those of a rectangular road tunnel. Furthermore, sufficient length is available downstream of the fire to observe the effects of smoke and temperature stratification. A service tunnel beneath the roadway allows for relatively easy measurement of pressure differences between the tunnel and the service tunnel.

The fire source for the tests was formed by fire cups with areas of 4 m² (Tests 1 and 2) and 6.1 m² (Test 3), placed directly above the roadway. With fuel quantities of 150 liters (Tests 1 and 2) and 230 liters (Test 3), a fire duration of approximately 15 minutes was targeted. The fire power was limited to 10 MW due to fire protection restrictions in the tunnel. The test setup directly replicates the boundary conditions underlying the CFD simulations in the study [15].

The test tunnel is equipped with six powerful jet fans. The longitudinal flow in the tunnel can be influenced by switching on individual jet fans. For the tests, an inflow of 3 m/s was targeted, corresponding to the ventilation design for Swiss road tunnels [1]. In the tests, the flow velocity was adjusted by switching on one fan (Test 1) or two fans (Tests 2 and 3). Dynamic flow control based on flow measurements is not possible in the test tunnel.

The arrangement of the test instrumentation in the tunnel is outlined in Figure 9.

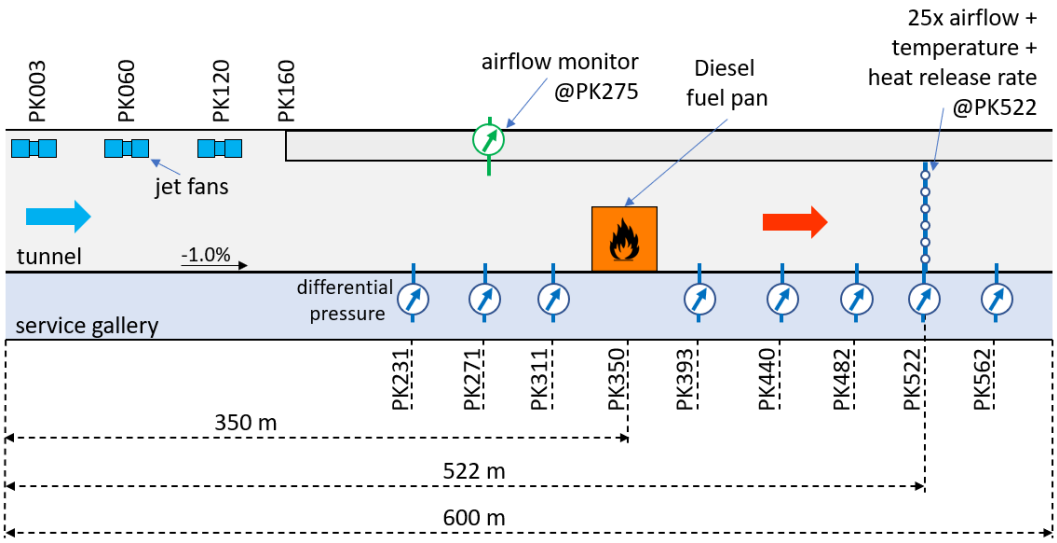

Figure 1: Test setup

According to the test design, the air flow measurement downstream from the fire was to consist of 25 independent airflow sensors to determine the average flow velocity in the tunnel and the flow profile in the cross-section. However, only six differential pressure sensors were available for the tests. This only allowed the recording of a vertical

flow profile, each with five pitot tubes, which recorded the average dynamic pressure in the tunnel.

For temperature measurement, 25 gas thermocouples were installed at PK522 at the same grid points as the airflow sensors.

The static pressure profile along the tunnel was measured as the differential pressure between the tunnel and the service gallery below. Inside the tunnel, the pressure measurement was located on the tunnel wall, approximately 2 m above the ground. The opening of the pressure tube was positioned perpendicular to the longitudinal flow to avoid any influence of the flow velocity. CFD simulations verified that the measured differential pressure during developed flow was representative of the average pressure in the tunnel cross-section.

An additional differential pressure measurement was located at PK231. The installation was similar to the differential pressure measurement described above. This pressure sensor was used to record short-term measurements with higher sampling frequencies of 100 to 2000 Hz.

The heat release rate was determined by measuring the total mass flow and various gas concentrations (CO, CO_2, O_2, and H_2O). The heat release rate was then derived from these mass flows. The measured heat release rate was additionally verified by the amount of fuel used and by the integral of the measured heat release.

1-D Model

Assuming that the mass of the fuel can be neglected relative to the total air flow, the 1-D calculation model can be formulated in a compact form. The equations require the definition of several locations along the tunnel. The tunnel is divided into three sections: upstream, fire, and downstream. It is also assumed that the length of the fire (section ①→②) can be neglected.

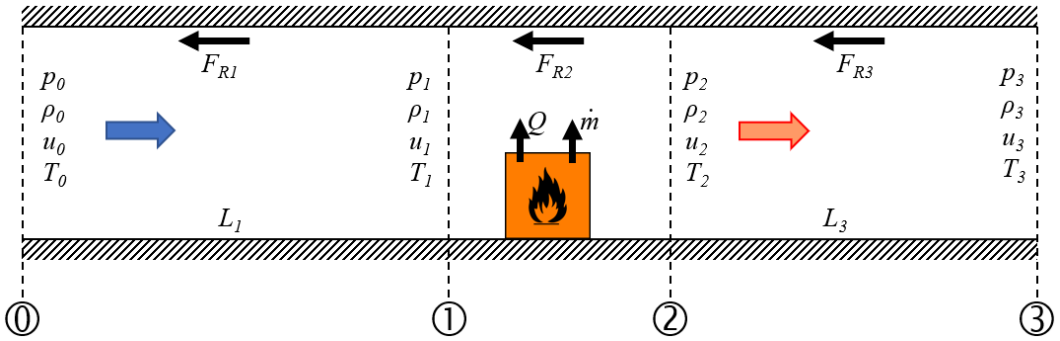

Figure 2: Definitions

The variation of static pressure due to wall friction in the inflow section results in

$$\Delta p_{0-1} = -\frac{\rho_0}{2} \cdot u_0^2 \cdot \frac{\lambda\, L_1}{D_h} \tag{1}$$

The change of static pressure at the fire location is simplified to

$$\Delta p_{1-2} = -\frac{Q_c\, u_0}{c_p A_T T_0} \tag{2}$$

The change in static pressure downstream from the fire includes several components:

- The wall friction corresponds to the inflow section. However, the flow velocity is increased and the density reduced. This results in an increased pressure drop.

$$\Delta p_{2-3A} = -\frac{\rho_0}{2} \cdot u_0^2 \cdot \frac{\lambda}{D_h} \cdot \left[\frac{Q_c}{\alpha U_T T_0}\left(1 - exp\left(-\frac{\alpha U_T L_3}{\rho_0 u_0 A_T c_p}\right)\right) + L_3\right] \tag{3}$$

- The recovery of static pressure by cooling and the resulting deceleration of the flow is

$$\Delta p_{2-3B} = \frac{Q_c\, u_0}{c_p A_T T_0}\left(1 - exp\left(-\frac{\alpha U_T L_3}{\rho_0 u_0 A_T c_p}\right)\right) \tag{4}$$

The research report [15] describes an additional pressure loss due to temperature stratification, see chapter 2.2.3. This contribution was derived from CFD simulations. The evaluation of the test data showed that this additional pressure loss was an artifact of the CFD simulations.

For the analysis of the experimental data in this report, the 1-D model following the equations given above was implemented into the 1-D numerical model Spitfire ([29] to [32]) to compare it with the experimental data and with further CFD simulations.

3-D CFD Simulations

In addition to the 1-D simulations, three different 3-D CFD codes were used for the preparation of the fire tests and for a comparison with the collected data:

- RANS, Star-CCM+
- LES, Fire Dynamic Simulator
- DES, ANSYS Fluent

A detailed documentation of the CFD simulations, i.e. geometry, sub-models, boundary conditions etc. are described in chapter 5.

The Star-CCM+ version v2302 was used for the RANS simulations. The simulations were carried out in stationary mode with 2nd order coupled flow and energy. Due to the expected high temperature gradients, the air is assumed to be compressible. Viscosity, thermal conductivity and heat capacity of the air are calculated as a function of

temperature using Sutherland's Law. The gravity term is included to take account of buoyancy forces. For inclined tunnel geometries, only the gravity vector is modified.

Fire Dynamic Simulator FDS v6.8.0 was used for the LES simulations. For analysis of the pressure curve of fires in long tunnels, the transient Very Large Eddy Simulation VLES in combination with the standard FFT-based solver has been used, as recommended in the FDS user manual.

Detached Eddy Simulation (DES) is a hybrid turbulence model that combines RANS and Large Eddy Simulation (LES). Near solid boundaries and close to the fire, where turbulence scales are small and resolving them is computationally expensive, DES applies RANS to model turbulence efficiently. Away from walls, in regions with large turbulent structures, DES switches to LES, which directly resolves unsteady eddies. DES provides a balance between accuracy and cost, capturing large-scale turbulent motions in separated flows while avoiding the excessive computational demand of a full LES.

Test Results

The complete results of the comparison of measurements and simulations are described in chapter 5.6. Individual results for Test 1 are presented here as an example.

Figure 3 shows the course of the differential pressure measurements during Test 1. The measurements were adjusted by setting the pressure difference to 0 Pa before the fire started. Furthermore, the signals were shifted in time so that the time is set to t = 0 min when the jet fan is switched on. The fire was ignited after 12:52 min. The fire lasted until 40:38 min. The pressure measurements show a calm course before the ventilation is switched on. Turbulence increases with ventilation operation. During the fire, significant pressure fluctuations occur, especially in the second half of the fire.

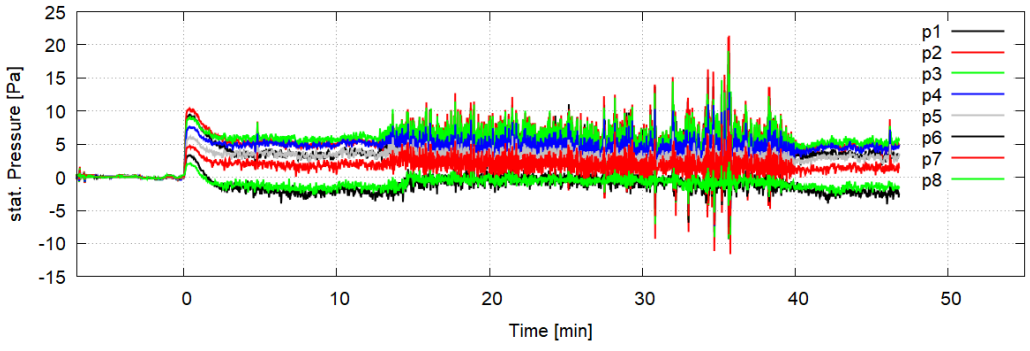

Figure 3: Differential pressure measurements for Test 1.

Figure 4 shows a comparison of the four pressure profiles along the tunnel with the measured differential pressure. Three of the pressure monitors (PK231, PK482, and PK562) exhibited irregular behavior in both the dynamic variation and the mean values of the pressure profile. The installation was rechecked after the test, but no explanation could be found. The data is shown in the graph but is not included in the analysis. The measurement on PK231 was replaced by the high-frequency sensor.

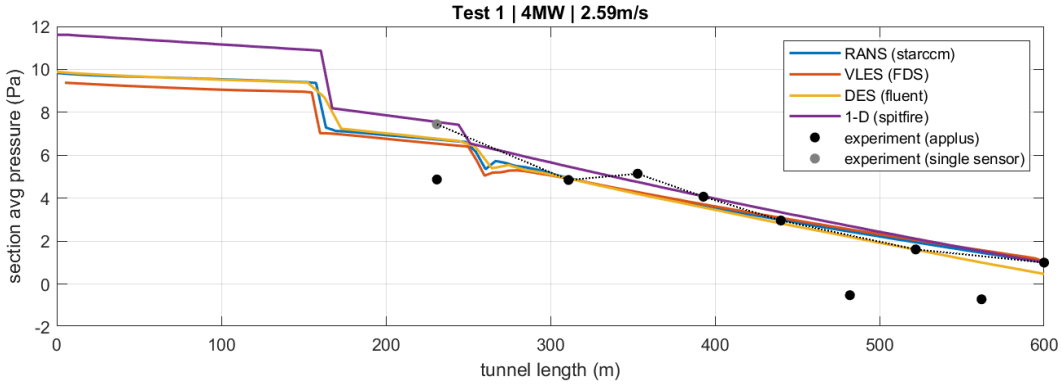

Figure 4: Comparison of the pressure curve along the tunnel from simulation data with the measured values for Test 1.

The three CFD simulations show good agreement with the measurements, within the expected measurement accuracy. The 1-D simulation shows a slightly increased wall friction downstream and an increased pressure drop at the cross-section change at PK160.

The comparison of the temperature distribution along the tunnel is shown in Figure 5. Only the mean value of the temperature measurements from the network measurement at PK522 is available as a single point.

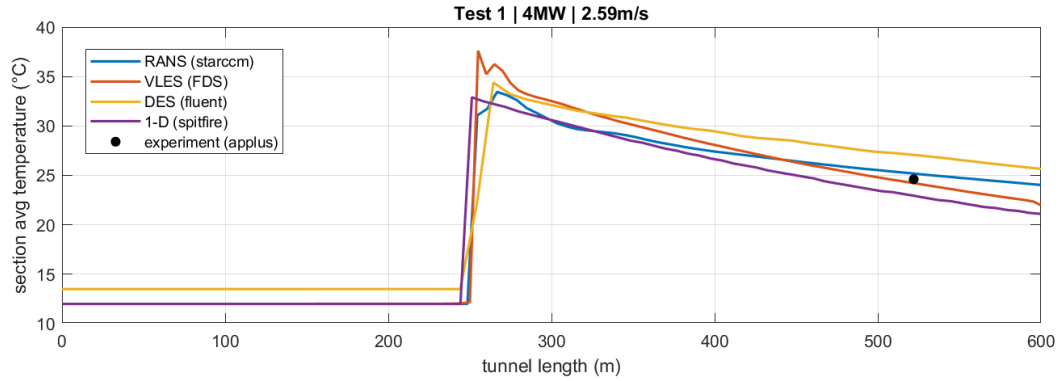

Figure 5: Comparison of the temperature curve along the tunnel from simulation data with the measured values for Test 1.

A comparison of the temperature and flow profiles downstream of the fire is shown in Figure 6. The measurements show a slightly stronger temperature stratification than the CFD simulations. In contrast, the flow profile in the simulation is balanced, with slightly higher velocities in the upper half of the cross-section. The measurements show lower flow velocities in the upper half of the tunnel profile. While the CFD simulations reveal a similarity between the temperature and flow profiles (if the measurement point with 0 m/s flow at the wall is omitted), this is not the case with the measurements.

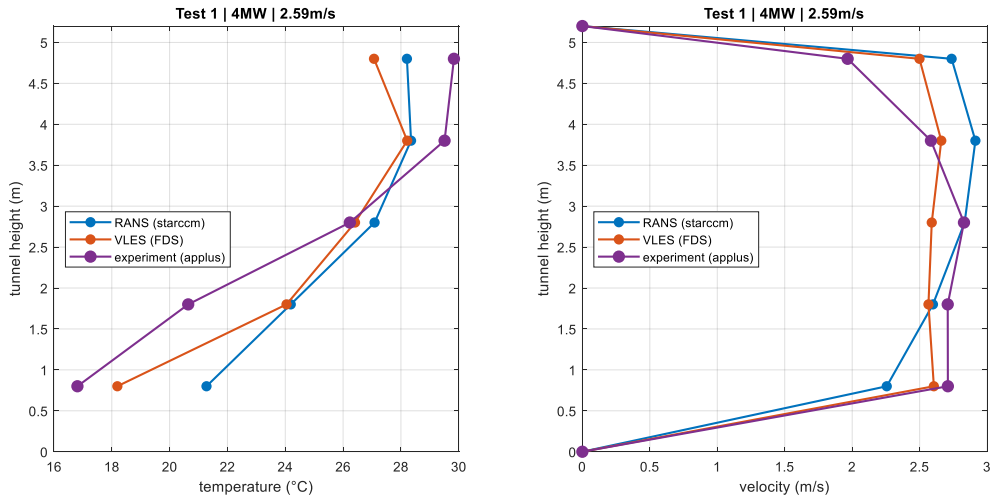

Figure 6: Temperature and velocity profile on PK522 for Test 1.

This result appears to be typical for 3D CFD simulations. Very similar differences between simulation and measurement were observed for a recalculation of fire tests in the Memorial Tunnel [27]. Note the similarity between the simulation profiles and the different measurement profiles.

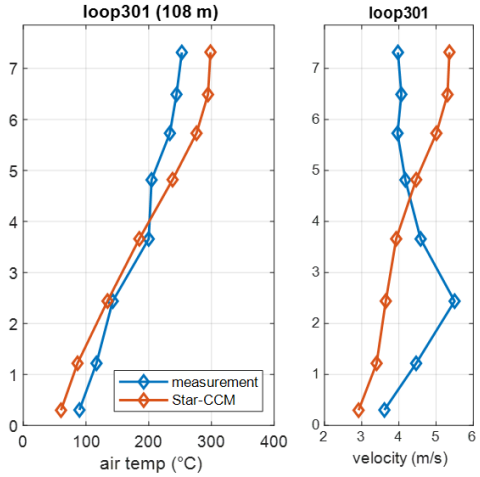

Figure 7: RANS vs. experiment of temperature and velocity profile of memorial measurement case 610 at loop 301 [27].

Additional CFD-Simulations

One goal of the research project was to scale the results to larger fire performances and other geometries typical for tunnels on ASTRA's national roads. The results should also be compared to the design of the ventilation systems according to ASTRA 13001. These simulations are documented in chapter 1 of the report.

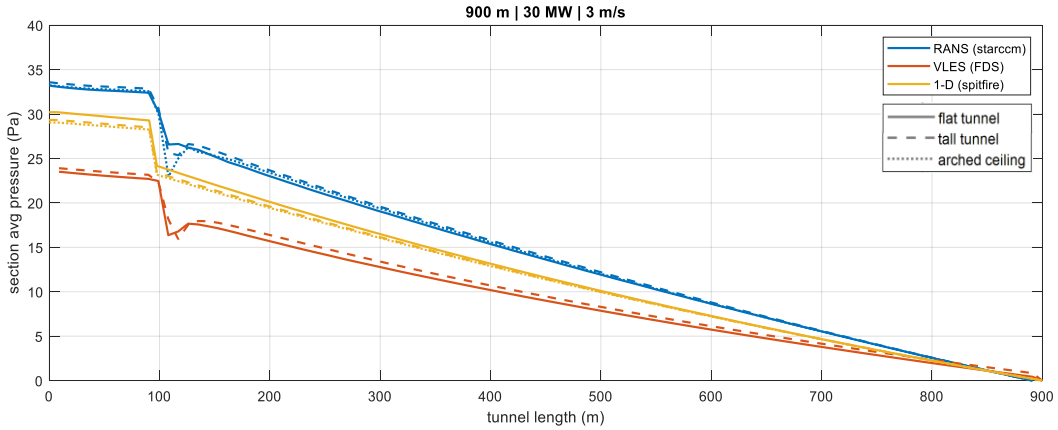

Figure 8: The average pressure along the tunnel for a 30MW fire

Figure 8 shows the pressure distribution along the tunnel for three tunnel cross-sections of the same area and for three calculation models. The influence of the tunnel profile is small. The differences between the calculation models are greater than the influence of the cross-sectional geometry. However, the differences between the models become smaller for a tunnel without a longitudinal gradient. The modeling of heat transfer and buoyancy play a significant role in the pressure distribution.

These simulations show that

- The shape of the tunnel cross-section (rectangular or horseshoe) has only a minor influence on the pressure distribution.
- The differences between the models increase with the heat release rate. This is partly due to the heat transfer model, i.e. the buoyancy in the inclined tunnel.
- Simulations with FDS versions v6.8.0, v6.9.1, and v6.10.0 showed significant differences between them, so these versions cannot be considered validated models for this application.

Further simulations were conducted using the DES methodology. The aim was, on the one hand, to investigate the variation in fire size and its influence on pressure drop, and, on the other hand, to investigate turbulence structures as a source of oscillations, the stability of smoke stratification, and the effect of smoke plume bifurcation in longitudinal flow.

The RANS turbulence model can be used to assess time-averaged flow properties. Furthermore, it allows for a low grid resolution. In comparison, DES requires higher grid and time resolution. As the heat release rate increases, oscillations increase. Therefore, a higher sampling rate is required to achieve stable mean flow properties. However, DES captures the details of turbulent structures and high-frequency oscillations, especially at and downstream of the fire.

Application

Using a parameter study, the effects of the flow resistance of a tunnel fire on the design of longitudinal ventilation systems are estimated (see Chapter 7.1). Longitudinal ventilation is calculated for three typical tunnels on the national road network without including the flow resistance of the fire. The influence of individual parameters is then quantified, where conservative assumptions lead to implicit safety margins. The flow resistance of the fire in this design case is compared with these safety margins.

The additional flow resistance is in every case lower than expected according to the research report [15]. Therefore, the implicit design safety margins are sufficient to allow control of most fire incidents. There is no immediate need for action for tunnels in operation. When designing new systems or during refurbishments, the flow resistance of a tunnel fire should be considered.

The throttling effect does not have to be considered if the ventilation is designed for a flow velocity of 1.5 m/s. Also, in tunnels with local smoke extraction in the event of an incident, the flow resistance of the fire does not need to be considered.

The equations for the throttling effect can be implemented in 1-D simulation programs, see Chapter 7.3. The change in static pressure at the fire location is given by

$$\Delta p_{1-2} = -\frac{Q_c\, u_0}{c_p A_T T_0} \tag{5}$$

The change in static pressure downstream from the fire includes two components. For the calculation of wall friction, the flow velocity is increased and the density reduced. This results in the increase of the wall friction as

$$\Delta p_{2-3A} = -\frac{\rho_0}{2} \cdot u_0^2 \cdot \frac{\lambda}{D_h} \cdot \frac{Q_c}{\alpha U_T T_0}\left(1 - exp\left(-\frac{\alpha U_T L_3}{\rho_0 u_0 A_T c_p}\right)\right) \tag{6}$$

Additional aerodynamic resistance of standing vehicles downstream of the fire or changes of the tunnel cross-section must be treated accordingly.

The recovery of static pressure by cooling and the resulting deceleration of the flow is given as

$$\Delta p_{2-3B} = \frac{Q_c\, u_0}{c_p A_T T_0}\left(1 - exp\left(-\frac{\alpha U_T L_3}{\rho_0 u_0 A_T c_p}\right)\right) \tag{7}$$

If these equations are integrated in an existing 1-D model, some modifications may be required.

CFD simulations can be used for investigation of flow resistance of the tunnel fire, see Chapter 7.4. The following aspects needs to be considered:

- Turbulence models such as SST k-ω provide a good estimate of the average flow resistance. However, they do not provide detailed information on dynamic turbulent flow characteristics.
- LES is computationally intensive, but a combined model such as DES offers a good compromise between computational effort and the capture of turbulent behavior in the tunnel.
- Both DES and LES require preliminary investigation using RANS or URANS simulations to refine the grid to the point where 80 percent of the turbulent kinetic energy is represented.
- In addition, the estimate of eddy viscosity and effective thermal conductivity from URANS simulations can be used to optimize the grid for DES.
- Higher heat release rates lead to stronger high-frequency pressure fluctuations. This must be considered when evaluating the results.

Zusammenfassung

Ausgangslage

Das Forschungsprojekt "Strömungswiderstand von Bränden in Strassentunneln" (AGT 2017/005) [15] kam zum Schluss, dass heutige Tunnellüftungen für den Brandfall unterdimensioniert sind. Der Strömungswiderstand werde gemeinhin unterschätzt. Das Projekt beinhaltete die theoretische Untersuchung des Strömungswiderstandes und seiner Relevanz für die Auslegung der Ereignislüftung. Mit den Ergebnissen der Studie kann der Strömungswiderstand bestimmt werden – zur Verwendung bei der Dimensionierung von Lüftungsanlagen mit 1-D Berechnungsprogrammen.

Für den Strömungswiderstand eines Brandes in einer Längslüftung beschreibt der Schlussbericht ein Gleichungssystem, das die Beiträge zum Gesamtwiderstand quantifiziert. Das Gleichungssystem wurde analytisch hergeleitet, beinhaltet aber auch einen Beitrag, der empirisch aus CFD-Simulationen abgeleitet wurde.

Die Richtlinie ASTRA 13001 [1] wurde im Forschungsprojekt auf inhärente Sicherheitsmargen untersucht. Der in [15] ausgewiesene Strömungswiderstand eines Brandes wurde in Relation zu diesen Sicherheitsmargen gesetzt. Die Analyse kam zum Schluss, dass der Strömungswiderstand die Sicherheitsmargen übersteige und dass Lüftungsanlagen somit stärker dimensioniert werden sollten.

Die Studie [15] basiert auf theoretischen Ansätzen und Strömungssimulationen, da praktisch keine geeigneten experimentellen Daten vorliegen. Vor einer praktischen Anwendung der Ergebnisse für die Planung und Auslegung von Lüftungsanlagen müssen die Simulationen anhand von Strömungsversuchen im grossen Massstab validiert werden. Als Validierung bezeichnet man die Überprüfung eines rechnerischen Modells mit Messungen. Versuche im kleinen Massstab haben nicht die gleiche Aussagekraft, weil Skaleneffekte die Resultate verfälschen können.

Im vorliegenden Forschungsbericht sind die Durchführung der Messungen und die Ergebnisse dieser Validierung dokumentiert. Zusätzlich sind weitere CFD-Simulationen dokumentiert, mit denen die Ergebnisse der Messungen auf andere Geometrien oder Brandgrössen übertragen wurden.

Literaturrecherche

In den Jahren nach Abschluss der Studie [15] haben sich weitere Forscher mit der Untersuchung des Strömungswiderstandes von Bränden in Strassentunneln beschäftigt. Diese aktuelle Literatur wird in Kapitel 2.2 dieses Berichts zusammengefasst und bewertet. Auch wird das Berechnungsmodell aus [15] nochmals zusammenfassend beschrieben.

Den Veröffentlichungen ist gemeinsam, dass sie ausschliesslich auf theoretischen Überlegungen, CFD-Simulationen und Modellexperimenten basieren. Es wurden keine Strömungsversuche in grossem Massstab durchgeführt, die für eine Validierung der Studie [15] verwendet werden könnten.

Brandversuche

In Kapitel 1 werden Vorbereitung und Durchführung der Brandversuche detailliert beschrieben. Die Brandversuche wurden im Versuchstunnel «San Pedro des Anes» in der Nähe von Gijon, Spanien durchgeführt. Der Tunnel ist für die Tests besonders geeignet, da er mit einer Länge von 600 m und einem Querschnitt von 48 m² zu einem Strassentunnel mit Rechteckprofil vergleichbare Abmessungen aufweist. Zudem steht stromab vom Brandort eine genügende Länge zur Verfügung, um den Einfluss einer Rauch- und Temperaturschichtung beobachten zu können. Ein Werkleitungskanal unter der Fahrbahn ermöglicht relativ einfach die Messung von Druckdifferenzen zwischen dem Tunnel und dem Werkleitungskanal.

Die Brandquelle für die Tests wurde durch Brandtassen mit Flächen von 4 m² (Tests 1 und 2) sowie 6.1 m² (Test 3) gebildet, aufgestellt direkt über der Fahrbahn. Mit Treibstoffmengen von 150 Liter (Tests 1 und 2) und 230 Liter (Test 3) wurde eine Branddauer von etwa 15 min angestrebt. Die Brandleistungen waren aufgrund von Beschränkungen des Brandschutzes im Tunnel auf 10 MW limitiert. Der Versuchsaufbau stellt direkt die Randbedingungen nach, die den CFD-Simulationen der Studie [15] zugrunde lagen.

Der Versuchstunnel ist mit sechs leistungsstarken Strahlventilatoren ausgerüstet. Mit dem Zuschalten einzelner Strahlventilatoren kann die Längsströmung im Tunnel beeinflusst werden. Für die Tests wurde eine Anströmung von 3 m/s angestrebt, entsprechend der Lüftungsauslegung für Schweizer Strassentunnel [1]. In den Tests wurde die Strömungsgeschwindigkeit durch das Einschalten von einem Ventilator (Test 1) bzw. von zwei Ventilatoren (Tests 2 und 3) eingestellt. Eine dynamische Regelung der Strömung aufgrund von Strömungsmessungen ist im Versuchstunnel nicht möglich.

Die Anordnung der Messgeräte im Tunnel ist in Figure 9 skizziert.

Die Luftströmungsmessung hinter dem Brand sollte gemäss Versuchsplanung aus 25 unabhängigen Geschwindigkeitssensoren bestehen, um die durchschnittliche Strömungsgeschwindigkeit im Tunnel sowie das Strömungsprofil im Querschnitt zu bestimmen. Für die Versuche standen jedoch nur sechs Differenzdrucksensoren zur Verfügung. Dies ermöglichte lediglich die Aufzeichnung eines vertikalen Strömungsprofils mit jeweils fünf Staurohren, die den durchschnittlichen dynamischen Druck im Tunnel aufzeichneten.

Zur Temperaturmessung wurden 25 Gasthermoelemente bei PK522 an denselben Rasterpunkten wie die Geschwindigkeitssensoren installiert.

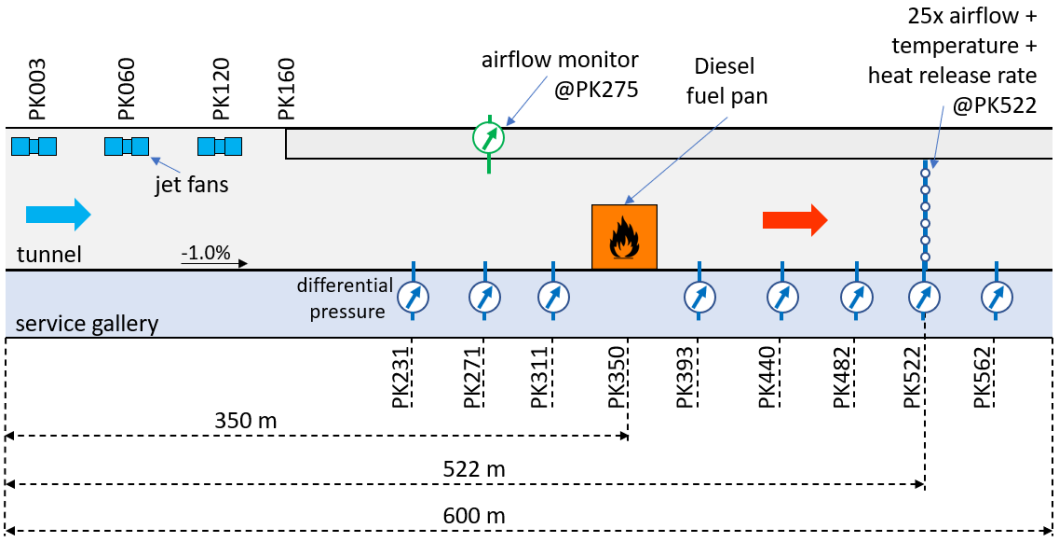

Figure 9: Testaufbau

Das statische Druckprofil entlang des Tunnels wurde als Differenzdruck zwischen dem Tunnel und dem darunterliegenden Servicestollen gemessen. Im Tunnel befand sich die Druckmessung an der Tunnelwand, ca. 2 m über dem Boden. Die Öffnung des Druckschlauchs war senkrecht zur Längsströmung angeordnet, um jeglichen Einfluss der Strömungsgeschwindigkeit zu vermeiden. In CFD-Simulationen wurde verifiziert, dass der gemessene Differenzdruck bei ausgebildeter Strömung repräsentativ für den durchschnittlichen Druck im Tunnelquerschnitt war.

Eine zusätzliche Differenzdruckmessung befand sich bei PK231. Die Installation ähnelte der oben beschriebenen Differenzdruckmessung. Dieser Drucksensor diente zur Erfassung von Kurzzeitmessungen mit höheren Abtastfrequenzen von 100 bis zu 2000 Hz.

Die Brandleistung wurde durch Messung des Gesamtmassenstroms und verschiedener Gaskonzentrationen (CO, CO_2, O_2 und H_2O) ermittelt. Aus diesen Massenströmen wurde dann die Brandleistung abgeleitet. Die gemessene Brandleistung wurde zusätzlich verifiziert durch die verwendete Brennstoffmenge und durch das Integral der Wärmefreisetzung.

1-D Modell

Mit der Annahme, dass die Masse des Brennstoffs gegenüber der Luftströmung vernachlässigt werden kann, lässt sich das 1-D Berechnungsmodell kompakt formulieren. Die Gleichungen verlangen die Definition mehrerer Punkte entlang des Tunnels. Der Tunnel wird in drei Abschnitte aufgeteilt: stromauf, Brand und stromab. Es wird zudem angenommen, dass die Länge des Brandes (Abschnitt ①→②) vernachlässigt werden kann.

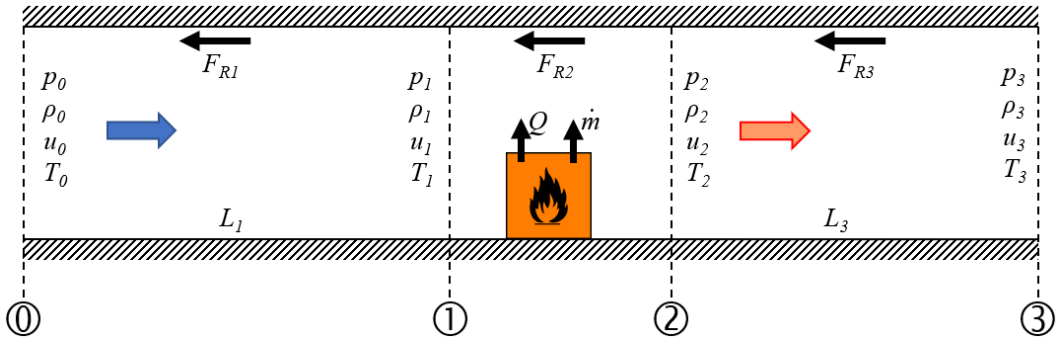

Figure 10: Definitionen

Im Abschnitt stromauf ändert sich der statische Druck aufgrund der Wandreibung.

$$\Delta p_{0-1} = -\frac{\rho_0}{2} \cdot u_0^2 \cdot \frac{\lambda\, L_1}{D_h} \tag{8}$$

Die Änderung des statischen Drucks am Brandort wird aus der Impulserhaltung abgeleitet.

$$\Delta p_{1-2} = -\frac{Q_c\, u_0}{c_p A_T T_0} \tag{9}$$

Stromab vom Brand ändert sich der Druck aufgrund von mehreren Einflusskomponenten:

- Die Berechnung der Wandreibung erfolgt wie im Abschnitt stromauf vom Brand. Allerdings ist aufgrund der Erwärmung der Luft die Strömungsgeschwindigkeit erhöht und die Luftdichte verringert. Daraus ergibt sich ein grösserer Druckabfall.

$$\Delta p_{2-3A} = -\frac{\rho_0}{2} \cdot u_0^2 \cdot \frac{\lambda}{D_h} \cdot \left[\frac{Q_c}{\alpha U_T T_0}\left(1 - exp\left(-\frac{\alpha U_T L_3}{\rho_0 u_0 A_T c_p}\right)\right) + L_3\right] \tag{10}$$

- Ein Teil des statischen Drucks wird zurückgewonnen, indem die Brandgase abkühlen und sich dadurch die Strömungsgeschwindigkeit verringert.

$$\Delta p_{2-3B} = \frac{Q_c\, u_0}{c_p A_T T_0}\left(1 - exp\left(-\frac{\alpha U_T L_3}{\rho_0 u_0 A_T c_p}\right)\right) \tag{11}$$

Der Forschungsbericht [15] beschreibt einen zusätzlichen Druckverlust durch Temperaturschichtung, vgl. Kapitel 2.2.3. Dieser Beitrag wurde aus CFD-Simulationen abgeleitet. Die Auswertung der Versuchsdaten in diesem Bericht zeigte, dass dieser zusätzliche Druckverlust ein Artefakt der CFD-Simulationen war.

Für diese Analyse der experimentellen Daten in diesem Bericht wurde das 1-D-Modell gemäss den oben angegebenen Gleichungen in das 1-D-numerische Modell Spitfire ([29] bis [32]) implementiert, um es mit den experimentellen Daten und mit weiteren CFD-Simulationen zu vergleichen.

3-D CFD Simulationen

Zusätzlich zu den 1-D Simulationen wurden drei verschiedene 3-D CFD-Programme zur Vorbereitung der Brandversuche und zum Vergleich mit den erhobenen Daten verwendet:

- RANS, Star-CCM+
- LES, Fire Dynamic Simulator
- DES, ANSYS Fluent

Eine detaillierte Dokumentation der CFD-Simulationen, d. h. Geometrie, Teilmodelle, Randbedingungen usw. ist in Kapitel 5 beschrieben.

Für die RANS-Simulationen wurde Star-CCM+ Version v2302 verwendet. Die Simulationen wurden stationär mit gekoppelter Strömung und Energie 2. Ordnung durchgeführt. Aufgrund der zu erwartenden hohen Temperaturgradienten wird die Luft als kompressibel angenommen. Viskosität, Wärmeleitfähigkeit und Wärmekapazität der Luft werden als Funktion der Temperatur nach dem Sutherlandschen Gesetz berechnet. Der Gravitationsterm wird zur Berücksichtigung der Auftriebskräfte einbezogen. Bei geneigter Tunnelgeometrie wird lediglich der Gravitationsvektor modifiziert.

Für die VLES-Simulationen wurde der Fire Dynamic Simulator FDS v6.8.0 verwendet. Zur Analyse des Druckverlaufs von Bränden in langen Tunneln wurde die transiente Very Large Eddy Simulation (VLES) in Kombination mit dem standardmässigen FFT-basierten Solver verwendet, wie im FDS-Benutzerhandbuch empfohlen.

Detached Eddy Simulation (DES) ist ein hybrides Turbulenzmodell, das RANS und Large Eddy Simulation (LES) kombiniert. In der Nähe von festen Wänden und in Brandnähe, wo die Turbulenzskalen klein und ihre Auflösung rechenintensiv ist, wendet DES RANS an, um die Turbulenz effizient zu modellieren. Entfernt von Wänden, in Bereichen mit grossen turbulenten Strukturen, wechselt DES zu LES, das instationäre Wirbel direkt auflöst. DES bietet ein ausgewogenes Verhältnis zwischen Genauigkeit und Kosten, indem es grossräumige turbulente Bewegungen in abgelösten Strömungen erfasst und gleichzeitig den grossen Rechenaufwand einer vollständigen LES vermeidet.

Ergebnisse

Die vollständigen Ergebnisse des Vergleichs von Messungen und Simulationen sind in Kapitel 5.6 beschrieben. Als Beispiel werden hier einzelne Ergebnisse für Test 1 dargestellt.

Figure 11 zeigt den Verlauf der Differenzdruckmessungen während Test 1. Die Messungen wurden eingestellt, indem die Druckdifferenz vor Brandbeginn auf 0 gestellt wurde. Zudem wurden die Signale zeitlich verschoben, dass bei Einschalten des Strahlventilators die Zeit auf t = 0 min eingestellt ist. Der Brand wurde nach 12:52 min gezündet. Die Branddauer währte bis 40:38 min. Die Druckmessungen zeigen vor Einschalten der Lüftung einen ruhigen Verlauf. Mit dem Lüftungsbetrieb nimmt die

Turbulenz zu. Während des Brandes treten deutliche Druckstösse auf, insbesondere in der zweiten Hälfte des Brandes.

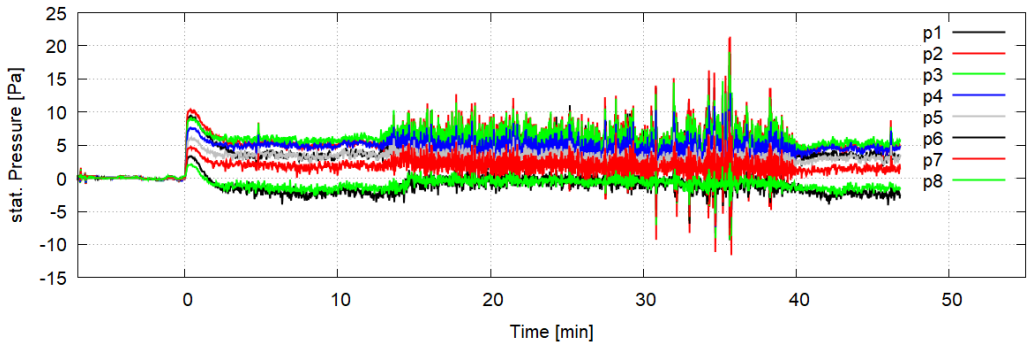

Figure 11: Differenzdruckmessungen für Test 1.

Figure 12 zeigt einen Vergleich der vier Druckprofile entlang des Tunnels mit dem gemessenen Differenzdruck. Drei der Druckmonitore (PK231, PK482 und PK562) zeigten sowohl in der zeitlichen Variation als auch in den Mittelwerten des Druckprofils ein irreguläres Verhalten. Die Installation wurde nach dem Test erneut überprüft. Es wurde dennoch keine Erklärung dafür gefunden. Die Daten sind in der Grafik dargestellt, werden aber in der Analyse nicht berücksichtigt. Die Messung an PK231 wurde durch den Hochfrequenzsensor ersetzt.

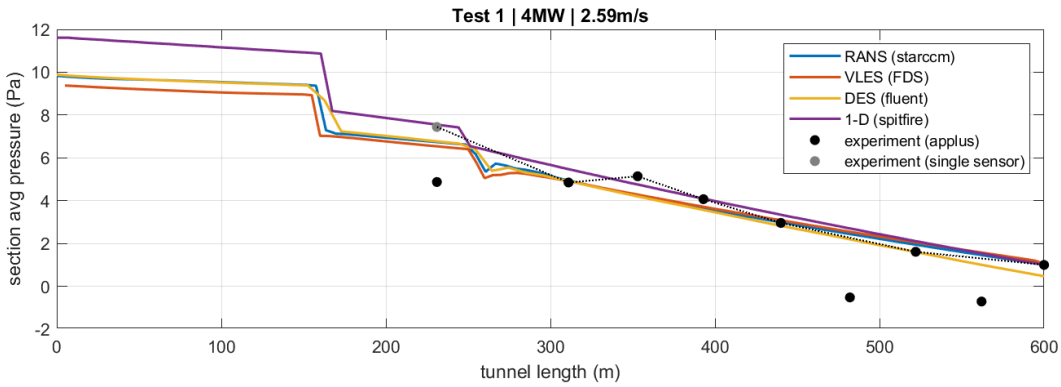

Figure 12: Vergleich der Profile des statischen Drucks entlang des Tunnels, Messung und Simulationen.

Die drei CFD-Simulationen zeigen eine gute Übereinstimmung mit den Messungen, im Rahmen der erwarteten Messgenauigkeit. Die 1-D-Simulation zeigt eine leicht erhöhte Wandreibung stromabwärts und einen erhöhten Druckabfall am Querschnittswechsel bei PK160.

Der Vergleich der Temperaturverteilung entlang des Tunnels ist in Figure 13 dargestellt. Als Messpunkt steht nur der Mittelwert der Temperaturmessungen der Netzmessung bei PK522 zur Verfügung.

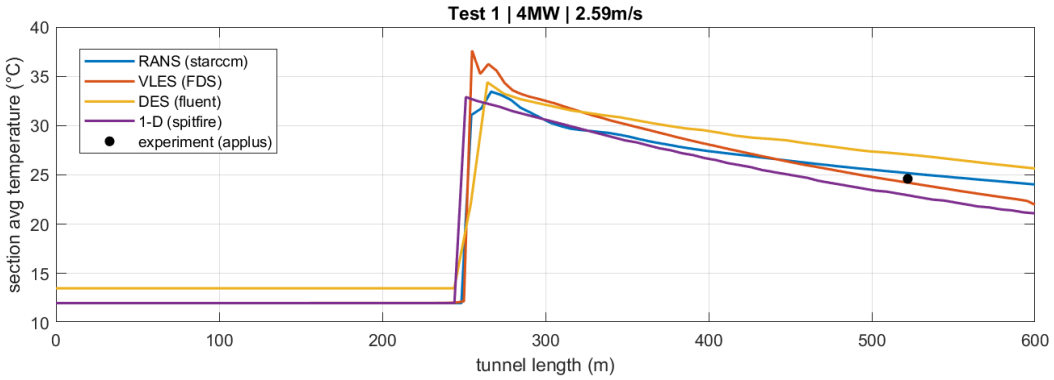

Figure 13: Vergleich der Profile der Temperatur entlang des Tunnels, Messung und Simulationen.

Der Vergleich der Temperatur- und Strömungsprofile stromab vom Brand bei PK522 ist in Figure 14 dargestellt. Die Messung zeigt eine etwas stärkere Temperaturschichtung als die CFD-Simulationen. Hingegen ist das Strömungsprofil in der Simulation ausgeglichen, mit etwas grösserer Geschwindigkeit in der oberen Hälfte des Querschnitts. Die Messung ergibt in der oberen Hälfte des Tunnelprofils geringere Strömungsgeschwindigkeiten. Während die CFD-Simulationen eine Ähnlichkeit zwischen Temperatur- und Strömungsprofil erkennen lassen, wenn man den Messpunkt mit Strömung 0 m/s an der Wand weglässt, ist dies bei der Messung nicht gegeben.

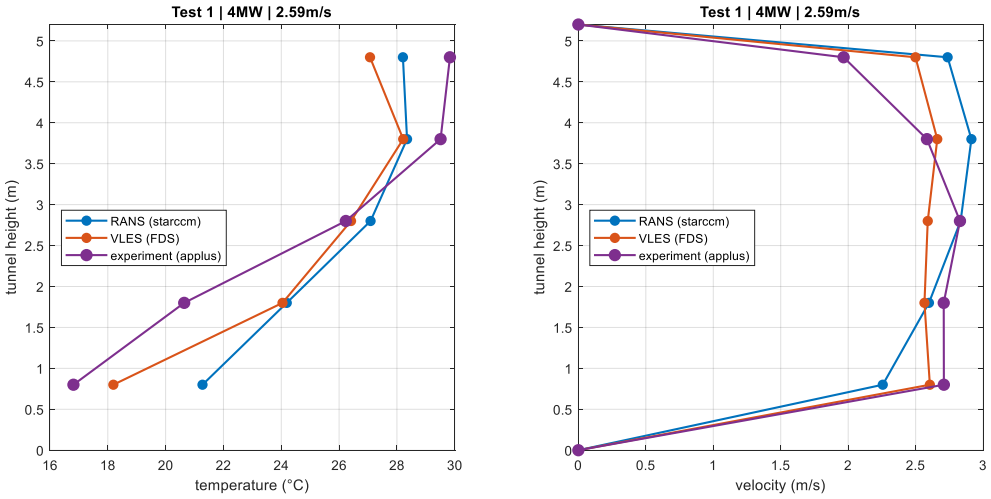

Figure 14: Vergleich der vertikalen Profile der Temperatur und der Strömungsgeschwindigkeit, Messung und Simulation.

Dieses Ergebnis scheint typisch zu sein für 3-D CFD Simulationen. Sehr ähnliche Unterschiede zwischen Simulation und Messung ergeben sich für eine Nachrechnung von Brandversuchen im Memorial Tunnel [27]. Zu beachten ist die Ähnlichkeit der Profile der Simulation und die unterschiedlichen Profile der Messung.

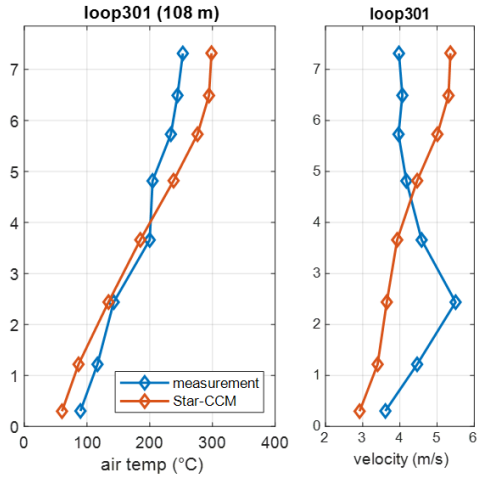

Figure 15: Vergleich Temperatur und Strömungsgeschwindigkeit, Messung und Simulation Memorial Tunnel Tests [27].

Weitere CFD-Simulationen

Ein Ziel des Forschungsprojekts bestand in der Skalierung der Ergebnisse auf grössere Brandleistungen und weitere Geometrien, die für Tunnel auf den Nationalstrassen des ASTRA typisch sind. Auch sollten die Ergebnisse in Relation zur Auslegung der Lüftungsanlagen nach ASTRA 13001 gestellt werden. Diese Simulationen sind in Kapitel 1 des Berichts dokumentiert.

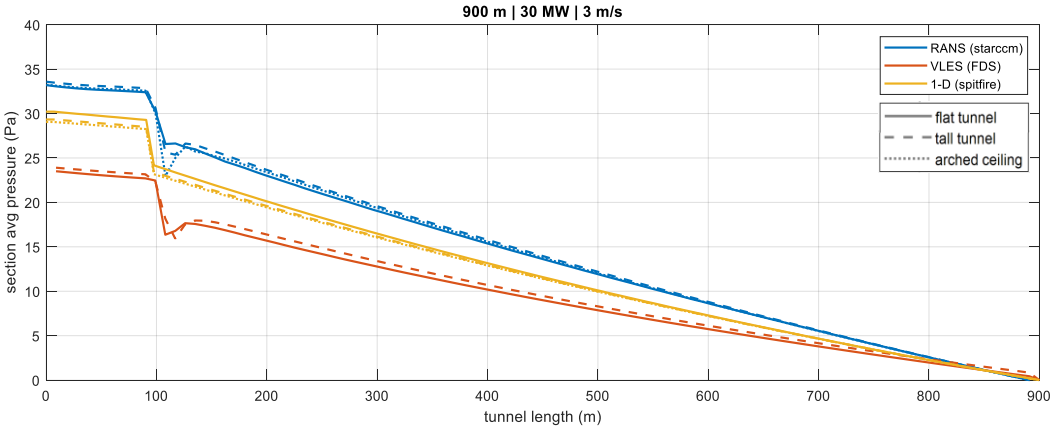

Figure 16: Profile des statischen Drucks für einen 30 MW-Brand

Figure 16 zeigt für drei Tunnelquerschnitte gleicher Fläche und für drei Berechnungsmodelle den Druckverlauf entlang des Tunnels. Der Einfluss des Tunnelprofils ist gering. Es zeigt sich, dass die Unterschiede der Berechnungsmodelle grösser sind als der Einfluss der Querschnittgeometrie. Die Unterschiede zwischen den Modellen werden jedoch geringer für einen Tunnel ohne Längsneigung. Die Modellierung des Wärmeübergangs hat einen wesentlichen Anteil an der Druckverteilung im geneigten Tunnel.

Die Ergebnisse dieser Simulationen zeigen:
- Die Form des Tunnelquerschnitts (Rechteck oder Hufeisen) hat auf die Druckverhältnisse nur einen geringen Einfluss.
- Die Unterschiede zwischen den Modellen nehmen mit der Brandleistung zu. Dies ist zum Teil auf das Modell der Wärmeleitung, d.h. auf den Auftrieb in der geneigten Tunnelröhre zurückzuführen.
- Simulationen mit FDS Versionen v6.8.0, v6.9.1 und v6.10.0 zeigten untereinander deutliche Unterschiede, so dass diese Versionen für diesen Anwendungsfall nicht als validierte Modelle angesehen werden können.

Weitere Simulationen wurden mit der DES Methodik durchgeführt. Ziel war zum einen die Variation der Brandgrösse und deren Einfluss auf den Druckverlust, zum anderen die Untersuchung von Turbulenzstrukturen als Quelle von Oszillationen, der Stabilität einer Rauchschichtung und des Effekts der Aufsplittung des Rauchplumes in der Längsströmung.

Es lässt sich feststellen, dass das RANS-Turbulenzmodell zur Beurteilung der zeitgemittelten Strömungseigenschaften verwendet werden kann. Darüber hinaus erlaubt es eine geringere Gitterauflösung. Im Vergleich dazu erfordert DES eine höhere Gitter- und Zeitauflösung. Bei zunehmender Wärmefreisetzungsrate nehmen Oszillationen zu. Darum ist eine höhere Abtastrate erforderlich, um stabile mittlere Strömungseigenschaften zu erzielen. DES erfasst jedoch die Details turbulenter Strukturen und hochfrequenter Oszillationen, insbesondere am und stromab vom Brand.

Anwendung

Anhand einer Parameterstudie werden die Auswirkungen des Strömungswiderstandes eines Brandes im Tunnel auf die Auslegung von Längslüftungssystemen nach ASTRA 13001 [1] abgeschätzt, vgl. Kapitel 7.1. Für drei typische Tunnel auf dem Nationalstrassennetz wird die Längslüftung ohne Strömungswiderstand des Brandes berechnet. Anschliessend wird der Einfluss von einzelnen Parametern quantifiziert, bei denen konservative Annahmen zu impliziten Reserven der Auslegung führen. Der Strömungswiderstand des Brandes in diesem Auslegungsfall wird mit diesen Reserven verglichen.

Der zusätzliche Strömungswiderstand ist in jedem Fall geringer als nach dem Forschungsbericht [15] erwartet. Entsprechend genügen auch die impliziten Reserven der Auslegung, um die meisten Brandereignisse beherrschen zu können. Ein unmittelbarer Handlungsbedarf bei in Betrieb befindlichen Tunneln ist nicht gegeben. In der Planung von neuen Anlagen oder bei Erneuerungen soll der Strömungswiderstand eines Tunnelbrandes berücksichtigt werden.

Der Widerstand muss nicht berücksichtigt werden, wenn die Lüftung für eine Strömungsgeschwindigkeit von 1,5 m/s ausgelegt ist. Auch in Tunneln mit Absaugung im Ereignisfall muss der Strömungswiderstand des Brandes nicht berücksichtigt werden.

Die Gleichungen für den Throttling Effect können in 1-D Simulationsprogrammen implementiert werden, vgl. Kapitel 7.3. Die Änderung des statischen Drucks am Brandort ist gegeben durch

$$\Delta p_{1-2} = -\frac{Q_c\, u_0}{c_p A_T T_0} \tag{12}$$

Die Änderung des statischen Drucks stromab vom Brand enthält zwei Beiträge. Für die Berechnung der Wandreibung wird die Strömungsgeschwindigkeit erhöht und die Luftdichte vermindert. Dies führt zu einer Erhöhung der Wandreibung gemäss

$$\Delta p_{2-3A} = -\frac{\rho_0}{2} \cdot u_0^2 \cdot \frac{\lambda}{D_h} \cdot \frac{Q_c}{\alpha U_T T_0}\left(1 - exp\left(-\frac{\alpha U_T L_3}{\rho_0 u_0 A_T c_p}\right)\right) \tag{13}$$

Ein erhöhter Strömungswiderstand durch Fahrzeuge oder Querschnittänderungen stromab vom Brand muss entsprechend behandelt werden.

Der Rückgewinn von statischem Druck aufgrund der Abkühlung der Brandgase und der entsprechenden Verringerung der Strömungsgeschwindigkeit ist gegeben durch

$$\Delta p_{2-3B} = \frac{Q_c\, u_0}{c_p A_T T_0}\left(1 - exp\left(-\frac{\alpha U_T L_3}{\rho_0 u_0 A_T c_p}\right)\right) \tag{14}$$

Wenn diese Gleichungen in ein bestehendes 1-D Modell integriert werden, müssen die Gleichungen gegebenenfalls modifiziert werden.

CFD-Simulationen können zur Untersuchung des Strömungswiderstands von Tunnelbränden eingesetzt werden, vgl. Kapitel 7.4. Dabei sind folgende Aspekte zu beachten:

- Turbulenzmodelle wie SST k-ω liefern eine gute Einschätzung des durchschnittlichen Strömungswiderstands. Sie liefern aber keine detaillierten Informationen zu dynamischen turbulenten Strömungsmerkmalen.
- LES ist rechenintensiv, ein kombiniertes Modell wie DES bietet jedoch einen guten Kompromiss zwischen Rechenaufwand und der Erfassung des turbulenten Verhaltens im Tunnel.
- Sowohl DES als auch LES erfordern eine Voruntersuchung mittels RANS- oder URANS-Simulation, um das Gitter so weit zu verfeinern, dass 80 Prozent der turbulenten kinetischen Energie dargestellt wird.
- Darüber hinaus kann die Einschätzung Wirbelviskosität und effektiven Wärmeleitfähigkeit aus URANS-Simulationen genutzt werden, um das Gitter für DES zu optimieren.
- Grössere Brandleistungen führen zu stärkeren hochfrequenten Druckschwankungen. Dies ist bei der Auswertung der Ergebnisse zu beachten.

Résumé

Situation initiale

Le projet de recherche « Résistance à l'écoulement des incendies dans les tunnels routiers » (AGT 2017/005) [15] conclut que les systèmes de ventilation actuels des tunnels sont sous-dimensionnés pour les situations d'incendie. La résistance à l'écoulement est généralement sous-estimée. Le projet comprend une étude théorique de la résistance à l'écoulement et de sa pertinence pour la conception de la ventilation de secours. Les résultats de cette étude peuvent être utilisés pour déterminer la résistance à l'écoulement, en vue de la conception de systèmes de ventilation à l'aide de programmes de calcul 1D.

Pour la résistance à l'écoulement d'un incendie en flux d'air longitudinal, le rapport final décrit un système d'équations quantifiant les contributions à la résistance totale. Ce système d'équations a été calculé analytiquement, mais inclut également une contribution empirique issue de simulations CFD.

La directive ASTRA 13001 [1] a été examinée dans le cadre du projet de recherche concernant les marges de sécurité inhérentes. Dans [15], la résistance à l'écoulement d'air d'un attendue incendie a été comparée à ces marges de sécurité. L'analyse a conclu que la résistance à l'écoulement d'air dépasse les marges de sécurité et que les systèmes de ventilation doivent donc être conçus pour une poussée accrue.

L'étude [15] s'appuie sur des approches théoriques et des simulations d'écoulement, car il n'existe pratiquement aucune donnée expérimentale pertinente. Avant de pouvoir appliquer les résultats à la planification et à la conception des systèmes de ventilation, les simulations doivent être validées par des essais d'écoulement en grandeur réelle. La validation consiste à vérifier un modèle informatique à l'aide de mesures. Les essais à petite échelle sont moins pertinents, car les effets d'échelle peuvent conduire à des résultats erronés.

Ce rapport de recherche documente les mesures et les résultats de cette validation. D'autres simulations CFD sont également documentées, permettant d'extrapoler les résultats de mesure à d'autres géométries de tunnel ou tailles d'incendie.

Étude de la littérature

Dans les années qui ont suivi la finalisation de l'étude [15], d'autres chercheurs ont étudié la résistance à l'écoulement des incendies dans les tunnels routiers. Cette littérature actuelle est résumée et évaluée au chapitre 2.2 de ce rapport. Le modèle de calcul de [15] est également résumé.

Ces publications ont en commun de se fonder exclusivement sur des considérations théoriques, des simulations CFD et des expériences sur modèle. Aucun essai d'écoulement à grande échelle n'a été réalisé pour valider l'étude [15].

Essais au feu

Le chapitre 1 décrit en détail la préparation et la réalisation des essais au feu. Ces essais ont été réalisés dans le tunnel d'essai « San Pedro des Anes », près de Gijón, en Espagne. Ce tunnel est particulièrement adapté aux essais car, avec une longueur de 600 m et une section de 48 m², ses dimensions sont comparables à celles d'un tunnel routier de section rectangulaire. De plus, une longueur suffisante est disponible en aval de l'incendie pour observer les effets de la fumée et la stratification thermique. Un tunnel de service sous la chaussée permet de mesurer relativement facilement les différences de pression entre le tunnel et le tunnel de service.

Le foyer d'incendie pour les essais était constitué de bacs de combustible de 4 m² (essais 1 et 2) et de 6,1 m² (essai 3), placées directement au-dessus de la chaussée. Avec des quantités de combustible de 150 litres (essais 1 et 2) et de 230 litres (essai 3), une durée d'incendie d'environ 15 minutes était visée. La puissance de feu était limitée à 10 MW en raison des restrictions de protection incendie dans le tunnel. La configuration de test reproduit directement les conditions limites sous-jacentes aux simulations CFD dans l'étude [15].

Le tunnel d'essai est équipé de six puissants ventilateurs à jet. L'écoulement longitudinal dans le tunnel peut être influencé par la mise en marche de chaque ventilateur. Pour les essais, un débit d'air entrant de 3 m/s a été ciblé, conformément à la conception de la ventilation des tunnels routiers suisses [1]. Lors des essais, la vitesse d'écoulement a été ajustée par la mise en marche d'un ventilateur (essai 1) ou de deux ventilateurs (essais 2 et 3). Un contrôle dynamique du débit basé sur des mesures de débit n'est pas possible dans le tunnel d'essai.

La disposition de l'instrumentation d'essai dans le tunnel est illustrée à la Figure 17.

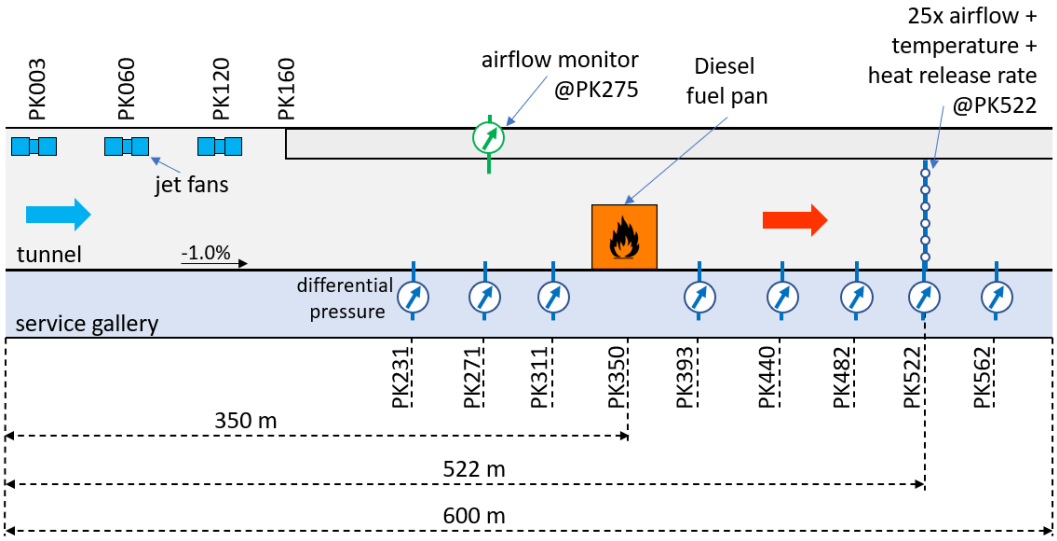

Figure 17: Configuration de test

Conformément au plan d'essai, la mesure du débit d'air en aval de l'incendie devait être effectuée par 25 capteurs indépendants afin de déterminer la vitesse moyenne d'écoulement dans le tunnel et le profil d'écoulement en coupe transversale. Cependant, seuls six capteurs de pression différentielle étaient disponibles pour les essais. Cela n'a permis d'enregistrer qu'un profil d'écoulement vertical, chacun avec cinq tubes de Pitot, enregistrant la pression dynamique moyenne dans le tunnel.

Pour la mesure de la température, 25 thermocouples ont été installés au PK522, aux mêmes points de grille que les capteurs de débit d'air.

Le profil de pression statique le long du tunnel a été mesuré comme la pression différentielle entre le tunnel et la galerie de service située en dessous. À l'intérieur du tunnel, la mesure de pression était située sur la paroi du tunnel, à environ 2 m du sol. L'ouverture de la prise de pression était positionnée perpendiculairement à l'écoulement longitudinal afin d'éviter toute influence sur la vitesse d'écoulement. Des simulations CFD ont vérifié que la pression différentielle mesurée pendant l'écoulement développé était représentative de la pression moyenne dans la coupe transversale du tunnel.

Un dispositif de mesure de pression différentielle supplémentaire était situé au PK231. L'installation était similaire à celle décrite précédemment. Ce capteur de pression permettait d'enregistrer des mesures à court terme avec des fréquences d'échantillonnage plus élevées, de 100 à 2000 Hz.

Le taux de dégagement de chaleur a été déterminé en mesurant le débit massique total et diverses concentrations de gaz (CO, CO_2, O_2 et H_2O). Le taux de dégagement de chaleur a ensuite été déduit de ces débits massiques. Le taux de dégagement de chaleur mesuré a également été vérifié par la quantité de combustible utilisée et par l'intégrale du dégagement de chaleur mesuré.

Modèle 1-D

En supposant que la masse du combustible puisse être négligée par rapport au débit d'air total, le modèle de calcul 1D peut être formulé de manière compacte. Les équations nécessitent la définition de plusieurs emplacements le long du tunnel. Ce dernier est divisé en trois sections : amont, incendie et aval. On suppose également que la longueur de l'incendie (section ①→②) peut être négligée.

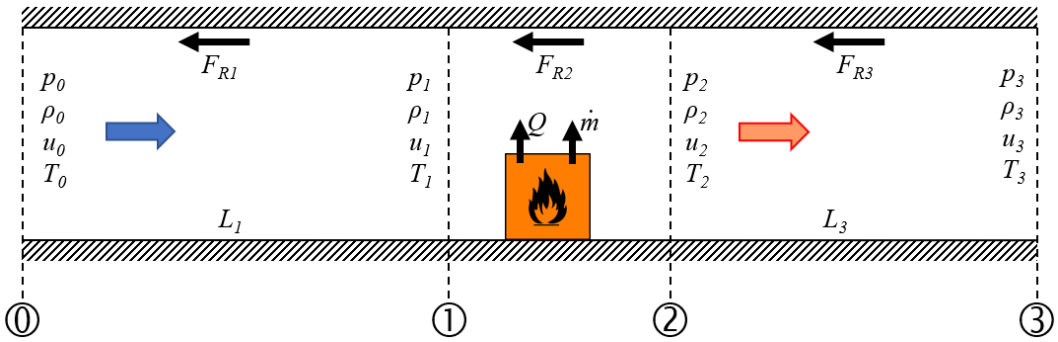

Figure 18: Définitions

La variation de la pression statique due au frottement des parois dans la section d'entrée entraîne

$$\Delta p_{0-1} = -\frac{\rho_0}{2} \cdot u_0^2 \cdot \frac{\lambda\, L_1}{D_h} \tag{15}$$

Le changement de pression statique au niveau du lieu de l'incendie est simplifié ainsi

$$\Delta p_{1-2} = -\frac{Q_c\, u_0}{c_p A_T T_0} \tag{16}$$

La variation de la pression statique en aval de l'incendie comprend plusieurs composantes :

- Le frottement pariétal correspond à la section d'entrée. Cependant, la vitesse d'écoulement augmente et la densité diminue, ce qui entraîne une perte de charge accrue.

$$\Delta p_{2-3A} = -\frac{\rho_0}{2} \cdot u_0^2 \cdot \frac{\lambda}{D_h} \cdot \left[\frac{Q_c}{\alpha U_T T_0}\left(1 - exp\left(-\frac{\alpha U_T L_3}{\rho_0 u_0 A_T c_p}\right)\right) + L_3\right] \tag{17}$$

- La récupération de la pression statique par refroidissement et la décélération de l'écoulement qui en résulte sont

$$\Delta p_{2-3B} = \frac{Q_c\, u_0}{c_p A_T T_0}\left(1 - exp\left(-\frac{\alpha U_T L_3}{\rho_0 u_0 A_T c_p}\right)\right) \tag{18}$$

Le rapport de recherche [15] décrit une perte de pression supplémentaire due à la stratification thermique. Cette contribution est issue de simulations CFD. L'analyse des données d'essai a montré que cette perte de pression supplémentaire était un artefact des simulations CFD.

Pour l'analyse des données expérimentales de ce rapport, le modèle 1D suivant les équations ci-dessus a été implémenté dans le modèle numérique 1D Spitfire ([29] à [32]) afin de le comparer aux données expérimentales et à d'autres simulations CFD.

Simulations CFD 3-D

En plus des simulations 1-D, trois codes CFD 3-D différents ont été utilisés pour la préparation des essais au feu et pour une comparaison avec les données collectées :
- RANS, Star-CCM+
- LES, Fire Dynamic Simulator
- DES, ANSYS Fluent

Une documentation détaillée des simulations CFD, c'est-à-dire la géométrie, les sous-modèles, les conditions aux limites, etc., est décrite au chapitre 5.

La version Star-CCM+ v2302 a été utilisée pour les simulations RANS. Celles-ci ont été réalisées en mode stationnaire avec un couplage écoulement-énergie d'ordre 2. En raison des gradients de température élevés attendus, l'air est supposé compressible. La viscosité, la conductivité thermique et la capacité thermique de l'air sont calculées en fonction de la température selon la loi de Sutherland. Le terme de gravité est inclus pour tenir compte des forces de flottabilité. Pour les géométries de tunnel inclinées, seul le vecteur de gravité est modifié.

Le simulateur de dynamique des incendies FDS v6.8.0 a été utilisé pour les simulations LES. Pour l'analyse de la courbe de pression des incendies dans les tunnels longs, la simulation transitoire des très grandes échelles VLES, associée au solveur FFT standard, a été utilisée, conformément aux recommandations du manuel d'utilisation de FDS.

La simulation des tourbillons détachés (DES) est un modèle de turbulence hybride combinant RANS et la simulation des grandes échelles (LES). À proximité des limites solides et de l'incendie, où les échelles de turbulence sont petites et leur résolution coûteuse en calculs, DES utilise la méthode RANS pour modéliser efficacement la turbulence. Loin des parois, dans les régions présentant de grandes structures turbulentes, DES passe à LES, qui résout directement les tourbillons instables. DES offre un équilibre entre précision et coût, en capturant les mouvements turbulents à grande échelle dans des écoulements séparés tout en évitant les exigences de calcul excessives d'une LES complète.

Résultats des tests

Les résultats complets de la comparaison des mesures et des simulations sont décrits au chapitre 5.6. Les résultats individuels du test 1 sont présentés ici à titre d'exemple.

La Figure 19 illustre l'évolution des mesures de pression différentielle lors du test 1. Les mesures ont été ajustées en réglant la différence de pression à 0 Pa avant le début de l'incendie. De plus, les signaux ont été décalés dans le temps afin que l'instant t = 0 min soit fixé à la mise en marche du ventilateur à jet. Le feu s'est déclaré après 12 min 52 s et a duré jusqu'à 40 min 38 s. Les mesures de pression montrent une évolution calme avant la mise en marche de la ventilation. Les turbulences augmentent avec le fonctionnement de la ventilation. Pendant l'incendie, d'importantes fluctuations de pression se produisent, en particulier dans la seconde moitié de l'incendie.

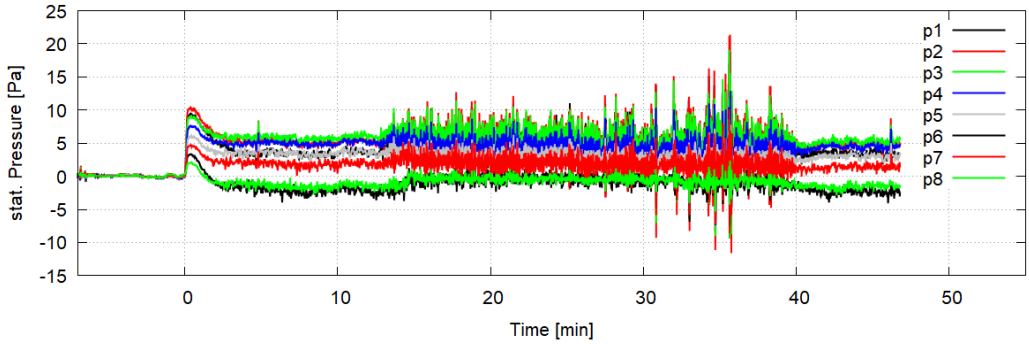

Figure 19: Mesures de pression différentielle pour le test 1.

La Figure 20 compare les quatre profils de pression le long du tunnel avec la pression différentielle mesurée. Trois des moniteurs de pression (PK231, PK482 et PK562) ont présenté un comportement irrégulier, tant au niveau de la variation dynamique que des valeurs moyennes du profil de pression. L'installation a été revérifiée après l'essai, mais aucune explication n'a été trouvée. Les données sont présentées dans le graphique, mais ne sont pas incluses dans l'analyse. La mesure sur le PK231 a été remplacée par le capteur haute fréquence.

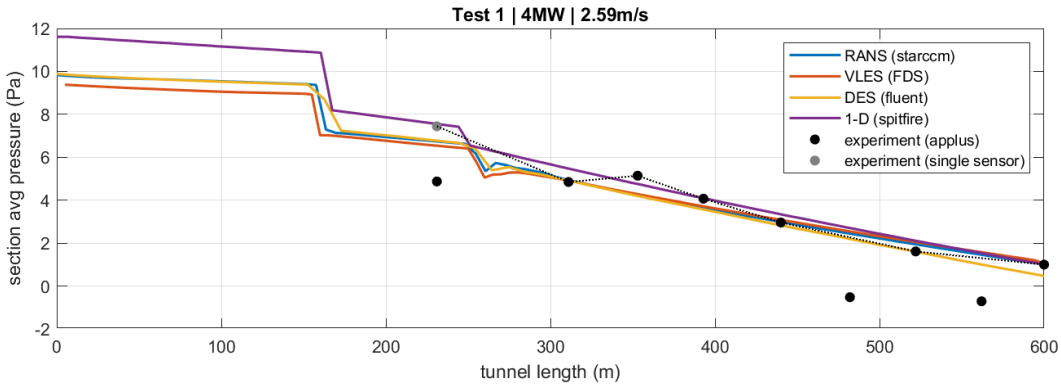

Figure 20: Comparaison de la courbe de pression le long du tunnel à partir des données de simulation avec les valeurs mesurées pour le test 1.

Les trois simulations CFD présentent une bonne concordance avec les mesures, dans les limites de la précision attendue. La simulation 1D montre une légère augmentation du frottement pariétal en aval et une perte de charge accrue au niveau du changement de section au PK160.

La comparaison de la distribution de température le long du tunnel est présentée à la Figure 21. Seule la valeur moyenne des mesures de température issues du réseau au PK522 est disponible en un seul point.

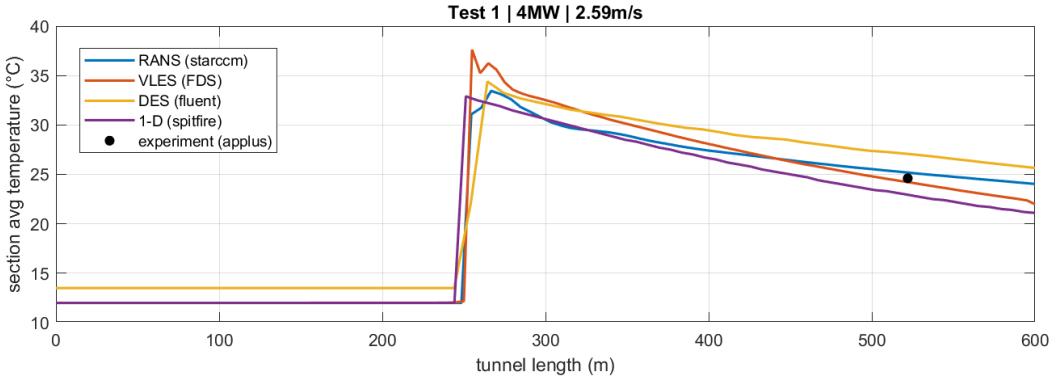

Figure 21: Comparaison de la courbe de température le long du tunnel à partir des données de simulation avec les valeurs mesurées pour le test 1.

Une comparaison des profils de température et d'écoulement en aval de l'incendie PK522 est présentée à la Figure 22. Les mesures montrent une stratification de température légèrement plus marquée que les simulations CFD. En revanche, le profil d'écoulement dans la simulation est équilibré, avec des vitesses légèrement plus élevées dans la moitié supérieure de la section transversale. Les mesures montrent des vitesses d'écoulement plus faibles dans la moitié supérieure du profil du tunnel. Si les simulations CFD révèlent une similitude entre les profils de température et d'écoulement (si l'on omet le point de mesure avec un écoulement de 0 m/s à la paroi), ce n'est pas le cas avec les mesures.

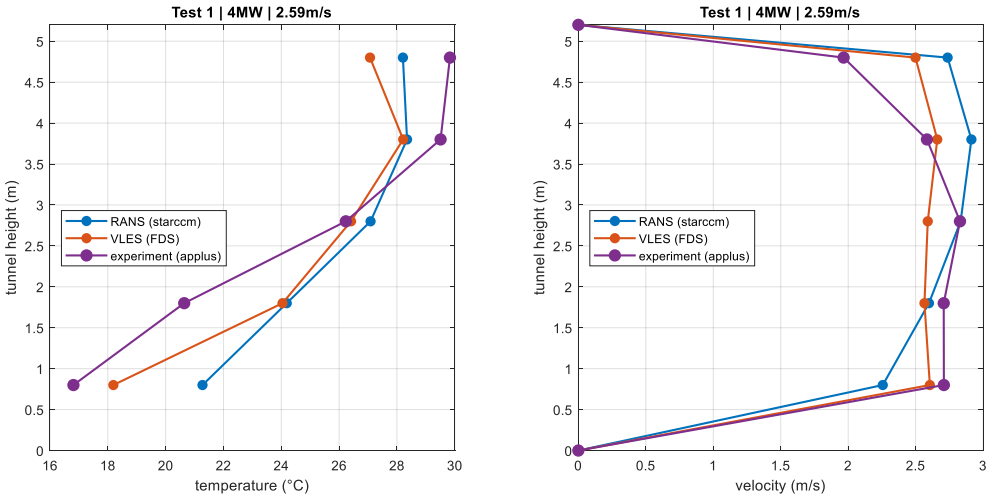

Figure 22: Profil de température et de vitesse sur PK522 pour le test 1.

Ce résultat semble typique des simulations CFD 3-D. Des différences très similaires entre simulation et mesure ont été observées lors d'un recalcul des essais d'incendie dans le Memorial Tunnel [27]. Notez la similitude entre les profils de simulation et les différents profils de mesure.

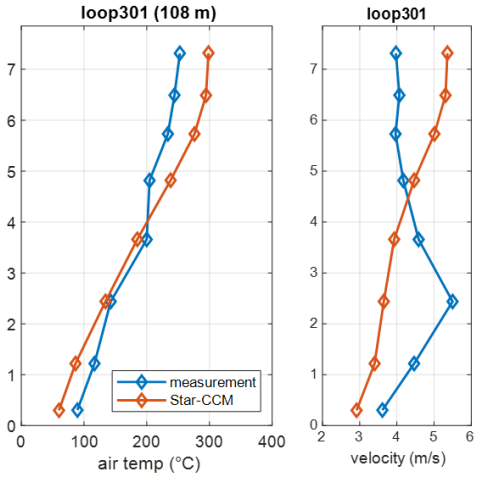

Figure 23: RANS vs. expérience du profil de température et de vitesse du cas de mesure commémoratif 610 à la boucle 301 [27].

Simulations CFD supplémentaires

L'un des objectifs du projet de recherche était d'adapter les résultats à des performances d'incendie plus importantes et à d'autres géométries typiques des tunnels des routes nationales suisses. Les résultats doivent également être comparés à la conception des systèmes de ventilation selon la norme ASTRA 13001. Ces simulations sont décrites au chapitre 1 du rapport.

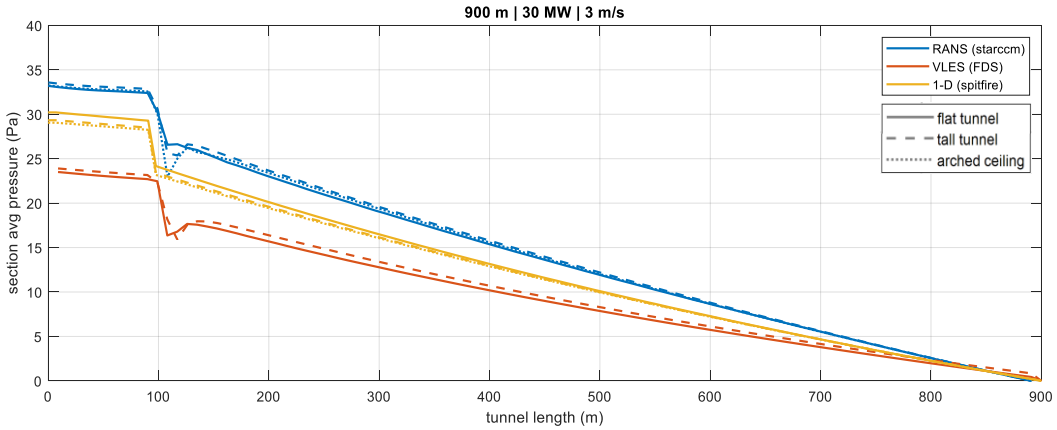

Figure 24: La pression moyenne le long du tunnel pour un incendie de 30 MW

La Figure 24 illustre la distribution de pression le long du tunnel pour trois sections transversales de même surface et pour trois modèles de calcul. L'influence du profil du tunnel est faible. Les différences entre les modèles de calcul sont supérieures à celle de la géométrie de la section transversale. Cependant, les différences entre les modèles

s'atténuent pour un tunnel sans gradient longitudinal. La modélisation du transfert de chaleur et de la flottabilité joue un rôle important dans la distribution de pression.

Ces simulations montrent que
- La forme de la section du tunnel (rectangulaire ou en fer à cheval) n'a qu'une influence mineure sur la distribution de pression.
- Les différences entre les modèles augmentent avec le taux de dégagement de chaleur. Cela est en partie dû au modèle de transfert de chaleur, c'est-à-dire à la flottabilité dans le tunnel incliné.
- Les simulations avec les versions 6.8.0, 6.9.1 et 6.10.0 de FDS ont montré des différences significatives entre elles ; ces versions ne peuvent donc pas être considérées comme des modèles validés pour cette application.

D'autres simulations ont été réalisées à l'aide de la méthodologie DES. L'objectif était, d'une part, d'étudier la variation de la taille de l'incendie et son influence sur la perte de charge, et, d'autre part, d'étudier les structures turbulentes comme source d'oscillations, la stabilité de la stratification des fumées et l'effet de la bifurcation du panache de fumée sur l'écoulement longitudinal.

Le modèle de turbulence RANS permet d'évaluer les propriétés d'écoulement moyennées dans le temps. De plus, il permet une faible résolution de grille. En comparaison, le DES nécessite une résolution de grille et une résolution temporelle plus élevées. Plus le taux de dégagement de chaleur augmente, plus les oscillations augmentent. Par conséquent, une fréquence d'échantillonnage plus élevée est nécessaire pour obtenir des propriétés d'écoulement moyennes stables. Cependant, le DES capture les détails des structures turbulentes et des oscillations à haute fréquence, notamment au niveau et en aval de l'incendie.

Application

À l'aide d'une étude paramétrique, les effets de la résistance à l'écoulement d'un incendie de tunnel sur la conception des systèmes de ventilation longitudinale sont estimés (voir chapitre 7.1). La ventilation longitudinale est calculée pour trois tunnels typiques du réseau routier national, conformément aux spécifications de la norme ASTRA 13001 [1]. L'influence de chaque paramètre est ensuite quantifiée, des hypothèses prudentes conduisant à des marges de sécurité implicites. La résistance à l'écoulement de l'incendie dans ce cas de conception est comparée à ces marges de sécurité.

La résistance supplémentaire à l'écoulement est systématiquement inférieure aux prévisions du rapport de recherche [15]. Par conséquent, les marges de sécurité implicites de conception sont suffisantes pour permettre la maîtrise de la plupart des incendies. Aucune action immédiate n'est nécessaire pour les tunnels en exploitation. Lors de la conception de nouveaux systèmes ou de rénovations, la résistance à l'écoulement d'un incendie de tunnel doit être prise en compte.

L'effet d'étranglement n'a pas à être pris en compte si la ventilation est conçue pour une vitesse d'écoulement de 1,5 m/s. De même, dans les tunnels avec désenfumage en cas d'incendie, la résistance à l'écoulement de l'incendie n'a pas à être prise en compte.

Les équations de l'effet d'étranglement peuvent être implémentées dans des programmes de simulation 1D (voir chapitre 7.3). La variation de pression statique au point d'incendie est donnée par

$$\Delta p_{1-2} = -\frac{Q_c\, u_0}{c_p A_T T_0} \tag{19}$$

La variation de la pression statique en aval de l'incendie comprend deux composantes. Pour le calcul du frottement pariétal, la vitesse d'écoulement est augmentée et la densité est réduite. Il en résulte une augmentation du frottement pariétal.

$$\Delta p_{2-3A} = -\frac{\rho_0}{2} \cdot u_0^2 \cdot \frac{\lambda}{D_h} \cdot \frac{Q_c}{\alpha U_T T_0}\left(1 - exp\left(-\frac{\alpha U_T L_3}{\rho_0 u_0 A_T c_p}\right)\right) \tag{20}$$

La résistance aérodynamique supplémentaire des véhicules stationnés en aval de l'incendie ou les modifications de la section transversale du tunnel doivent être traitées en conséquence.

La récupération de la pression statique par refroidissement et la décélération résultante de l'écoulement sont données par

$$\Delta p_{2-3B} = \frac{Q_c\, u_0}{c_p A_T T_0}\left(1 - exp\left(-\frac{\alpha U_T L_3}{\rho_0 u_0 A_T c_p}\right)\right) \tag{21}$$

Si ces équations sont intégrées dans un modèle 1D existant, certaines modifications peuvent être nécessaires.

Les simulations CFD peuvent être utilisées pour étudier la résistance à l'écoulement lors d'un incendie en tunnel (voir chapitre 7.4). Les aspects suivants doivent être pris en compte :

- Les modèles de turbulence tels que SST k-ω fournissent une bonne estimation de la résistance moyenne à l'écoulement. Cependant, ils ne fournissent pas d'informations détaillées sur les caractéristiques dynamiques de l'écoulement turbulent.
- Les modèles LES nécessitent des calculs intensifs, mais un modèle combiné tel que DES offre un bon compromis entre effort de calcul et capture du comportement turbulent dans le tunnel.
- Les modèles DES et LES nécessitent tous deux une étude préliminaire à l'aide de simulations RANS ou URANS afin d'affiner la grille jusqu'à ce que 80 % de l'énergie cinétique turbulente soit représentée.
- De plus, l'estimation de la viscosité turbulente et de la conductivité thermique effective à partir des simulations URANS peut être utilisée pour optimiser la grille pour les modèles DES.

- Des taux de dégagement de chaleur plus élevés entraînent des fluctuations de pression à haute fréquence plus importantes. Ceci doit être pris en compte lors de l'évaluation des résultats.

1 Introduction

1.1 Initial situation

The research project "Flow resistance of fires in road tunnels" (AGT 2017/005) [15] concluded that today's tunnel ventilation systems were under-dimensioned for fires. The project includes a theoretical investigation of flow resistance and its relevance for the tunnel ventilation design for smoke control.

The results of the study can be used to determine flow resistance - for application in the dimensioning of ventilation systems with 1-D simulation software. The flow resistance of a fire consists of several contributions. Some can be determined from the one-dimensional conservation equations:

- Decrease in static pressure at the fire site due to heating, expansion and acceleration of the tunnel air,
- Increased wall friction downstream of the fire due to increased flow velocity with reduced air density,
- Increase in static pressure due to the deceleration of the air flow due to cooling on the tunnel wall.

There remained a pressure loss due to spatial effects. This was determined from a series of 3-D flow simulations: FDS Version 6.7.0 and OpenFoam/FireFoam Version 1812. In the simulations, the temperature stratification of the flow downstream of the fire had a strong influence on the flow profile, which in turn resulted in the increased flow resistance due to temperature stratification downstream of the fire.

The study determined key parameters. These are the heat release rate, flow velocity and tunnel profile (cross-section and height). A total of more than 200 simulations were carried out. Around 60 simulations were included in the evaluation. Key variables were varied as follows:

- Heat release rate — 2 MW - 34 MW
- Flow velocity — 1 m/s - 4 m/s
- Tunnel cross-section — 2-lane rectangular profile
  4-lane horseshoe profile

For the flow resistance of a fire in a longitudinal ventilation system, the report describes a system of equations that quantifies the contributions to the total resistance. The ASTRA 13001 guideline [1] was examined in the research project for inherent safety margins. The flow resistance of a fire was put in relation to these safety margins. It was shown that the flow resistance exceeds the safety margins, and that longitudinal ventilation should therefore include additional jet fan thrust.

The study [15] is based on theoretical approaches and flow simulations, since practically no suitable experimental data were available at the time. Before the results can be applied in practice, the simulations must be validated using large-scale fire tests.

1.2 Objectives

Validation is the verification of a computational physical model with experimental measurements. Validation pursues the following objectives:

- Measurement of the physical quantities required to validate the results of the study. For the study [15], the pressure distribution along the tunnel (see Figure 25) and the cross-sections of the flow velocity and temperature downstream of the fire are to be determined (see Figure 26).
- Comparison of the measurements with the results of the study.

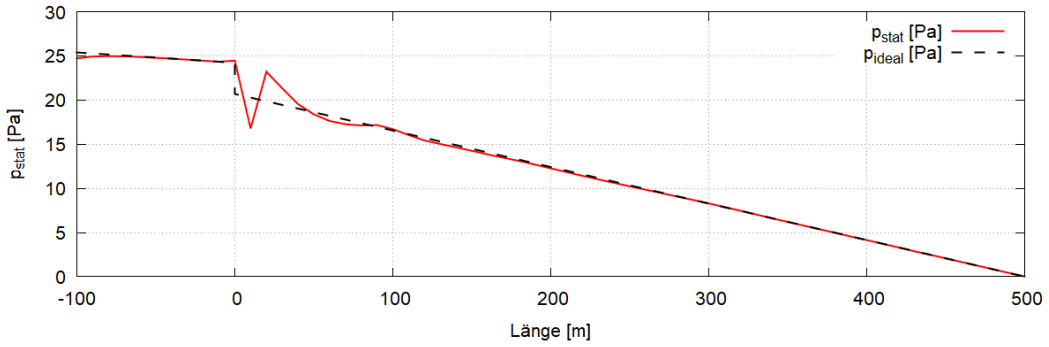

Figure 25: Static pressure distribution, 10 MW fire in 3 m/s airflow, red: simulation OpenFOAM, black: idealised distribution [15]

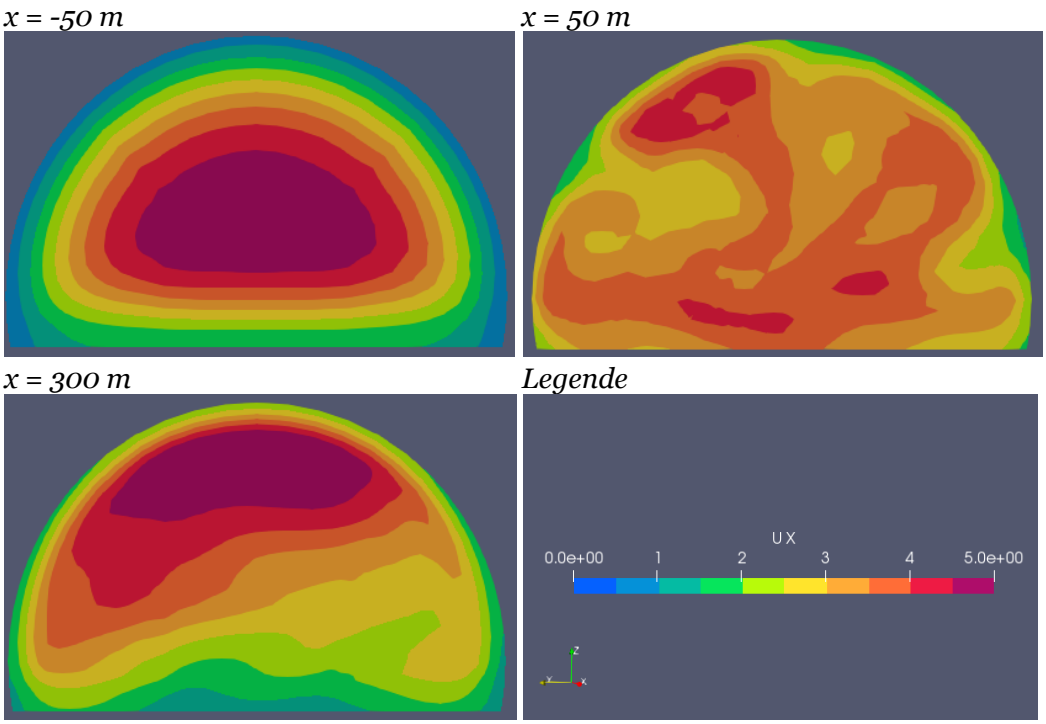

Figure 26: Sections of the airflow velocity for the pressure distribution shown in Figure 25 [15]

The research study consists of seven work packages:

- WP1 Literature study, test preparation: This work package consists of a review of scientific literature on the throttling effect, that has not been included in the previous study [15], [16]. This is documented in chapters 1 and 1 of this report.

- WP2 Preparatory CFD simulations. In a series of CFD simulations, the fire test conditions are anticipated to support the preparation of the tests and to serve as a basis of a comparison of CFD simulations and test data.
- WP3 Fire test preparation. This work package mostly includes the preparation of the fire tests in collaboration with the Spanish partner Applus+ TST, documented in chapter 1 of this report.
- WP4 Fire tests. The observations of the fire tests are described in chapter 1 of this report.
- WP5 Processing the test data. The CFD simulations have been adapted to match the boundary conditions of the fire tests for a validation of the models. The comparison of the CFD models to the test data is described in chapter 5.6.
- WP6 Application to typical ASTRA tunnels. This work package included the application of the CFD models to typical tunnels on the Swiss national road network. Following the fire tests, this work package was amended to further investigate strengths and weaknesses of the various tested CFD models. This is documented in chapter 1 of this report.
- WP7 documentation. The research study is documented in this report. Further documentation (drawings, photos, videos, raw data) are provided for free download.

2 Fundamental Information

This chapter provides general information on the flow resistance of a tunnel fire in a longitudinal flow. To avoid repetition, reference is made here to the study [15]. An English translation of the study [15] is provided in [16]. The compilation of literature in the following chapters is limited to new sources since 2020 and to sources discovered after completion of the study [15].

2.1 The *Throttling Effect*

It has been known since the 1960s that a fire in a closed channel results in an additional pressure loss. The phenomenon is described in the literature but only based on a few research results and only rarely in relation to tunnel fires.

The studies that dealt with the *Throttling Effect* usually focused on the local flow resistance at the fire site, which is mainly determined by the heating and expansion of the air. For the present work, we assume, in accordance with the study [15], that the flow resistance consists of several contributions:

- Decrease in static pressure at the fire site due to the heating, expansion and acceleration of the tunnel air,
- Increased wall friction downstream of the fire due to the increased flow velocity with reduced air density,
- Increase in static pressure due to the deceleration of the airflow due to cooling at the tunnel wall and
- Increased flow resistance due to the temperature stratification downstream of the fire.

The flow resistance in the tunnel with fire (at x = 0 m) is compared with the flow resistance without fire, see Figure 27.

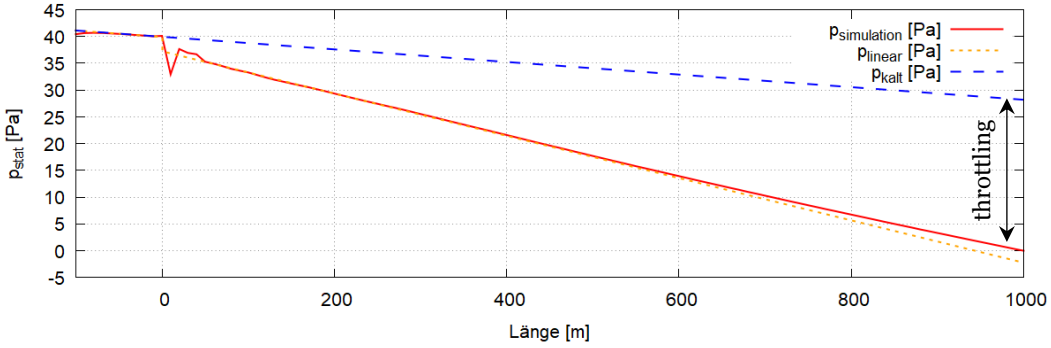

Figure 27: Static pressure distribution [15]

The throttling effect, as defined for this study, excludes buoyancy pressure from temperature differences and a tunnel gradient. For measurements in an inclined tunnel, these effects must be separated if possible.

2.2 Previous studies

The reports [15] and [16] include an extensive list of previous publications and literature on the throttling effect. These citations shall not be repeated here. Instead, the following chapters include further references that have been published in recent years or some that have been missed in the reports.

2.2.1 Carlotti & Salizzoni (2017) [11]

The study consists of a dimensional analysis of the throttling effect of a tunnel fire in longitudinal ventilation and a validation based on model experiment data.

The dimensional analysis is based on the hypothesis that the flow resistance of a tunnel fire is governed by the following relations:

$$\zeta_{fire} = f\left(\rho_0, D_h, B, \nu, u_0, g\frac{\Delta\rho}{\rho_0}\right) \quad with\ B = \frac{gQ}{\rho_0 c_p T_0} \tag{22}$$

ζ_{fire} represents a local pressure loss coefficient. The term B represents the heat release rate as a source of buoyancy with the somewhat strange unit of [m⁴/s²]. We also note that the gravitational constant is written in terms of the density difference between the fire fumes and the initial temperature.

The authors further assume that the flow is independent of the (large) Reynolds number and that the Froude number has very little impact on the flow resistance as it would not vary significantly for typical tunnels or design fires. Consequently, the pressure drop of a tunnel fire in longitudinal ventilation can be approximated as

$$\zeta_{fire} = \frac{B}{gD_h^2 u_0} = \frac{Q}{\rho_0 c_p T_0} \cdot C_1 \tag{23}$$

And

$$\Delta p_{1-2} = -\frac{\rho_0}{2} u_0^2 \zeta_{fire} = -\frac{Q u_0}{2 c_p T_0 D_h^2} \cdot C_1 \tag{24}$$

With values for C_1 ranging from 1.84 (small scale experiments) to 5.7 (CFD simulations for tunnel fires up to 30 MW).

The structure of this term for the local pressure loss at the fire is very similar to the term that is derived from the energy equation and the pressure balance across the fire, see e.g. chapter 2.2.3. The main differences are the replacement of the square of the hydraulic diameter by the tunnel cross-section and the usage of the convective part of the heat release rate. Both relations cannot be distinguished by dimensional analysis. C_1 must be determined from CFD simulations or model experiments, as full-scale experimental data is not available. For a typical tunnel with cross-section 59 m², hydraulic diameter 7.9 m and for a convective part of 75% of the heat release rate the relations give $C_1 = 3.17$, well in the range proposed in the paper.

2.2.2 Li et al. (2018) [12]

The objective of the study was the provision of a formula of the local pressure drop of a tunnel fire in longitudinal ventilation at critical velocity for engineering design purposes. The study is based on an analytical approach, on an empirical parameter derived from model scale experiments and on validation by CFD simulation.

The analytical approach differs from previous methods. It assumes that the longitudinal airflow provides mechanical work on the fire plume or vice versa, i.e. an energy balance is instigated

$$C_1 Q \approx \Delta p_{1-2} \cdot u_0 A_T \tag{25}$$

$$\Delta p_{1-2} \approx \frac{Q}{u_0 A_T} \cdot C_1 \quad with\ C_1 = 8 \cdot 10^{-5} \tag{26}$$

The empirical constant C_1 is determined in small scale experiments. For this formula, it is assumed that the volume flow rate across the fire does not change, referring to many studies that have shown that the added smoke volume from burnt fuel would be negligible. This may be a misconception, as many studies, e.g. [15], have shown that the added mass flow from burnt fuel is negligible, but not the volume change across the fire.

While the proposed formula has similarities to the relation proposed by CETU [5]

$$\Delta p_{1-2} = -\frac{Q_C}{u_0 D_h^2} \cdot C_2 \quad with\ C_2 = 9 \cdot 10^{-5} \tag{27}$$

It should describe a pressure rise instead of a pressure drop. The approach of an energy balance also does not allow for the introduction of an empirical constant α, except as some form of efficiency. Even then, the loss of energy should be accounted for.

The validation is based on CFD simulations using FDS version 6. The tunnel section is rather short with length 40 m, width 8 m and height 5 m. The pressure difference is measured 5 m upstream and 5 m downstream of the fire source. In this distance downstream, is must be assumed that the flow profile is still highly disturbed by the intermittent fire plume. Therefore, a point measurement of the static pressure may not be representative for the pressure in the tunnel cross-section.

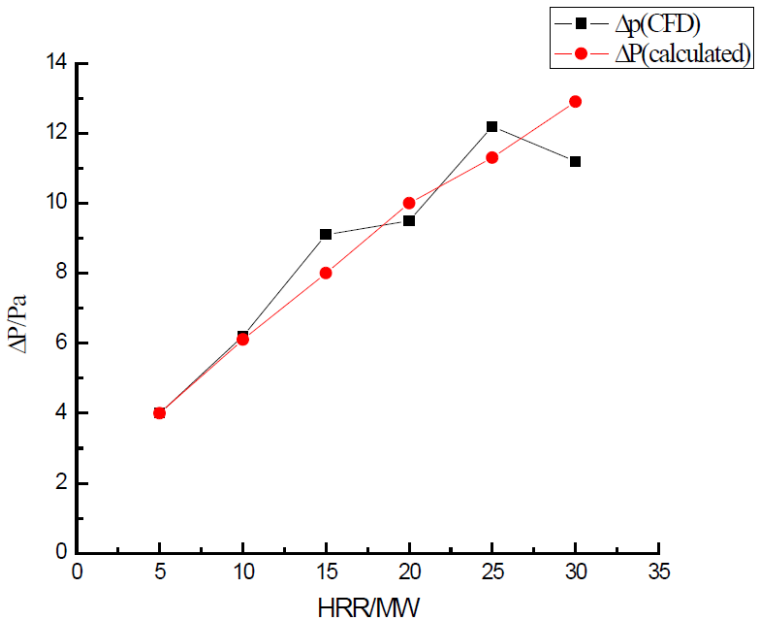

Figure 28: Comparison of the proposed model and CFD results [12]

The simulations include a variation of the heat release rate, see Figure 28. This only demonstrates that the pressure drop is roughly proportional to the heat release rate. This is the case for most models that have been proposed previously.

2.2.3 Riess et al. (2020) [15], [16]

The objective of the project was the quantification of the airflow resistance of a tunnel fire – of the "throttling effect". The findings of the study allow a calculation of this resistance based on the relevant parameters – for application in the design of tunnel ventilation systems using one-dimensional flow models.

In an extensive parameter study, involving CFD simulations using large eddy simulation in OpenFoam/FireFoam, the governing parameters for the airflow resistance of a tunnel fire were determined. These are the heat release rate, the upstream airflow velocity and the tunnel geometry (cross-section area and height of the tunnel profile). For the parameter study, more than 200 simulation runs were performed. About 60 simulations were analysed in the final processing.

With the assumption that fuel mass flow is neglected, the calculation model is presented in a compact formulation. Equations (28) to (31) were developed from classical fluid dynamic analysis, such as pipe flow pressure drop and momentum balance. Equation (32) was developed from an empirical analysis of the CFD simulations.

The set of equations requires the definition of several positions along the tunnel, see Figure 29. The tunnel is divided into three sections: upstream L_1, fire L_2 and downstream L_3. It is furthermore assumed $L_2 = 0$, i.e. there is no wall friction in this section.

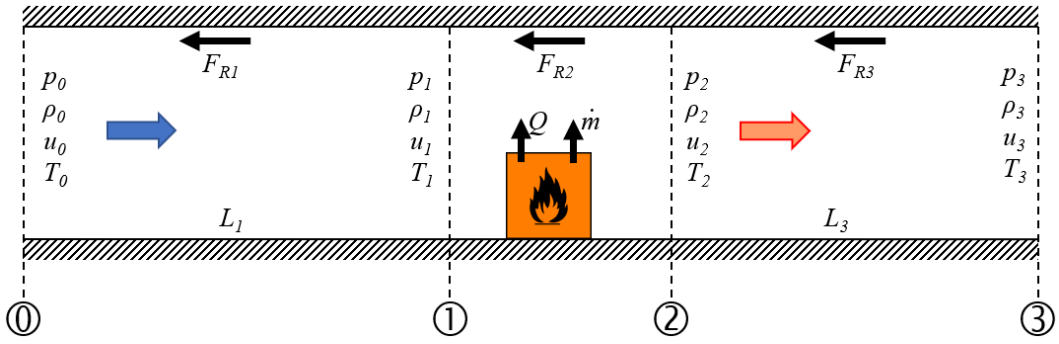

Figure 29: Definitions

The variation of static pressure due to wall friction in the inflow section results in

$$\Delta p_{0-1} = -\frac{\rho_0}{2} \cdot u_0^2 \cdot \frac{\lambda\, L_1}{D_h} \tag{28}$$

The change of static pressure at the fire location is simplified to

$$\Delta p_{1-2} = -\frac{Q_c\, u_0}{c_p A_T T_0} \tag{29}$$

The change in static pressure downstream from the fire includes three components:

- The wall friction corresponds to the inflow section. However, the flow velocity is increased and the density reduced. This results in an increased pressure drop.

$$\Delta p_{2-3A} = -\frac{\rho_0}{2} \cdot u_0^2 \cdot \frac{\lambda}{D_h} \cdot \left[\frac{Q_c}{\alpha U_T T_0}\left(1 - exp\left(-\frac{\alpha U_T L_3}{\rho_0 u_0 A_T c_p}\right)\right) + L_3\right] \tag{30}$$

- The recovery of static pressure by cooling and the resulting deceleration of the flow is

$$\Delta p_{2-3B} = \frac{Q_c\, u_0}{c_p A_T T_0}\left(1 - exp\left(-\frac{\alpha U_T L_3}{\rho_0 u_0 A_T c_p}\right)\right) \tag{31}$$

- The additional static pressure loss due to temperature stratification (friction and energy dissipation in the secondary flow) was determined from the CFD simulations. The simulations include a low mass flow of the combustible material (methane). The pressure loss results from

$$\Delta p_{2-3C} = -1.894 \cdot \frac{Q^{0.315}\, u_0^{1.136}\, H_T^{0.608}}{A_T^{1.295}} \cdot \frac{L_3}{500m}\ [Pa] \tag{32}$$

From these equations, the contribution of each component to the total pressure drop in the tunnel can be calculated. For the following example, the equations have been modified to show the friction of the cold tunnel flow vs. the contributions of the throttling effect. It appears that the throttling effect is dominated by the pressure drop due

to flow stratification downstream. It is interesting to note that the recovery of the static pressure due to cooling and decelerating the airflow downstream *Δp 2-3b* is non-negligible.

Throttling Effect Contributions

Parameters			
Tunnel length	1000 m	Air density	1.2 kg/m²
Cross-section	59 m²	Temperature	283 K
Hydr. Diameter	7.9 m	HRR	30 MW
Tunnel height	6.7 m	Conv. part	75%
Fire location	500 m	Flow velocity	3 m/s
Friction coeff.	0.015	Heat transfer coeff.	10 W/m²K
Results			
Cold flow friction	Δp 0-3 cold	-10.3 Pa	27%
Local expansion	Δp 1-2	-4.0 Pa	11%
Friction increase	Δp 2-3a warm	-1.4 Pa	4%
Pressure recovery	Δp 2-3b	2.0 Pa	-5%
Flow stratification	Δp 2-3c	-24.1 Pa	64%
Total	Δp 0-3 total	-37.8 Pa	100%

Table 1: Different contributions to the throttling effect

The report also includes a designated section on oscillations observed in CFD simulations of tunnel fires. Oscillations in tunnel fires are a phenomenon that is rarely described in the literature. However, oscillations have repeatedly occurred in simulations with FDS and FireFoam. This justifies a more detailed consideration. The report compares physical effects of a tunnel fire with the respective frequencies and compares those frequencies with oscillations observed in the simulation:

- Flame oscillations with a characteristic frequency of the fire source
- Air column oscillations with the acoustic frequency of the tunnel tube
- Coupling of airflow oscillations and heat transfer, the Rijke tube
- Coupling of airflow oscillations and heat release rate, the Runehamar fire tests

The study [15] is based only on computer simulations using standard CFD models. At the time, there were no experimental data available to verify the results. The authors recommended that the findings of this study are validated against fire tests. For this purpose, the report includes a designated section on appropriate fire tests to be performed in a full-size tunnel.

2.2.4 Ang et al. (2021) [17]

The article by Ang et al. [17] is based on the relations described in [15] with several significant differences. For the temperature distribution downstream of the fire, the model TE1D does not assume a constant heat transfer coefficient α, but an exponential function of the temperature $T_2(x)$.

$$T_2(x) = T_0 + (T_2(0) - T_0)\left(0.57\exp\left(-0.13\frac{x}{H_T}\right) + 0.43\exp\left(-0.021\frac{x}{H_T}\right)\right) \quad (33)$$

with the height of the tunnel H_T. The temperature distribution is derived empirically from large scale fire tests. The friction coefficient is not assumed constant, but as a function of the Reynolds number using the Colebrook formula.

$$\lambda = \left\{2\log\left(\frac{\varepsilon}{3.715} + \frac{5.72}{Re^{0.9}}\right)\right\}^{-2} \quad ; \quad 65 < Re < 1300 \tag{34}$$

with the relative surface roughness ε and the local Reynolds number Re. Furthermore, the pressure gain by cooling and slowing down of the airflow downstream and any pressure effects by stratification are neglected.

The results of the 1-D model were compared to a simulation using Fire Dynamic Simulator FDS.

A significant difference between the model TE1D and FDS is visible downstream of the fire, where the FDS simulation indicates an additional pressure drop, here marked as ΔP_{smoke}.

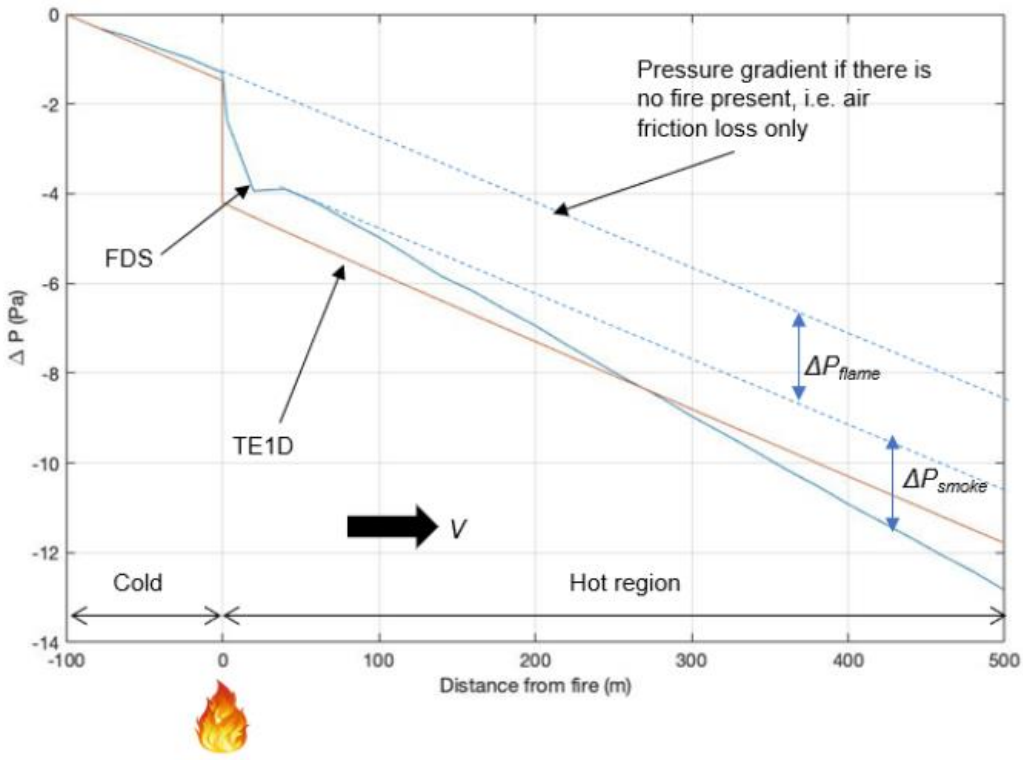

Figure 30: Comparison TE1D and FDS pressure distribution for a 10 MW fire in 4 m/s airflow [17]

The paper concludes that the 1-D model is in reasonable agreement with the FDS simulation. Elevated temperature downstream of the fire is one of the main contributors to the fire throttling effect, although there may be other effects such as stratification that could contribute to the total pressure loss. A 1-D model can produce instantaneous results that can be used to assess the fire throttling effect for a fire size of 10 MW, noting

the trade-off between prediction discrepancy to CFD models against the computation time.

2.2.5 Ang et al. (2022) [19]

In this article, the model proposed in [17] is developed further. The initial model TE1D is labelled TE1D (Energy). Then, for the pressure drop at the fire, an alternative method is proposed by applying the maximum ceiling temperature T_p from plume theory instead of the average Temperature T_2 derived from the heat release rate and the ventilation airflow.

$$\Delta p_{1-2} = \rho_0 u_0^2 \left(1 - \frac{T_p}{T_0}\right) \tag{35}$$

with (for airflow u_o above critical velocity)

$$T_p = min\left(T_0 + \frac{Q}{u_0 b_0^{1/3} H_T^{5/3}} \;;\; 1350°C\right) \tag{36}$$

In equation (36), b_o is the radius of the fire source. H_T is the height of the tunnel (resp. the height between the fire and the tunnel ceiling) and Q is the heat release rate of the fire. This model is labelled TE1D (Plume).

The two models TE1D (Plume) and (Energy) are compared to CFD simulations using OpenFoam and FDS 6.7.6.

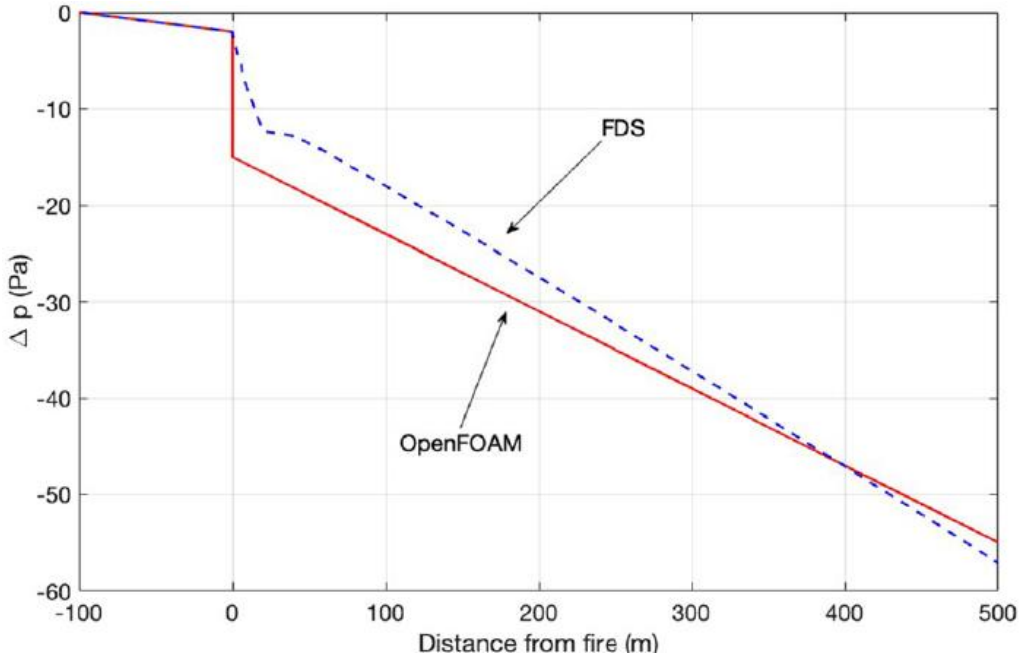

Figure 31: Comparison OpenFoam and FDS pressure distribution for a 34 MW fire in 4 m/s airflow [19]

Both CFD simulations show a significant, but different pressure resistance downstream of the fire. The comparison in [19], however, evaluates the local pressure drop

at the fire ΔP_{flame} (see Figure 32). This pressure drop is calculated for various heat release rates between 10 MW and 50 MW and for rectangular and arched tunnel cross-sections.

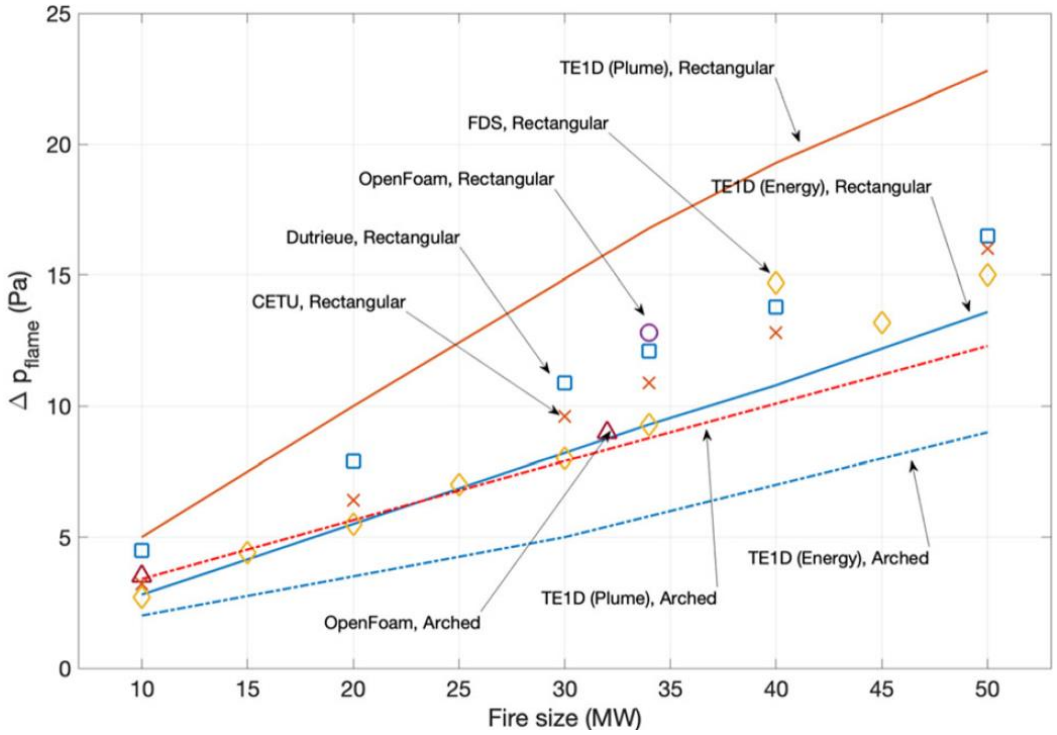

Figure 32: Comparison of the static pressure drop, derived from various models as a function of heat release rate [19]

The comparison shows that the (Plume) and (Energy) variants of the model TE1D provide an upper and lower limit of the local pressure loss at the fire when compared to the CFD simulations.

Regarding the comparison in Figure 32, it must be noted that the comparison includes the TE1D model and CFD simulations, but no experimental data. Data given as CETU are based on a design code [5] and Dutrieue refers to an article [9] that is also based on CFD simulations. The Dutrieue data includes the local pressure drop at the fire as well as any potential downstream pressure drop.

The paper includes a section dedicated to the pressure loss ΔP_{smoke} downstream of the fire. The 1-D models do not include these effects, which were especially visible in the CFD simulations for fire heat release rates above 30 MW. Figure 33 shows the difference between the 1-D model and the LES simulations using FDS and OpenFoam, noted as “error”. This error is a relative difference of the longitudinal pressure gradient in the hot-smoke region of the tunnel. For heat release rates above 30 MW, there is an additional pressure drop visible in the 3-D CFD simulations when compared to the TE1D model. The authors conclude that for such scenarios, CFD models should be used instead of 1-D approximations. But even so, it is acknowledged that the availability of only a small number of experiments and fire tests to validate CFD models is a challenge that the tunnel fire safety community has faced for a long time.

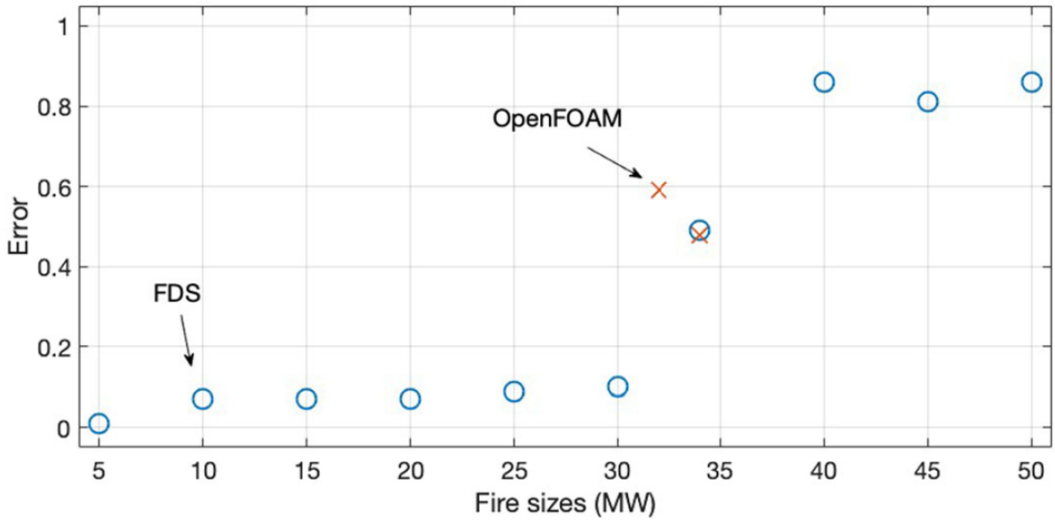

Figure 33: Comparison of "error" of TE1D to FDS and OpenFOAM regarding the pressure loss Δp_{2-3} [19]

2.2.6 Hansen (2022) [20]

This paper investigates the throttle effect for a blower fan and an exhaust fan case in a mine drift. The study is based on model fire experiments and CFD simulations. In the test setup, the position of the exhaust fan was varied from upstream from the fire, i.e. supplying air towards the fire, to downstream, i.e. extracting smoke.

Twelve model fire experiments were conducted with a 1:15 scaled tunnel, using wooden pallets as fuel. Ventilation speeds varied between 0.3 m/s, 0.6 m/s and 0.9 m/s. CFD models were used to simulate heat transfer and flow dynamics during the fire. The simulations showed deviations in the mass flow rate, especially during the critical phases of the fire. Hansen recommends using CFD models primarily for qualitative analyses of the throttling effect.

For a fan positioned downstream of the fire, the mass flow rate is affected by the reduced density of the fire gases. Cooling of the fire gases increases with increasing distance from the fire, which increases the density and reduces the throttling effect.

It appears that Hansen defines the throttling effect differently from our study, chapter 2.1 above. In the model fire tests as well as the CFD simulations, Hansen really investigates the reduced efficiency of an axial fan operating downstream in hot smoke versus a fan operating upstream in cool ambient air. The increased flow resistance of the fire in longitudinal ventilation is only a secondary effect in his study.

2.2.7 Gay (2022) [21]

In Gay's master thesis, a study on the influence of the fire throttling effect in tunnels is documented. A 1-D model based on pipe flow engineering principles is formulated and verified against STAR-CCM+ CFD simulations. The results obtained via STAR-CCM+ are then compared to FDS simulations to identify any similarities or differences between the CFD software.

The thesis is closely related to the work of Edmund Ang [17], [19]. The described 1-D model for the pressure drop is equivalent to TE1D (Energy) as described by Ang et al. [19], see equation (29).

A comparison is made between CFD simulations with Star-CCM+ and FDS using the same boundary conditions and starting parameters. The static pressure profile along the tunnel is shown in Figure 34. The results from STAR-CCM+ and FDS agree with each other until the fire location, where they deviate. The simulation done through STAR-CCM+ matches with the 1-D theory in the hot smoke region but varies significantly with FDS simulation. The pressure gradient in the hot smoke region for the FDS simulation result is considerably greater than that of STAR-CCM+ as well as the 1-D model.

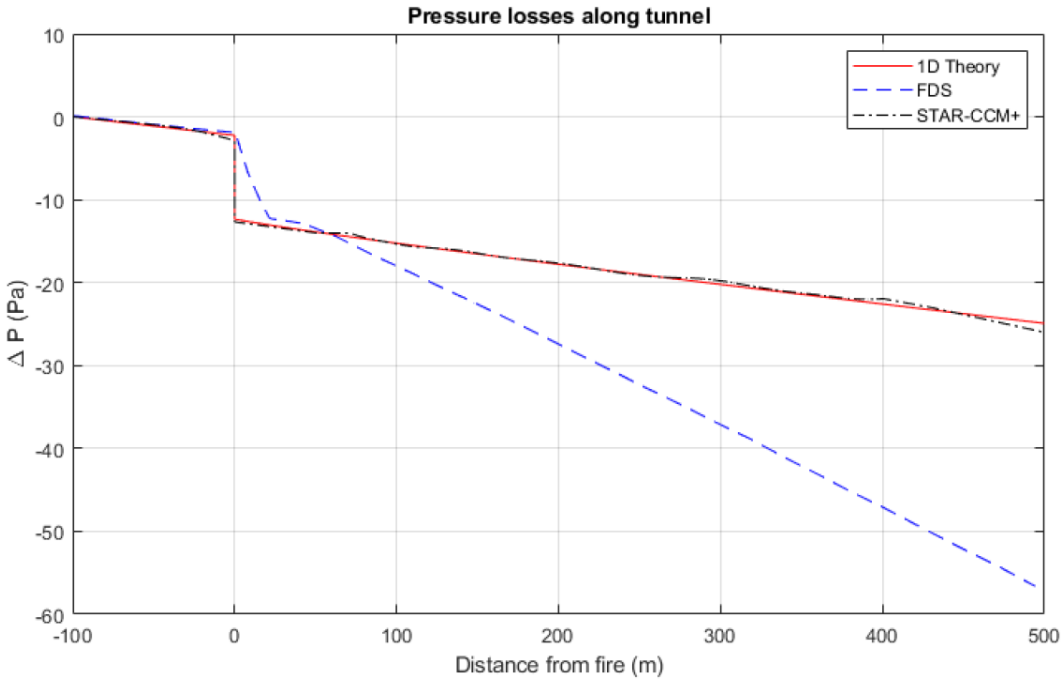

Figure 34: Comparison 1-D model, Star-CCM+ and FDS pressure distribution for a 34 MW fire in 4 m/s airflow [21]

It is argued that smoke bifurcation flow present under high ventilation velocities is a plausible explanation for the absence of smoke stratification. Smoke bifurcation is a phenomenon in which smoke flow is divided into two streams that flow along the sidewalls of the tunnel. This destroys the stability of smoke stratification and ultimately affects the pressure losses across the hot smoke region. But the absence of smoke stratification could also be caused by the RANS turbulence model used in STAR-CCM+, which may be unable to capture the 3-D effects of smoke stratification.

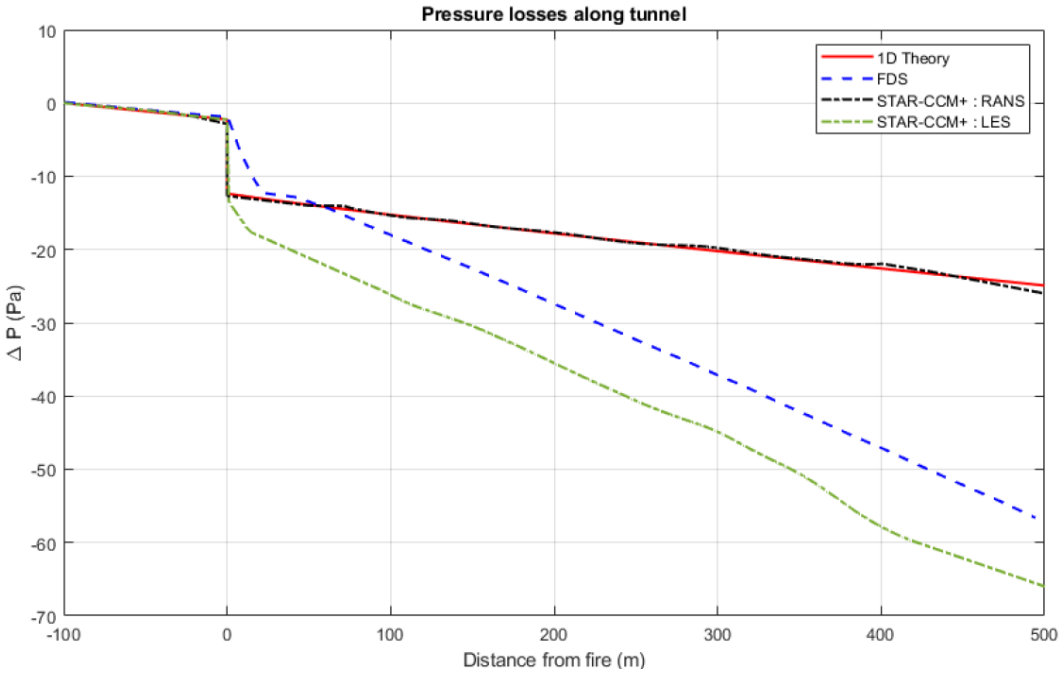

Figure 35: Comparison 1-D model, Star-CCM+ and FDS pressure distribution for a 34 MW fire in 4 m/s airflow [21]

To exclude the selection of the turbulence model as reason for the discrepancy, the simulation with STAR-CCM+ was repeated with the LES turbulence model. Figure 35 shows the pressure gradient in the hot smoke region. Using a LES turbulence model in STAR-CCM+ gives significantly greater pressure losses than both 1-D theory and RANS. The results match the FDS simulation. Since FDS uses large eddy simulation, it can be inferred that LES simulations predict much higher pressure losses than both RANS simulations and 1-D theory.

The differences between the two turbulence models are investigated further. The paper by Ang et al. [19] assumes flow stratification downstream as a possible reason for the increased pressure drop. The RANS simulation with Star-CCM+ does not show flow stratification downstream while the LES simulation shows peak flow velocity at the tunnel ceiling, see Figure 36.

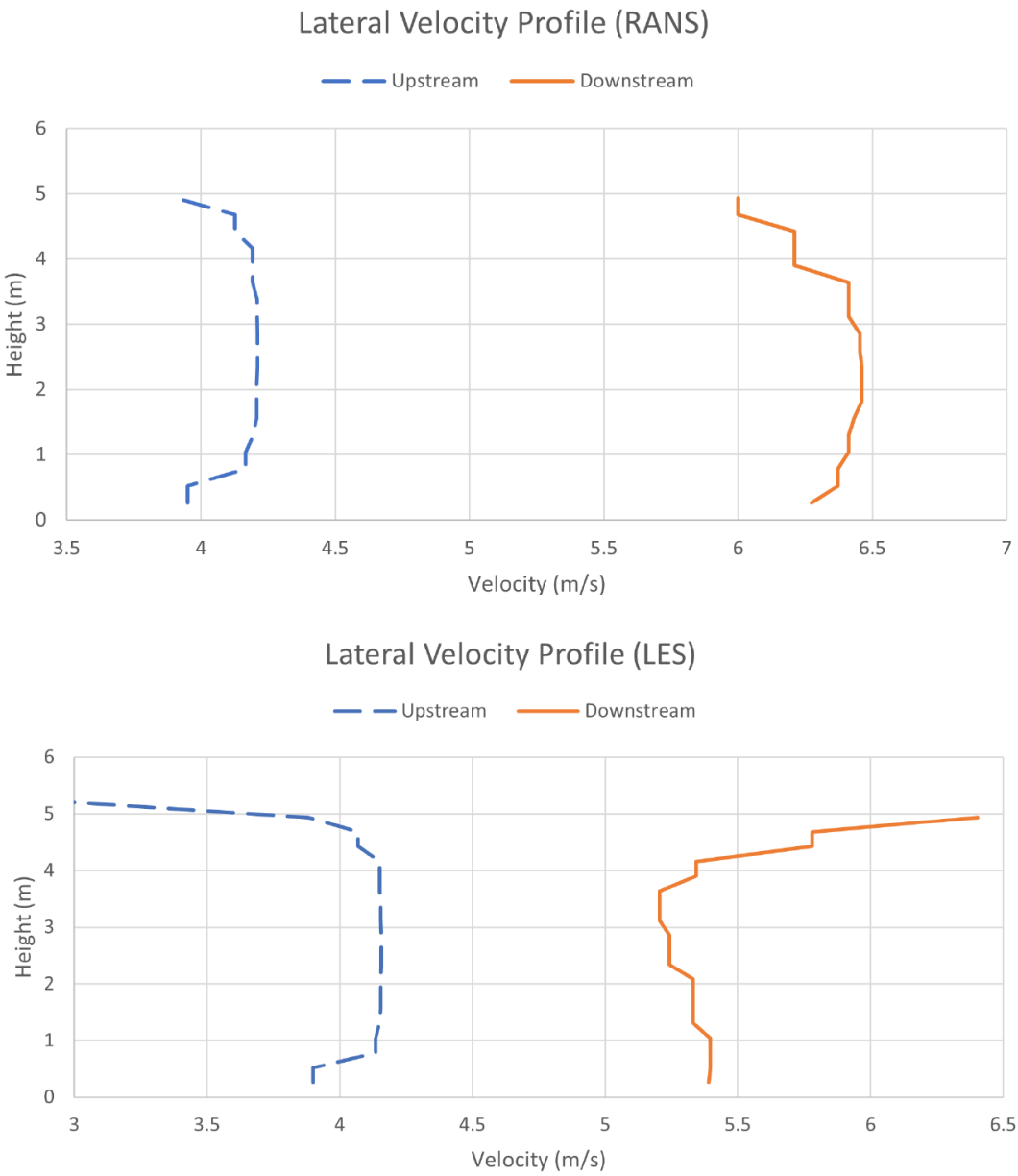

Figure 36: Lateral velocity plots upstream and downstream of the fire source, STAR-CCM+ simulation RANS vs. LES [21]

Gray recommends further validation of the CFD models as the tunnel fire application of STAR-CCM+ and FDS is only validated against measured temperature distributions and not static pressure profiles. Based on available data, it cannot be determined which of the models (if any) represents the physics correctly. The author appears to prefer the LES simulation.

Furthermore, the bifurcation flow at the fire shall be investigated to find the impact of smoke stratification and smoke bifurcation on the pressure losses downstream of the fire.

2.2.8 Ang (2024) [22]

In this PhD thesis [22], Edmund Ang (aka Chin Ding Ang) concentrates on engineering simulations for tunnel fire safety and ventilation. The numerical simulations for the

study have been performed with Fire Dynamic Simulator FDS, demonstrating advantages and problems with the application of this model. FDS versions 6.5.3 to 6.7.6 have been used. The thesis considers the following topics:

- Limitations of Carbon Monoxide modelling in FDS.
- Performance of the pressure solver in FDS, especially with the observation of unexpected oscillations.
- Understanding of the fire throttling effect using a 1-D model (TE1D) in comparison to FDS simulations.

As CO modelling is not part of our study, we concentrate on the other two topics of Ang's thesis.

Chapter 2 of the thesis [22] describes the application of FDS for tunnel fires. It describes the approximations necessary to represent a curved tunnel profile, e.g. a circular profile by an orthogonal numerical grid. The more pressing issues are in the pressure solver settings. This issue is due to the low Mach number formulation of FDS which assumes instantaneous pressure propagation in a tunnel model. This topic is further analysed in chapter 4 of the thesis.

Due to the extended length of a tunnel, and the incompressible flow configuration (pressure changes propagate instantaneously where in reality they travel below the speed of sound), the pressure solver settings when modelling a fire in a tunnel needs special attention. Otherwise, this results in pressure oscillation, or numerical instability, both of which render the results useless. It is recommended to use the TUNNEL_PRECONDITIONER in FDS with an increased setting of the number of pressure iterations to 30 or more.

Even with these settings, misleading pressure oscillations may be observed. Figure 37 shows a comparison of the mass flow for a 55 MW fire with default settings and with increased pressure solver iterations. But while the mass flow oscillations were greatly reduced, other properties, such as the maximum velocity error continued to oscillate. A key issue is the need for validation of the CFD models due to the unique nature of LES, compared to other turbulent models such as RANS.

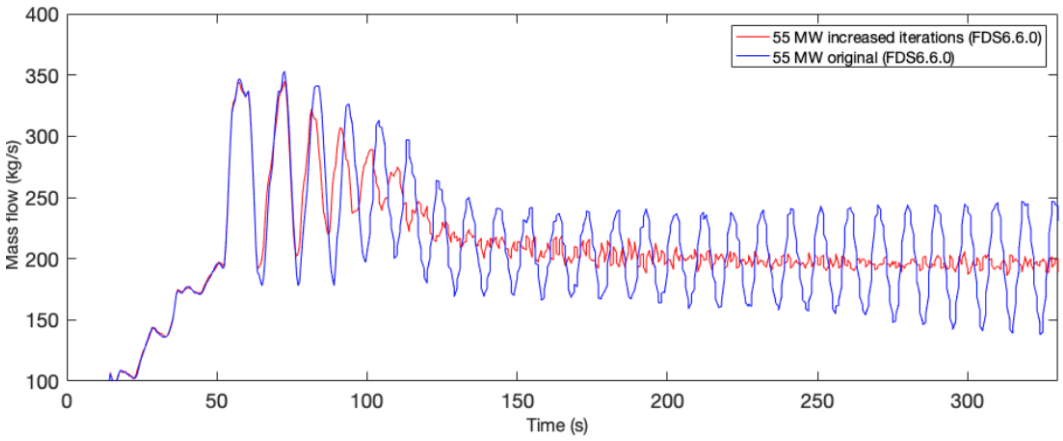

Figure 37: Comparison of mass flow between default and increased pressure solver iterations [22]

The FDS developers suggest the application of “micro-vents” (size of 1 cell) along the tunnel to reduce oscillations. But if the goal of the simulation is the evaluation of a longitudinal pressure profile, these “micro-vents” should not be relied upon as a numerical solution.

Chapter 5 of the thesis describes the 1-D model, which is taken from the previously published article [19] with the two models TE1D (Plume) and TE1D (Energy) , see chapter 2.2.5. Considering the results of the comparison between 1-D and CFD models, Ang concludes that a 1-D model, when there is a sufficiently large fire where significant stratification is expected to occur, cannot capture the 3-D effect of a fire, which is the bigger contributor to the pressure loss. CFD models should be used in scenarios with fire sizes above 5 to 15 MW.

It is critical for the tunnel fire safety community to have access to more relevant fire experiments. Fire tests can form a basis of validation for CFD models and assist engineers and researchers to better understand the limitations of these CFD models.

2.2.9 Luo & Nie (2024) [23]

This study documents an CFD simulation of three tests of the Memorial Tunnel test program [27]. For the simulations, FDS version 6.9.1 has been used. The intent of the simulations is to quantify the reduction of longitudinal flow during the tests. This is described as the “throttling effect”.

A grid dependency study is performed concentrating on the temperature. It is not clear, which temperature the graphs refer to. The length D is not defined. It may be the characteristic dimension of the fire source. But as the CFD model is be validated according to the experiment, the size should be given by the test geometry.

The study does not differentiate between the throttling effect as defined in our study and the buoyancy due to the increased temperature on the downward gradient downstream of the fire. A considerable part of the paper also discusses the variation of the critical velocity for smoke control on different tunnel gradients.

In recent years, the critical velocity has been rediscovered as a research topic. In this context, the authors should refer to these recent discussions of CFD modelling of the Memorial Tunnel and the updated formulation for the confinement velocity, e.g. in [25] and [26].

3 Methodology

3.1 Model vs. full-scale test

Road tunnels are rarely available for airflow measurements or fire tests. Due to the easier repeatability and lower costs, small-scale model tests are often used for tests simulating large fires in road tunnels.

3.1.1 Similarity

To ensure that model tests can be transferred to full scale, similarity must be maintained. This first concerns geometric similarity. Increased wall friction downstream was identified as a factor in the fire's flow resistance. Geometric similarity therefore includes the roughness of the tunnel surfaces.

In flow tests, similarity is assessed using dimensionless parameters. The Reynolds number (ratio of inertia forces to viscosity forces) is considered as the key indicator for most flow tests. For instance, the Reynolds number can be used to estimate whether the flow is laminar or turbulent.

In the case of buoyant flows, the Froude number (ratio of inertial forces and gravitational forces) is relevant as a measure of the temperature stratification in the longitudinal flow.

In model tests, some studies used the injection of a light gas instead of a fire source. The inflow of salt water into a water tank can also be used to simulate the spread of smoke in a tunnel. When investigating the pressure loss of a fire, these methods have the disadvantage that the cooling of the smoke gases downstream cannot be reproduced. In addition, the amount of substance added has a significant influence on the mass and thus on the momentum balance and the pressure difference across the injection point. In addition, on a small scale and in tests with water, the Reynolds numbers that prevail in a tunnel can hardly be achieved.

3.1.2 Problem

It is practically impossible to simulate the flow resistance of a tunnel fire in a model test. This was confirmed during the development of the NFPA 502 standard [7]. The formula for calculating the critical velocity for avoiding back-layering of smoke was adjusted in the 2017 and 2020 editions based on model tests. The corresponding chapter in the 2020 edition of NFPA 502 had to be withdrawn one year after publication [8], [13].

The conclusion in [13] is:

- *The conclusion is that the important physical effects and flow characteristics for determining critical velocity in real tunnels are different to those in scale model tunnels, especially those used to support the 2020 NFPA 502 Annex D equation, and they do not scale to full size. The 2020 Annex D equation does not predict critical velocity in real tunnels.*

The flow processes at the critical velocity are practically identical to the flow processes that are decisive for this study on the flow resistance of a fire in longitudinal flow. It is obvious that model tests cannot be transferred to the full scale here either.

It would be desirable to carry out the tests on a full scale with a nominal fire output of 30 MW. This is not possible due to restrictions on the part of the operator. The maximum permissible fire output is 10 MW. In the study [15], the fire output varied between 2 MW and 34 MW. This had no fundamental influence on the flow processes. The results for the pressure drop due to the fire could be easily scaled with the fire output. In the evaluation of all the described parameters (fire output, flow, tunnel cross-section, height of the tunnel profile), the fire output shows the smallest sampling error (cf. [15], Chapter 5.4.2, Table 10). For this reason, we believe it is justified to carry out the tests with a fire output of 10 MW. Since the CFD simulation is carried out with the same fire output, the transferability of the results is guaranteed.

3.2 Summary of Tasks

The following subtasks had to be solved to measure the flow resistance of a tunnel fire:

- Fire heat release rate 5 to 10 MW
- Protection of the installations and measuring devices from the heat of the fire
- Setting a constant and repeatable adjustable longitudinal flow
- The fire tests aim to achieve as stationary conditions as possible.
- Flow towards the fire with a developed turbulent flow profile
- Measurement of air temperature and pressure to determine the air density
- Measurement of pressure differences from -20 to +20 Pa over distances of 100 to 300 m
- Measurement of a temperature and flow profile in the flow downstream from the fire.

3.3 Test tunnel

The test facility for this project Iss in Spain at "San Pedro de Anes" and is operated by the company Tunnel Safety Testing S.A. (Applus TST). Applus TST was involved as a sub-contractor in this research project, responsible for the test tunnel including the fire source, the measurements of flow velocity and temperature in a cross-section downstream of the fire (25 points) as well as seven differential pressure monitors between the tunnel and the service gallery at eight locations along the tunnel.

The tunnel consists of an open-cut tunnel with a concrete vault. The dimensions correspond approximately to a two-lane road tunnel. The facility has two ventilation centers, a utility duct and three emergency exits. The normal profile of the test tunnel is shown in Figure 38 and the situation in Figure 39. Key figures are:

- Length: 600 m
- Width: 9.50 m
- Height: 8.12 m
- Height under the intermediate ceiling: 5.17 m
- Cross section (without ZD): 66 m²
- Cross section (with ZD): 48 m²
- Min. curve radius: 400 m
- Longitudinal gradient: -1% south to north
- Transverse gradient: 2%
- Service tunnel: 4 m wide and 2.50 m high
- Emergency exits: 3 (distance 150 m)

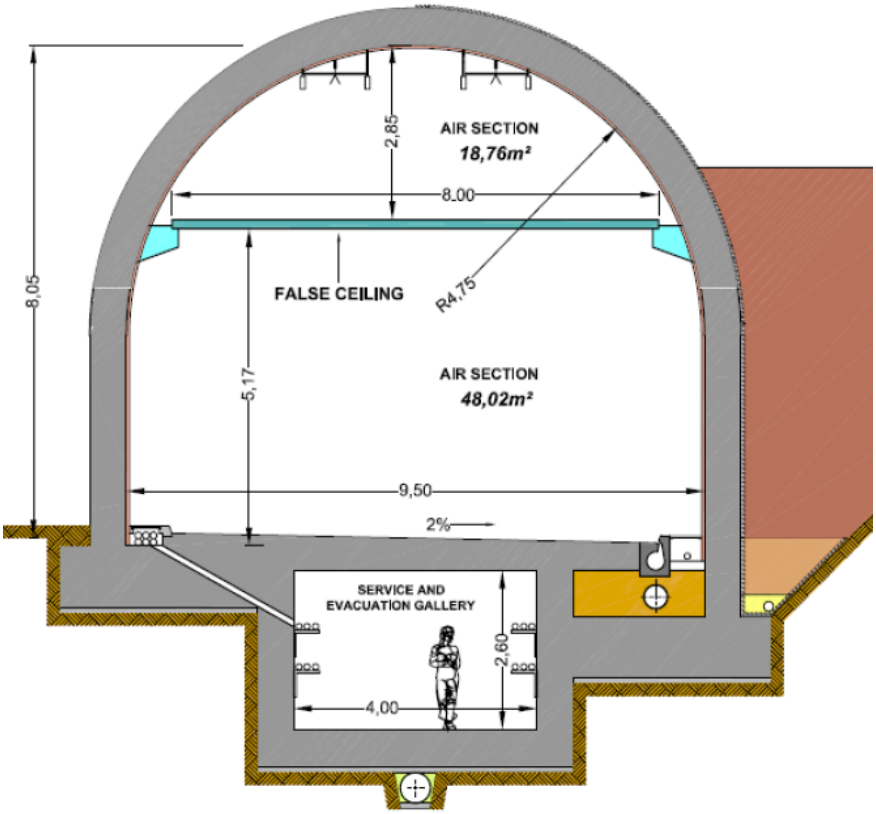

Figure 38: Normal profile of the test tunnel San Pedro des Anes

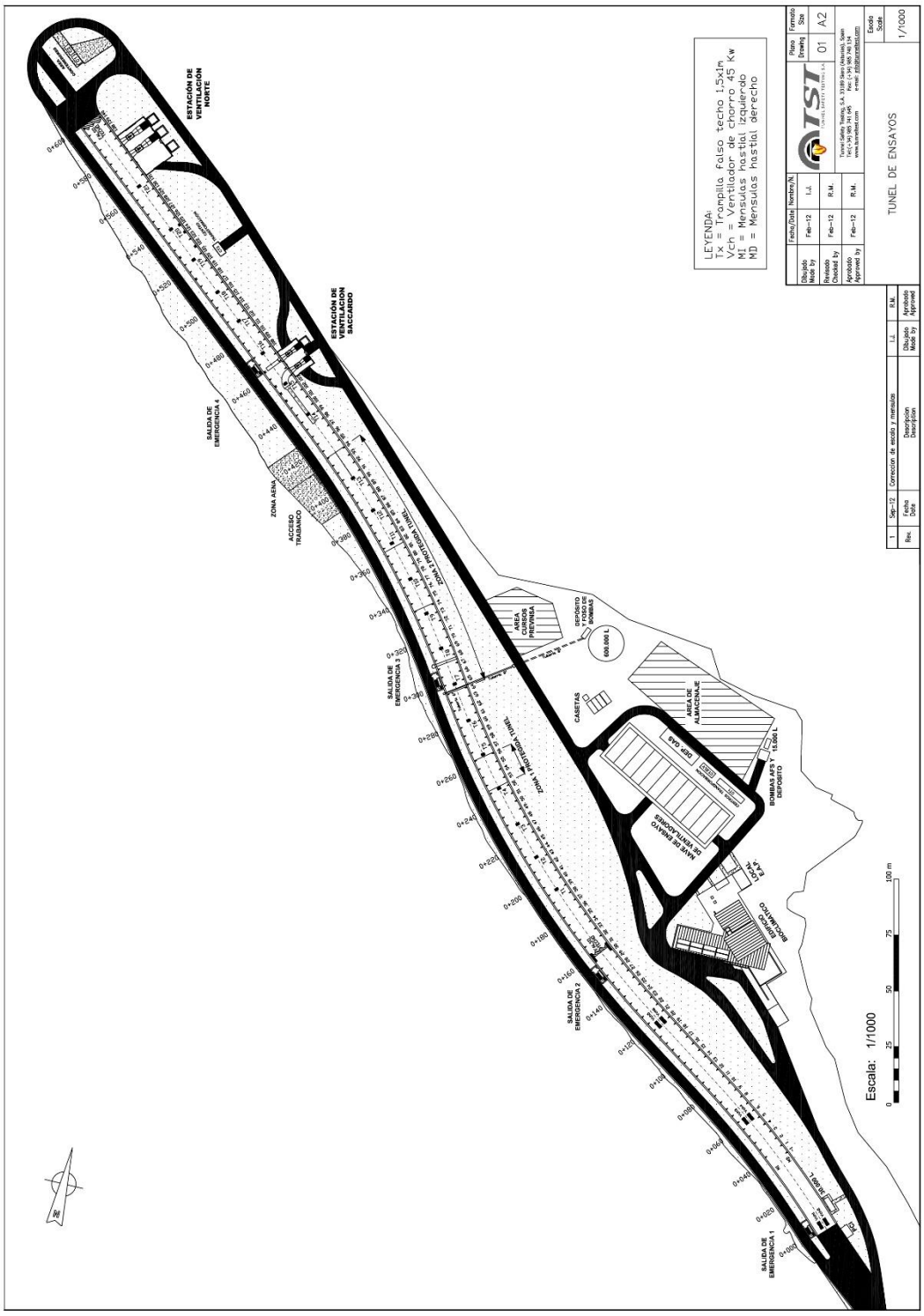

Figure 39: Situation of the test tunnel San Pedro des Anes

Figure 40: South portal San Pedro des Anes with jet fans

Figure 41: North portal San Pedro des Anes with false ceiling

3.4 Fire source

The fire was formed by fire pans that were placed close to the road surface. Based on the study [15], this appears to be a critical case for the pressure loss. Fire pans represent a minimal geometric pressure loss, see Figure 42. The heat release was determined before the test from the area of the fire pans. In the test, it was verified using gas analysis of the exhaust air. The average heat release rate was also determined by the amount of fuel and the duration of the fire.

Figure 42: Fire pan as used in Tests 1 and 2

For tests 1 and 2, a fire pan of 4 m² and dimensions 2500 x 1600 x 500 mm was filled with diesel fuel, see Figure 42. Based on the assumption of a specific fire heat release rate of 2.5 MW/m2, this should provide a nominal 10 MW fire. This assumption was supported by the Memorial Tunnel tests, which gave a nominal 10 MW for a 4.5 m² pan fire with Diesel oil and petrol in a pan that was partly filled with water [27].

For test 3 a second diesel fuel pan of 2.16 m² sized 1800 x 1200 x 500 mm was added to increase the heat release rate to a maximum of 15 MW. The following amounts of fuel were used for each test:

- Test 1: 147 l
- Test 2: 150 l
- Test 3: 230 l

The fire was located in the tunnel at pk. 255 (i.e. 255 m from the south portal). The fuel pans were laid on the ground as flat and low as possible, avoiding any inclination angles. Water was used to level the fuel and to achieve constant heat release.

Figure 43: Test 2

3.5 Ventilation

The test tunnel is equipped with six jet fans. The jet fan technical data is listed in

Jet fan data	
Manufacturer	Zitron
Model	JZR 12-45/4
Internal diameter	1200 mm
Nominal thrust	1487 N
Flow rate	38.2 m^3/s
Nominal flow velocity	33.8 m/s
Nominal power	45 kW
Rotation speed	1500 r.p.m.
Weight	1100 kg
Locations	2 jet fans @ pk.005
	2 jet fans @ pk.060
	2 jet fans @ pk.120

Table 2: Jet fan characteristics

The target value of the longitudinal ventilation is an airflow of 3 m/s towards the fire, corresponding to the design value of a longitudinal flow according to the ASTRA 13001 guideline [1]. The jet fans are supplied via soft starter on/off. Adjustable speed control is not possible. The flow velocity during the tests had to be adjusted by using a fixed number of jet fans.

As a closed-loop control of the jet fans is not possible, the jet fans were be pre-set to achieve the intended airflow. The airflow was expected to change during the test due to the resistance of the fire and due to buoyancy pressure against air-flow direction. To estimate the air-flow velocity, 1-D simulations have been performed, as shown in Figure 44. The figure shows the (cold) airflow in the open tunnel section (red) and under the false ceiling (green). The flow resistance of the fire was estimated according to the report [15]. One jet fan was expected to be sufficient to accelerate the airflow approaching the fire to 3.1 m/s. When the fire starts, the flow velocity is reduced. The simulation in Figure 44 includes the expected reduction of the flow velocity due to the throttling effect according to the report [15].

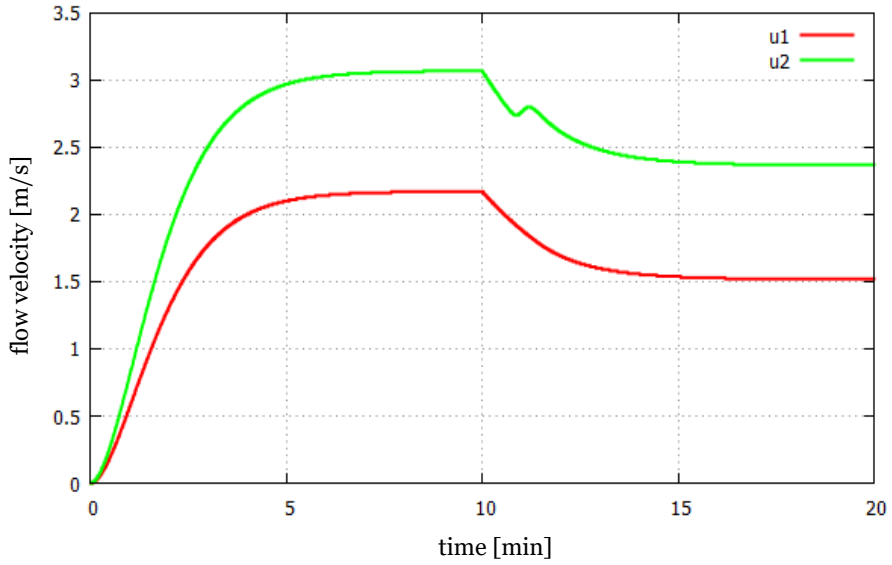

Figure 44: Expected airflow velocity upstream of the fire, operation of 1 jet fan, fire start at t = 10 min

3.6 Instrumentation

The setup of the tests is shown in Figure 45.

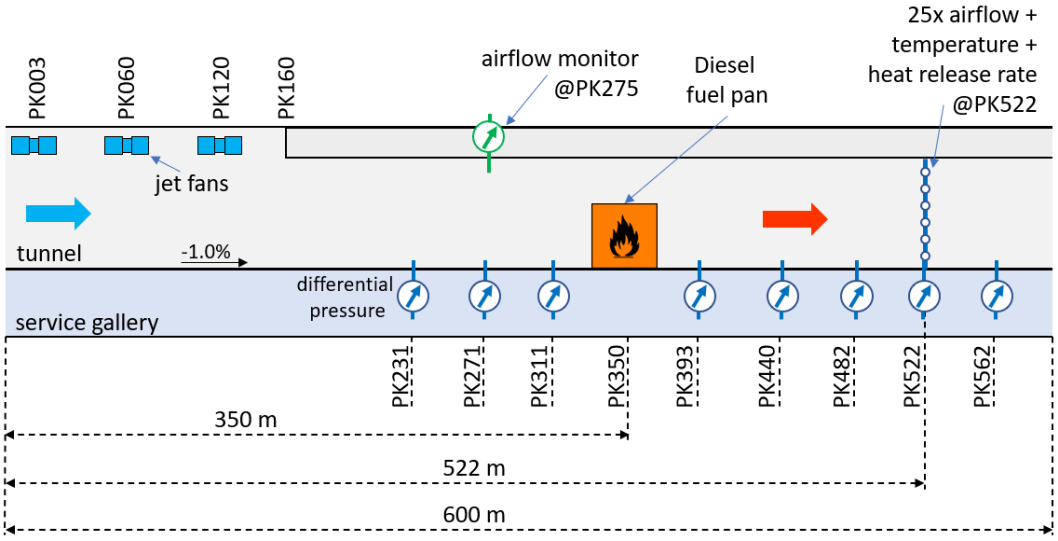

Figure 45: Test setup

In comparison to the test plan, some minor adjustments had to be made to match the setup to the test tunnel facilities. The exact location of the monitors is described in this chapter.

3.6.1 Airflow velocity at pk.522

The airflow measurement downstream of the fire was supposed to consist of 25 independent velocity monitors to assess the average flow velocity in the tunnel as well as the flow profile in the cross-section. However, upon arrival, the installation was reduced to 25 Prandtl tubes connected to 6 differential pressure monitors. This set-up only allows to record a vertical flow profile with five pitot tubes recording the average pressure across the tunnel, see Figure 48.

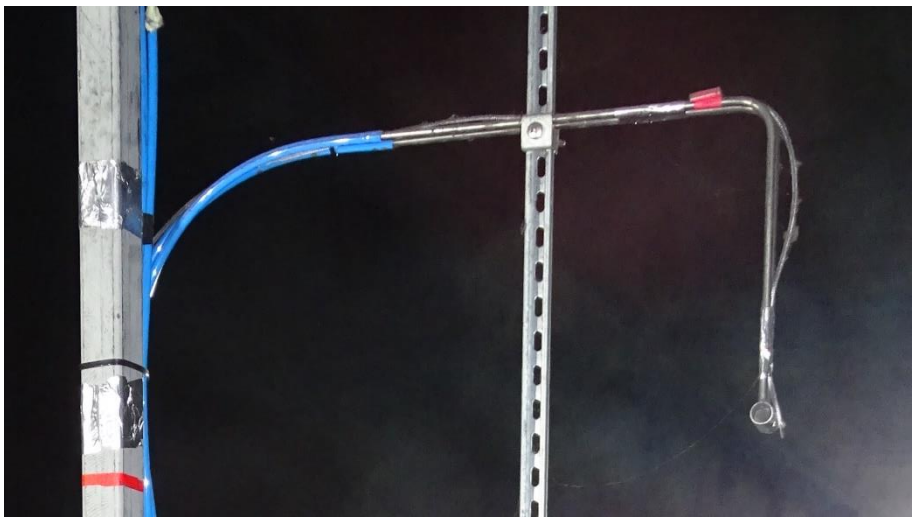

Figure 46: Prandtl pitot tube

Figure 47: Air velocity and temperature grid installation

Symbol	Description
	Prandtl pitot tube velocity 1
	Prandtl pitot tube velocity 2
	Prandtl pitot tube velocity 3
	Prandtl pitot tube velocity 4
	Prandtl pitot tube velocity 5
	Prandtl pitot tube velocity 6
	Differential pressure transmitter
	Gas thermocouple

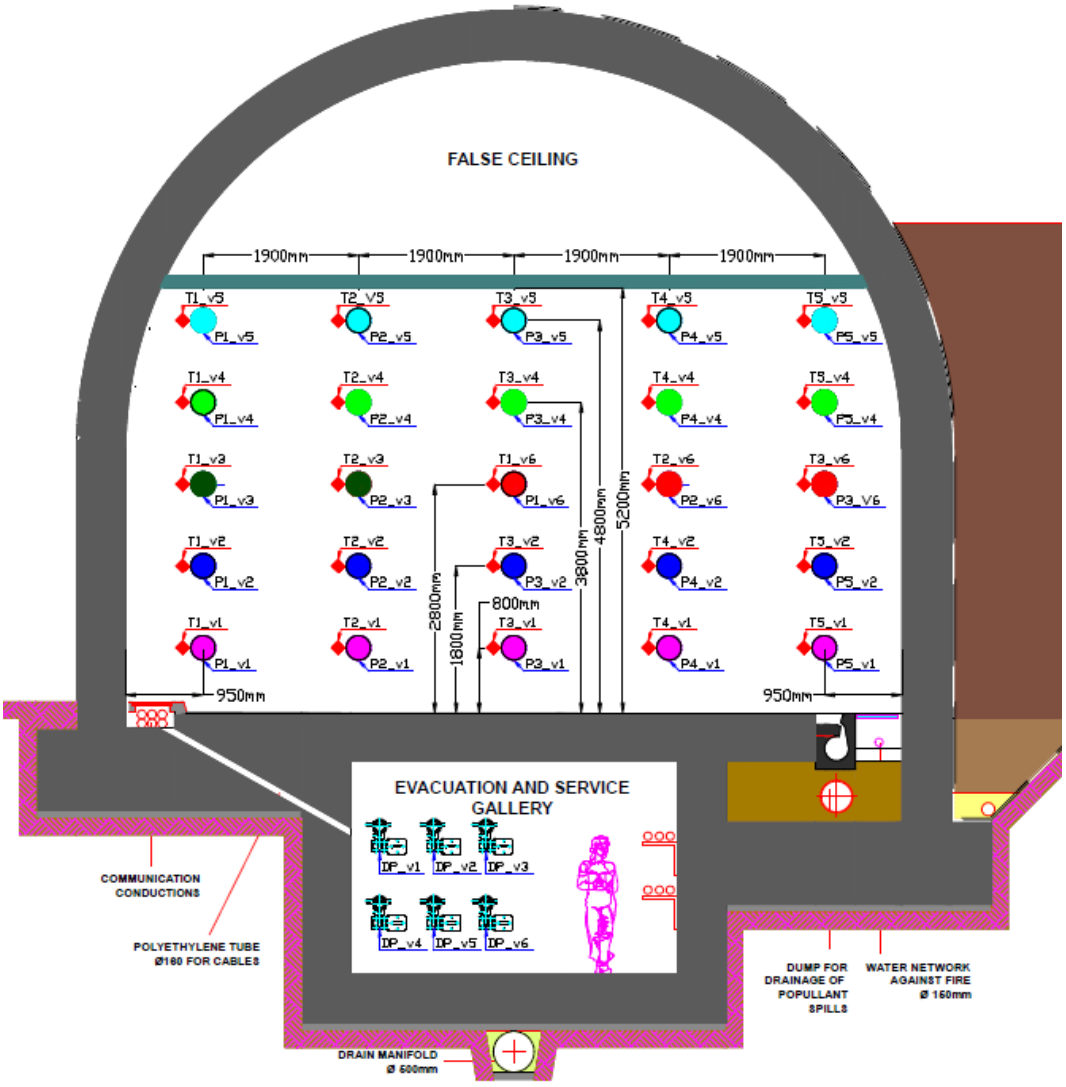

Figure 48: Velocity section at pk.522

The pressure transmitters were ABB 2600T Series 265DS. According to the specifications, the measuring error is given as ±0.04% of the set measurement span. The pressure transmitters have been calibrated against an acceptable error of ±0.8 Pa. At a flow velocity of 3 m/s, this gives an uncertainty of each flow measurement of ±0.22 m/s. Airflow data was recorded at a sampling frequency of 1 Hz.

Figure 49: Differential pressure monitors for airflow measurement at pk.522 (located in the service gallery)

One additional airflow monitor was installed at PK275. This airflow monitor is a fixed installation in the test tunnel. It was used for reference during the tests, but no additional information was made available (type of sensor, calibration etc.).

3.6.2 Temperature

For temperature measurement, 25 gas thermocouples were installed at pk.522 in the same grid setting as the air velocity measurement equipment in the same points as the velocity probes, as shown in Figure 48.

Three additional thermocouples were used as temperature reference along the tunnel. However, these instruments were not previously calibrated and were used as reference of the temperature in the tunnel concrete structure. The details of these thermocouples are shown in Table 3.

Additional temperature monitors

Location	Description	Type of instrument	Position
Pk.275	Gas thermocouple	Thermocouple Type K	Ceiling
Pk.390	Gas thermocouple	Thermocouple Type K	Ceiling
Pk.415	Gas thermocouple	Thermocouple Type K	Ceiling

Table 3: Additional temperature measurements

The accuracy of the thermocouples is given as ±3K @ 1200°C. Temperature measurements were recorded at a sampling frequency of 1 Hz.

3.6.3 Differential pressure

The static pressure profile along the tunnel was measured as a differential pressure between the tunnel and the service gallery underneath.

Figure 50: Differential pressure monitor (located in the service gallery)

Differential pressure monitors

Location	Description	Type of instrument	Position
PK231	Pressure transmitter	ABB 2600T Series 265DS	231 m
PK311	Pressure transmitter	ABB 2600T Series 265DS	311 m
PK353	Pressure transmitter	ABB 2600T Series 265DS	353 m
PK393	Pressure transmitter	ABB 2600T Series 265DS	393 m
PK440	Pressure transmitter	ABB 2600T Series 265DS	440 m
PK482	Pressure transmitter	ABB 2600T Series 265DS	482 m
PK522	Pressure transmitter	ABB 2600T Series 265DS	522 m
PK562	Pressure transmitter	ABB 2600T Series 265DS	562 m

Table 4: Differential pressure measurements in the service gallery

The pressure transmitters were ABB 2600T Series 265DS. According to the specifications, the measuring error is given as ±0.04% of the set measurement span. The pressure transmitters have been calibrated against an acceptable error of ±0.8 Pa.

In the tunnel, the pressure measurement was located at the tunnel wall, ca. 2.5 m above ground. The opening of the pressure tube was arranged perpendicular to the longitudinal flow to avoid any influence of the flow velocity.

For the pressure measurements downstream of the fire, the temperature difference between the tunnel and the service gallery could have a significant impact on the pressure measurements. At a height difference of 6.5 m between the measurement points, a

temperature variation of ±1 K (inside vs. outside the measurement tube) could cause a pressure difference of ±0.27 Pa. In CFD simulations, it was verified that the measured differential pressure was representative for the average pressure in the tunnel cross-section.

Static pressure data was recorded at a sampling frequency of 1 Hz.

3.6.4 High frequency differential pressure

An additional differential pressure measurement was located at PK231. The installation of the sensor with the pressure tubes was like the installation of the differential pressure measurement described in chapter 3.6.3.

Figure 51: Differential pressure monitor Sensirion SDP810-500Pa

The pressure transmitter was a Sensirion SDP810-500Pa. According to the specifications, the measuring error is total of 0.1 Pa zero offset and 3% measurement error. For a measured pressure of 5 Pa, this represents an absolute error ±0.25 Pa.

As this measurement was located upstream from the fire, it was not influenced by temperature variations during the tests. This pressure sensor was used to collect short time measurements at sampling frequencies of 100 and 2000 Hz.

3.6.5 Heat release rate measurement

The heat release rate was not measured directly. It was evaluated by measuring the total mass flow rate and various gas concentrations (CO, CO_2, O_2 and H_2O). The heat releases rate is then derived from these mass flow rates.

Calorimetry equations were employed to compute the heat release rates. The two methods, CDG (Carbon Dioxide Generation) and OC (Oxygen Consumption) were used to ensure a relevant evaluation by comparing both approaches using the data acquisition program to provide the HRR variation with time.

The equipment used to measure the relevant variables is described in Table 5.

Heat Release Rate Measurement

Measured Variable	Measurement Principle	Calibrated range	Accuracy
Flue Gases composition - HRR			
CO	NDIR (non-dispersive infrared)	0-10000 ppm	±1.2% full scale value
CO_2	NDIR (non-dispersive infrared)	0-20%	±1.2% full scale value
O_2	Paramegnetic	0-21%	±1% full scale value or 0.02 vol% O_2
Air velocity – Ventilation			
Bidirectional probe	Differential Pressure		
Differential pressure transducer	Capacitive Sensor	1-4 m/s	±15% measured value
Flue Gases – Temperature, HRR and Test Conditions			
Temperature	Thermocouple K	20-1200°C	±3°C @1200°C
Absolute pressure	Capacitive Sensor	900-1200 hPa	±0.7% full scale value
Humidity	Capacitive Sensor	0-100%	±2% relative humidity

Table 5: Heat release rate measurement

Figure 52: Installation of the heat release rate measurement in the service tunnel at PK522

4 Results

For interpretation of the measurements, the raw data was recalibrated to correct zero offset of the pressure and to align the time according to the begin of the test:

- The initial time is set to t = 0 min for the start of the jet fan(s)
- For each test, the initial differential pressure (without ventilation) is corrected to a 0 Pa time average.
- It is noted that the airflow measurements at PK522 cannot measure airflow against the ventilation direction.
- The recorded data from the airflow measurement at PK275 apparently gives the flow velocity without information on flow direction (always positive).

4.1 Results of Test 1

The first fire test was conducted on 12th June 2024. One jet fan situated at the tunnel portal was switched on at 09:14:37 (t = 0). The time stamps of the test are given in Table 6.

Time Stamps Test 1

Event	Time (hh:mm:ss)	t (mm:ss)
Start measurement	09:07:31	-07:06
Start ventilation 1 jet fan	09:14:37	0:00
Start fire	09:27:29	12:52
Fire extinguished	09:55:15	40:38
Stop measurement	10:01:24	46:47

Table 6: Time stamps of Test 1

Figure 53 shows the heat release rate as measured in Test 1. The heat release rate increased quickly to values between 3 and 4.5 MW. This corresponds to a specific heat release rate of 0.95 MW/m² fuel pan. At t = 38 min, the fuel was depleted, and the heat release rate was reduced. Although the fire was out at t = 40:38, the heat release rate measurement still showed ~0.5 MW, which indicates the accuracy of the measurement. The total heat release of the fire can be calculated using the calorific value of diesel fuel 9.95 kWh/l. The calorific value of 147 l diesel fuel is 1463 kWh, while the measured heat release between t = 0 and t = 40 min was 1560 kWh (+6.6%).

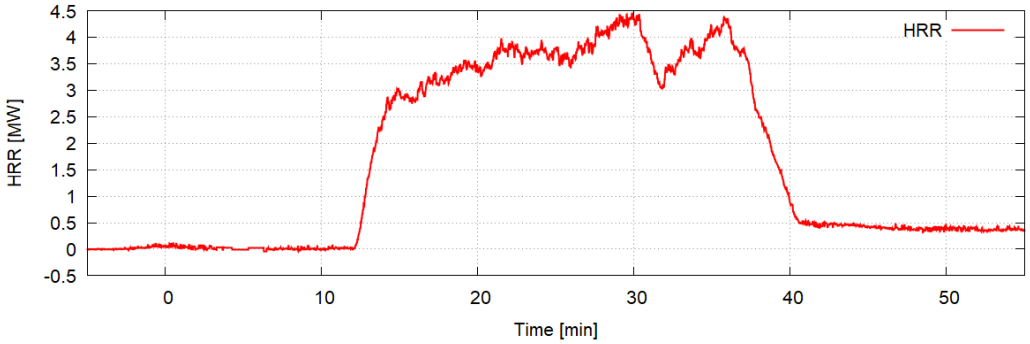

Figure 53: Heat release rate Test 1

Figure 54 shows the measured flow velocity, i.e. the average of the 25 measurements at PK522 and the measurement at PK275. Prior to the start of the jet fan, the airflow was directed towards the southern portal, against the airflow during the test. Both airflow monitors showed a positive flow velocity, but the measurement at PK275 did not give a flow direction and the measurement at PK522 was set up only to measure airflow in positive direction south to north.

When the jet fan was switched on, both measurements showed an increase of the flow velocity up to 2.8 m/s. The measurement at PK275 showed significant flow fluctuations, while the measurement at PK522 was smoother. This was not caused by a time average signal processing, but by taking the average of 25 anemometers. The individual anemometers showed fluctuations like the measurement at PK275. These fluctuations can be attributed to flow turbulence.

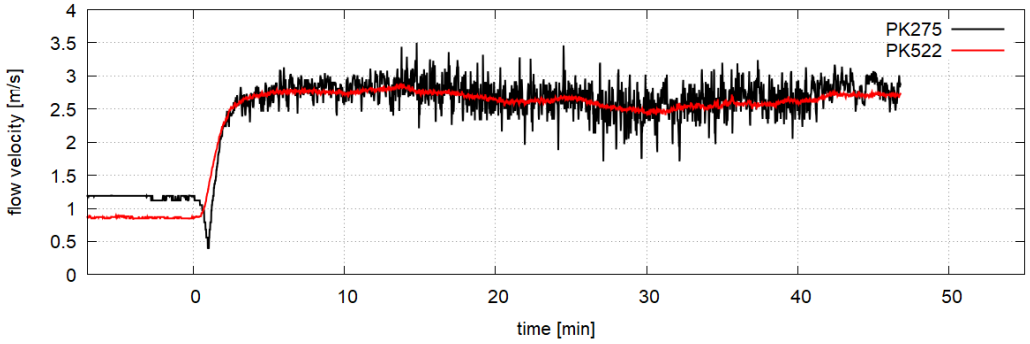

Figure 54: Airflow measurement during Test 1

At t = 12:52, the fire was started. Figure 54 shows a minor decrease of the flow velocity and an increase of the fluctuations. The decrease of the flow velocity was caused by the flow resistance of the fire as well as the buoyancy of the hot smoke downstream. When the fire was burnt out, the flow velocity increased close to the original value. The increased fluctuations can be attributed to additional turbulence generation by the fire.

Figure 55 shows the differential pressure measurements during the test. Before the jet fan was switched on, there were very little disturbances to the differential pressure. In the morning, there were little disturbances from meteorological conditions outside the tunnel.

Switching on the jet fan caused an increase of the static pressure in the tunnel, while the tunnel air was accelerated. When the flow balance was reached (jet fan pressure equals the friction in the tunnel), the pressure measurements settled according to the pressure profile along the tunnel.

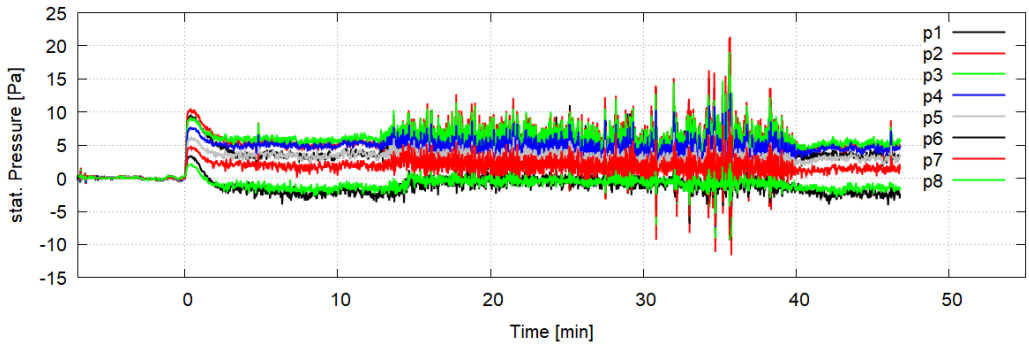

Figure 55: Differential pressure measurements during Test 1

When the fire was started, pressure fluctuations increased significantly. It is also visible that the pressure measurements settled to a different equilibrium. Pressure fluctuations increased towards the end of the fire test, e.g. at t = 35 min. In this phase, the water in the fire pan was boiling. This led to irregular eruptions from the fire pan, which are visible in the video recording of the fire test. At about t = 40 min, the fire pan was burnt out. The pressure fluctuations were diminished and the pressure measurements settled to values close to the measurements at t = 3 to 12 min.

Figure 56 shows the pressure difference between the tunnel and the service tunnel for various averaging periods. The averaging times have been varied to assess the impact of different periods. The first four periods refer to the ventilation operation prior to ignition. The last two periods refer to a mostly stable period of the fire. Two measurements (6 @ PK482 and 8 @PK562) show a pressure higher in the service tunnel than in the test tunnel. Furthermore, the difference between the data with and without fire were very different from the other measurements. The installation of these measurements has been checked prior to the tests and again after the test data was evaluated. No explanation has been given for these results. For the comparison of the tests with CFD analysis later in this report, these measurements have been disregarded. Also, the measurement 1 at PK231 does not fit in a linear pressure profile that was expected without the fire. For this location, we have the additional high-frequency measurement, which has been used for comparison with the CFD analysis.

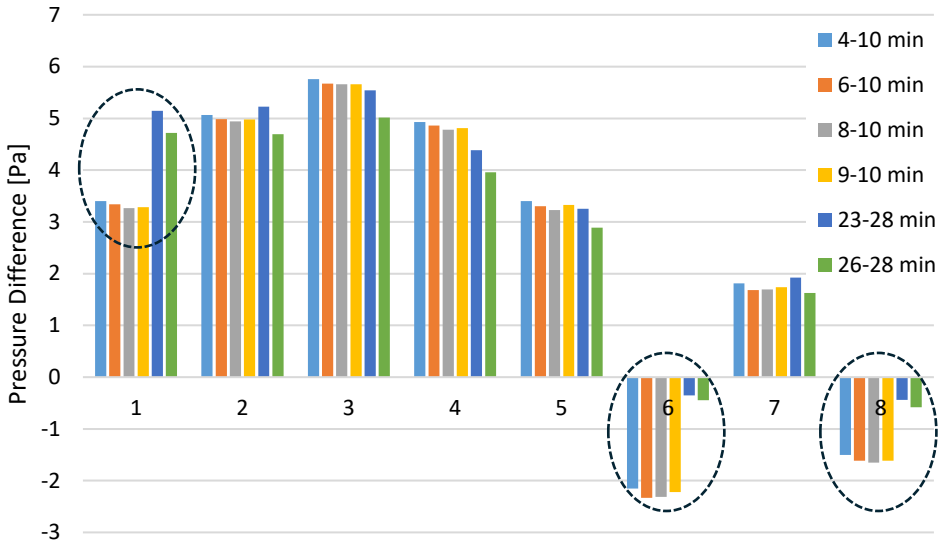

Figure 56: Pressure Difference between Tunnel and Service Tunnel, Test 1

The measurements also show very little difference between the pressure difference with and without fire. Only the measurement upstream of the fire shows a significant increase with the fire. Although the heat release rate in Test 1 was relatively small, this indicates that the throttling effect of the fire has been relatively small and difficult to measure.

Figure 57 shows the pressure difference between tunnel and service tunnel at the location PK231. These measurements have been taken with a sampling frequency of 100 Hz and 2000 Hz. As in Figure 55, the measurements show little disturbances before the ventilation was started, slightly more with the jet fan operating. With the fire, the fluctuations increased significantly.

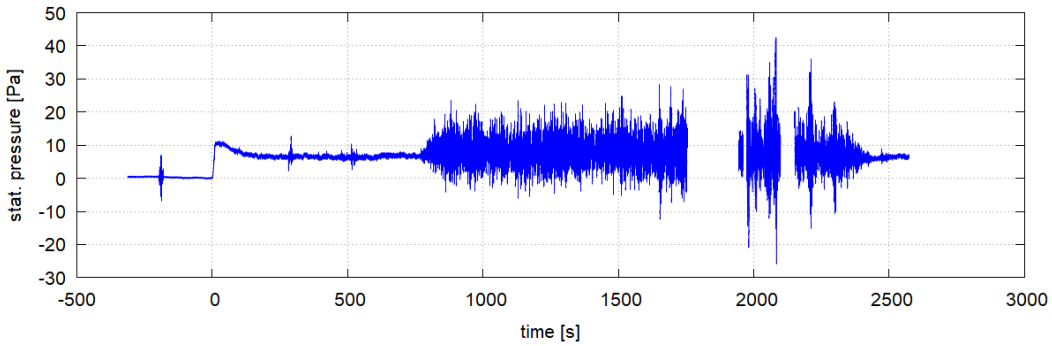

Figure 57: High frequency measurement at PK231, Test 1

Figure 58 shows a small section of the measurement in Figure 57. The fluctuations appear to contain bursts of different frequencies. An initial analysis shows bursts dominated by a frequency of ~1.30 Hz and of ~0.30 Hz. These frequencies can be compared to the natural frequency of the tunnel

$$f_{tunnel} = \frac{speed\ of\ sound}{2 \cdot tunnel\ length} = 0.29\ Hz \tag{37}$$

and the characteristic frequency of the fire with D_B = 2 m as the characteristic length of the square fuel pan [10].

$$f_{fire} = \frac{1.9}{\sqrt{D_B}} = 1.34\ Hz \tag{38}$$

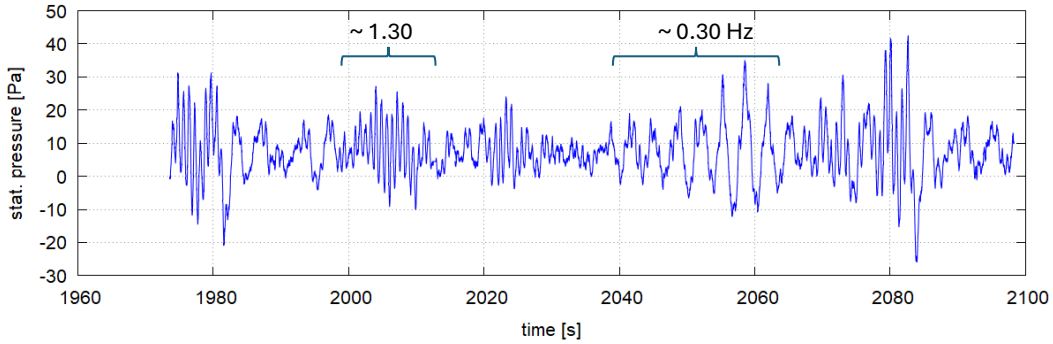

Figure 58: High frequency measurement at PK231, Test 1 (detail)

The dynamic pressure data is better represented by a frequency analysis for a longer period with developed fire. For Test 1, this is shown in Figure 59. The oscillations include the dominant oscillations as well as the turbulence frequency spectrum. A dominant oscillation is visible at ~0.30 Hz, which represents the natural frequency of the tunnel tube. Higher order natural frequencies (n·0.29 Hz) are not visible.

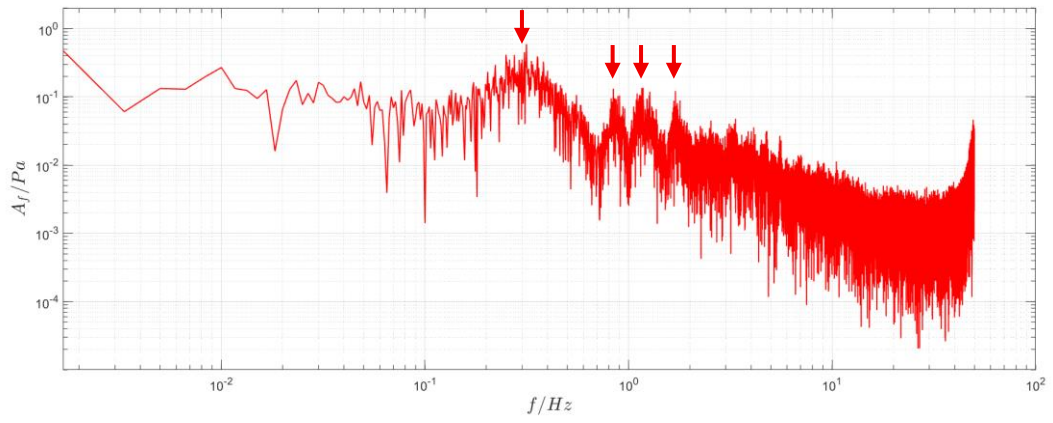

Figure 59: Frequency analysis Test 1, Sampling Rate 100 Hz

The graph also includes three local maximums at 0.85 Hz, 1.1 Hz and 1.5 Hz. Although this does not match the frequency of the flame oscillation, the maximums are most likely driven by the fire. Further research is required to evaluate possible causes, e.g. eddy separation of the plume in crossflow.

Figure 60 shows the airflow and temperature profiles at the measurement location PK522. For these profiles, the average of the five sensors at equal height has been

taken. The red lines refer to the measurement prior to the fire and the green lines refer to a period with fire. The graphs show a significant temperature stratification, but no stratified airflow. The measurements even indicate a slightly higher flow velocity in the lower half of the tunnel profile.

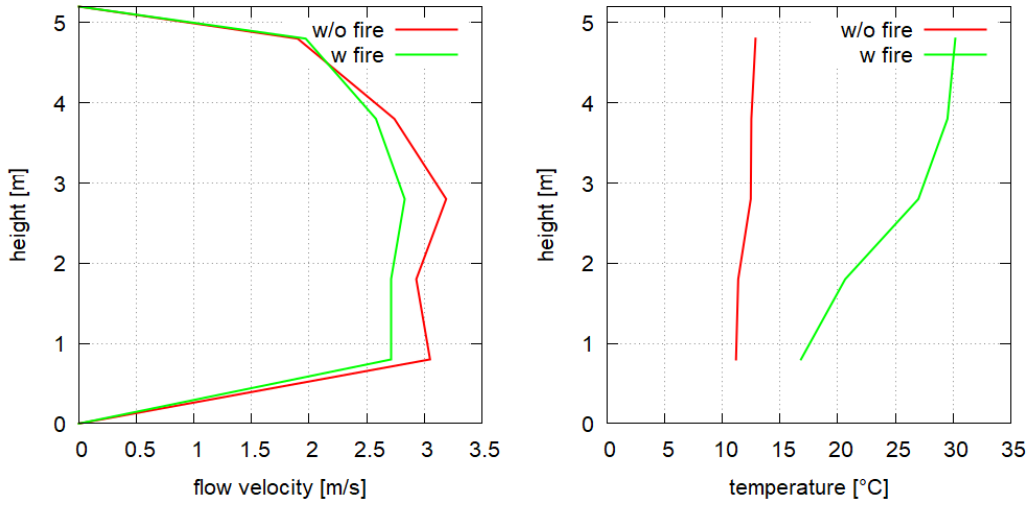

Figure 60: Airflow and Temperature Profiles at PK522, Test 1

4.2 Results of Test 2

The second fire test was conducted on the same day 12th June 2024. Two jet fans situated at the tunnel portal were switched on at 12:02:29 (t = 0). The time stamps of the test are given in Table 7.

Time Stamps Test 2

Event	Time (hh:mm:ss)	t (mm:ss)
Start measurement	11:57:07	-5:22
Start ventilation 2 jet fans	12:02:29	0:00
Start fire	12:12:28	9:59
Fire extinguished	12:48:37	46:08
Stop measurement	12:56:06	53:37

Table 7: Time stamps of Test 2

Figure 61 shows the heat release rate as measured in Test 2. The heat release rate increased quickly to values between 3 and 4.5 MW. As in the first test, this corresponds to a specific heat release rate of 0.95 MW/m² fuel pan. At t = 20 min, the heat release rate was reduced. About 10 min later, the heat release rate increased again up to 3.5 MW. Most of the fuel was burnt at t = 38 min, but small flames continued until the fire was put out at t = 46:08, the heat release rate measurement still showed ~0.3 MW, which indicates the accuracy of the measurement. The total heat release of the fire can be calculated using the calorific value of diesel fuel 9.95 kWh/l. The calorific value of

150 l diesel fuel is 1493 kWh, while the measured heat release between t = 0 and t = 47 min was 1735 kWh (+16.2%).

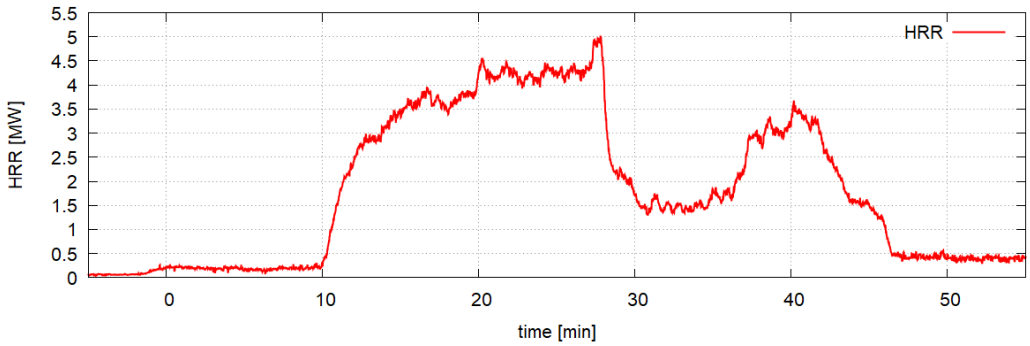

Figure 61: Heat release rate Test 2

Figure 62 shows the measured flow velocity, i.e. the average of the 25 measurements at PK522 and the measurement at PK275. Prior to the start of the jet fan, the airflow is directed towards the southern portal, against the airflow during the test. Both airflow monitors showed a positive flow velocity, but the measurement at PK275 did not give a flow direction and the measurement at PK522 was set up only to measure airflow in positive direction south to north.

When the two jet fans were switched on, both measurements showed an increase of the flow velocity up to 3.6 and 4.0 m/s. The measurement at PK275 showed significant flow fluctuations, while the measurement at PK522 was smoother. This was not caused by a time average signal processing, but by taking the average of 25 anemometers. The individual anemometers showed fluctuations like the measurement at PK275. These fluctuations can be attributed to flow turbulence.

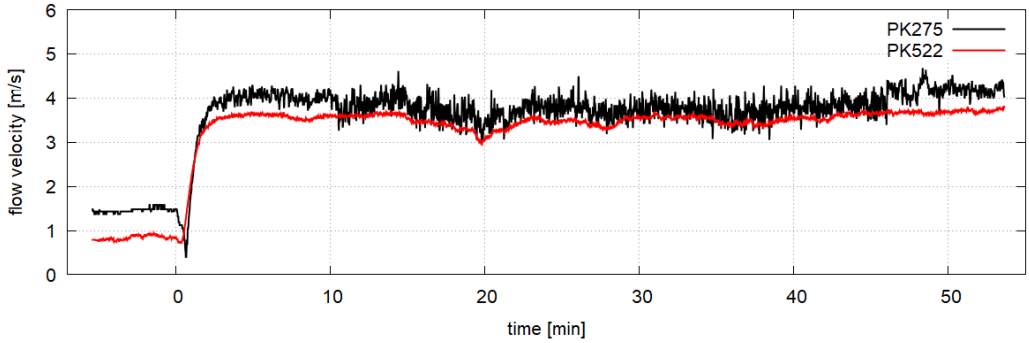

Figure 62: Airflow measurement during Test 2

At t = 9:59, the fire was started. Figure 62 shows a minor decrease of the flow velocity and an increase of the fluctuations. The decrease of the flow velocity was caused by the flow resistance of the fire as well as the buoyancy of the hot smoke downstream. When the fire was burnt out, the flow velocity increased close to the original value. The increased fluctuations can be attributed to additional turbulence generation by the fire.

Figure 63 shows the differential pressure measurements during the test. Before the jet fan was switched on, there already were small disturbances to the differential pressure. At midday, there were increased disturbances from meteorological conditions outside the tunnel, especially the ambient wind conditions were less favourable than during Test 1.

Switching on the jet fan caused an increase of the static pressure in the tunnel, while the tunnel air was accelerated. When the flow balance was reached (jet fan pressure equals the friction in the tunnel), the pressure measurements settled according to the pressure profile along the tunnel.

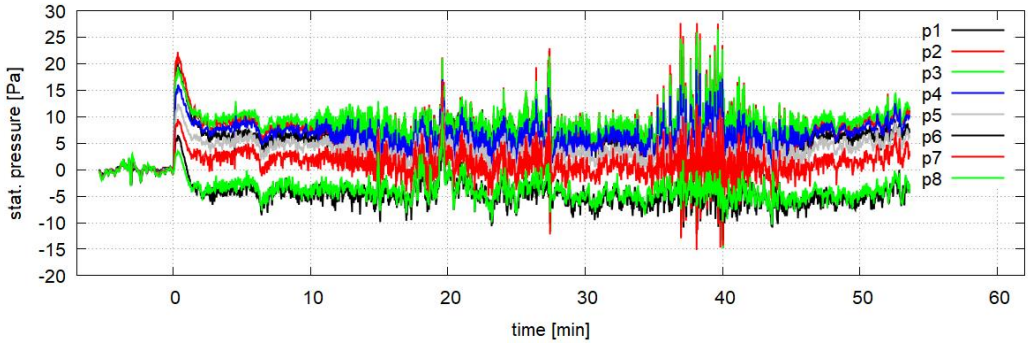

Figure 63: Differential pressure measurements during Test 2

When the fire was started, pressure fluctuations increased. Pressure fluctuations increased towards the end of the fire test, especially visible at t = 35 min. In this phase, the water in the fire pan was boiling. This led to irregular eruptions from the fire pan, which are visible in the video recording of the fire test. At about t = 46 min, the fire pan was burnt out. The pressure fluctuations were diminished and the pressure measurements settled to values close to the measurements at t = 3 to 9 min.

Figure 64 shows the pressure difference between the tunnel and the service tunnel for various averaging periods. The averaging times have been varied to assess the impact of different periods. The first two columns refer to the ventilation operation prior to ignition. The third column refers to a period when the heat release rate still increased. The fourth column refers to a period where the fire was fully developed and quasi steady state. The last two columns refer to a period where the heat release rate was decreasing with significant pressure fluctuations, with flame oscillations visible also in the video.

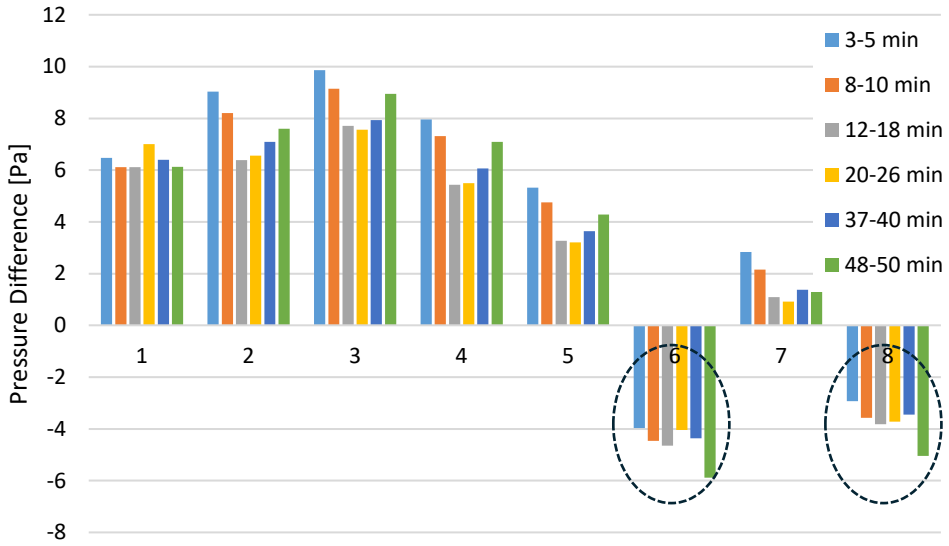

Figure 64: Pressure Difference between Tunnel and Service Tunnel, Test 2

Two measurements (6 @ PK482 and 8 @PK562) show a pressure higher in the service tunnel than in the test tunnel. Furthermore, the difference between the data with and without fire were very different from the other measurements. The installation of these measurements has been checked prior to the tests and again after the test data was evaluated. No explanation has been given for these results. For the comparison of the tests with CFD analysis later in this report, these measurements have been disregarded.

The measurements also show very little difference between the pressure difference with and without fire. Although the heat release rate in Test 2 was relatively small, this indicates that the throttling effect of the fire has been relatively small and difficult to measure.

Figure 65 shows the pressure difference between tunnel and service tunnel at the location PK231. These measurements have been taken with a sampling frequency of 100 Hz and 2000 Hz. With the fire, the pressure fluctuations increased significantly.

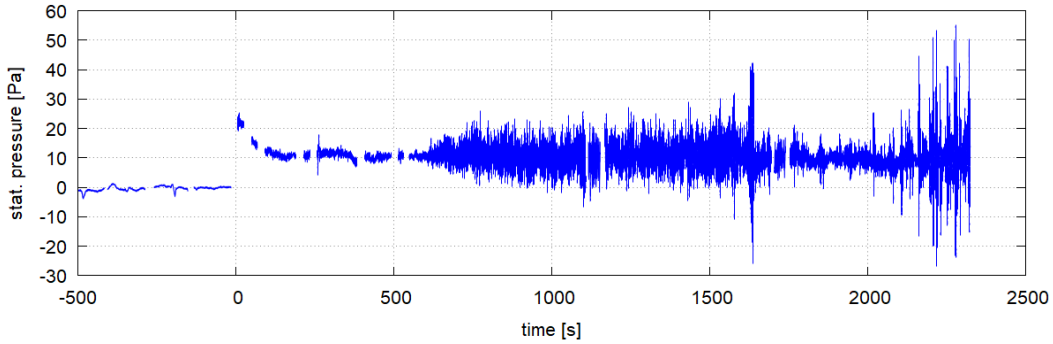

Figure 65: High frequency measurement at PK231, Test 2

Figure 66 shows a small section of the measurement in Figure 65. The oscillations are more continuous than in Figure 58. It appears that the natural frequency of the tunnel is prominent, but the data requires a more detailed frequency analysis.

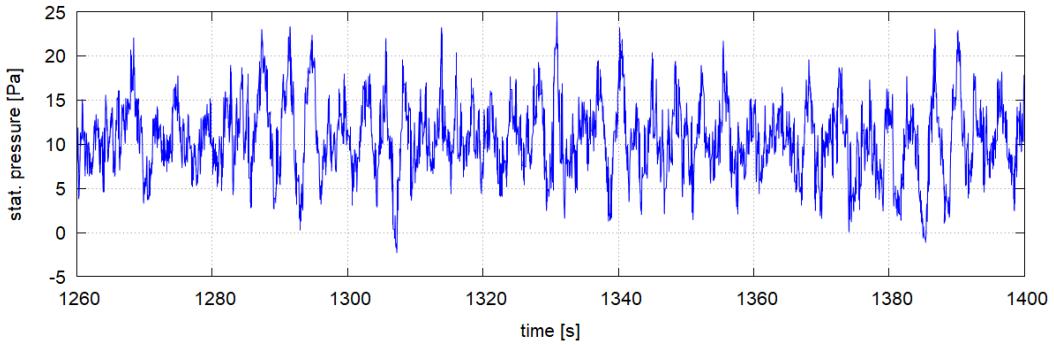

Figure 66: High frequency measurement at PK231, Test 2 (detail)

Figure 67 shows the frequency analysis for a longer period with developed fire. The oscillations include the dominant oscillations as well as the turbulence frequency spectrum. A dominant oscillation is visible at ~0.30 Hz, which represents the natural frequency of the tunnel tube. Higher order natural frequencies (n·0.29 Hz) are not visible.

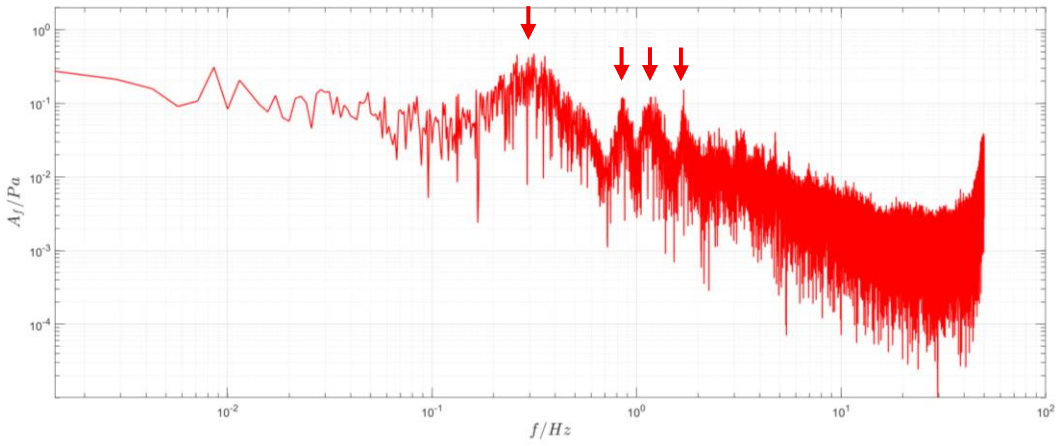

Figure 67: Frequency analysis Test 2, Sampling Rate 100 Hz

The graph also includes three local maximums at 0.85 Hz, 1.1 Hz and 1.5 Hz. This matches the maximums observed in Test 1. Although this does not match the frequency of the flame oscillation, the maximums are most likely driven by the fire. Further research is required to evaluate possible causes, e.g. eddy separation of the plume in crossflow.

Figure 68 shows the airflow and temperature profiles at the measurement location PK522. For these profiles, the average of the five sensors at equal height has been taken. The red lines refer to the measurement prior to the fire and the green lines refer to a period with fire. The graphs show a significant temperature stratification, but no stratified airflow. The measurements even indicate a slightly higher flow velocity in the lower half of the tunnel profile. In comparison to Figure 60, the flow velocity is significantly higher and – consequently -the temperature lower.

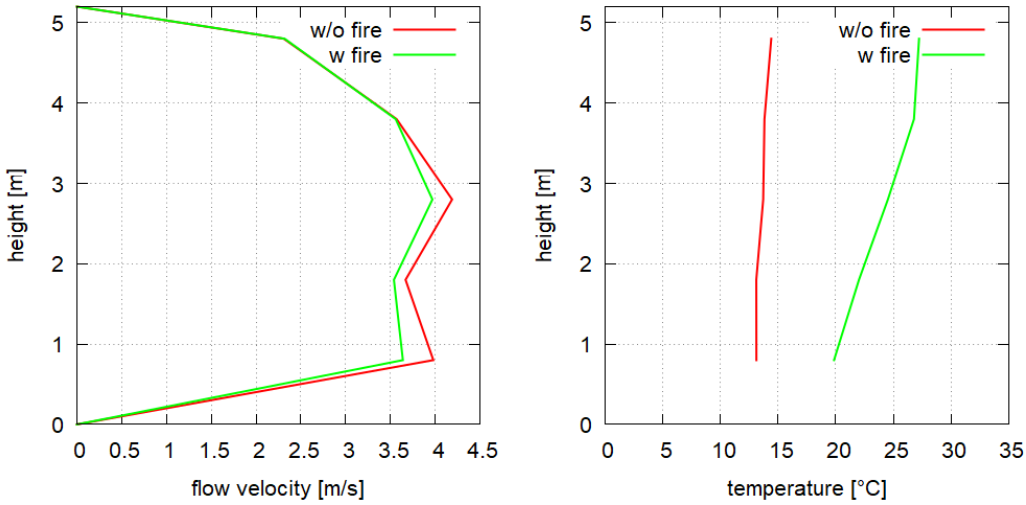

Figure 68: Airflow and Temperature Profiles at PK522, Test 2

4.3 Results of Test 3

The third fire test was conducted on the same day 12th June 2024. Two jet fans situated at the tunnel portal were switched on at 12:02:29 (t = 0). The time stamps of the test are given in Table 8.

Time Stamps Test 3

Event	Time (hh:mm:ss)	t (mm:ss)
Start measurement	16:04:37	-5:50
Start ventilation 2 jet fans	16:10:27	0:00
Start fire	16:20:57	10:30
4 m² pool burnt out	16:34:27	24:00
2.16m² pool extinguished	17:06:40	56:13
Stop measurement	17:16:42	1:06:15

Table 8: Time stamps of Test 3

Figure 69 shows the heat release rate as measured in Test 3. The heat release rate increased quickly to 8 MW and then more slowly up to 12 MW. A maximum heat release rate of 12 MW corresponds to a specific heat release rate of 1.95 MW/m² fuel pan. Between t = 22 min and 25 min, the heat release rate was reduced, as the downstream situated 4 m² fuel pan burnt out. The small fuel pan continued to burn until the fire was suppressed at t = 56:13. The total heat release of the fire can be calculated using the calorific value of diesel fuel 9.95 kWh/l. The calorific value of 230 l diesel fuel is 2289 kWh (most of the fuel was burnt), while the measured heat release between t = 0 and t = 54 min was 2600 kWh (+13.6%).

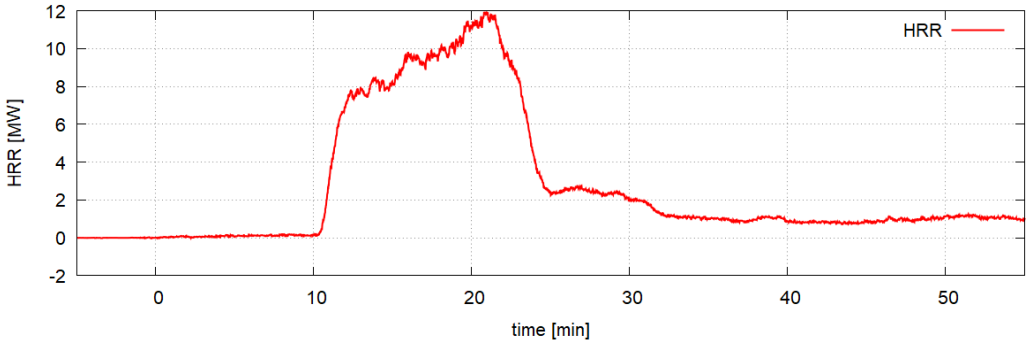

Figure 69: Heat release rate Test 3

Figure 70 shows the measured flow velocity, i.e. the average of the 25 measurements at PK522 and the measurement at PK275. Prior to the start of the jet fan, the airflow is directed towards the southern portal, against the airflow during the test. Both airflow monitors showed a positive flow velocity, but the measurement at PK275 did not give a flow direction and the measurement at PK522 was set up only to measure airflow in positive direction south to north. Even without ventilation or any vehicle movement in the tunnel, the flow velocity varied considerably. This was due to adverse wind conditions outside the tunnel. The fluctuations of ambient wind made the interpretation of the in-tunnel airflow and pressure measurements more difficult.

When the two jet fans were switched on, the measurements showed an increase of the flow velocity up to 3.4 and 3.8 m/s. The measurement at PK275 showed significant flow fluctuations, while the measurement at PK522 was smoother. This was not caused by a time average signal processing, but by taking the average of 25 anemometers.

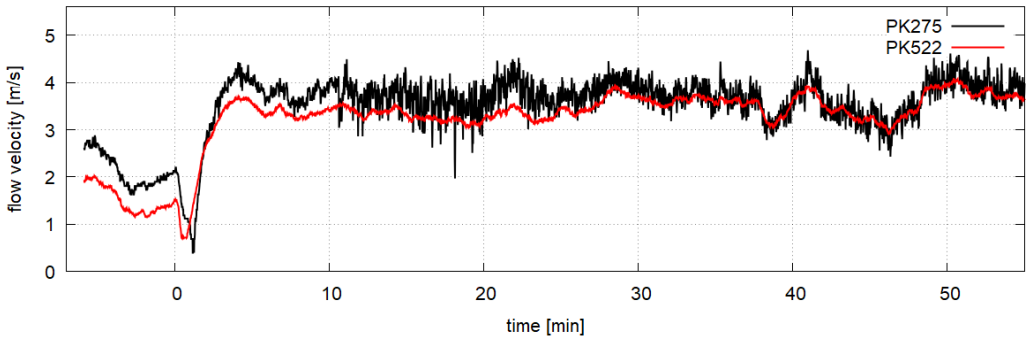

Figure 70: Airflow measurement during Test 3

At t = 10:30, the fire was started. Figure 70 indicates a minor decrease of the flow velocity and an increase of the fluctuations. The impact of the throttling effect and the thermal buoyancy were significant less than the fluctuations due to changes of the ambient conditions, especially wind.

Figure 71: Smoke plume from the north portal, left: Test 1 (quiet atmosphere), right Test 3 (gusty wind)

Figure 72 shows the corresponding differential pressure measurements during the test. Before the jet fan was switched on, there already were significant disturbances to the differential pressure. As the weather conditions changed, there were increased disturbances especially from gusty wind, which made interpretation of the data even more difficult.

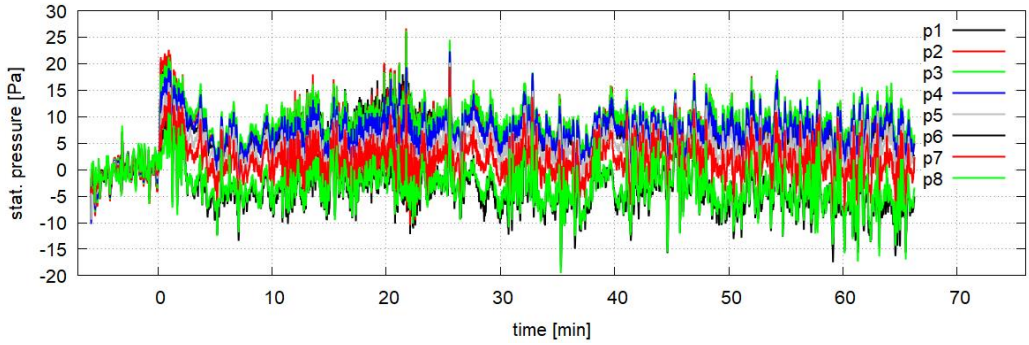

Figure 72: Differential pressure measurements during Test 3

Figure 73 shows the pressure difference between the tunnel and the service tunnel for various averaging periods. The first column refers to the ventilation operation prior to ignition. The second column refers to a period where the fire was fully developed and quasi steady state. The last column refers to a period where the larger fuel pan was burnt out and the heat release rate reduced.

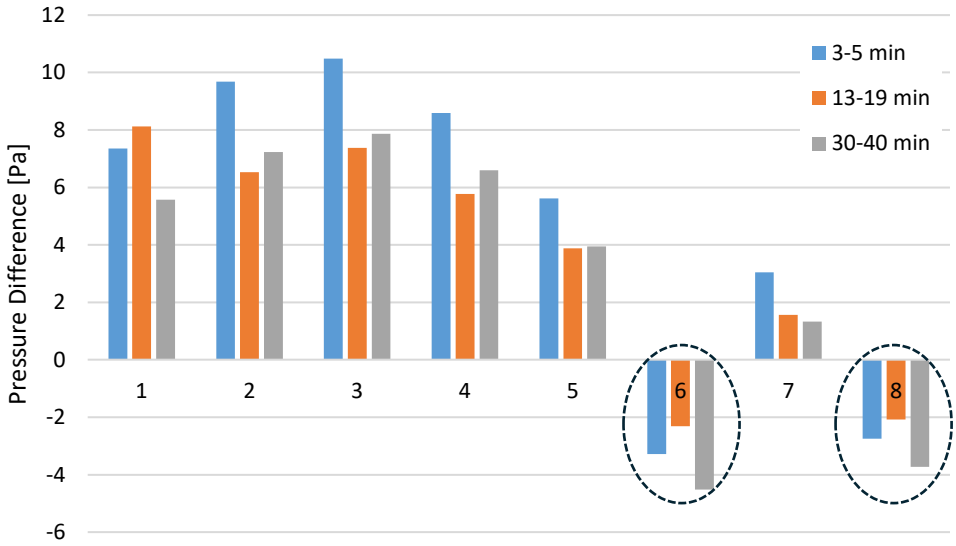

Figure 73: Pressure Difference between Tunnel and Service Tunnel, Test 3

Two measurements (6 @ PK482 and 8 @PK562) show a pressure higher in the service tunnel than in the test tunnel. The installation of these measurements has been checked prior to the tests and again after the test data was evaluated. No explanation has been given for these results. For the comparison of the tests with CFD analysis later in this report, these measurements have been disregarded.

Figure 74 shows the pressure difference between tunnel and service tunnel at the location PK231. These measurements have been taken with a sampling frequency of 100 Hz and 2000 Hz. The measurements show low frequency disturbances before the fire was started. With the fire, the fluctuations increased significantly. Only when the downstream fire pan was burnt out, the fluctuations were reduced again.

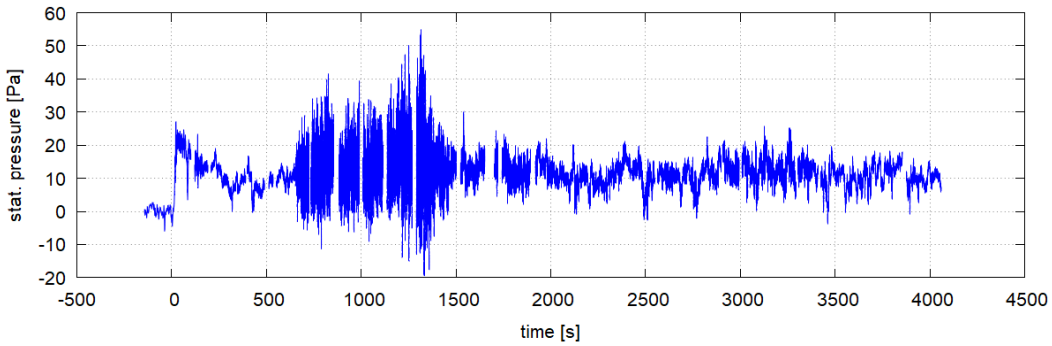

Figure 74: High frequency measurement at PK231, Test 3

Figure 75 and Figure 76 show small sections of the measurement in Figure 74. It is visible that the jet fan operation increased turbulence. But the intensity of the fluctuations is much more pronounced with the fire.

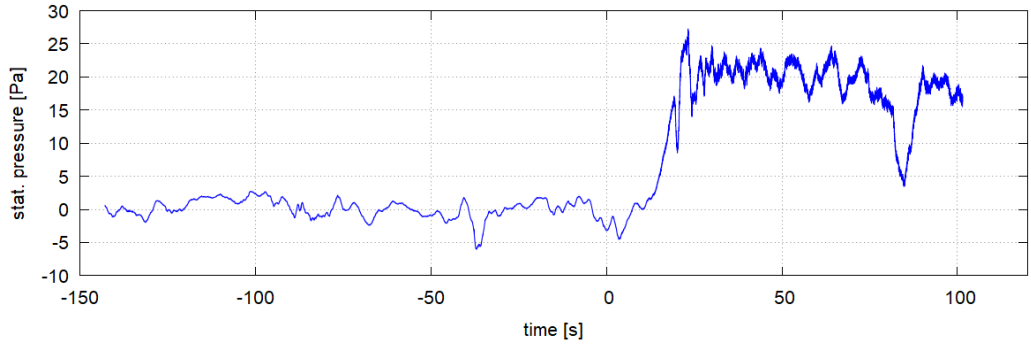

Figure 75: High frequency measurement at PK231, Test 3 (detail jet fans on)

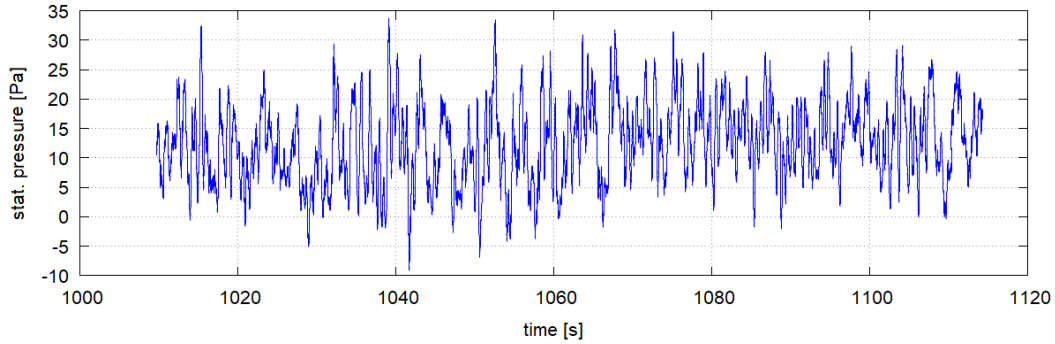

Figure 76: High frequency measurement at PK231, Test 3 (detail fire developed)

The fluctuations are more difficult to interpret than in Test 1. The data requires a more detailed frequency analysis. In Test 3, the fire source is significantly larger. The fuel pan area of 6.16 m² corresponds to a characteristic length D_B of 2.48 m and a frequency of the fire of 1.21 Hz [10].

$$f_{fire} = \frac{1.9}{\sqrt{D_B}} = 1.21\ Hz \tag{39}$$

Figure 77 shows the frequency analysis for a longer period with developed fire. The maxima are less obvious, as the oscillations of the fire test are superimposed by oscillations driven by the dynamic weather conditions outside the tunnel. Still, the oscillations include the dominant oscillations as well as the turbulence frequency spectrum. A dominant oscillation is visible at ~0.30 Hz, which represents the natural frequency of the tunnel tube. Higher order natural frequencies (n·0.29 Hz) are not visible.

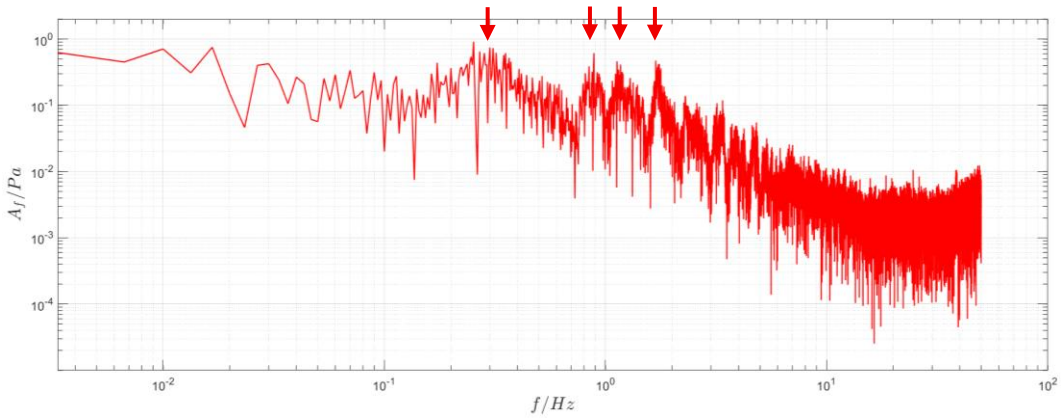

Figure 77: Frequency analysis Test 3, Sampling Rate 100 Hz

The graph also includes three local maximums at 0.85 Hz, 1.1 Hz and 1.5 Hz. This matches the maximums observed in Test 1 and Test 2. It does not match the frequency of the flame oscillation, as the increased heat release rate and the larger fire pan should lead to a reduced frequency of the flame oscillations. Further research is required to evaluate possible causes, e.g. eddy separation of the plume in crossflow.

Figure 78 shows the airflow and temperature profiles at the measurement location PK522. For these profiles, the average of the five sensors at equal height has been taken. The red lines refer to the measurement prior to the fire and the green lines refer to a period with fire. The graphs show a significant temperature stratification, but no stratified airflow. The measurements even indicate a slightly higher flow velocity in the lower half of the tunnel profile. In comparison to Figure 68, the temperature is significantly higher due to the increased heat release rate and similar flow velocity.

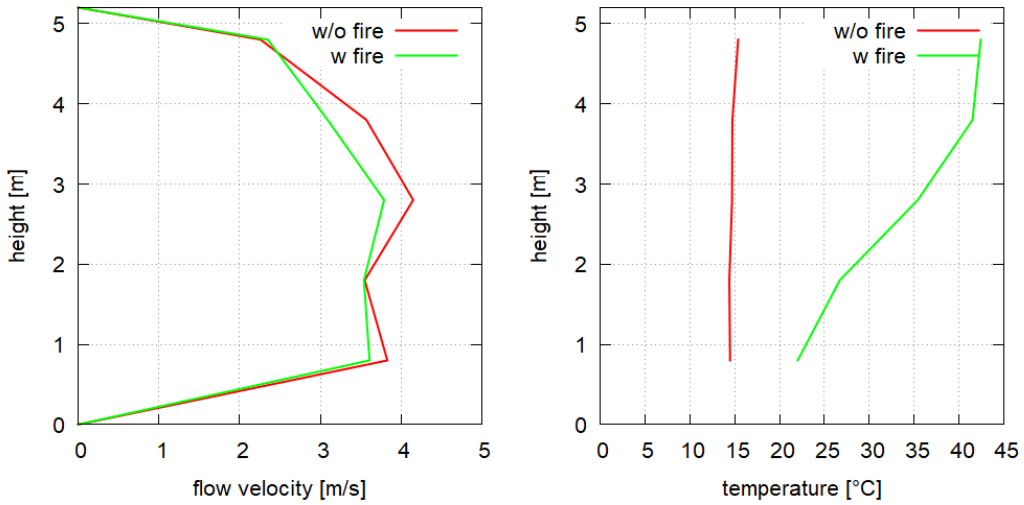

Figure 78: Airflow and Temperature Profiles at PK522, Test 3

5 CFD Simulation – Validation

Numerous examples can be found in the literature in which numerical simulations are used to calculate the air flow in tunnels in the event of fire, e.g. [25], [26]. These mostly refer to experimental measurement data from the fire tests in the Memorial Tunnel, [27], whereby only flow velocities and temperatures were measured in these tests, but not the pressure curve along the tunnel axis.

Other researchers used tunnel models on a smaller scale to measure velocity, temperature and pressure during a fire and to validate the simulation models [15]. As explained in chapter 3.1, small-scale models cannot be used to achieve adequate flow, temperature and pressure conditions for long tunnels in case of fire due to non-compliance with the similarity laws. Only 1:1 scale tunnels can be used for this purpose.

The fire test in the test tunnel at "San Pedro de Anes" represents an ideal starting point for the validation of numerical simulations of air flows in tunnels in the event of fire. In chapter 1, the calculations of the 1-D tool Spitfire show a good agreement with the measured data with regard to the total flow resistance and thus the air flow generated by the fans in operation as well as the temperature development along the tunnel axis. Temperature and velocity profiles at PK522 cannot, of course, be calculated with this 1-D software.

In the first steering committee meeting, the two software packages Star-CCM+ for the Reynolds Averaged Navier-Stokes (RANS) and Fire Dynamics Simulator FDS for the Very Large Eddy Simulations (VLES) were chosen for the 3-D CFD simulation. FDS is the standard application for 3-D simulations of fires and is frequently used by fire protection experts. The software revealed two weaknesses in the research project [15]. There is the problem with pressure and velocity oscillations occurring under certain conditions. Although this problem has been resolved in the latest version, the question of the loss of accuracy caused by this change remains unanswered. Secondly, the applied standard involves the use of large calculation elements in the order of 30 - 50 cm, which do not fulfil the requirements of classic LES simulations. For these reasons, high-resolution detached eddy simulations with mesh sizes in the range of 5 cm were carried out in Ansys Fluent in parallel. A total of four software packages were used in this project:

- Spitfire 1-D
- Star-CCM+ for RANS
- FDS for VLES (Very Large Eddy Simulation)
- Ansys Fluent for DES

5.1 Simulation Setup 1-D

Traditionally, tunnel ventilation systems are designed by 1-D steady state calculations of ventilation operation against the resistance of friction due to tunnel walls and traffic. With little modifications, these calculations can be turned into dynamic 1-D models of

tunnel ventilation systems. The main advantage of 1-D simulation is the rapid simulation time, which allows the simulation of a multitude of dynamic scenarios with very little effort and costs.

There are two weaknesses in 1-D tunnel ventilation models: Effects that are caused by 3-D flow phenomena must be included by sub-models – including smoke stratification and smoke back-layering. And every physical effect that is relevant for the flow regime must be included explicitly, for example the throttling effect or the inertia of ventilation control.

Spitfire is a model for analysing fire scenarios with arbitrary ventilation systems. The model is based on the one-dimensional time-dependent momentum and energy equations. The underlying equations have been published before [28]. The equations for the longitudinal airflow in the tunnel are the core of the model: Friction, pressure force of moving and standing vehicles against the longitudinal airflow, local losses at the portals, stack effect due to longitudinal gradient and the temperature distribution. These equations are given in [29] for longitudinal ventilation and in [30] for combined ventilation systems. In the simplest form for the tunnel without traffic or fire, we note

$$\frac{dp}{dx} = -\rho\frac{du}{dt} - \frac{\rho}{2}u^2\left(\frac{\lambda}{D_h} + \zeta\right) - k\rho u\frac{du}{dx} + ig\rho_0\frac{T(x) - T_0}{T(x)} \tag{40}$$

The model has been extended to include a transport equation for smoke concentration and a deterministic egress model [31]. The most notable inclusion in Spitfire is the propagation of hot smoke under the tunnel ceiling. The model can predict back-layering of smoke with the density-driven smoke propagation superimposed to the 1-D analysis. Smoke propagation is driven by density differences between the hot smoke and the cooler tunnel air [32]. Spitfire also includes a sub-model for smoke stratification [32] to interact with the egress model.

The model was re-written, simplified, extended and validated several times. The sub-model for the in-tunnel temperature now follows and is calibrated against the model described in Austrian design guideline RVS 09.02.32 [3]. Radiation is accounted for by applying the convective part of the heat release rate Q_c.

$$T(x) = T_0 + \frac{Q_c}{\rho_0 u_0 A_T \cdot c_p} \cdot e^{-\frac{\alpha U_T \cdot x}{\rho_0 u_0 A_T \cdot c_p}} \tag{41}$$

For the application in this research project, Spitfire was modified to adjust the throttling effect of the fire. The main contribution to the pressure profile is now given by the local expansion at the fire

$$\Delta p_{1-2} = -\frac{Q_c\, u_0}{c_p A_T T_0} \tag{42}$$

The other contributions to the tunnel aerodynamics due to wall-friction, vehicles' piston effect and jet fan operation are calculated from the local temperature-dependent

air density $\rho(x,T)$. In the calculations for this study, of these contributions only the wall friction and local pressure losses are relevant.

Throttling Effect Contributions			
Parameters			
Tunnel length	600 m	Air density	1.2 kg/m²
Cross-section	48 m²	Temperature	285 K
Hydr. Diameter	6.6 m	HRR	10 MW
Fire location	250 m	Conv. part	90%
Friction coeff.	0.015	Heat transfer coeff.	10 W/m²K
Flow velocity	3 m/s		
Results			
Cold flow friction	Δp 0-3 cold	-7.4 Pa	81%
Local expansion	Δp 1-2	-2.0 Pa	22%
Friction increase	Δp 2-3a warm	-0.6 Pa	7%
Pressure recovery	Δp 2-3b	0.9 Pa	-10%
Total	Δp 0-3 total	-9.0 Pa	100%

Table 9: Different contributions to the throttling effect

Table 9 gives an example for the various contributions to the throttling effect for the geometry of the test tunnel. The locations 0 to 3 refer to the definitions in Figure 29. The calculation does not include the local pressure losses at the tunnel portals as well as the cross-section change upstream. It also does not include the buoyancy due to the downward gradient of the tunnel. The pressure drop is dominated by cold flow friction. The contributions of the throttling effect compensate each other partly, i.e. the pressure drop at the fire and the pressure recovery from cooling downstream.

5.2 Simulation Setup for RANS

Prior to the fire tests at Applus TST, simulation models were developed on the basis of literature references. For example, the model was largely based on the research of Beyer et al 2024 [25], who in turn based his model broadly on previous research work and which thus corresponds to the current state of the art in the simulation of tunnel fires. The simulation model for RANS developed for the validation is explained below. The models for VLES (FDS) and DES (Fluent) are structured in the same way as far as possible. Deviations are also described in this chapter.

5.2.1 Solver

The Star-CCM+ version v2302 from Siemens was used for the RANS simulations. The simulations were carried out in stationary mode with 2nd order coupled flow and energy. Due to the high temperature gradients to be expected as a result of the fire, the air is assumed to be a compressible fluid. The viscosity, thermal conductivity and heat capacity of the air are calculated as a function of temperature using Sutherland's Law. The gravity term is included to take account of buoyancy forces. For inclined tunnel geometries, only the gravity vector is modified.

5.2.2 Physical sub-models and boundary conditions

Various turbulence models were considered, including the 6-equation Reynolds Stress Transport model (RST), to account for the anisotropic turbulence effects of a tunnel fire. For this purpose, the RST was compared with the Realisable k-epsilon and the k-omega SST model for a 10 MW fire with 3 m/s longitudinal flow. The differences between them in terms of the pressure and temperature curves are marginal, see Figure 79. Since the calculation time, convergence and complexity of the RST model are also higher, the k-omega SST turbulence model was chosen. The jump in the pressure curve at metre -100 is due to the start of the false ceiling in this section.

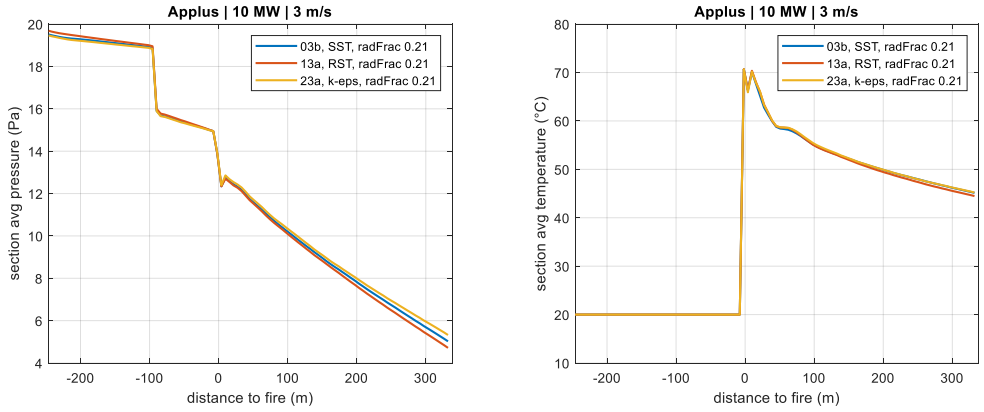

Figure 79: Pressure and temperature curve along the tunnel axis for the Applus geometry

To model the source of the fire, the volumetric heat source was compared with the eddy-dissipation combustion model. The area of the fire in the combustion model corresponds to the area of the two diesel fuel pans in Applus TST, totalling 4.32 m². The size of the volumetric heat source was varied in order to analyse the influence and finally fixed at a size of fire side length of 2.08 Meter and a height of 2 Meter. When comparing the two models and varying the size, it was found that the influence is only significant in the immediate vicinity of the fire and therefore also affects the back-layering. After 50 metres downstream, however, the influence is only marginal with regard to the velocity and temperature distribution, see Figure 80. With regard to the pressure and temperature profile over the entire tunnel and the velocity and temperature profile at PK522, which is the focus of this project, no major differences can be identified, see Figure 80. The simpler of the two models, namely the volumetric heat source, was therefore chosen.

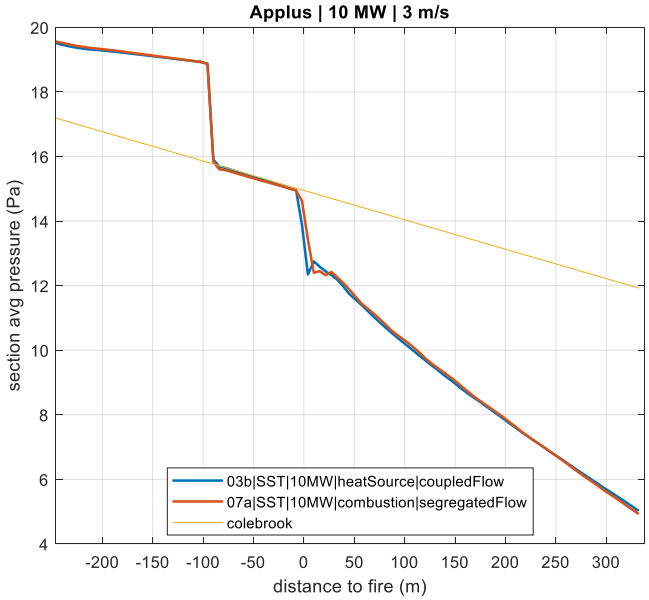

Figure 80: Comparison of pressure curve for volumetric heat source (blue) and combustion model (red)

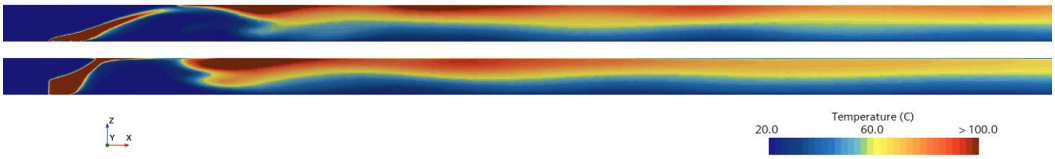

Figure 81: Temperature profile on the centre vertical plane along the Applus TST tunnel with the fire on the left-hand side of the images; combustion model (top); volumetric heat source (bottom)

The radiation is not simulated and instead the radiative fraction is introduced - a factor for the reduction of the HRR. This procedure is also used in FDS and is a robust method in which the temperature of the fire does not influence the radiative fraction. The standard value for a tunnel fire of the order of 10 MW in FDS is 0.35. Beyer et al. [25] used a value of 0.21 in their studies and comparisons with the Memorial measured values. For the Applus case, the radiative fraction was varied between the values 0.15 and 0.35 and compared with the model in which the radiation of the fire is calculated, see Figure 82. The value 0.21 is closest to the model with radiation calculation. The value 0.21 was therefore fixed in advance and no longer changed. It later became apparent that this value was a good representation of the experimental data from the fire tests.

For the temperature boundary condition of the tunnel wall, an isothermal temperature is defined equal to the inlet air temperature. This boundary condition is described in Beyer et al. [25]. The wall roughness is set to 2.5 mm.

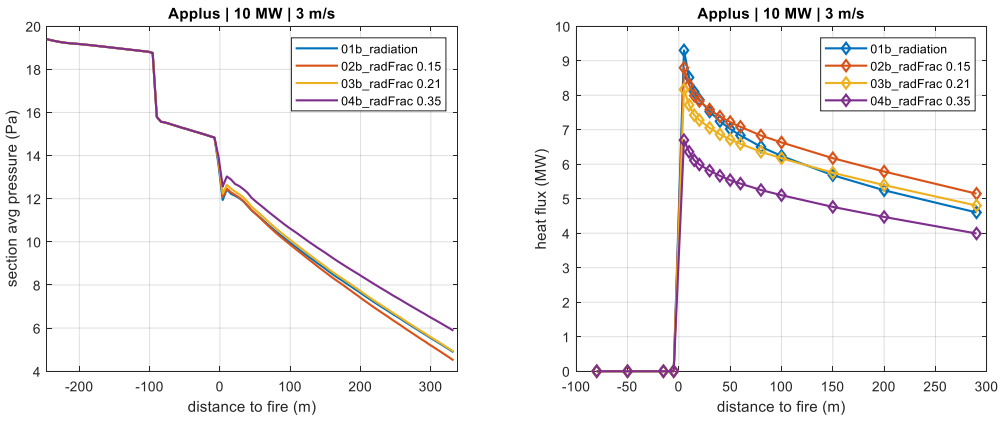

Figure 82: Simulation of the Applus TST tunnel with (blue) and without radiation modelling and with different radiative fractions

The averaged velocity profile at PK522 is used to determine the total mass flow, which is entered as a uniform velocity for the inlet boundary condition.

5.2.3 Meshing

For the RANS simulations in Star-CCM+, a poly mesh with an element size of approx. 30 cm, wall inflation layers to correspond to 100 < yPlus < 200 with approx. 1.8 million elements is used.

5.3 Simulation Setup for VLES

Where possible, the same settings are made for the VLES as for the RANS simulations. Deviations from this are explained below.

5.3.1 Solver

FDS version 6.8.0 is used for the validation. For analyses of the pressure curve of fires in long tunnels, the transient and Very Large Eddy Simulation (VLES) in combination with the standard FFT-based solver is recommended in the FDS user manual chapter 21.3 [33]. VLES in FDS is an implicit LES approach utilizing empirical wall functions for the velocity and the convective heat transfer.

5.3.2 Physical sub-models

The fire is simulated with the combustion model for n-heptane, whereby the area for the inflowing medium corresponds to the area of the two diesel fuel pans, 4.32 m².
TUNNEL_PRECONDITIONER=T

5.3.3 Geometry

FDS requires that the calculation mesh consists exclusively of cuboids. As a result, curvatures in the geometry cannot be resolved without steps. The curved roof of the Applus TST tunnel is therefore converted into a rectangular cross-section with the same area and the slight curvature of the tunnel is neglected. Simulations with the RANS model show that this simplification is permissible in relation to the pressure and temperature profile and the area of interest, see Figure 83. Only at the transition from full profile to profile with intermediate ceiling is there a difference of approx. 1 Pa.

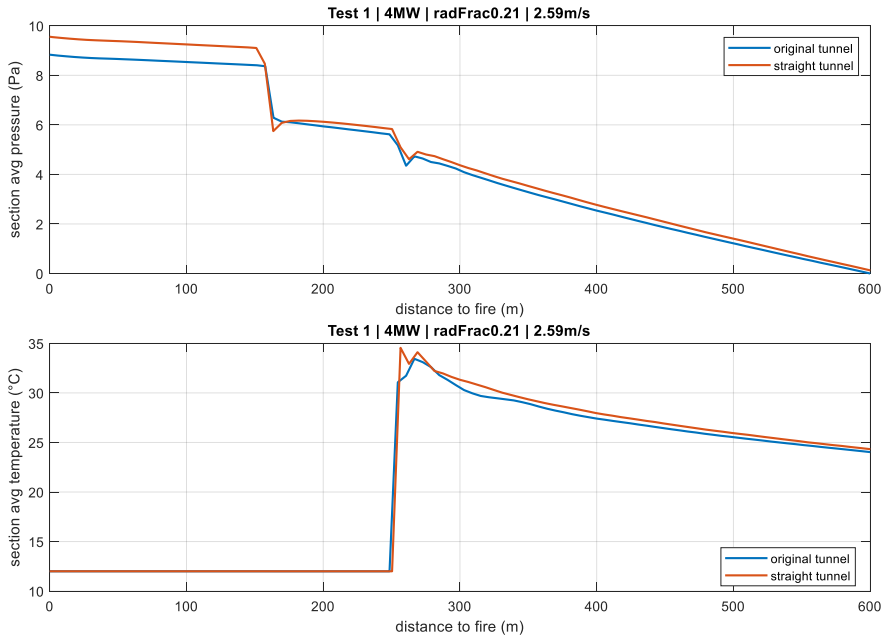

Figure 83: Comparison of pressure curve (top) and temperature curve (bottom) along the tunnel between original geometry (blue) and simplified geometry (red)

5.3.4 Meshing

According to the FDS user guide, chapter 6.3.6, the mesh resolution should correspond to the HRR. Equation (43) is provided for calculating the characteristic fire diameter.

$$D^* = \left(\frac{\dot{Q}}{\rho_\infty c_p T_\infty \sqrt{g}}\right)^{\frac{2}{5}} \tag{43}$$

In our application with HRR between 4 and 50 MW, the characteristic fire diameter is between 1.7 and 4.6 metres. For the VLES in FDM, a mesh with hexagonal elements with a side length of 30 cm and a total of 1.2 million elements is used. This means that characteristic fire diameter is resolved with 6 to 15 mesh elements. Compared to the table in 3.4.3 of the FDS Validation Guide, this is in the range of the studies mentioned. An analysis of technical articles on the engineering application of FDS for road tunnels shows that a grid resolution in the range of 0.25 m to 1.0 m is often chosen, typically 0.5 m. The selected element size of 0.3 metres therefore corresponds to the available specifications.

The wall regions are not provided with mesh layers and the boundary layer is not represented by a turbulence model. Instead, empirical wall functions are used for shear stresses and heat. The user manual [33] shows that the VLES solver in FDS achieves sufficient accuracy even with relatively coarse elements in the boundary layer and a correspondingly high yPlus in the range of 5,000.

5.3.5 Postprocessing

The "section average pressure" and "section average temperature" values in the diagrams for the pressure and temperature profile along the tunnel are determined by averaging the areas on a total of 100 transverse planes.

The same approach is used for the flow and temperature profiles over the tunnel height as for the measuring grid in PK522. There, the measuring points are arranged on a total of 5 horizontal planes. The profiles from the simulations are also calculated from the mean values of these 5 horizontal planes or lines.

The sensor signals from the fire tests for velocity, pressure and temperature from the fire tests fluctuate quite strongly, which makes time averaging necessary for comparison with the steady-state RANS simulations. The following time periods apply to fire tests 1-3, whereby the time is set to zero when the fans are switched on:

- Test 1: Minute 26:00 - 28:00
- Test 2: Minute 23:00 - 25:00
- Test 3: Minute 17:00 - 19:00

The x-axis in the diagrams corresponds to the length of the tunnel from 0 to 600 metres. The following sections are worth mentioning:

- PK159: Start of the suspended ceiling
- PK252: Position of the fire
- PK522: Position of the measuring grid

The positions for the eight pressure differential measurements are PK231, PK311, PK353, PK393, PK440, PK482, PK522 and PK562. At position PK232, the pressure difference is recorded with an additional pressure transmitter with a higher sampling rate.

5.4 Simulation Setup for DES

In this section, numerical simulation of the three testcases is performed using detached eddy simulation (DES) the Ansys-FLUENT is used to implement the DES simulation. The pressure-based solver with bounded second order implicit second-order method is used. In addition, SIMPLE scheme is used for pressure-velocity coupling. The same software and solver are also used for the simulation of unsteady Reynolds averaged Navier-Stokes (URANS) equation, which is performed in this section. The following section describes shortly the governing equations for DES.

5.4.1 Model Description for DES

The Detached Eddy Simulation (DES) considers implementing a blending between scale resolving LES and turbulence models. This model was introduced by Spalart et. al. [34] and tailored for Spalart-Allmaras turbulence model. The main idea was to resolve the turbulent eddies away from wall and therefore in the original model, a distance from wall-based implementation was used to switch between turbulence model and LES. Later, the concept was more generalized to consider the switching between two-equation transport model and LES by using the length scale of eddy viscosity as a measure of the switch. Therefore, in the case of low grid resolution for eddy size, the RANS is used and is switched to LES when the grid resolution is small enough to resolve the eddy size. The eddy length scale in the RANS context can be estimated as

$$L^e_{RANS} = \frac{\sqrt{k}}{C_k \omega} \tag{44}$$

where k corresponds to turbulent kinetic energy and ω represents specific dissipation rate. The term C_k represents a constant term and its value is usually 0.61. This length scale is compared with mesh size estimate to define a generalized eddy size length scale as

$$L^e_{DES} = min(L^e_{RANS}, C_{DES}\Delta) \tag{45}$$

where Δ is the maximum dimension of the local control volume CV of the mesh element. In a more generalized sense for unstructured mesh, Δ can be estimated as

$$\Delta = (CV)^{\frac{1}{3}} \tag{46}$$

The recommended value of model constant C_{DES} is usually 0.65. In the two-equation turbulence model such as SST k- ω transport equation, this switch property of the eddy size length scale is directly implemented in the transport equation for turbulent kinetic energy k in the dissipation term, which is obtained as

$$\frac{\partial(\bar{\rho}k)}{\partial t} + \frac{\partial\left(\overline{\rho\tilde{u}_j}k\right)}{\partial x_j} = \frac{\partial}{\partial x_j}\left(\left(\mu + \frac{\mu_T}{\sigma_k}\right)\frac{\partial k}{\partial x_j}\right) + P_k - \frac{\rho k^{\frac{3}{2}}}{L^e_{DES}} \tag{47}$$

It is to be noted that the modification in transport equation for k adjusts the eddy viscosity automatically as we solve the SST transport equation. However, in Ansys-Fluent simulation set-up, the eddy viscosity is replaced in the LES region by the following equation for viscosity

$$\mu_t^{DES} = \rho L^2_{DES}|S| \; \forall \; L^e_{DES} = C_{DES} \tag{48}$$

DES suffers from the intrusion of LES mode into attached boundary layer. This is remedied using delayed-DES (DDES) approach, where a shielding function f_d is introduced to allow a smooth transition from RANS to LES in the attached boundary layer region [35]. This leads to the estimate of eddy size length scale as

$$L^e_{DDES} = L^e_{RANS} - f_d \max(0, L^e_{RANS} - C_{DES}\Delta) \tag{49}$$

The shielding function is estimated as

$$f_d = 1 - \tanh[(8r_d)^3] \tag{50}$$

$$r_d = \frac{\mu_t + \mu}{max\left(\sqrt{\frac{\partial \widetilde{u_i}}{\partial x_j}\frac{\partial \widetilde{u_j}}{\partial x_i}}, 10^{-10}\right)\rho\kappa^2 d_w^2} \tag{51}$$

where d_w represents the distance from nearest wall and κ corresponds to von Kármán constant and usually estimated to be 0.41. The DDES version is used in this project.

5.4.2 Domain Discretization using URANS

URANS corresponds to the unsteady RANS simulation. The meshing requirement for DES is estimated by performing a precursor URANS. This provides

- The discretization requirement for DES simulation, by estimating turbulent eddy size to mesh size ratio and
- The timestep and time sampling rate to estimate the time average of DES simulations.

The URANS used SST k-ω turbulence model. Five different mesh size is tested here to obtain an optimized grid size for DES studies, which captures the energy containing scales away from the wall and computationally not very expensive simulation. The Applus tunnel geometry is discretized using Fluent meshing software, with two regions of interest with increased grid resolutions. These are the heat source region, which models the fire and a subdomain of the tunnel around the fire, where flow behaviour observed to have maximum changes with time and space.

Discretisation Details

Mesh Name	N_c	N_c^f	N_c^t	$S_B^f(m)$	$S_B(m)$
Mesh02	5.83 x 10^5	2.69 x 10^4	5.56 x 10^5	0.1	0.75
Mesh0	8.67 x 10^5	2.70 x 10^4	8.40 x 10^5	0.1	0.5
Mesh1	1.726 x 10^6	2.70 x 10^4	1.699 x 10^6	0.1	0.25
Mesh3	1.027 x 10^7	1.90 x 10^5	1.008 x 10^7	0.05	0.125
Mesh5	1.742 x 10^7	1.427 x 10^6	1.599 x 10^7	0.025	0.1

Table 10: Discretization details of different mesh types used in DES simulations

Table 10 obtains the details of different mesh types with the description of maximum mesh volume size for the heat source region and a sub-domain around the fire, which is denoted as body of influence (BOI). The mesh types are denoted with specific numbering e.g. Mesh1. The term N_c corresponds to the total number of cells in the discretized tunnel domain. The corresponding cells in the fire zone and tunnel zone are indicated by the terms N_c^f and N_c^t respectively. The maximum cell volume in the fire region and tunnel BOI are indicated using terms S_B^f and S_B respectively. The coarsest mesh has around half a million cells. The finest mesh has about 17 million cells. The mesh is generated using polyhedral meshing with prism layers near the tunnel walls. The coarsest mesh type has maximum cell-size of 10 cm and 75 cm for heat source region and BOI respectively. The finest mesh type has a maximum cell-size of 2.5 cm and 10 cm for heat source region and BOI respectively.

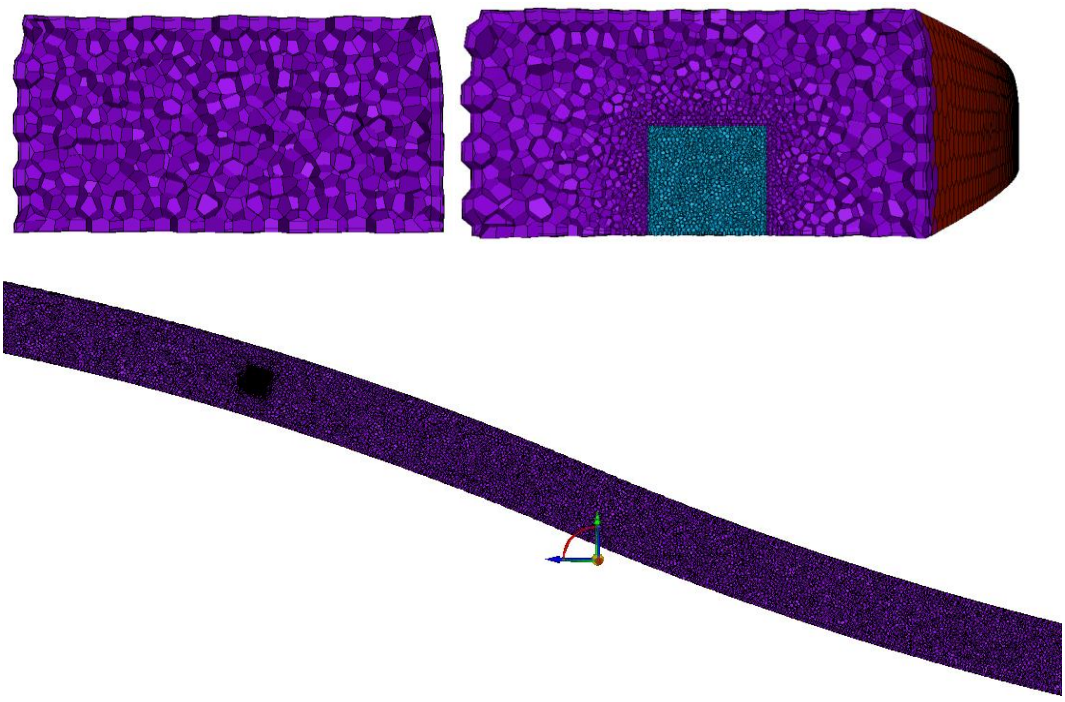

Figure 84: The meshed geometry is depicted for a cross-section at the heat source location (top right), away from heat source region (top left) and along a plane parallel to tunnel at a height of one metre

Figure 84 depicts the meshed geometry using polyhedral meshes using Fluent-meshing software for three different cross-sections. The top two figures correspond to the cross-section of tunnel at heat source region (top right) and downstream from the heat source region (top left). The heat source region is coloured in mild-green to depict the separate mesh resolution of the heat source region. Further a cross-section along the tunnel axis, passing though the heat source region is depicted in the bottom figure. This encompasses the BOI and heat source region and therefore contain high mesh resolution compared to the rest of the domain of Applus tunnel.

A test case is chosen with high heat release rate of 10MW to find the optimal mesh requirement, where the meshing properties are mainly varied in heat source and BOI region. Initial URANS simulation is used with a timestep size of 0.05s for about 800s of simulation of the fire inside the tunnel. After that, a smaller timestep of 0.01s is used for about 25s of simulation to obtain different samples of the solution over time to estimate mean properties over these time samples. A sampling rate of 0.4s is chosen to obtain the time averaged solutions. The URANS also obtains the eddy size for turbulent eddies and a ratio of eddy size to cell size (Δ) is estimated. Such estimation provides the refinement requirement for next finer mesh, which is described in the paper by Deb et. al. [24]. A ratio of eddy size to cell size of less than five indicates that the LES cannot resolve such eddies and therefore cannot capture the full spectrum of energy containing scale (more the 80% of turbulent kinetic energy [36]).

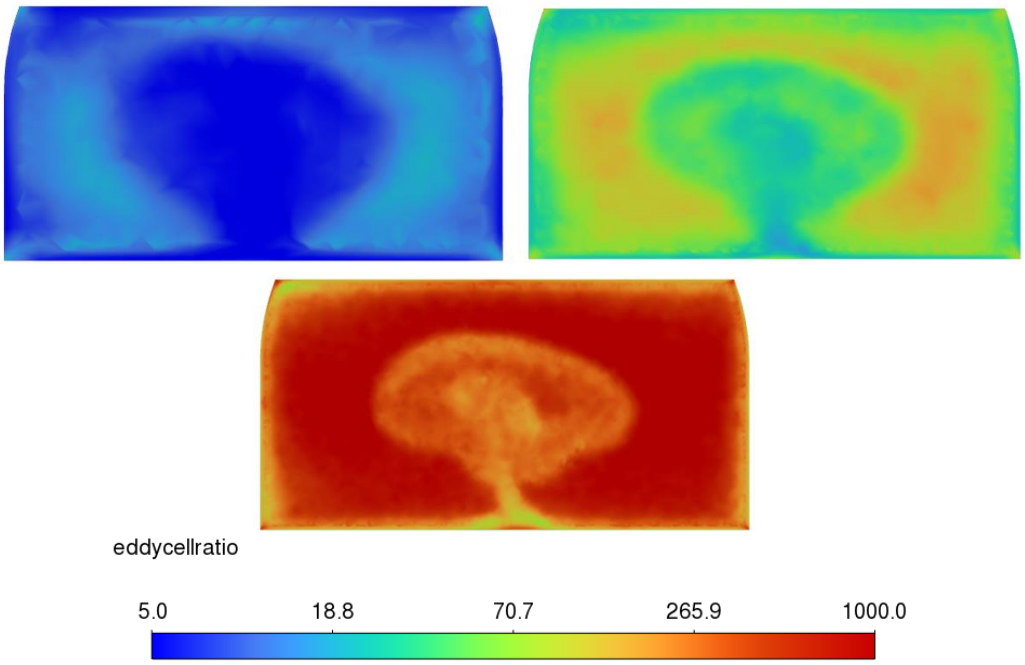

Figure 85: Eddy size to cell size ratio for three different mesh types of Mesh0 (top left), Mesh1 (top right) and Mesh3 (bottom figure) at a cross section of 5m downstream of the fire

Figure 85 obtains the eddy size to mesh size ratio for three different mesh resolutions. The mesh type Mesh0 under resolves the eddy size. However, the mesh type of Mesh1 has small under resolved regions near the boundary. The mesh resolution type Mesh3 resolves well most of the domain including the region near the wall.

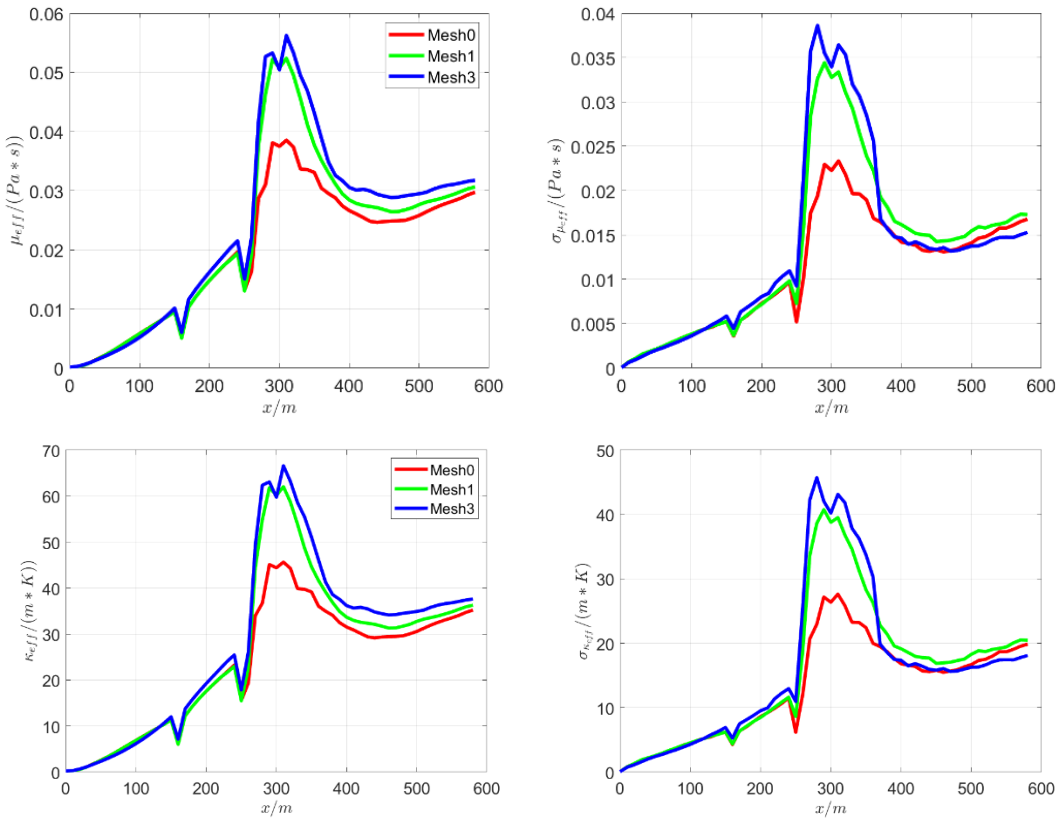

Figure 86: Average effective viscosity and standard deviation of effective viscosity on a plane perpendicular to tunnel axis at different tunnel axis location is depicted in the top left and right plots. The same is obtained for effective thermal conductivity in the bottom left and right plots.

It is observed from mean effective viscosity and thermal conductivity plots in the left column of Figure 86 that Mesh1 and Mesh3 finally converged for such solutions in terms of mean properties. The right column represents the standard deviation of the corresponding quantities on the cross-sectional planes of the tunnel at different locations, which approximately also converges for Mesh1 and Mesh3 grid resolutions.

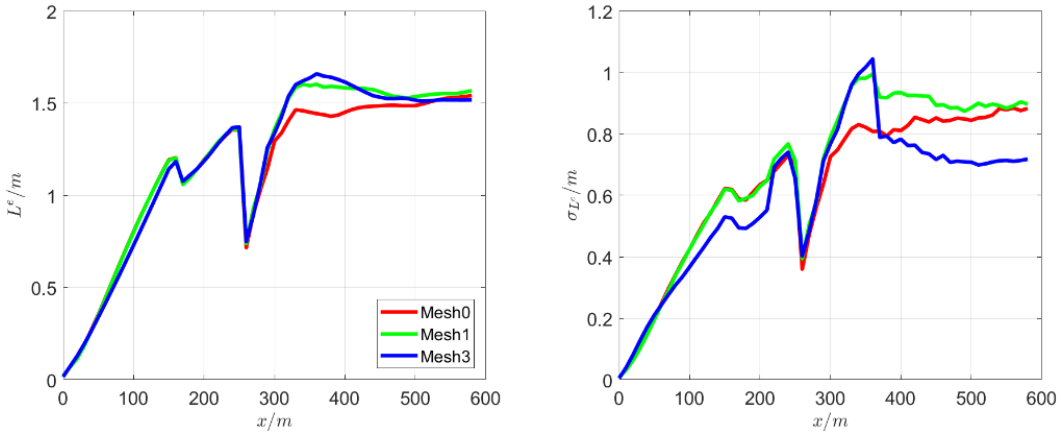

Figure 87: Average eddy size and standard deviation of eddy size on a plane perpendicular to tunnel axis at different tunnel axis location is depicted in the left and right plots respectively.

Figure 87 obtains the mean eddy size estimated using turbulent properties (k, ε). The mean eddy size also converges for Mesh1 and Mesh3 types in the downstream of the heat source region. Based on these initial analysis using URANS, DES simulations are performed for testcases 1,2 and 3 using Mesh type 3. Further, to test the convergence of results, a high order grid resolution of type Mesh5 is also simulated in DES.

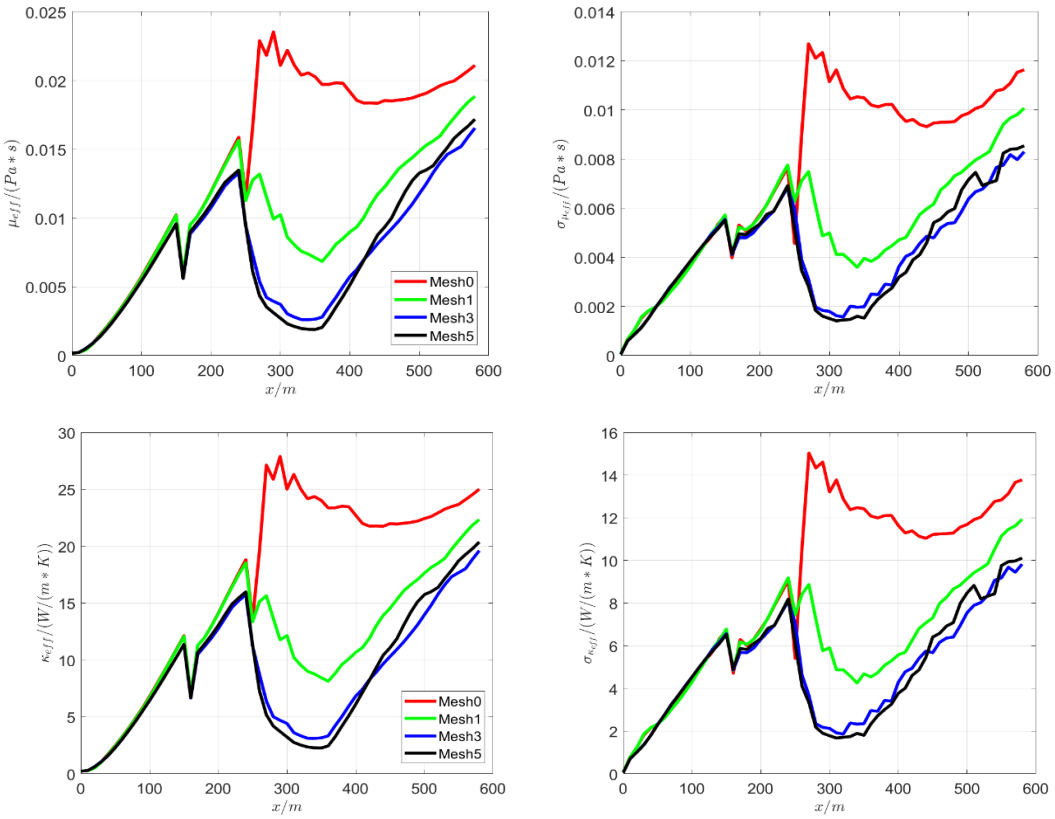

Figure 88: Average effective viscosity and standard deviation of effective viscosity on a plane perpendicular to tunnel axis at different tunnel axis location is depicted in the top left and right plots using DES simulation. The same is also obtained for effective thermal conductivity in the bottom left and right plots.

Figure 88 obtains the effective viscosity and thermal conductivity using DES simulation with different mesh resolutions. It is observed that, Mesh0 and Mesh1 solves the turbulent modelling SST simulation as the eddy size in these cases are smaller than the mesh size. The mesh size Mesh3 and Mesh5 obtains the DES simulation with lower viscosity and thermal conductivity, which indicates that viscosity and thermal conductivity in these cases corresponds to LES in the interior of the domain. Further, Mesh3, mesh5 converges and therefore it is enough to use low resolution Mesh3 for the analysis of tunnel fire with heating rate of 10MW or lesser values.

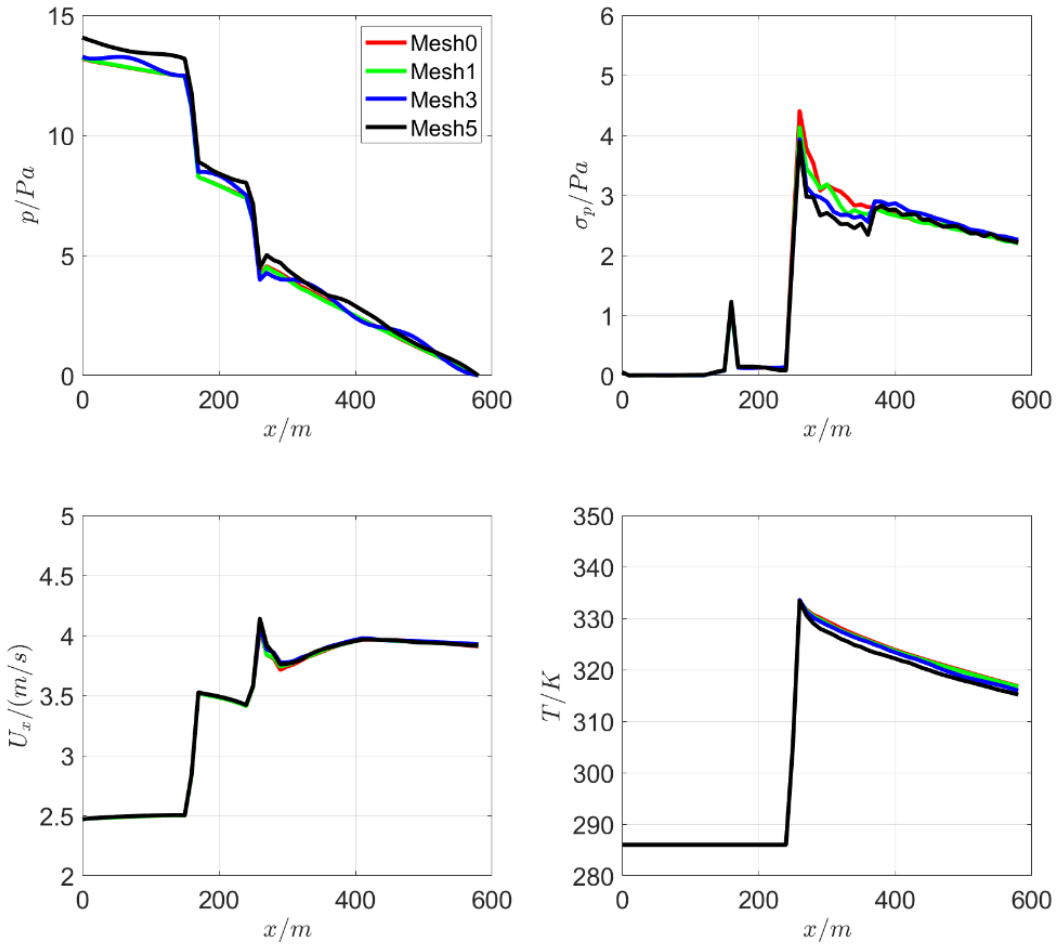

Figure 89: Top: Average pressure solution and its standard deviation at different mesh resolution using DES simulation. Bottom: Average fluid speed (left) and average fluid temperature (right).

Figure 89 obtains pressure averaged solutions (top left), temperature (bottom right) and fluid speed along the tunnel (bottom left) and standard deviation in pressure solution (top right) solution using different mesh resolutions and DES simulation type. The average quantities converge with increasing mesh resolution.

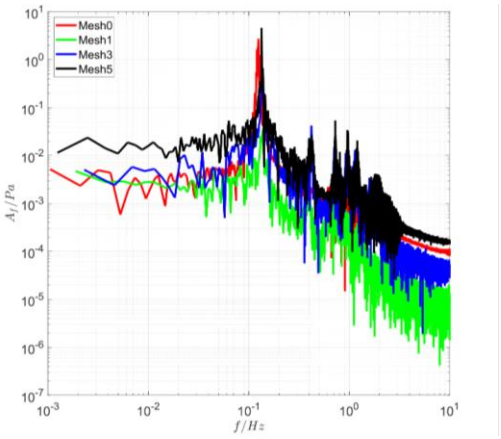

Figure 90: Fourier transformed solution at different mesh resolution for pressure solutions.

Figure 90 obtains frequency domain solution of pressure solution at a point 50m downstream of the fire. The Fourier transformed solution is obtained from a time sample of 0.01s over a time window of 24s. All the four-mesh resolution obtains a similar peak around 0.11Hz and some high frequency peaks around 0.4Hz and 1Hz. The presence of such high frequency peaks makes it necessary to estimate mean over time with higher sampling rate (0.4s or 2.5Hz). Therefore, all the averaged solutions are reported after estimating mean over time samples with time interval of 0.4s.

5.4.3 URANS vs DES Comparison

In this section the results estimated using URANS is compared with DES results for qualitative flow features and mean behaviours for the mesh resolution type Mesh3.

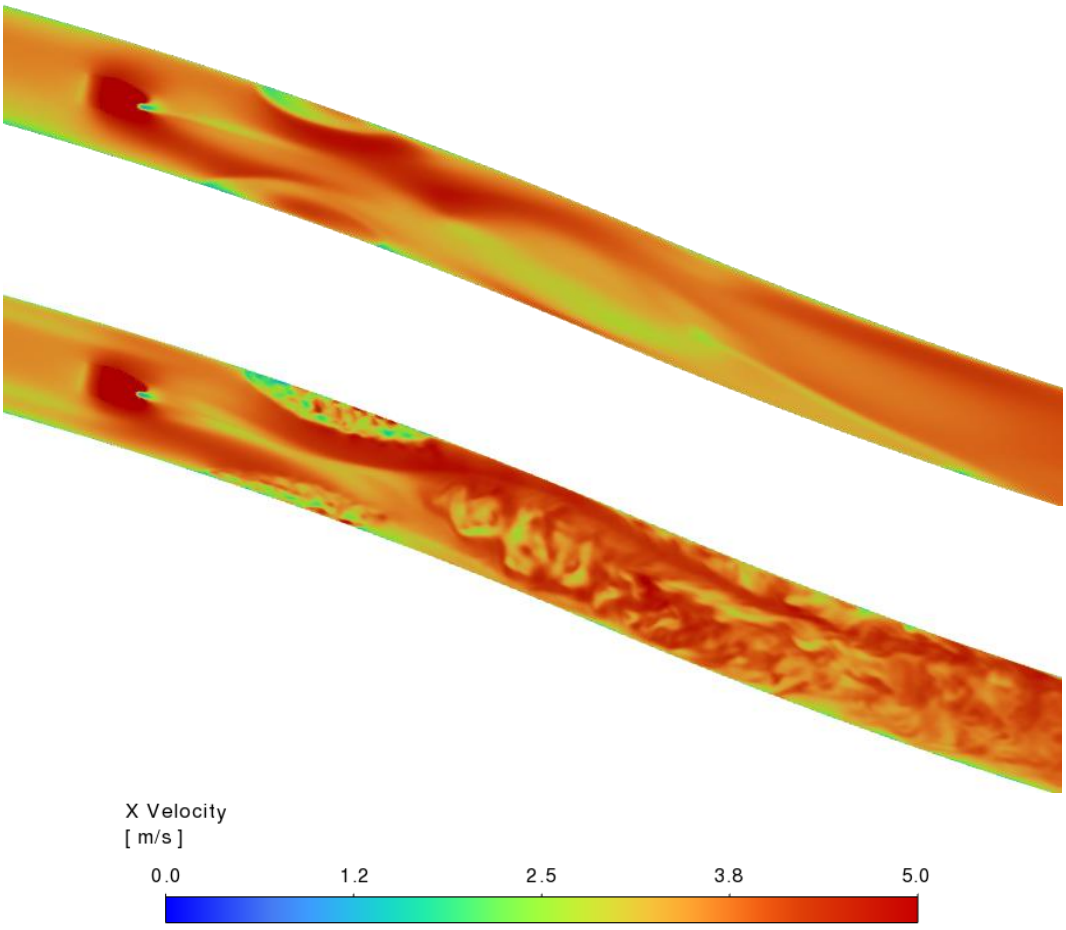

Figure 91: Comparison of fluid speed along the tunnel for URANS (top figure) and DES (bottom figure) at a tunnel height of 2.5m.

Figure 91 obtains a snapshot of flow speed along x-direction (tunnel axial direction) using URANS (top figure) and DES (bottom figure) at a plane of Z=2.5m tunnel height. The more detailed flow features are observed using DES due to reduced viscosity owing to mesh adjusted eddy length scale. However, the larger flow features are approximately captured well using URANS.

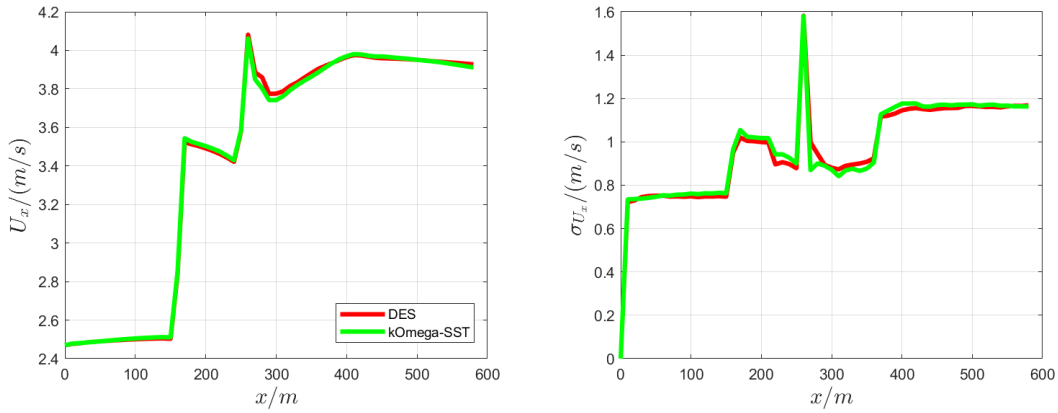

Figure 92: Average fluid speed and fluid speed standard deviation along the tunnel cross section at different tunnel axial location using DES and URANS.

Figure 92 estimates the flow speed average using DES and URANS. Average and first order statistical moments compares well using DES and URANS.

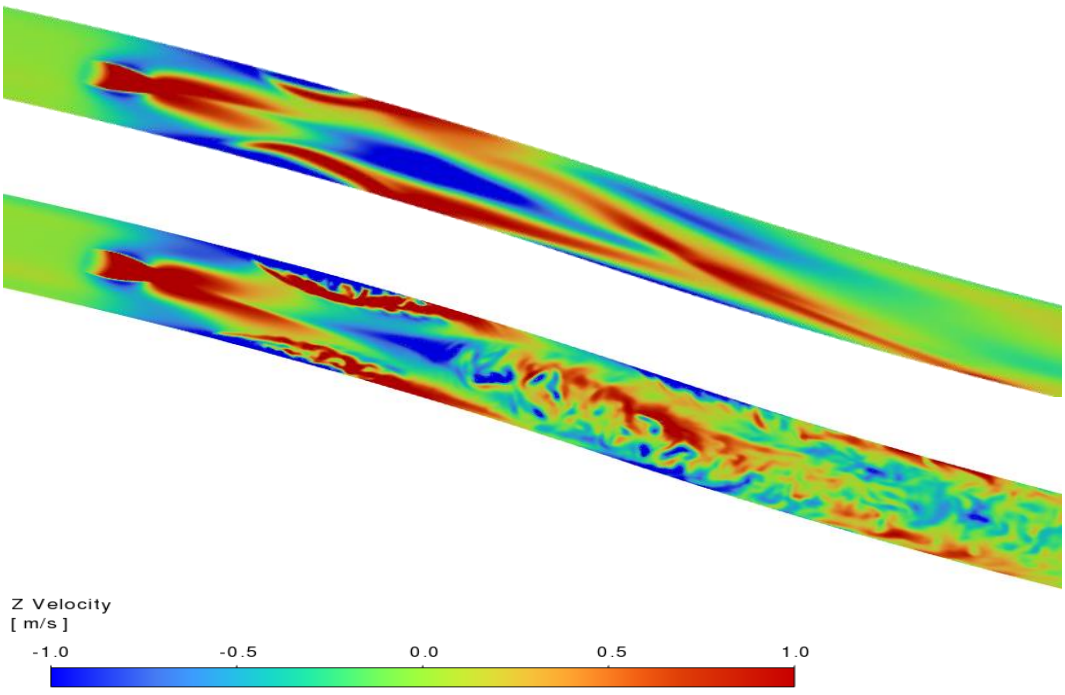

Figure 93: Comparison of vertical fluid speed along tunnel height of 2.5m for URANS and DES simulation.

Figure 93 observes the vertical fluid speed along tunnel height using URANS and DES. The detailed flow features and turbulent eddies are well visible in DES simulation compared to URANS.

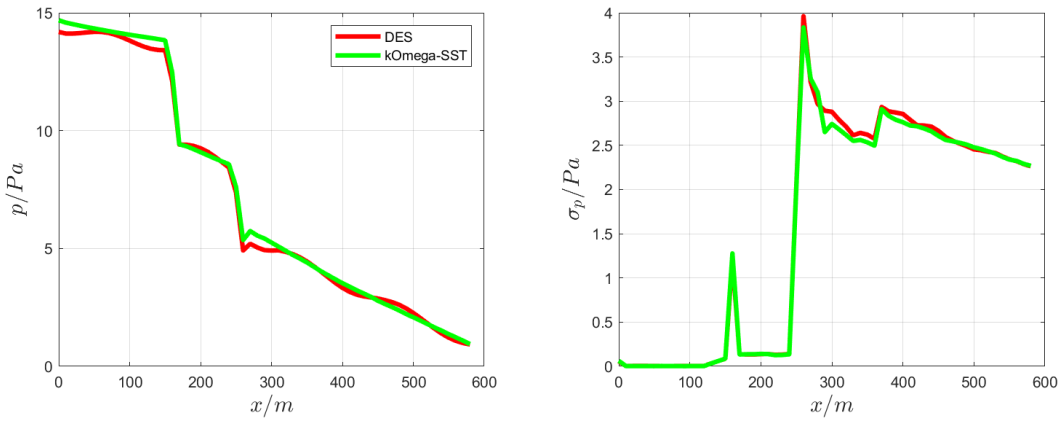

Figure 94: Average static pressure and static pressure standard deviation along the tunnel cross section at different tunnel axial location using URANS and DES.

Figure 94 obtains the average pressure solution and its first order statistical moment (Standard Deviation) using DES and URANS simulation. It also matches well for both the methods.

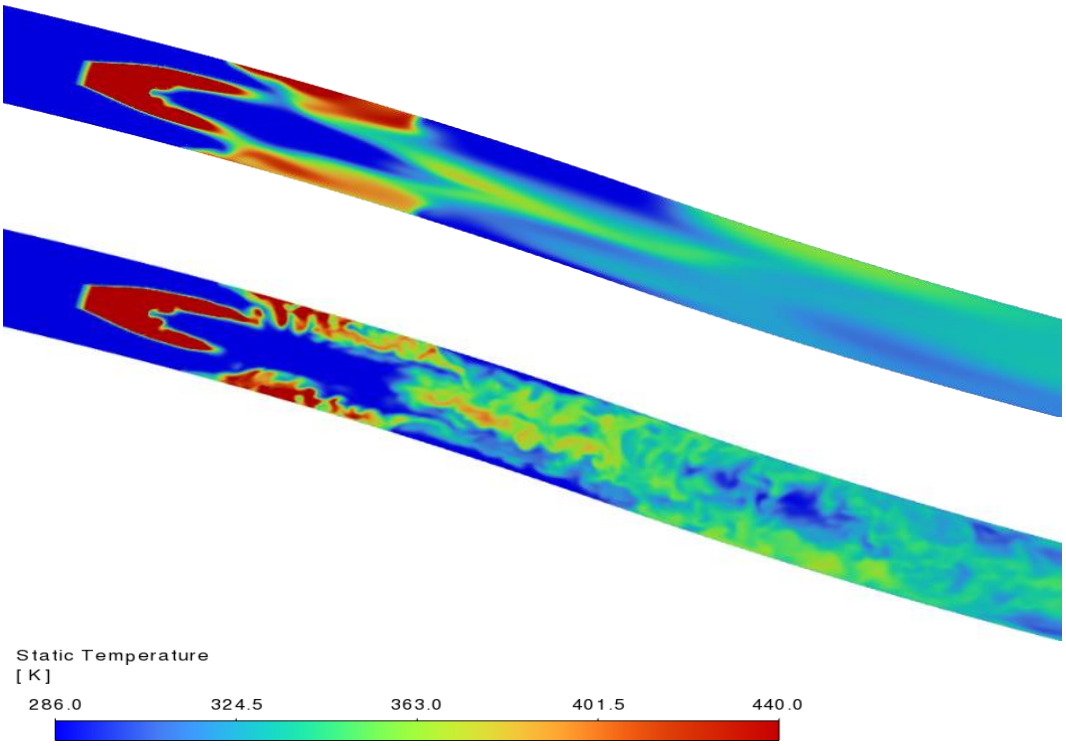

Figure 95: Comparison of URANS and DES simulation for fluid temperature along tunnel height z = 2.5m.

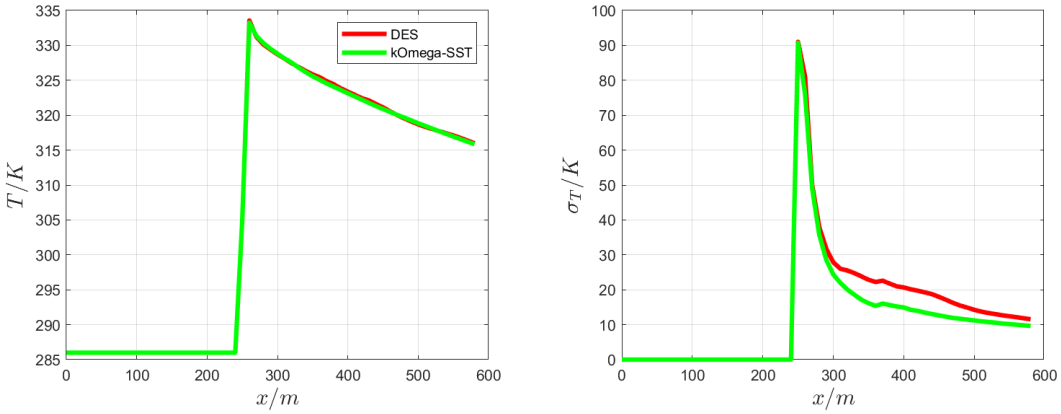

Figure 96: Average fluid temperature and fluid temperature standard deviation along the tunnel cross section at different tunnel axial location.

Figure 95 observes a snapshot of fluid temperature along the tunnel height of 2.5m using DES and URANS. It further confirms the detailed flow features captured using DES simulation. Figure 96 obtains the mean and standard deviation of the fluid temperature. The mean properties are similar for URANS and DES. However, the scale resolving properties of DES leads to higher standard deviation along the cross-sectional planes compared to URANS.

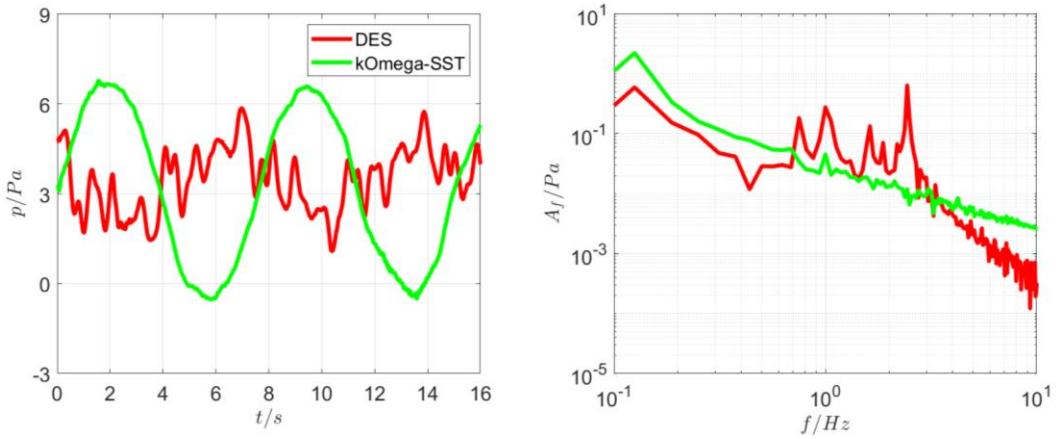

Figure 97: Time domain and frequency domain solution for static pressure at a point located 50m upstream of the fire for DES and URANS simulations.

Finally, time domain and frequency domain solution for static pressure at a location of 50m upstream of the fire is observed in the plots of Figure 97. Scale resolving nature of DES allows to capture higher order fluctuations in pressure compared to URANS. The maximum value of y^+ obtained for DES lies in the range of 13 to 15 over the simulation time. The same for URANS lies in the range of 9 to 11. However, the average y^+ lies within 5 for both DES and URANS.

5.5 Simulation parameters

The parameters from Table 11 are derived from the evaluation of the three fire tests carried out at Applus TST. The same values are used for the RANS simulations as well as for the VLES and the DES.

Simulation Parameters

Parameter	Unit	Test 1	Test 2	Test 3
Velocity PK522	m/s	2.59	3.70	3.34
Temperature inlet	°C	12.0	13.5	15.0
HRR	MW	4.00	4.22	10.00
Radiative fraction	-	0.21	0.21	0.21

Table 11: Simulation parameters for the fire tests 1-3

5.6 Results

5.6.1 Test 1 - 4 MW, 2.59 m/s

For the pressure curve along the tunnel, the values from RANS, VLES and 1-D are compared with the experimental data, see Figure 98.

As mentioned above, the two pressure difference signals PK482 and PK562 are questioned (red cross). The line for the pressure curve from the measurement data therefore does not run through these two points. In addition, the measurement signal on PK231 is difficult to interpret and does not match the measurement signal of the additional sensor. The additional sensor on PK231 shows more plausible values in relation to the pressure curve. The violet line for the measured pressure curve therefore runs through it and not through the value measured by Applus (third red cross). The pressure at the tunnel portal at PK600 was not measured. For better visualisation and comparison with the simulation data, this measurement point was added retrospectively.

With these interpretations, all simulations show good agreement with the measured data with a maximum deviation of 1 Pa, mostly within the expected measurement accuracy. It should be noted here that neither the simulation model nor its parameters from chapter 5.2.2 or 5.2.2 were changed from the preliminary study to achieve this agreement. The only changes are the adjustments of the boundary conditions to the parameters for the fire tests 1-3 (HRR, inlet temperature, inlet velocity).

The slight increase at measuring point PK353 can be observed in all three fire tests, but not in the simulation data. It was not possible to determine whether there is a measurement uncertainty or whether this pressure increase is significant of a physical effect.

To assess the resulting wall friction and the usage of the wall function of the solvers without a heat source, the tunnel section from the tunnel entrance to the start of the false ceiling can be used (PK0 until PK160). The pressure drop in this section for the used solver is:

- RANS (Star-CCM+): 0.42 Pa

- VLED (FDS): 0.47 Pa
- DES (fluent): 0.51 Pa
- 1-D (spitfire): 0.74 Pa

For comparison, the pressure loss using the empirical Colebrook–White equation in this section is 0.75 Pa, which is closest to the 1-D solution. The reason for the three 3-D solvers having approximately the same deviation was not investigated further.

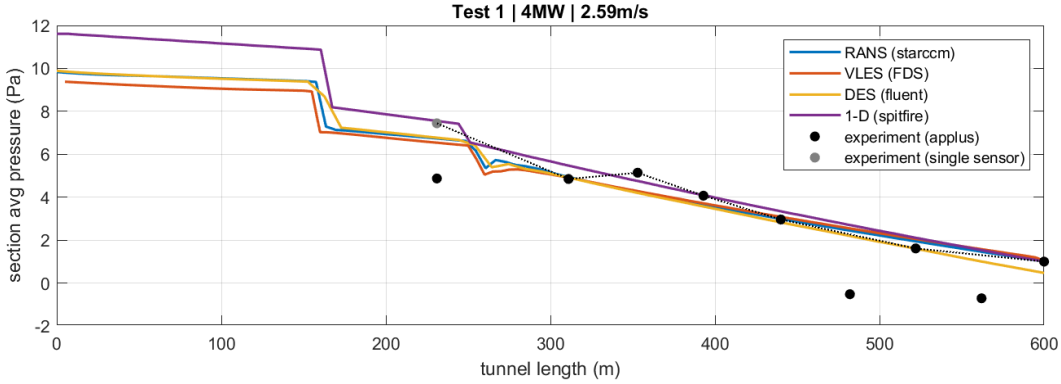

Figure 98: Comparison of the pressure curve along the tunnel from simulation data with the measured values for Test 1.

The temperature curve along the tunnel also shows relatively good agreement between the simulation models, see Figure 99. The data point from the fire test is the averaged value at the PK522 measuring grid and lies within the simulation curves.

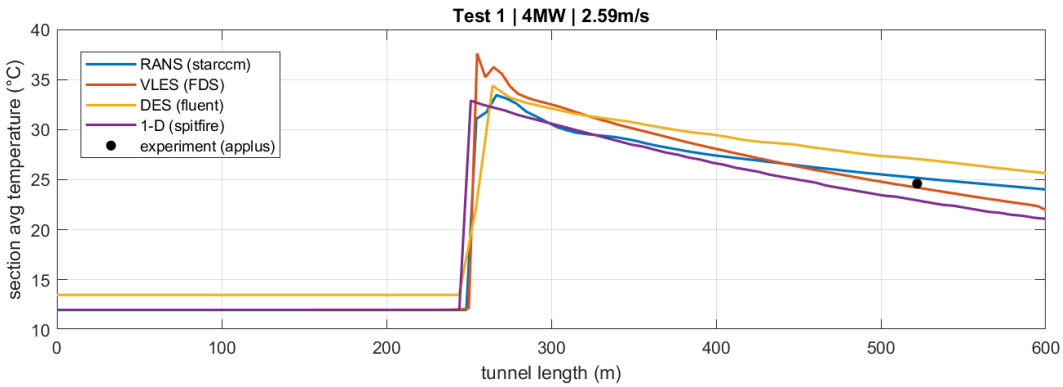

Figure 99: Comparison of the temperature curve along the tunnel from simulation data with the measured values from fire test 1.

The velocity and temperature profiles were created from the sensor data of the measurement grid at PK522 (5 horizontal levels of measurement points) and compared with the data from the RANS simulations and VLES, see Figure 100. The simulation data is averaged across the tunnel profile. The temperature profiles from all three data sets show good agreement with a maximum deviation of 2 K. The temperature stratification is visibly pronounced. The agreement is less good for the velocity profiles. The profile from the measurement data shows higher velocities in the lower half of the tunnel profile, i.e. like an inverted temperature stratification, while the RANS simulations show this temperature stratification (higher velocities in the upper half of the tunnel profile). In the VLES data, the profile is relatively flat with a very marginal stratification effect.

The report [15], [16] refers to the Reynolds analogy: The Reynolds analogy combines turbulent impulse and heat transport. In turbulent flow, impulse transport and heat transport depend on the same turbulence elements. Accordingly, similar distributions should result for the temperature and for the flow velocity. The Reynolds analogy was experimentally proven for pipe flows and flows on flat plates. It applies if the turbulent Prandtl number is close to 1.0 and if there is no form resistance, i.e. flow separation. While the CFD simulations indicate a similarity of the temperature and flow profiles, the experiment shows a different flow profile with the flow maximum closer to the centre of the tunnel cross-section.

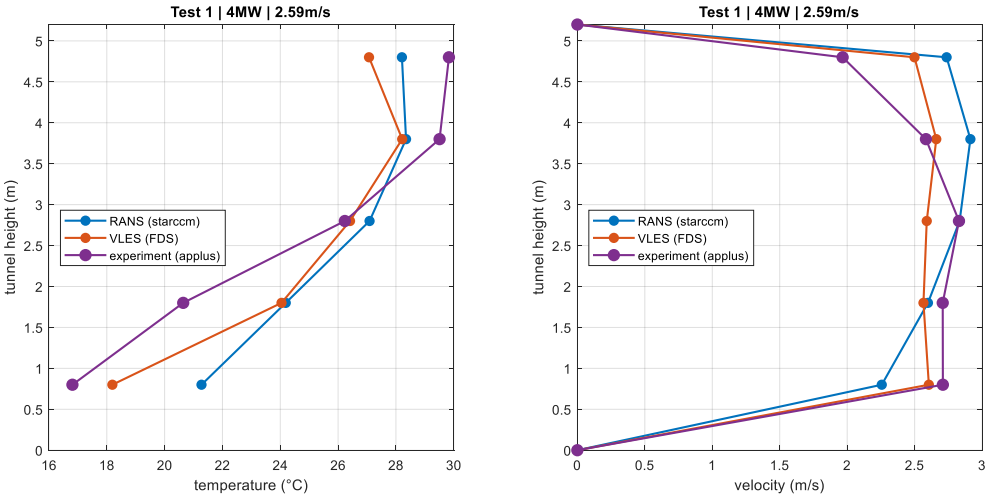

Figure 100: Temperature and velocity profile on PK522 for fire test 1

The dynamic 1-D simulation also allowed a comparison of the variation of the flow velocity during the test with the measurements at PK522, see Figure 101. While the simulation shows the start of the jet fan delayed against the measurement1, the target velocity agrees well. During the fire, the flow velocity is slightly reduced due to the resistance of the fire and – more importantly – due to increased buoyancy along the downward gradient of the tunnel. When the fire is out, the flow velocity returns to the initial value.

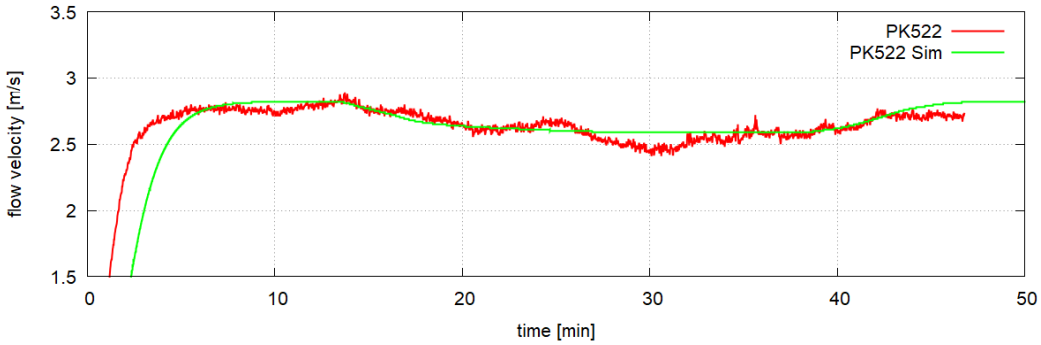

Figure 101: Comparison of the flow velocity, 1-D simulation vs. measurement at PK522

[1] In the 1-D model, the jet fan startup is defined to allow the simulation of PID jet fan control.

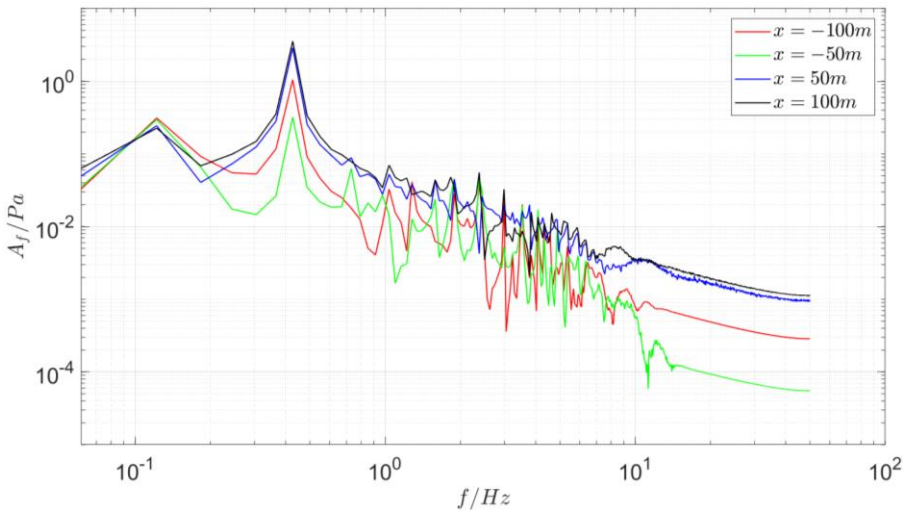

Figure 102: Frequency analysis Test 1, DES simulation

Figure 102 shows the frequency analysis for the DES simulation Test 1. We observe a peak frequency at 0.43 Hz, which matches the second harmonic frequency of a tube with the length of the test tunnel, but with one closed and one open end (0.425 Hz). The boundary conditions of the CFD model cause the tunnel oscillations to behave like a tube closed at one end. At the upstream portal, the flow rate is set to a fixed value. At the downstream portal, the pressure is set to ambient pressure. For the oscillation, the fixed flow rate represents a closed tunnel. In this respect, the CFD model behaves different from the physical tunnel, see Figure 59.

5.6.2 Test 2 - 4.22 MW, 3.7 m/s

Fire test 2 with a similar HRR but with two operating fans shows a similar picture to fire test 1, see Figure 103. The agreement in the pressure curve between the experiment and the simulation models is good, mostly within the expected measurement accuracy.

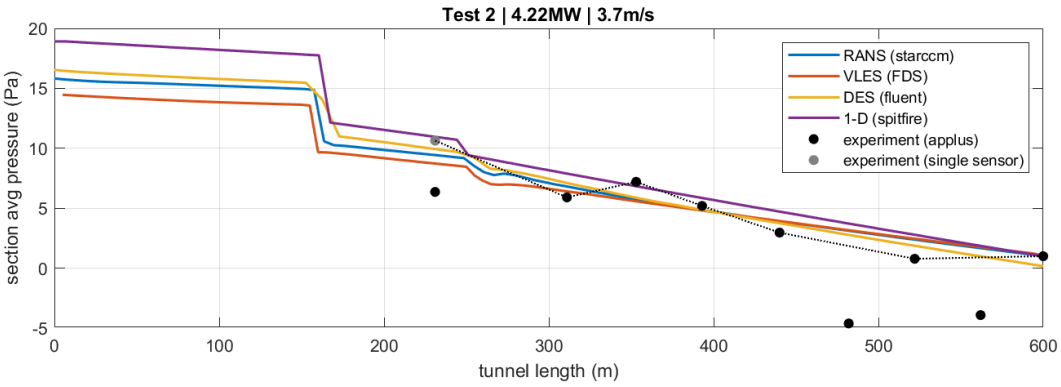

Figure 103: Pressure curve for fire test 2

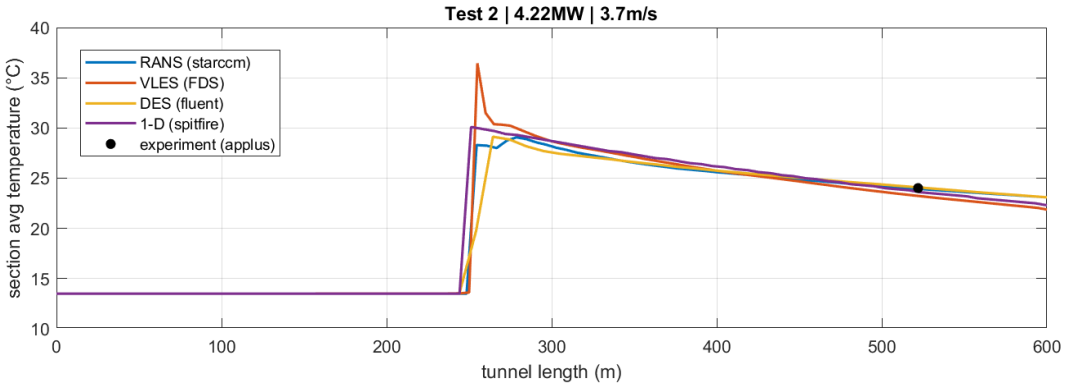

Figure 104: Temperature curve for fire test 2

The picture with the temperature and velocity profile is also very similar to fire test 1, only with slightly lower temperatures and slightly higher velocities, see Figure 105.

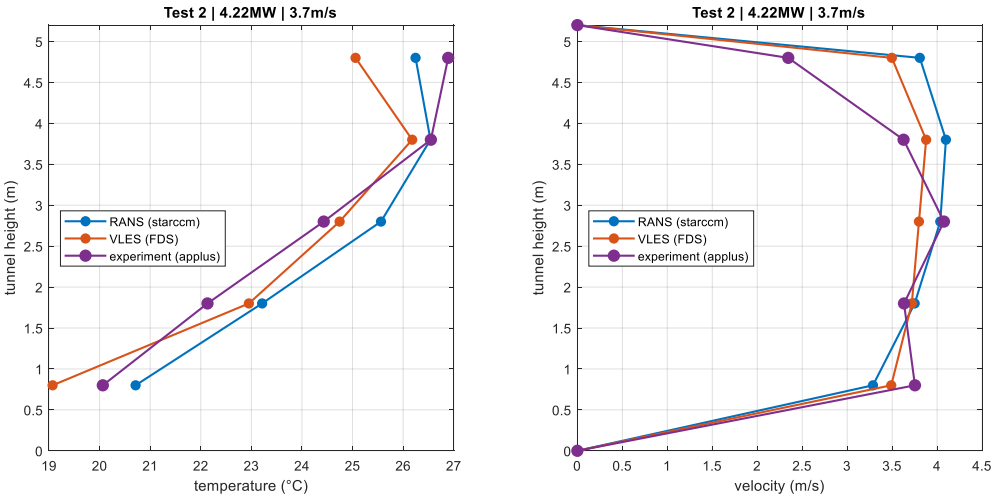

Figure 105: Temperature and velocity profile on PK522 for fire test 2

In Test 2, the comparison between the flow velocity of the 1-D simulation vs. the measurement at PK522 shows a higher flow velocity than the measurement. This could be corrected by assuming a smaller installation efficiency of the two jet fans vs. the one jet fan in Test 1 or by adjusting the meteorological boundary conditions. The parameters of the simulation were not adjusted, as it was the intention to evaluate the accuracy of the predicted airflow.

Like Test 1, the flow velocity is slightly reduced due to the resistance of the fire and due to increased buoyancy along the downward gradient of the tunnel. When the fire is out, the flow velocity returns to the initial value. The effect is less visible, as the flow resistance is dominated by increased friction due to the higher flow velocity. Also, the buoyancy is reduced with lower temperature downstream due to the increased velocity.

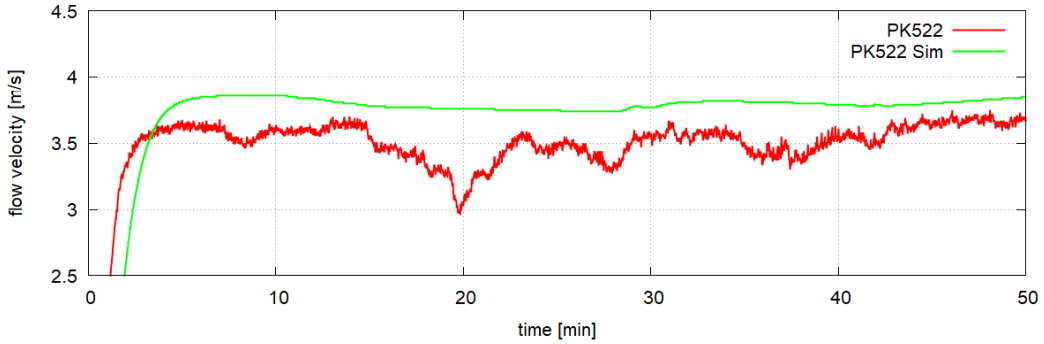

Figure 106: Comparison of the flow velocity, 1-D simulation vs. measurement at PK522

The measured flow velocity is more variable in Test 2 compared to Test 1. This is due to the variations of the external pressure on the tunnel portals.

5.6.3 Test 3 - 10 MW, 3.34 m/s

Fire test 3 is interesting because it uses 10 MW HRR. Here too, the simulation models show good agreement between the pressure curve and the measured data. Only the additional monitoring point at PK231 is slightly higher than in the previous tests, see Figure 107.

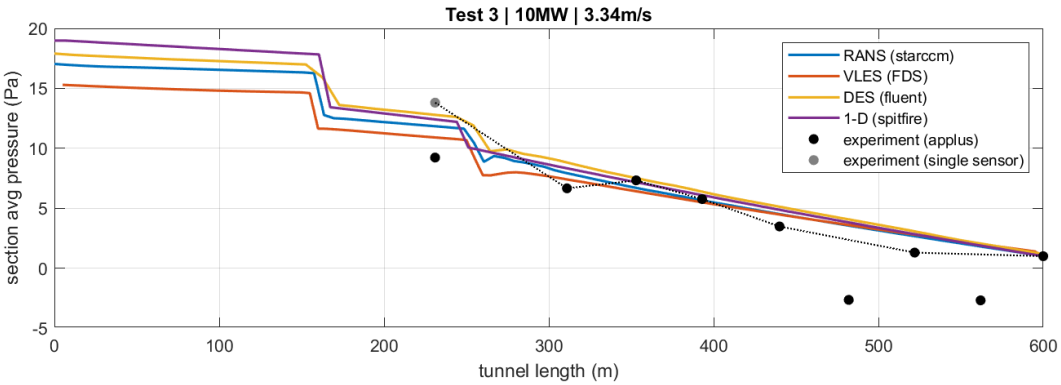

Figure 107: Pressure curve for fire test 3

In the temperature curve, the two 3-D simulation models are approx. 6 K higher than the experimental data point and the 1-D simulation. This could be a consequence of the relatively strong transients caused by the wind during this fire test. Both 3-D simulations were carried out with constant boundary conditions, while the spitfire simulation partially reproduces these transients.

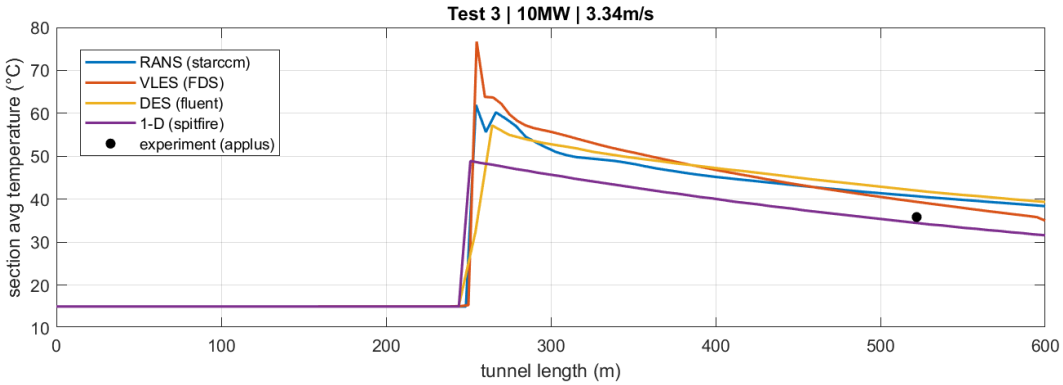

Figure 108: Temperature curve for fire test 3

The average 6 K lower temperature of the fire test can also be seen in the temperature profile. The "reversed" velocity stratification in the experiment is quite pronounced in this test.

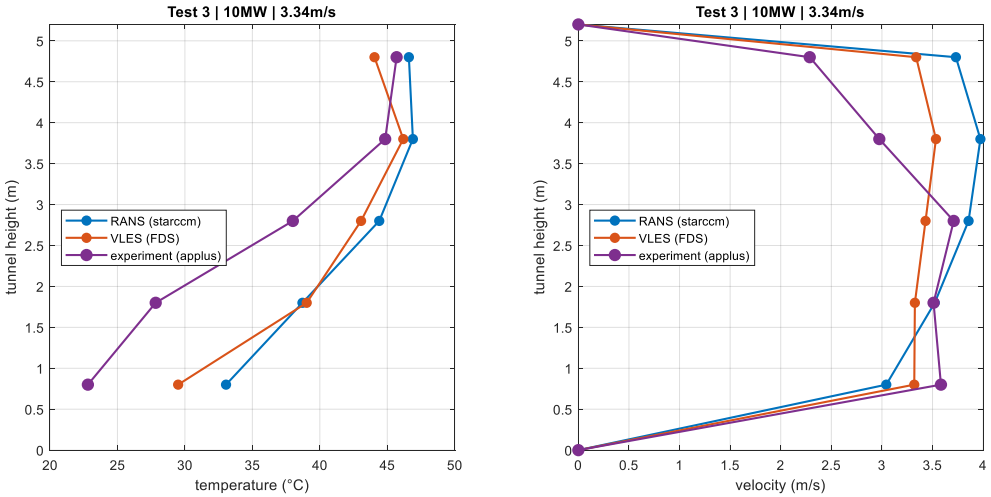

Figure 109: Temperature and velocity profile on PK522 for fire test 3

Many publications describe a layering effect in the velocity profile in the simulations, e.g. [26], with higher flow velocities at the tunnel ceiling. However, this effect cannot be seen in any of the three Applus TST fire tests. Even in the measured data from the Memorial tests, the velocity profiles tend to be the opposite of the stratification effect, as in case 610 with 54.3 MW and 4.3 m/s longitudinal velocity depicted in Figure 110.

The same case was simulated during this project with the RANS model. The temperature stratification is present in both the measurement and simulation data, but not in the velocity profile. However, this last measurement level is only 108 m downstream of the fire and not 270 m as in the Applus fire tests. At this point, the question arises as to whether the expected temperature stratification is actually present in the velocity profile or not.

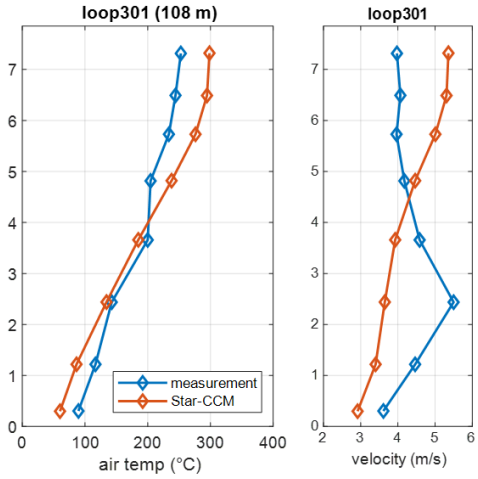

Figure 110: RANS vs. experiment of temperature and velocity profile of memorial measurement case 610 at loop 301

In Test 3, the comparison between the flow velocity of the 1-D simulation vs. the measurement at PK522 shows a slightly higher flow velocity than the measurement. The parameters of the simulation were not adjusted, as it was the intention to evaluate the accuracy of the predicted airflow.

Like Test 2, the flow velocity is reduced due to the resistance of the fire and due to increased buoyancy along the downward gradient of the tunnel. In Test 3, the reduction is more pronounced than Test 2, due to increased HRR. When the fire is out, the flow velocity returns to the initial value.

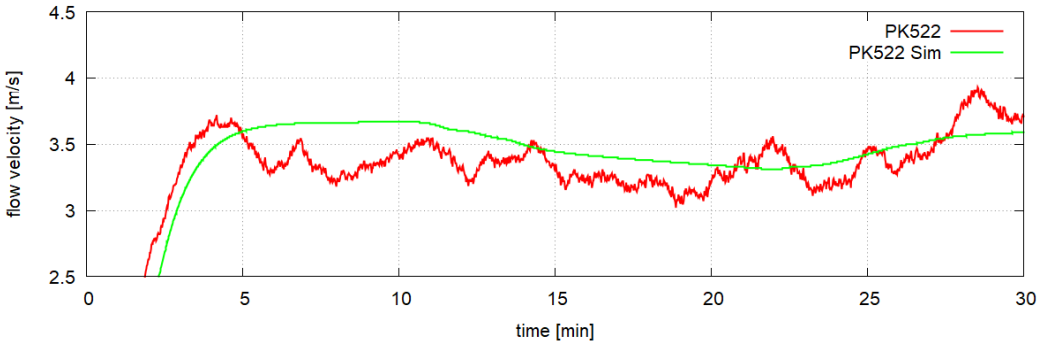

Figure 111: Comparison of the flow velocity, 1-D simulation vs. measurement at PK522

The measured flow velocity is more variable in Test 3 compared to Test 1. This is due to the variations of the external pressure on the tunnel portals.

5.7 Conclusion Results

- The 1-D, RANS and VLES simulation models show relatively little deviation from each other in the pressure and temperature curves for all three fire tests. They show good agreement with the measured values, meaning that the validation in this project can be considered successful.

- The temperature profiles for PK522 show a clear stratification effect in both the simulations and the measured values.
- The situation is different for the velocity profiles at PK522, 270 m downstream of the fire. Only the profiles from the RANS simulations show a clear stratification effect. The measured values show a "reverse" stratification effect in all three tests. The reasons for this are unclear. The velocity profiles from the VLES are rather flat with only a marginal stratification effect.
- URANS can be used as an effective precursor to DES to estimate the mesh requirement in scale resolving simulations.
- Two counter-rotating vortices are observed in the downstream of volumetric heat source, which initially transport the high temperature gas into the tunnel downstream. These vortices diffuse at certain downstream distance and leading to more turbulent mixing of the fluid and therefore more homogenized flow field.

6 Simulation Part B

Based on the numerical simulations and experimental observations performed during the project, it can be concluded that the simulation of Applus tunnel setup shows good agreement across the models for low heat release rates (up to 10 MW). However, a preliminary investigation of a longer tunnel with a higher heat release rate (30 MW) revealed some deviations between the models.

Therefore, this chapter introduces an objective: to perform simulations for a long tunnel under increased heat release conditions. In addition, the experience gained with the Applus tunnel is extended to investigate the varying high heat release rate effect for the same tunnel.

The simulation type considered here includes RANS with SST k-ω type turbulence closure. In addition, Very Large Eddy Simulation (VLES) implemented in Fire Dynamic Simulation (FDS) software is also used for such simulations. Further, scale-resolving DES is used for fire strength up to 30MW while simulating Applus tunnel geometry. The unsteady DES is also compared with unsteady version of RANS with same turbulence closure type of SST k-ω. The main objective of the current section includes:

- An investigation into the throttling effect for varying heat release rate, varying cross-section types and a comparison of the results across software platform and simulation models.
- An analysis of the differences in the flow resistance estimates (pressure drop) between steady-state RANS with VLES for varying heat release rate and further comparison with the 1-D Spitfire model.
- Application of DES to investigate average flow properties for varying heat release rate in the case of the Applus tunnel. Choice of DES as against LES is to avoid high computational cost near the wall, while capturing the turbulent flow features and dynamics within the tunnel especially downstream of the fire.

Two different tunnel geometries are simulated in this section, which include:

- In the first case, a 900m long straight tunnel is simulated for tunnel volumetric heat source strength of 4, 10, 30 and 50MW. In addition, one percent slope against the flow is also considered. This tunnel is denoted as long tunnel in the rest of the chapter.
- In the second case, the Applus tunnel is simulated with no slope and volumetric heat source strength of 10, 20 and 30MW.

6.1 Long Tunnel simulation results

A straight 900m long tunnel with fire placement at 100m after the entry location is considered. Three different types of cross section geometry are used for the tunnel with height of and breadth described in the following table.

Tunnel Cross-sections

	Flat tunnel	Tall tunnel	Arched ceiling
Width B [m]	12.5	8.5	9.5
Height H [m]	5.2	7.65	8.0
Area A [m²]	65.0	65.0	65.0

Table 12: Tunnel cross-sections used in the long tunnel simulation

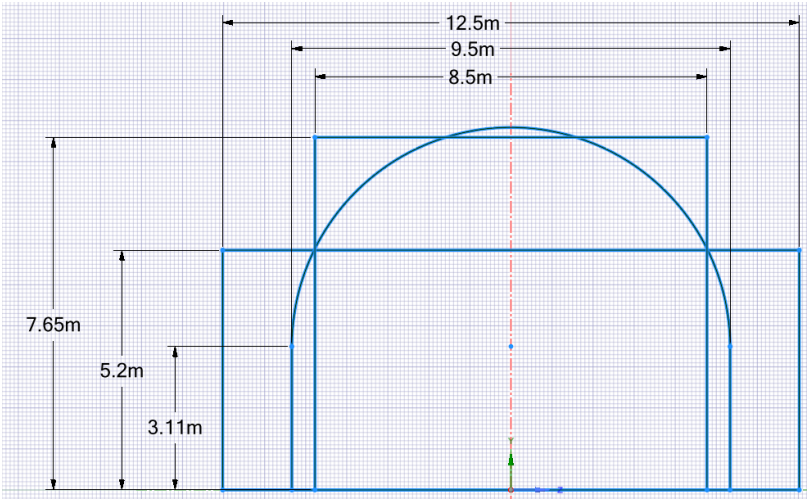

Figure 112: Tunnel cross section geometric parameters for three types of cross section as flat, tall and arched ceiling

As obtained in Table 12, three different cross-sections with the same cross-sectional area of 65m² and varying height (H) and width (B) are used in the simulation. The cross-section types are denoted as flat tunnel, tall tunnel and arched ceiling. Both flat tunnel and tall tunnel correspond to rectangular cross-sections. The flat tunnel has a larger width of 12.5m compared to 8.5m in the case of the tall tunnel. The arched tunnel has a cross-section with a rectangular bottom part of height 3.11m and width 9.5m. The top part is semi-circular with a diameter of 9.5m.

The simulation models considered here are VLES and RANS and for comparison the 1-D model spitfire. FDS is used for VLES and StarCCM is used for RANS simulations. The tunnel entry flow velocity of 3m/s is considered, and inlet temperature was kept at 286K. Same simulation set-up as described in section 5.3 is also used here. Two FDS versions are tested here. The version FDS 6.8.0 is also used in the simulation of Applus tunnel testcase. A new version FDS 6.9.1 is used to compare the results for higher heat release rates. The RANS simulation is used for all comparison of all three types of cross-sections. However, FDS is used only for rectangular cross-section. The 1-D spitfire model effectively considers the effect of each cross-section into the solution of the smoke and temperature convection and therefore separate estimation can be performed using 1-D model for each type of cross-section.

Figure 113 and Figure 114 obtain the average pressure along the tunnel for heat release rate case of 30MW for the two case of one percent slope and no slope respectively. It is also obtained for three different types of simulation models. The variation in average pressure solution for all different cross-sections is minor while using RANS simulation

and one percent slope. In case of no-slope, the arched type of cross-section observes more pressure-drop across the fire. Physical reasoning or numerical issue regarding this observation could not be identified at this moment and requires further investigation. The average pressure for one percent slope case decreases while using VLES as compared to RANS simulations, whereas 1-D results observe intermediate values for pressure between the two different 3-D simulation approaches.

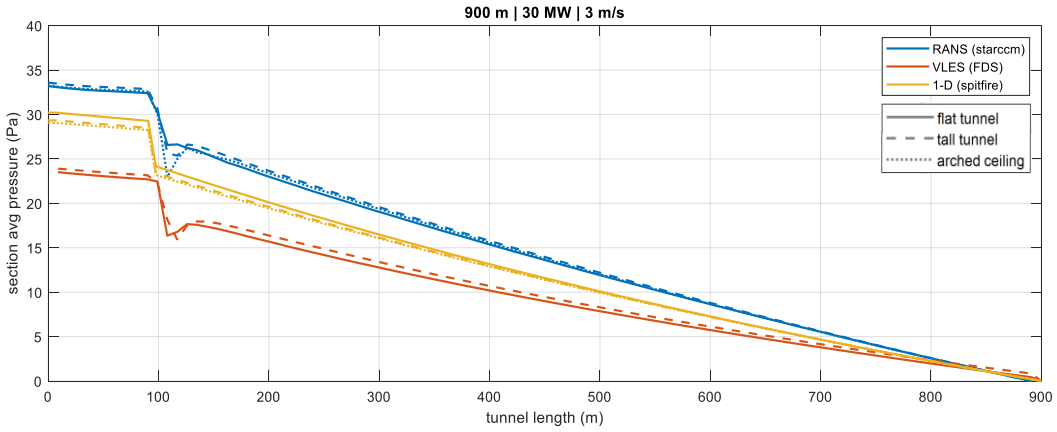

Figure 113: The average pressure for a 30MW fire along the tunnel with a 1% incline in the direction of the flow

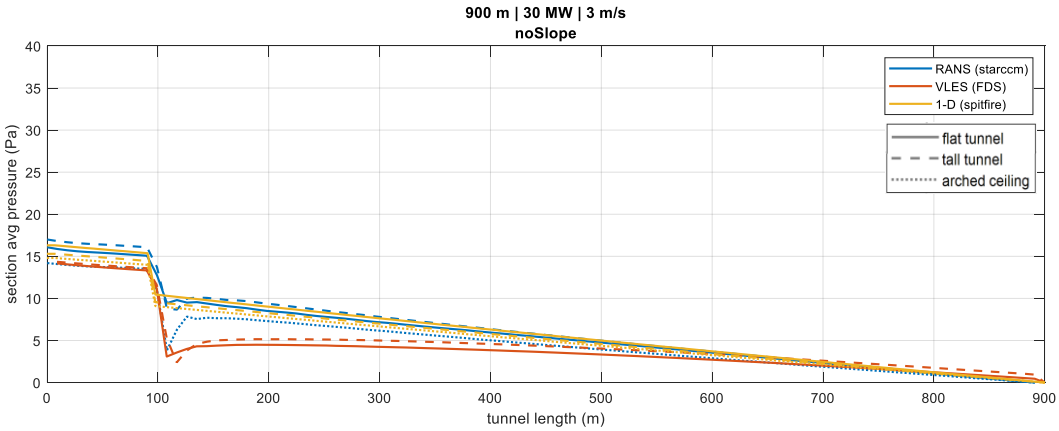

Figure 114: The average pressure along the tunnel using 30MW tunnel fire strength and no slope of the tunnel and FDS 6.9.1

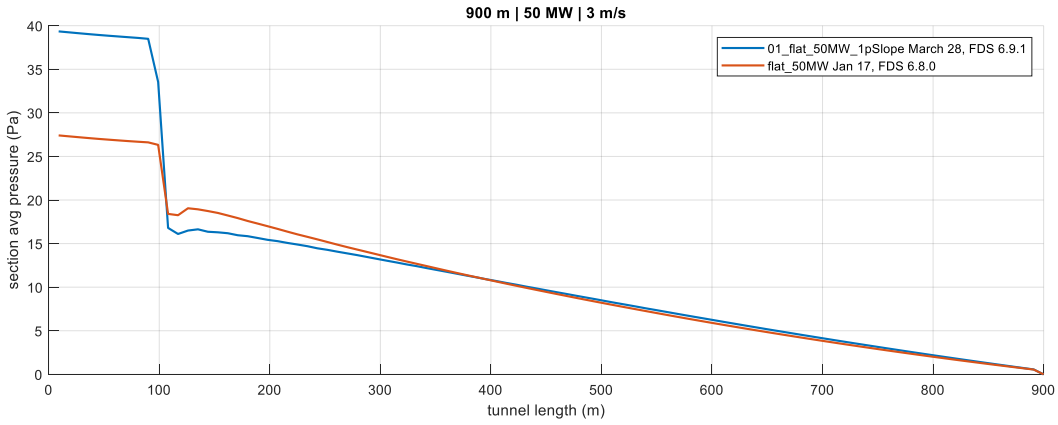

Figure 115: Comparison of FDS 6.8.0 and FDS 6.9.1 in the case of 50MW fire

The pressure solution obtained using FDS results with version 6.9.1 is observed to be much larger compared to FDS 6.8.0 version for the case of 50MW fire case, see Figure 115. This, therefore, indicates the uncertainty in using VLES modelling and FDS software to estimate the pressure-drop in the case of higher value of heat source terms. It appears that significant changes have been made to the pressure solver of FDS between versions 6.8.0, 6.9.1 and 6.10.0, see Figure 116. This indicates limitations of any validation of Fire Dynamic Simulator for tunnel fire applications.
The other two software packages used, Star-CCM+ (version v2302) and Fluent (2024R2), were not examined for variations in the results. However, due to the large number of applications in various projects in recent years, such large fluctuations have never been observed, and it was therefore decided not to test different versions for the tunnel application.

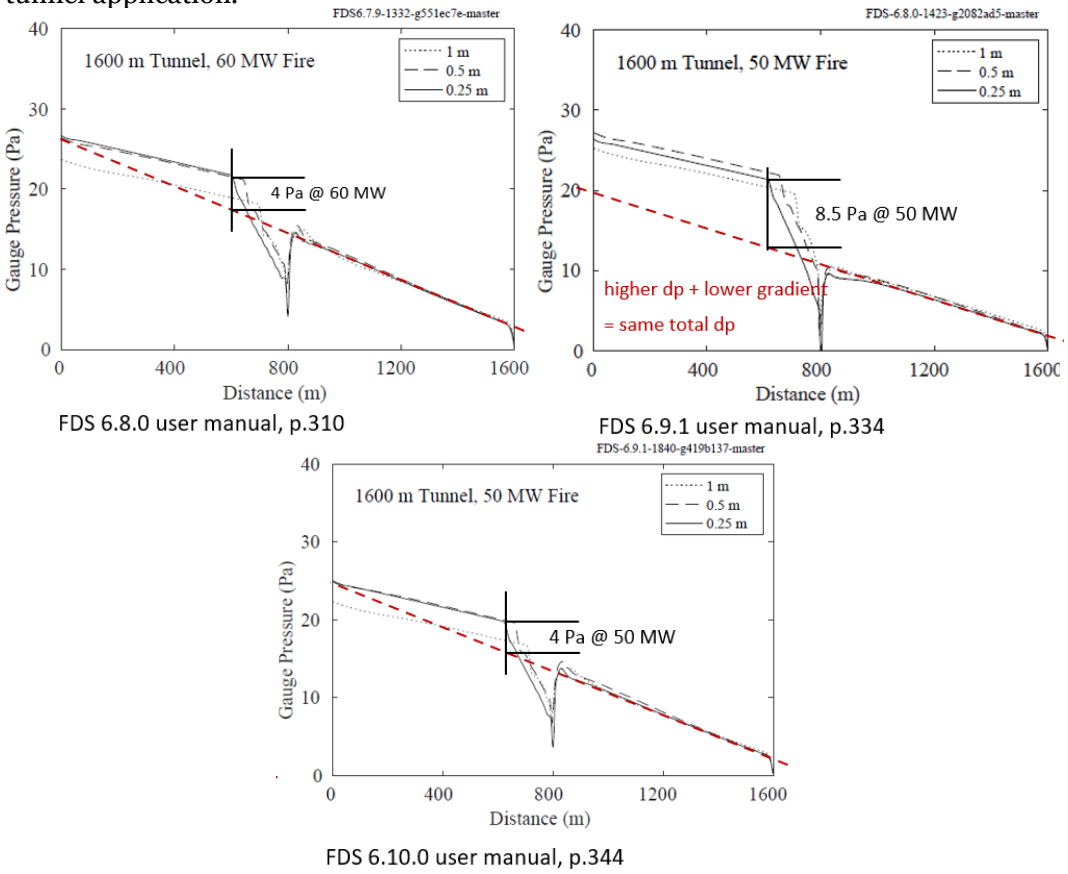

Figure 116: Comparison of FDS 6.8.0, FDS 6.9.1 and FDS 6.10.0 (graphs taken from different versions of the FDS user guide [33])

The combined results of varying heat release rates for the pressure drop along the tunnel are presented in the following set of figures.

In Figure 119 the average pressure drop obtained from RANS (Star-CCM+) simulations for three different tunnel cross-section types under varying heat release rates are reported. The solutions are obtained for the one percent slope case. The left plot presents the pressure-drop along the entire tunnel (Δp_t). The centre plot obtains the pressure-drop across the fire location (Δp_f), and the right plot corresponds to the pressure drop (Δp_pf) in the fire downstream section. To evaluate the pressure-drop across the fire and downstream regions, two monitoring points were selected: one at approximately

90 m from the tunnel inlet (just upstream of the fire, which is located at 100 m), and another at approximately 135 m from the inlet. The second point is placed far enough downstream of the fire so that the influence of fire-induced nonlinearities on the pressure drop is negligible. All three average pressure drop remains nearly unchanged while using different cross-section types in the case of one percent slope as observed in the Figure 119.

However, as reported in the Figure 118, RANS simulation observes non-monotonic trend in the fire downstream pressure-drop for heat release rate of 30 MW while using arched-ceiling cross-section and no-slope for the tunnel. This behaviour arises because the large pressure drop across the fire is not fully recovered downstream, unlike in the case of rectangular cross-sections.

Figure 117 and Figure 120 compare the pressure drop for the flat rectangular cross-section type by using three types of simulation models for one percent slope and no-slope case, respectively. The 1-D Spitfire model compares well with the RANS SST k-ω turbulence model for flat cross-section type. However, the VLES prediction varies significantly from RANS simulation. It obtains lower pressure-drop in all three plots in the case of one percent slope, see Figure 117. Further, in the case of no-slope in Figure 120, a decreasing pressure drop with increase in heat release rate is observed for the fire downstream region while using VLES. However, the pressure drop across the fire is higher in VLES compared to RANS and 1-D in the case of no-slope.

A similar decreasing trend for VLES, in the case of no-slope of tunnel, is also observed for cross-section type tall as observed in Figure 122 for fire downstream region. The one percent slope case for tall cross-section observes the lower pressure-drop using VLES as compared to RANS and Spitfire, see Figure 121. Finally, the 1-D model also observes non-monotonic pressure-drop in the case of no-slope simulations, see Figure 121. Such large variation in pressure-drop, non-monotonic behaviour and variation across the software versions (see Figure 115) demands a more detailed investigation using high-fidelity unsteady simulation types such as LES.

In the case of 4 and 10 MW, RANS corresponds very well with the Spitfire calculations, with deviations of <1 Pa (<5%). At higher HRRs of 30 or 50 MW, however, there are larger deviations of 5 Pa (approx. 10%) or, in the case of the curved ceiling, even approx. 30%, see Figure 121. As there is no measurement data available for the pressure drop at 30 or 50 MW, it is not possible to assess which of the two models provides the more accurate prediction.

In view of computational cost limit in resolving very small eddies near the wall, LES is replaced with relatively cheaper simulation type DES. Further, experiences with different mesh resolution types in DES for the case of relatively high heat release rate of 10MW is already developed in section 5.4.2. Therefore, further simulation is performed for Applus tunnel geometry with varying heat release rate. The subsequent sub-section describes about the simulation results with DES, and its comparison with unsteady RANS for the case of Applus tunnel while using volumetric heat release rate of 10,20 and 30MW.

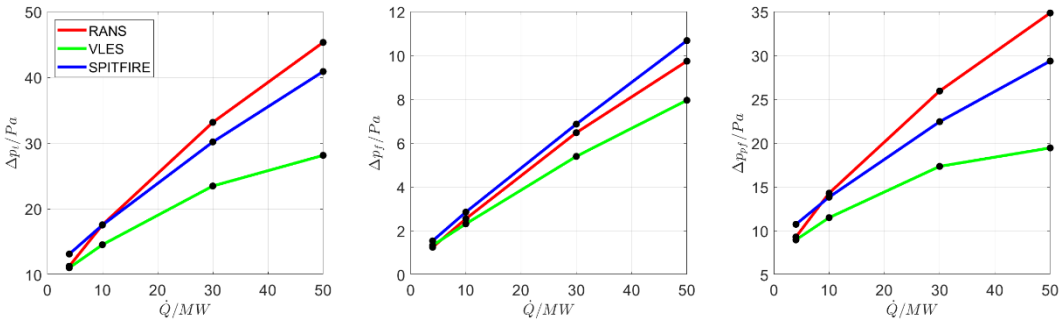

Figure 117: The pressure-drop along the tunnel (left plot), across the fire (centre plot) and along the tunnel downstream of the fire (right plot) for varying heat release rate and different simulation models using cross-section type **flat** and the case of one percent slope

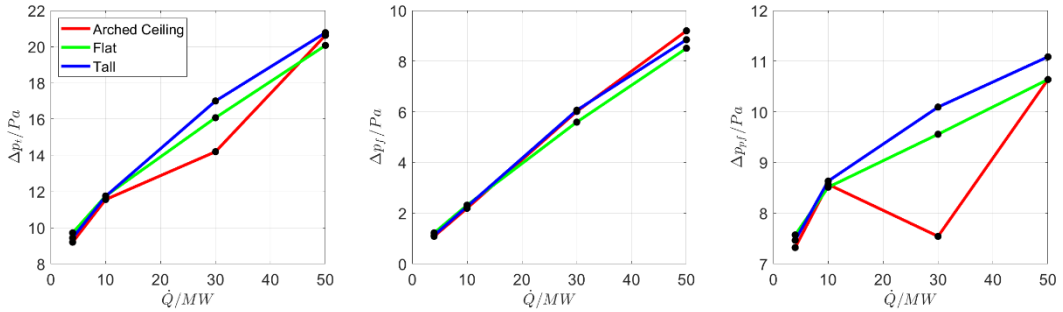

Figure 118: The pressure-drop along the tunnel (left plot), across the fire (centre plot) and along the tunnel downstream of the fire (right plot) for varying heat release rate and RANS simulation with no slope of tunnel

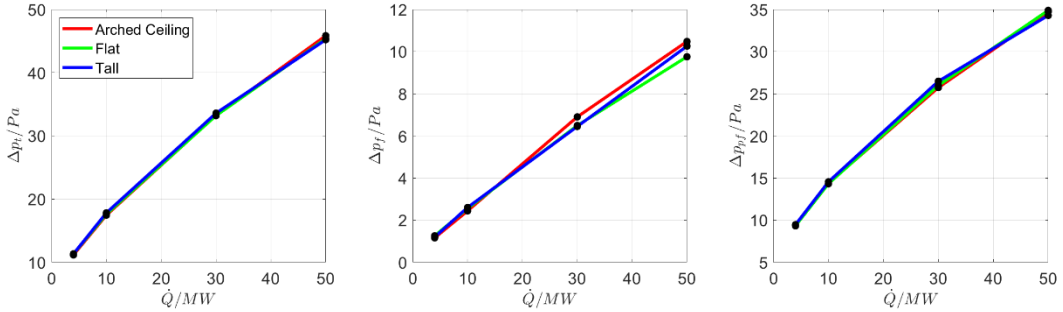

Figure 119: The pressure-drop along the tunnel (left plot), across the fire (centre plot) and along the tunnel downstream of the fire (right plot) for varying heat release rate and RANS simulation and the case of one percent slope

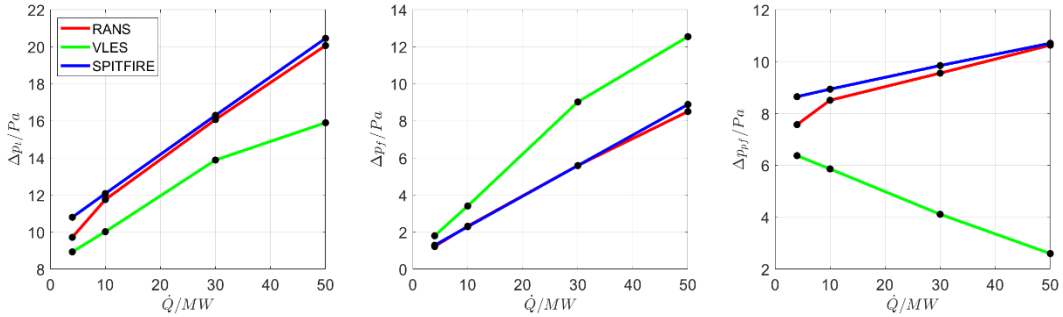

Figure 120: The pressure-drop along the tunnel (left plot), across the fire (centre plot) and along the tunnel downstream of the fire (right plot) for varying heat release rate and different simulation models using cross-section type **flat** and no slope of tunnel

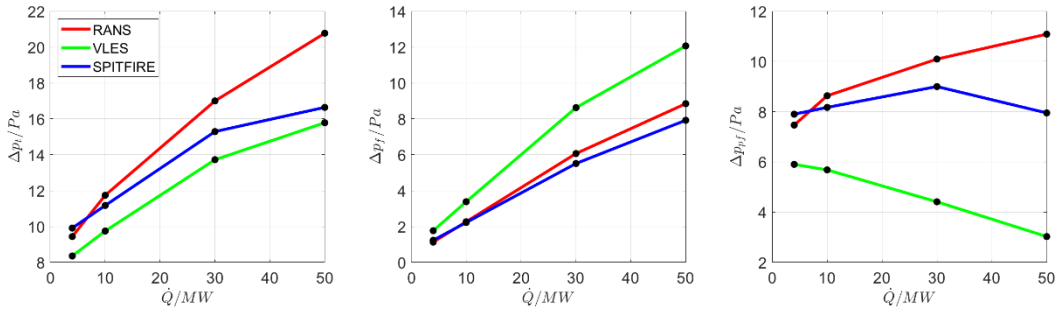

Figure 121: The pressure-drop along the tunnel (left plot), across the fire (centre plot) and along the tunnel downstream of the fire (right plot) for varying heat release rate and different simulation models using cross-section type **curved?** and no slope of tunnel

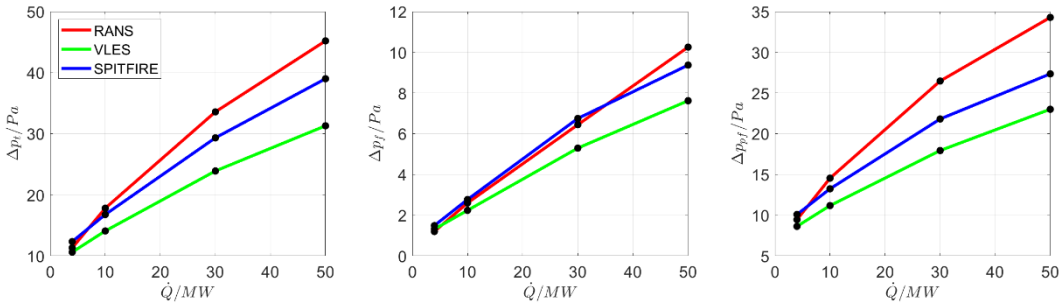

Figure 122: The pressure-drop along the tunnel (left plot), across the fire (centre plot) and along the tunnel downstream of the fire (right plot) for varying heat release rate and different simulation models using cross-section type **tall** and the case of one percent slope

6.2 Applus Tunnel with varying heat release rate

In this section a comparison of the effect of varying heat release rate on pressure drop is considered in the case of the Applus tunnel. No slope in the tunnel is considered and the volumetric heat release rate is varied from 10MW, 20MW and 30MW.

The simulation is performed using DES and URANS. The SST k-ω turbulence modelling is used for URANS. Further details about DES and URANS can be found in the section 5.4.2. In short, URANS is unsteady version of RANS and therefore requires time sampling of the simulation results. Also, as described in section 5.4.2, URANS is used to optimize mesh resolution requirement of DES for the case of 10MW fire with no slope. Table 10 provides the comparison of different mesh types used in DES and URANS. It is established in section 5.4.2 that mesh type Mesh3 has enough resolution to resolve the eddy size interior of the tunnel while using DES. Therefore, DES using Mesh3 is compared with computationally cheaper URANS using Mesh1 for the test-cases 10MW, 20MW and 30MW fire strength. In the previous subsection, the long tunnel is simulated using steady state RANS with SST k-ω turbulence closure. Further Star-CCM+ software is used in the context of RANS solver for long tunnel. Here, both URANS and DES are performed for Applus tunnel using Ansys-FLUENT simulation software.

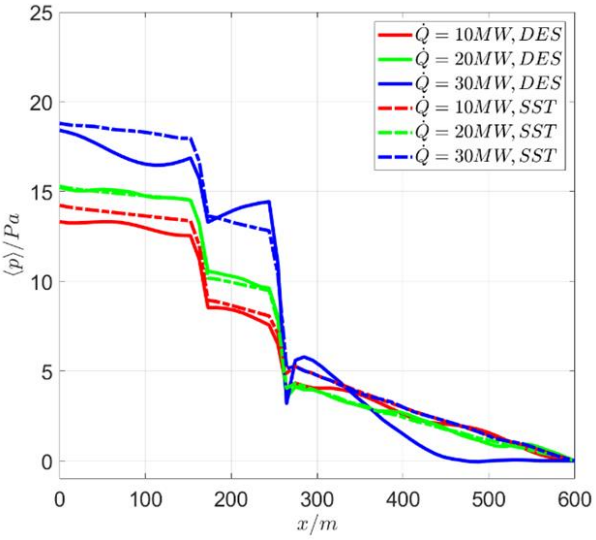

Figure 123: Comparison of average pressure for Applus tunnel using DES and varying heat release rate

The time dependent simulation further required data sampling in time for the simulation results to obtain average pressure values. For heat release rate cases of 10MW and 20MW, a time sampling of 0.4s is used. The high heat release rate of 30MW required higher sampling frequency to average out the high frequency pressure variations. Therefore, a sampling rate of 0.1s is considered for averaging in the case of 30MW fire. Figure 123 provides a comparison of DES and URANS simulation result for time averaged value of mean static pressure at different locations through the tunnel axis. It is observed that the URANS simulation with the low-resolution mesh (Mesh1) provides a smoother time-averaged pressure solution at the same sampling rate, compared to the DES simulation with a high-resolution mesh. For both test cases (10 MW and 20 MW fire), the DES results show mild variations in the time-averaged pressure relative to the expected linear pressure drop along the tunnel. Since DES is a blending method between URANS and LES, use of low-resolution DES is equivalent to using URANS and therefore it is of no advantage to capture the turbulent flow features by using low mesh resolution while using DES. High mesh resolution DES, as used here, is expected to perform better in estimating the average properties when higher time resolution is used both for sampling and simulation. The variation from URANS and expected linear pressure drop is more apparent in the case of DES while using it for high heat release rate value (30MW fire). In this case, use of higher time resolution for sampling (0.1s) is still not sufficient to remove the high frequency oscillations while using DES. The deviating behaviour of the '30 MW, DES' curve is therefore due to the insufficient sampling frequency for averaging.

DES also provides a recipe for using highly resolved LES. In LES, the wall modelling requires more higher resolution, and therefore it can be computationally further demanding to perform LES for long tunnels with higher heat release rate. However, using DES with higher time resolution, if a converged solution can be obtained, then it can be used to identify the spatio-temporal resolution requirement for LES. It can be a necessary condition for LES studies in tunnel fire to obtain a well resolved and converged DES at least in the sense of average flow and turbulent properties. To obtain a sufficient condition for mesh and timestep size requirement for LES, a further investigation into

near wall refinement is required. This is because, DES relaxes the wall resolution requirement by using RANS near the wall as described in section 5.4.1.

Figure 124 obtains the area averaged solutions for pressure (top left), standard deviation of pressure (top right), fluid speed (bottom left) and temperature (bottom right) using mesh type Mesh1 and URANS-SST at varying heat release rate. The sampling rate of 0.4s is used in this simulation.

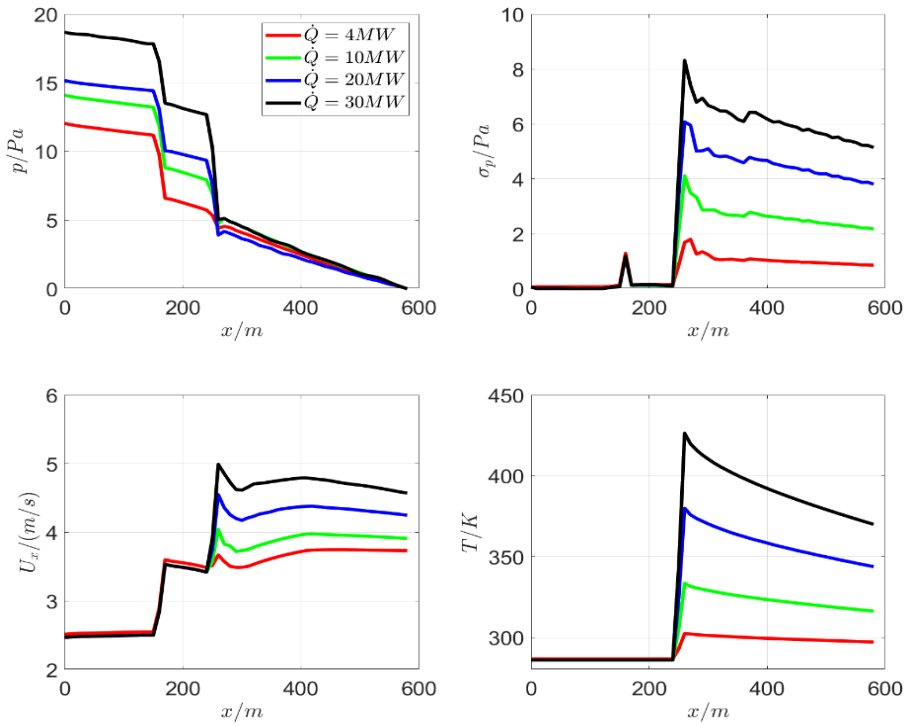

Figure 124: Comparison of average pressure, pressure deviation, average temperature and average flow speed for Applus tunnel using DES and varying heat release rate

URANS is used in this comparison because DES result shows nonlinear pressure drop due to inefficient time sampling in the case of 30MW fire. An increase in the standard deviation of pressure (top-right plot of Figure 124) is observed with higher heat release rates, particularly downstream of the fire location. The mean pressure along the tunnel (left plot of Figure 124) does not change significantly downstream of the fire. As expected, however, the pressure drop due to throttling effect increases with increase in heat release rate. The elevated standard deviation of pressure across the tunnel cross-section also indicates non-uniform flow behaviour and the presence of spatio-temporal features such as vortices and vortex breakdown downstream of the fire. While average quantities are sufficient to assess longitudinal ventilation strength, these cross-sectional deviations should be further investigated to understand their impact on ventilation requirements, especially under high heat release conditions.

The variation of flow properties near the fire is better understood by observing the temperature and longitudinal flow speed at different cross-sections downstream of the fire. In this regard, the cross-sectional temperature and flow speed along the tunnel

are obtained in the Figure 125 and Figure 126, respectively. Horizontal row of each of this figure corresponds to the solution (temperature and flow speed) at cross-section 10m, 14m, and 20m downstream of fire for a specific heat release rate value. The corresponding heat release rate ($\dot{Q}$) is mentioned in the left of the row. The corresponding distance from the fire is mentioned in the top of each column (x_f). Two distinct flow features are observed for low heat release rate value (3.33MW). Further investigation demonstrates the presence of two counter rotating vortices in the fire downstream. This corresponds to flow bifurcation downstream of the fire. These counter rotating vortices decay at a certain distance downstream of the fire and allow more mixing among eddies of different temperature.

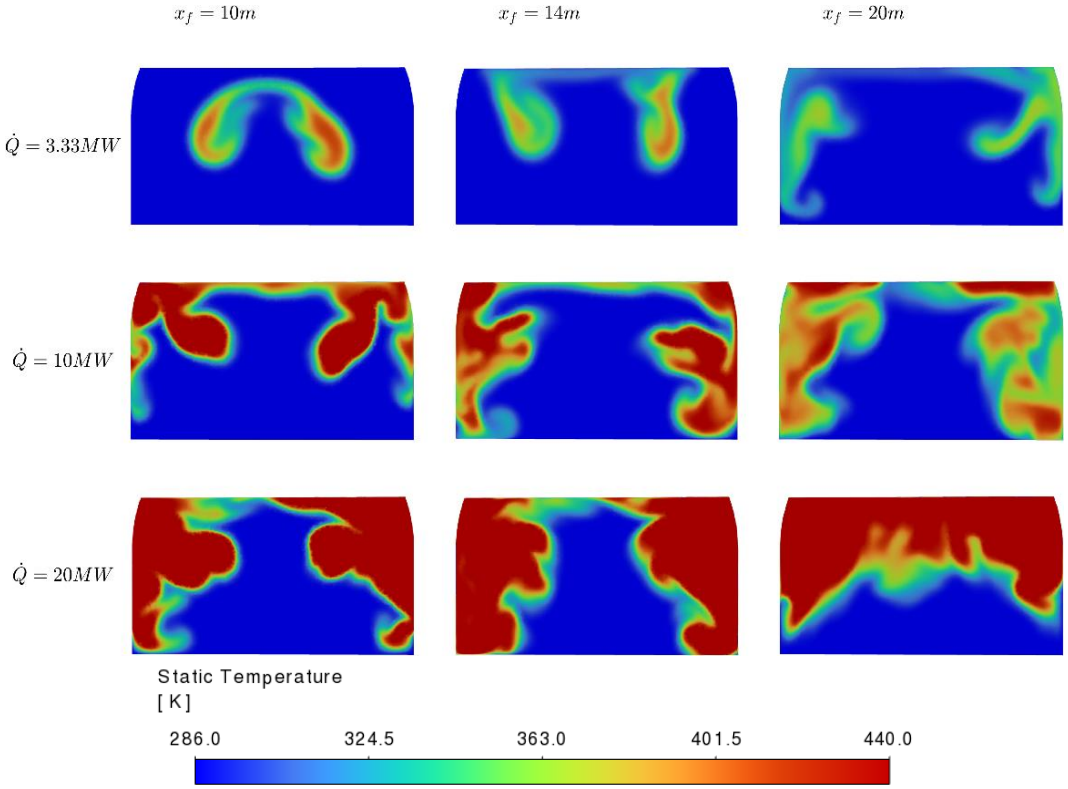

Figure 125: The temperature field along three different planes downstream of fire for three different heat release rates simulated using DES

The distance, up to which the stable counter rotating vortices are extended, depends on heat release rate and flow speed. This further contributes to temperature stratification. In the current simulation results, temperature stratification develops for heat release rate of 20MW at 20m downstream of the fire, see Figure 125. The low heat release rate values require longer distance downstream of the fire to establish the temperature stratification. As observed in Figure 126, momentum mixing along the tunnel axis can also be attributed to the extension and breakdown of such counter rotating vortices, which is more prominent for high heat release rate. Therefore, more uniform flow behaviour across the tunnel cross-section is observed for high heat release rate when compared to the low heat release rate case of 3.33MW.

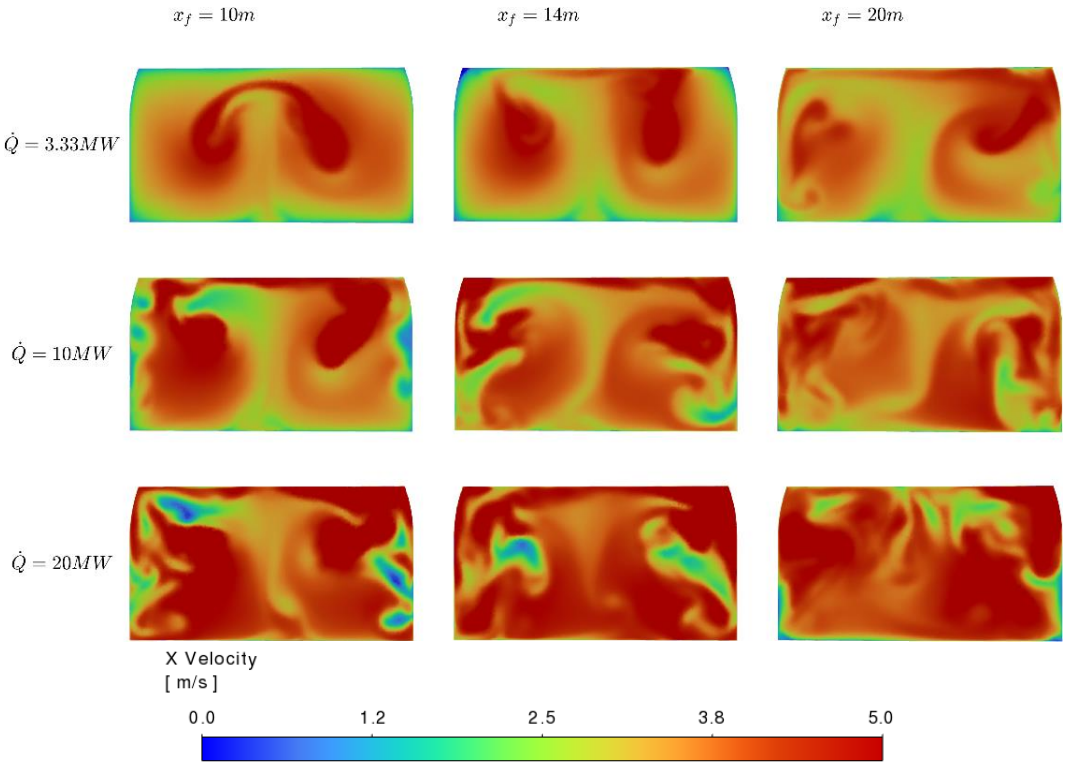

Figure 126: The fluid velocity along tunnel axis for three different planes downstream of fire for three different heat release rates simulated using DES

In conclusion, it is observed that URANS can be used to estimate the average flow properties with good sampling rate in time. In addition, it allows low mesh resolution to estimate the average quantities. Further investigations also portray that URANS can capture some dynamic flow features as well, for example the counter rotating vortices downstream of the fire. In comparison, DES requires more higher mesh resolution and time resolution. In addition, with increasing heat release rate, higher sampling rate is required in DES to obtain smooth average flow properties. However, it captures the details of turbulent features and high frequency oscillation especially around and downstream of the fire. In addition, the standard deviation of pressure increases with increase in heat release rate. Therefore, average estimates for ventilation studies have larger uncertainties with increase in heat release rate. This, therefore, demands high-fidelity simulation such as DES or even LES with increased heat release rate.

The simulation using steady state RANS as described in previous subsection is also useful for average pressure-drop estimation along the tunnel. However, by construction, it cannot capture the dynamics of flow during interaction with fire. Finally, while using FDS or any other software with scale resolving simulation types such as LES, a thorough pre-study for mesh resolution requirement must be performed with URANS/RANS. This provides the necessary conditions for mesh and timestep size in the context of LES. 1-D model such as Spitfire is very useful to estimate the average flow properties. However, such models cannot capture the uncertainties such as standard deviation or higher order statistics of the average quantities across the tunnel cross-sections.

7 Application

7.1 Sensitivity Study ASTRA 13001

In this chapter, the requirements of the guideline ASTRA 13001 on ventilation of road tunnels [1] are examined for inherent safety margins in the design of longitudinal ventilation systems. The sensitivity study represents an update to the study presented in [15] and [16], but updated to consider the revised model for the throttling effect.

It is explicitly not the intention of this investigation to show design reserves of the guidelines to promote a reduction of these reserves. The present study is concerned with an assessment of possible reserves against the influence of the flow resistance of a fire, which may not have been considered in the design.

This flow resistance is only considered for mechanical longitudinal ventilation system. Tunnel ventilation systems with local smoke extraction are not affected. When a smoke extraction system is operated according to the guideline ASTRA 13001 [1], the flow velocity at the fire is small. The local expansion of the airflow according to equation (52) does not add to an overall pressure drop. Also, there is no longitudinal airflow at high temperature downstream of the fire (equations (53) and (54)).

Ventilation systems with massive extraction downstream of a fire may require special analysis. In the tunnel section between the fire and the point of extraction can the throttling effect (equations (52) to (54)) be addressed like a tunnel with longitudinal ventilation between the fire and the downstream tunnel portal.

7.1.1 Methodology

Within the framework of tunnel ventilation design, the Swiss guideline [1] requires the consideration of scenarios for selection and distribution of jet fans. The considerations in this sensitivity study are limited to quasi-steady state conditions. The emergency ventilation is driving the design of ventilation systems with longitudinal ventilation. Thus, only these design cases are dealt with here.

The guideline ASTRA 13001 [1] defines methodology and boundary conditions to be used for the design of tunnel ventilation systems. If possible, the design conditions are derived from project-specific data. Individual contributions are assigned a probability of occurrence, such as the 95-percentile of the natural temperature difference between the tunnel and the ambient. The essential data required for ventilation design are:

- Tunnel geometry
  - Longitudinal gradient
  - Wall roughness
  - Local pressure losses
- Traffic
  - Traffic volume
  - Traffic composition

- Meteorology
  - Natural temperature difference
  - Wind loads
  - Barometric pressure differences
- Fire
  - Heat release rate
  - Location
- Ventilation mode
  - Design and specification of ventilation control

In the following, it is assumed that the input variables are independent of each other. In principle, dependencies are possible, e.g. between the share of heavy goods vehicles in the traffic mix and an expected heat release rate. However, these dependencies are excluded here.

An inherent safety margin cannot be generally determined from the percentile values of the thermal buoyancy and thus the heat release rate can be decisive for the design of the longitudinal ventilation system, whereas in an urban, congestion-prone but flat tunnel the flow resistance of the vehicles can be decisive. In a tunnel that cuts through a mountain range, however, the barometric pressure difference can determine the design of the ventilation system. For this reason, the following analysis is based on three sample tunnels. All three tunnels are equipped with longitudinal ventilation with jet fans in accordance with the design code.

Sample Tunnels

Parameter	Tunnel A	Tunnel B	Tunnel C
Type	Alpine tunnel	Near urban bypass tunnel	Urban tunnel
Length	1 km	2 km	1 km
Cross-section		2-lane arched profile	
Gradient	3%	0.5%	0.5%
Traffic characteristic	GV	RV1	RV2
Traffic volume	10’000	20’000	40’000
Share of heavy goods vehicles	10%	10%	10%
Natural temperature difference	2K per 450 m	1K per 450 m	1K per 450 m
Wind and barometric pressure	5 Pa	10 Pa	5 Pa
Heat release rate (nominal)	30 MW	30 MW	30 MW
Minimum airflow velocity (design)	1.5 m/s downhill	3.0 m/s downhill	3.0 m/s downhill
Airflow velocity (operation)	1.0 m/s	2.5 m/s	1.0 m/s

Table 13: Sample tunnels A, B and C

For the three tunnels, first a design calculation will be carried out without inclusion of the throttling effect. The design is then varied by using the mean value or median or the set-point value of operation for individual input variables. This results in a reduction of the required thrust of the jet fans. In this way the sensitivity of the design is determined.

7.1.2 Design Data

Regarding the tunnel geometry as well as the wall roughness, no statistical analysis is useful. The tunnel geometry is clearly defined in the design. λ=0.015 is used for the as wall-friction coefficient [1]. This includes a general assumption on the flow resistance of typical tunnel installations (cable trays, lighting, traffic signals). Installations may vary from tunnel to tunnel. Flow measurements in two-lane road tunnels indicate that the value of λ=0.015 does not include a safety margin. For large tunnel cross-sections (e.g. three-lane arched cross-sections) the real friction coefficient can be lower.

For traffic volume, a relevant hourly traffic volume is derived from the annual average daily traffic volume AADT and a traffic characteristic. As a rule, this is 11% of AADT. The correlation corresponds to an assumption of the 30th most heavily loaded hour of the year, i.e. a 99.7-percentile. If traffic volumes are high, a high frequency of congestion is assumed, according to which the traffic volume is derived from lane capacity. If the occurrence of a fire is independent of the traffic volume, the expected value of traffic volume is 1/24 or 4.2% of AADT.

The share of heavy goods vehicles HGV includes a safety margin by using a combination of an average HGV share and a high traffic volume for the design. Typical daily patterns are characterised by peaks in passenger traffic and a comparatively even load of heavy goods vehicles. This results in a relatively low share of heavy goods traffic during peak hours. Based on typical load curves for traffic and heavy goods vehicles, we estimate the average share of HGV in a peak hour at 60% of the daily average.

In ASTRA 13001 [1], a 95-percentile is specified for the determination of the stack effect due to the natural temperature difference between the inclined tunnel and the ambient. It is stated that the temperature is largely constant over the length of the tunnel and usually a few Kelvin above the mean annual temperature. In the absence of local data, the natural temperature difference is given as a 95-percentile with 1 to 2 K per 450 m tunnel length. For the sensitivity study we follow this specification. But we assume the expected value for the temperature difference as 0 K difference.

For adverse wind load on the tunnel portal, the dynamic pressure resulting from the mean value of the unfavourable wind directions is to be applied. If an evenly distributed wind rose is assumed, the unfavourable wind directions are defined as a 60° angle. It is postulated that the mean value of wind speed is close to the median. Then, this specification corresponds to a 92-percentile of wind speed. For the expected value of the wind pressure, we set the median at 0 Pa, since in more than half of all wind directions the wind does not affect the portal adversely.

For adverse barometric pressure, the 95-percentile shall be used. For tunnels that do not penetrate mountain ranges, the meteorological pressure is closely related to the local wind speeds. Barometric pressure differences are to be assumed as 5 Pa/km, related to the distance between the tunnel portals (not necessarily the tunnel length). For the expected value of the barometric pressure, we again use the median of 0 Pa.

In [1], a truck fire with a fire output of 30 MW is specified as the design fire. According to the explanations in [16], Appendix D, this nominal fire capacity corresponds to an

effective heat release rate of 20 MW. In the following, only the effective heat release rate is used. Data from the risk concept for tunnels of national roads [37] can be used for the statistical distribution of the fire heat release rate. In this report, the effective heat release rate was used. According to this, at an average heat release rate (derived from the traffic density) 90% of all fires can be represented by a 5 MW fire, 8% of all fires correspond to a heat release rate of 30 MW and 2% of the fires are to be represented by a 100 MW fire. This gives an expected heat release rate of 8.9 MW (weighted average). The buoyancy from a smaller heat release rate is estimated by extrapolating data from the Memorial fire tests [27]. The expected stack effect can be approximated in the ventilation design by reducing the buoyancy by 1/3. The buoyancy is not directly proportional to the heat release rate, since with decreasing fire size the heat transfer into the wall (heat radiation and conduction) also decreases. A smaller fire requires less thrust. The reduction is shown in the tables below. However, it is not regarded as a safety margin, as the objective of the specification is to be able to control a truck fire - without considering the probability of this event.

The fire location is also included in the ventilation design. Depending on the fire location, the number of vehicles in the tunnel may change. If the fire is located at the entrance portal, the traffic congestion will extend outside the tunnel portal. At the same time, more vehicles that were in the tunnel at the start of the fire can leave the tunnel. The location of the fire also affects buoyancy. This is the case when the fire is close to the exit portal or when the longitudinal gradient changes in the tunnel. The most unfavourable location in the tunnel is always assumed for the ventilation design. A variation of the fire location does not appear to be reasonable within the scope of this sensitivity study. The most unfavourable location for ventilation is assumed. The three sample tunnels each have a constant longitudinal gradient. The selected fire location is 800 m away from the lower tunnel portal to include the maximum of the buoyancy caused by the fire.

In the design of the longitudinal ventilation, a safety margin is included in that the ventilation is designed for a higher flow velocity than what is specified as the set-point for ventilation control. The respective set-point value of the control specifications is used as the expected value.

7.1.3 Tunnel A

The results of the sensitivity study for Tunnel A are summarised in Table 14. In the column "Base case", the input variables for the calculation of the base case are listed. In the column "Variation" the parameter is listed which is adjusted as a single input variable - the other input variables correspond to the base case. The variation of these individual input variables results in a reduction of the required total thrust in the cross-section - shown here as pressure reduction. In the last column, the pressure reduction is shown in relation to the required total thrust of the base case.

Example as read from Table 14: The base case calculation without throttling effect gives a total required jet fan thrust of 65.8 Pa. When the hourly traffic is reduced from 1'100 to 417 vehicles and the other parameters chosen according to the base case, the required thrust is 64.9 Pa – a reduction of 0.9 Pa or 0.9/65.8=1.4%. If the throttling effect is included, an additional 0.9 Pa is to be added to the 65.8 Pa of the base case.

When designing a tunnel with a clear longitudinal inclination, the stack effect drives the design above all other influences. Meteorological pressure differences also play a significant role, whereby the temperature difference in turn affects the ventilation design via the longitudinal inclination. The traffic data are of secondary importance.

Tunnel A

Parameter	Base Case	Variation	Thrust reduction	
Hourly traffic	1'100 Fz/h	417 Fz/h	0.9 Pa	1.4%
Truck partition	8%	4.8%	0.1 Pa	0.2%
Natural temperature difference	4.4K	0.0K	5.3 Pa	8.1%
Wind and barometric pressure	5 Pa	0 Pa	5.0 Pa	7.6%
Heat release rate (nominal)	20 MW	8.9 MW	16.5 Pa	25.1%
Minimum airflow velocity	1.5 m/s	1.0 m/s	3.3 Pa	5.0%
Total thrust in tunnel cross-section	65.8 Pa			
Throttling effect	0.9 Pa			

Table 14: Tunnel A

Due to the longitudinal gradient, the fire buoyancy and thus the fire heat release rate becomes the determining factor in ventilation design. The safety margin resulting from the difference between the set speeds in design and operation is only a small proportion of 5% of the total thrust. The natural temperature difference and wind loads provide an inherent safety margin of about 10%. The other contributions are of minor importance. As one input variable dominates the design, no excessive safety margin results from a combination of unlikely requirements.

For Tunnel A, the throttling effect adds a flow resistance of 0.9 Pa. This corresponds to approximately 1% of the nominal thrust. This influence is negligible against other model uncertainties and assumptions. The design is sufficient without considering the flow resistance of the fire.

7.1.4 Tunnel B

The results of the sensitivity study for Tunnel B are summarised in Table 15, for a description see Tunnel A in chapter 7.1.3.

In a tunnel with traffic without congestion RV1 and a small gradient, the largest safety margin is the difference in the target speed between design and operation. Since the main resistance to ventilation consists of losses due to friction on the tunnel and vehicles, the quadratic relationship between flow velocity and pressure losses has a very clear effect.

In urban tunnels with uni-directional traffic and low occurrence of congestion, a greater safety margin is obtained than in steep tunnels, by dividing the required thrust in similar proportions between assumptions on traffic and meteorology. A margin of 20% of the calculated total thrust results from the difference between the target speeds

in design and operation. This should be seen in connection with the assumptions on traffic volume.

Tunnel B

Parameter	Base Case	Variation	Thrust reduction	
Hourly traffic	2'200 Fz/h	833 Fz/h	9.1 Pa	14.1%
Truck partition	8%	4.8%	1.7 Pa	2.6%
Natural temperature difference	4.4K	0.0K	1.9 Pa	2.9%
Wind and barometric pressure	10 Pa	0 Pa	10.0 Pa	15.5%
Heat release rate (nominal)	20 MW	8.9 MW	2.9 Pa	4.5%
Minimum airflow velocity	3.0 m/s	2.5 m/s	12.6 Pa	19.5%
Total thrust in tunnel cross-section	64.5 Pa			
Throttling effect	3.5 Pa			

Table 15: Tunnel B

For Tunnel B, the throttling effect of the fire is 3.5 Pa. This corresponds to 5% of the nominal thrust. Formally, the design is not sufficient without considering the flow resistance of the fire. When designing the ventilation system for a tunnel of this type, a corresponding additional thrust should be considered.

7.1.5 Tunnel C

The results of the sensitivity study for Tunnel C are summarised in Table 16, for a description see Tunnel A in section 7.1.3.

Tunnel C

Parameter	Base Case	Variation	Thrust reduction	
Hourly traffic	165 pcu/km,lane	1'666 Fz/h	18.3 Pa	32.6%
Truck partition	8%	4.8%	2.0 Pa	3.6%
Natural temperature difference	2.2K	0.0K	0.5 Pa	0.9%
Wind and barometric pressure	5 Pa	0 Pa	5.0 Pa	8.9%
Heat release rate (nominal)	20 MW	8.9 MW	3.0 Pa	5.3%
Minimum airflow velocity	3.0 m/s	1.0 m/s	37.2 Pa	66.2%
Minimum airflow velocity	3.0 m/s	2.5 m/s	12.8 Pa	22.8%
Total thrust in tunnel cross-section	56.2 Pa			
Throttling effect	3.5 Pa			

Table 16: Tunnel C

In an urban tunnel with frequent occurrence of congestion RV2, the largest safety margin results from the assumed combination of the traffic situation congestion with the target speed of 3 m/s. This combination is excluded during operation, since a control to a longitudinal flow of 2.5 m/s is only required if traffic monitoring in the tunnel reliably indicates that there is no congestion. On the other hand, if congestion cannot be excluded, the longitudinal flow can only be controlled to 1.0 m/s. The combination of congestion and 3 m/s longitudinal flow in this example results in a safety reserve of

46% of the calculated total thrust. The decisive factor is operation with fluid traffic and control at 2.5 m/s, in which the safety factors of the input variables for traffic and ventilation set-point speed interact with detection of congested traffic.

For Tunnel C, the throttling effect of the fire is 3.5 Pa. This corresponds to 6% of the nominal thrust. Formally, the design is not sufficient without considering the flow resistance of the fire. If the emergency ventilation is operated at 1 m/s flow velocity, the safety margin for this type of tunnel is significant.

7.1.6 Summary

In chapter 7.1, the flow resistance of the fire is related to the ventilation design without inclusion of the throttling effect.

For three typical applications, the total thrust in the tunnel, as calculated without throttling effect, is compared with the flow resistance resulting from the 1-D model in chapter 5.1, resp. equations (52) to (54). It is shown that in the three sample tunnels the inherent safety margins of the guideline ASTRA 13001 [1] are sufficient to compensate for the flow resistance of the fire.

Although the effect is small when compared to inherent safety margins of the design code, it is recommended to consider the throttling effect for the design of new tunnels. Based on this study, no immediate action is required to upgrade existing tunnels.

7.2 Recommendation for ASTRA 13001

An update to the guideline ASTRA13001 [1] is not required. It is sufficient to include the throttling effect in the design calculations in the responsibility of the ventilation designer.

7.3 Application in 1-D design tools

The throttling effect can be included in dynamic or static 1-D tunnel ventilation models as described by the following equations. The equations are slightly different from the formulation in chapter 2.2.3, as the “cold” friction must be treated separately. Indices in the equations refer to the definitions in Figure 29.

The change of static pressure at the fire location is given as

$$\Delta p_{1-2} = -\frac{Q_c\, u_0}{c_p A_T T_0} \tag{52}$$

The change in static pressure downstream from the fire includes two components. For the calculation of wall friction, the flow velocity is increased and the density reduced. This results in the increase of the wall friction as

$$\Delta p_{2-3A} = -\frac{\rho_0}{2} \cdot u_0^2 \cdot \frac{\lambda}{D_h} \cdot \frac{Q_c}{\alpha U_T T_0} \left(1 - exp\left(-\frac{\alpha U_T L_3}{\rho_0 u_0 A_T c_p}\right)\right) \tag{53}$$

Additional aerodynamic resistance of standing vehicles downstream of the fire or changes of the tunnel cross-section must be treated accordingly. It may be easiest to treat the increased friction downstream of the fire by including flow velocity and air density as a function of the local temperature $u(x,T)$ and $\rho(x,T)$.

The recovery of static pressure by cooling and the resulting deceleration of the flow is given as

$$\Delta p_{2-3B} = \frac{Q_c\, u_0}{c_p A_T T_0} \left(1 - exp\left(-\frac{\alpha U_T L_3}{\rho_0 u_0 A_T c_p}\right)\right) \tag{54}$$

If these equations are integrated in an existing 1-D model, some modifications may be required.

7.4 CFD Models

CFD simulations can be used for investigation of flow resistance of the tunnel fire, however following important aspects needs to be considered while applying CFD simulation:

- RANS with turbulence models such as SST k-ω provides a good estimation of average flow resistance up to HRR of 10 MW but lacks the details of dynamic turbulent flow features. From 10 MW upwards, the models increasingly diverge and a reliable prediction of the pressure drop cannot be guaranteed with this model.
- LES is expensive computationally, but a blended model such as DES is a good compromise between computational cost and capturing turbulent behaviour inside the tunnel.
- Both DES and LES require a precursor investigation using RANS or URANS simulation to estimate optimized mesh refinement requirement to resolve 80 percent turbulent kinetic energy. This can be obtained by estimating turbulent eddy size to mesh size ratio by using URANS/RANS and a qualitative investigation of this ratio to be minimum five throughout the tunnel domain. Some relaxation near the wall is possible in DES while using this criterion for mesh resolution requirement study.
- In addition, estimation of average turbulent diffusivities (eddy viscosity and effective thermal conductivity) on tunnel cross-section along the tunnel axis by URANS simulation can be used to optimize the mesh refinement requirement for DES.
- Unsteady simulations will require enough time sampling rate of the simulation data to estimate mean flow properties along the tunnel. It is observed that larger values of fire heat source leads to more high frequency pressure fluctuation and therefore requires higher time resolution of simulation and higher sampling rate for time averaging of flow properties.
- The unsteady simulations such as URANS and DES observe enhanced standard deviation of average pressure on tunnel cross-section planes with increased heat release rate. This standard deviation can be used to quantify the uncertainty in

average solutions while using other steady state solvers such as RANS or 1-D Spitfire. In addition, this also demonstrates that turbulence in fire downstream leads to varying flow features, which can also have time dependent behaviour. Therefore, it is necessary to investigate the detailed flow feature with scale resolving simulations especially in the case of high heat release rate while developing ventilation design.

8 Further Research

In this chapter, ideas for further research are listed. It must be noted that the effect of fires on the flow resistance in tunnels is generally small. When compared to inherent safety margins of the design code ASTRA 13001, it could even be considered irrelevant in the design of tunnel ventilation systems. While further research in fire tests and CFD simulations is desirable, it may be more of academic value than of direct relevance to ASTRA.

8.1 Fire Tests

The fire test performed for this study were limited to heat release rates up to 10 MW. This was a boundary condition imposed by the requirement of a long tunnel section downstream of the fire and by the limited fire protection of the zone 1 of the test tunnel. The protected area zone 2 ranges from PK335 to PK415. This other section is fire rated for larger fires. In previous projects, it has been used for fires with heat release rates up to 200 MW.

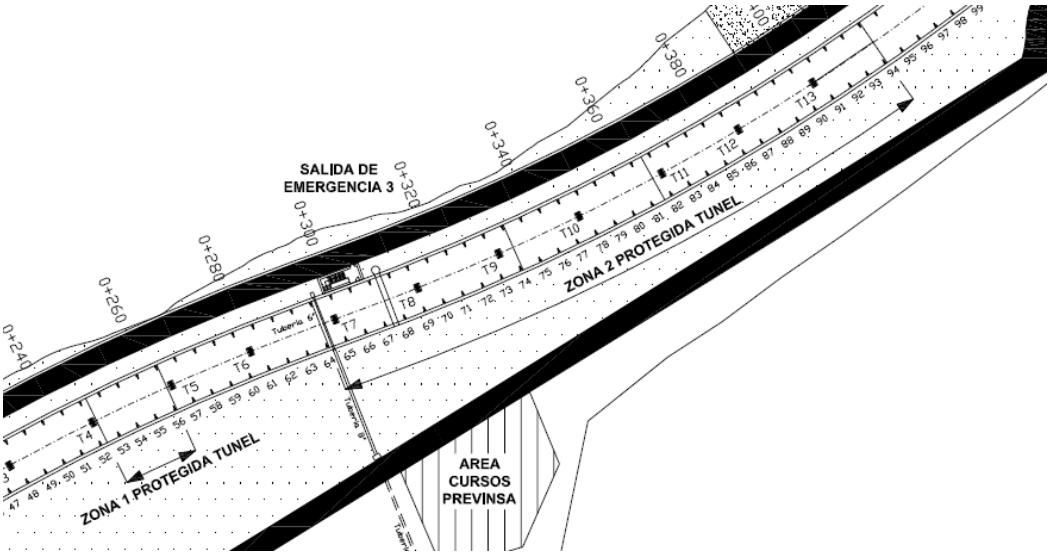

Figure 127: Fire protected zones of the test tunnel

The CFD models applied in this study have been validated using the test data with small heat release rates. The validation was deemed successful for the test scenarios. Upscaling the heat release rates to typical design fires of 20 to 50 MW, however, demonstrated significant differences between the CFD models. It appears desirable to validate the models for larger fires.

The test facility as described in chapter 3.3 appears ideal for these fire tests. The main advantage over other test tunnels is the service gallery underneath, which allow measurements of differential pressure relatively easily.

For the differential pressure measurements, it is recommended to use the high frequency pressure monitors described in chapter 3.6.4 – or an equivalent product. The relatively low price of these sensors would allow two (or more) pressure monitors for each location. The higher sampling rate allows to collect information on turbulence properties as well as acoustic effects of the tunnel. It would also make the fire tests less dependent of the services of the tunnel operators.

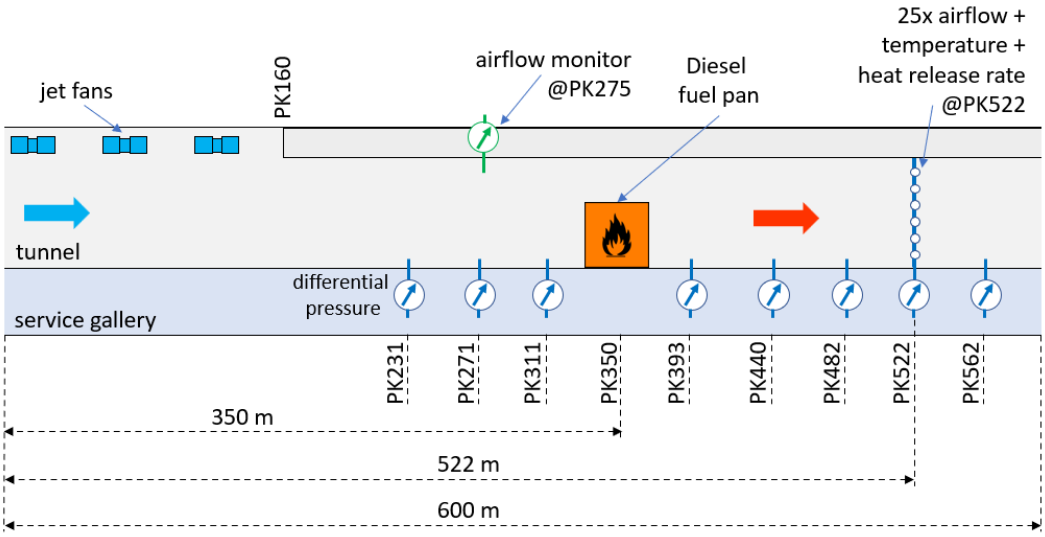

Figure 128: Test setup for large fires

This test setup could then also be used to investigate smoke back-layering and the critical ventilation velocity. In three articles [13], [25] and [26], researchers challenged the industry standard how to calculate critical velocity for the design of longitudinal tunnel ventilation systems. These papers finally lead to a new formulation of the critical velocity and to a revision of the internationally applied standard NFPA502 [7], [8]. The test setup as described in Figure 128 is suitable for further validating the new formulation.

8.2 Application of CFD Models

The simulation experience gained from this project provides following important research outlooks for future studies:

- It is observed that URANS with turbulence modelling can be used to qualitatively estimate the mesh refinement required for DES/LES investigation. It will be a research objective to define a quantitative criterion for tunnel simulation such that optimized mesh refinement can be performed for DES/LES.
- DES and URANS observe time dependent fluctuation in pressure solution with specific frequency. Furthermore, high frequency fluctuations are activated with increasing heat release rate. It is important to understand the physical or numerical reasoning for such fluctuations. Turbulence, fire volume and tunnel length play important role in analysing the dynamic features of the flow. Therefore, more detailed investigation into fire dynamics in the presence of longitudinal ventilation is required via computationally expensive scale resolving simulations.

- A more detailed investigation of flow bifurcation and the influence of buoyancy and turbulent momentum transport on this flow bifurcation will be an interesting study. Current simulations observe development of counter rotating vortices around the fire, which dissipate at a certain distance downstream of the fire. The role of tunnel cross-section, tunnel length, fire strength and fire volume on the vortex geometry and timescale of dissipation of these vortices are of interest from both fluid dynamics and tunnel ventilation point of view. How these counter rotating vortices contribute to the pressure drop downstream and, on the pressure, fluctuation can be valuable for ventilation design.
- In addition to ventilation objectives these counter rotating vortices also corresponds to plume bifurcation and therefore can provide important insight regarding pollutant dispersion along the tunnel. Especially, when it is intended to address the concern regarding distribution of harmful chemicals along the tunnel in case of electric vehicle fire, the detailed flow features around the fire are of utmost importance. Therefore, in future, a pollutant dispersion modelling based on flow features developed using detailed LES or DES simulation can be valuable.
- This draws also a further importance of obtaining highly resolved tunnel simulation in the case of high heat release rate using LES. Therefore, a computationally expensive LES can be used to further benchmark the criterion for mesh refinement and time sampling for low resolution simulations like URANS or VLES and intermediate resolution simulation types like DES.
- For longer, complicated and curved tunnels with multiple jet fans, it is always of importance to find a simple modelling approach to define minimum necessary design requirement. The 1-D Spitfire model works very well to define such simple estimation of average quantities. However, due to 1-D limitation, it cannot capture the details of fire volume and flow feature of the combustion at the fire. In future, a coupling of 1-D and 3-D scheme can be developed which combines an approximately 1-D flow feature away from the fire with detailed flow feature around the fire. Such coupled simulation allows reduction of computational cost for the entire tunnel by focusing with high fidelity simulation near the fire and jet fans and with 1-D simulation in rest of the tunnel.

Bibliography

[1] Bundesamt für Strassen ASTRA (2022), *Lüftung der Strassentunnel*, Richtlinie ASTRA 13001, V3.01.

[2] Bundesamt für Strassen ASTRA (2023), *Fachhandbuch BSA*, January 2023

[3] Forschungsgesellschaft Strasse, Schiene und Verkehr FSV (2014), *Richtlinie Tunnelausrüstung, Belüftung, Grundlagen*, RVS 09.02.31.

[4] Forschungsgesellschaft Strasse und Verkehr FGSV (2019), *Empfehlungen für die Ausstattung und den Betrieb von Strassentunneln mit einer Planungsgeschwindigkeit von 80 km/h oder 100 km/h*, EABT-80/100.

[5] Centre d'Etudes des Tunnels (2003), *Les dossiers pilotes du CETU – Section 4.1 Ventilation*, November 2003.

[6] Schweizerischer Ingenieur- und Architektenverein SIA (2023), *Projektierung Tunnel - Strassentunnel*, Norm SIA 197/2.

[7] NFPA 502, *Standard for Road Tunnels, Bridges and Limited Access Highways*, 2014, 2017 und 2020.

[8] TIA NFPA 502 (2021) *Tentative Interim Amendment*, 15 September 2021.

[9] Dutrieue, R., Jacques, E. (2006), *Pressure loss caused by a fire in a tunnel*, 12th International Symposium on Aerodynamics and Ventilation of Vehicle Tunnels, Portoroz.

[10] Ingason H., Zhen Li Y., Lönnermark A. (2015), *Tunnel Fire Dynamics*, Springer DOI 10.1007/978-1-4939-2199-7.

[11] Carlotti, P., Salizzoni, P. (2017), Pressure drop caused by a fire in a tunnel, 17th International Symposium on Aerodynamics and Ventilation of Vehicle Tunnels, Lyon.

[12] Li, J., Li, Y., Feng, X., Li, J. (2018), *Analysis on ventilation pressure of fire area in longitudinal ventilation of underground tunnel*, IOP Conf. Series: Materials Science and Engineering 322, DOI 10.1088/1757-899X/322/5/052020

[13] Stacey C., Beyer M. (2020), *Critical of critical velocity – an industry practitioner's perspective*, 10th International Conference Tunnel Safety and Ventilation, Graz.

[14] Riess I., Weber D., Steck M. (2020), *On the airflow resistance of fires in longitudinal ventilation – the throttling effect*, 10th International Conference Tunnel Safety and Ventilation, Graz.

[15] Riess I., Weber D., Steck M. (2020), *Strömungswiderstand von Bränden in Strassentunneln*, Report 1679 Project AGT 2017/005.

[16] Riess I. (2020), *Aerodynamic Resistance of Fires in Tunnels*, Riess Ingenieur-GmbH Report 1904002.

[17] Ang E., Riess I., Peiro J. & Rein G. (2021), *Understanding and modelling the fire throttling effect in longitudinally ventilated tunnels*, 12th Asia-Oceania Symposium on Fire Science and Technology, Brisbane.

[18] Hansen R. (2021), *Modelling the throttle effect in a mine drift*, Journal of Sustainable Mining, Volume 20 issue 4, https://doi.org/10.46873/2300-3960.1329

[19] Ang E., Peiro J., Riess I. & Rein G. (2022), *Analysis of fire throttling in longitudinally ventilated tunnels with a one-dimensional model*, Fire Technology, https://doi.org/10.1007/s10694-022-01285-4

[20] Hansen R. (2022), *The throttle effect – blower fan versus exhaust fan*, Mining Revue vol. 28 issue 3, 2022, https://doi.org/10.2478/minrv-2022-0016

[21] Gay D. (2022), *CFD Simulation of the Throttling Effect in Tunnels*, MSc Thesis, Imperial College London.

[22] Ang E. (2024), *Engineering simulations in the design and analysis of tunnels for fire safety and smoke ventilation*, PhD Thesis, Imperial College London.

[23] Luo, C., Nie, Y. (2024), *Numerical study on throttling effect of catastrophic tunnel fires in longitudinal ventilation tunnel*, http://dx.doi.org/10.2139/ssrn.4972103

[24] Deb R., Weber A., Riess I. (2024), *Numerical investigation of flow resistance of fires in road tunnels*, 20th International Symposion on Aerodynamics, Ventilation and Fire in Tunnels, Copenhagen.

[25] Beyer M., Stacey C. (2022), *CFD Validation for Tunnel Smoke Control Design,* 11th International Conference Tunnel Safety and Ventilation, Graz.

[26] Beyer M., Stacey C., Brenn G. (2024), *A Mixed Convection Model for Estimating the Critical Velocity to Prevent Smoke Backlayering in Tunnels,* Fire Technology, 61, 295–342, 2025

[27] MTFVTP (1995), *Memorial tunnel fire ventilation test program—comprehensive test report*, Bechtel/Parsons Brinckerhoff, Boston

[28] Ackeret, J. Haerter, A., Stahel, M. (1967). *Die Lüftung der Autotunnel*, Mitteilung Nr. 10, Institut für Strassenbau, ETH Zürich.

[29] Riess, I., Bettelini, M. (1999). *The prediction of smoke propagation due to tunnel fires*. ITC Conference Tunnel Fires and Escape from Tunnels. Lyon

[30] Riess, I., Bettelini, M., & Brandt, R. (2000). *Sprint - a design tool for fire ventilation*. 10th International Symposion on Aerodynamics and Ventilation of Vehicle Tunnels. Boston.

[31] Riess, I., Brandt, R. (2010). *ODEM - a one-dimensional egress model for risk assessment*. 5th International Conference Tunnel Safety and Ventilation, Graz.

[32] Riess, I. (2020). *On smoke stratification in a 1-D tunnel ventilation model*, 11th International Conference Tunnel Safety and Ventilation, Graz.

[33] McGrattan K, Hostikka S, McDermott R, Floyd J, Weinschenk C, Overholt K. Fire dynamics simulator user's guide. NIST and VTT Technical Research Centre of Finland, sixth edition

[34] Spalart, P. R., Jou, W.-H., Strelets, M., & Allmaras, S. R. (1997), *Comments on the feasibility of LES for wings, and on a hybrid RANS/LES approach,* Proceedings of the First AFOSR International Conference on DNS/LES, Ruston, Louisiana, USA, Aug. 4–8, 1997.

[35] Spalart, P. R., Deck, S., Shur, M. L., Squires, K. D., Strelets, M. K., & Travin, A. (2006), *A new version of detached-eddy simulation, resistant to ambiguous grid densities*, Theoretical and Computational Fluid Dynamics, **20**, 181–195.

[36] Pope, S. B. (2000). *Turbulent Flows*. Cambridge: Cambridge University Press.

[37] Bundesamt für Strassen ASTRA (2014), Risikokonzept für Tunnel der Nationalstrassen, Dokumentation ASTRA 89005, V1.10.

Open Data Access
A detailed documentation of the fire tests and associated CFD simulations is available for download:
https://doi.org/10.5281/zenodo.17938708

The documentation includes
- This report
- The test report provided by Applus+TST
- Test facility
  - Drawings
  - Photos
- Instrumentation
  - Drawings
  - Data sheets
  - Photos
- Fire test documentation (3x)
  - Raw data
  - Photos
  - Video recording
- CFD data

Use of Data

No data from other studies or projects was used in this project. Sources for diagrams, illustrations, and quotations used in this report are marked and listed in the bibliography.

Apendix

DES Simulation for Test Cases 1 to 3

This section provides additional information extracted from the DES simulations for the test cases 1 to 3. It shall be read in the context of sections 5.4 and 5.6.

Figure 129 depicts the averaged pressure solution along the tunnel at different locations. Further, the comparison of solution with experimental results is also depicted in the plots for all three testcases. The left and central column plots observe the pressure in time domain and frequency domain at four different locations of 50m, 100m upstream of fire (x = -50m, x = -100m) and 50m and 100m downstream of fire (x = 50m and x = 100m) for each testcases. Small timescale pressure fluctuations are more prominent for high heat release rate case of Test3. The pressure fluctuation with large amplitude is observed for Test1 in the case of DES simulation. However, the time averaged results compare well with the observed pressure in the experiment.

The simulation results at different tunnel cross-sections are obtained in Figure 130 to Figure 132 for testcase Test1. Figure 130 presents the pressure distribution on the tunnel cross-section at four locations downstream of the fire, reported for Test1 at three-time instances. Two counter-rotating vortices, generated by the heat source, are evident in the downstream cross-sections near the fire (x_f = 5m, 10m). These vortices gradually dissipate due to turbulence and vanish approximately 20 m downstream of the fire.

Figure 131 and Figure 132 show the corresponding solutions for temperature and velocity. The temperature field illustrates that the vortices convect high-temperature gases downstream. However, further along the tunnel, turbulence enhances mixing, increasing the effective thermal diffusivity and leading to a more uniform temperature distribution across the cross-section.

The velocity field indicates that the flow remains quasi-steady in the near downstream region (up to 15 m). Beyond this point, turbulent momentum mixing produces a more homogeneous velocity profile. This behavior is supported by Figure 86, which depicts the mean effective viscosity and thermal conductivity. The results show a reduction in momentum and thermal diffusivity immediately after the fire, reaching a minimum, followed by a gradual increase farther downstream.

Finally, Figure 133 and Figure 134 present the temperature and vertical velocity along the tunnel axis at different tunnel heights, further highlighting the evolution of the flow and thermal structures downstream of the fire.

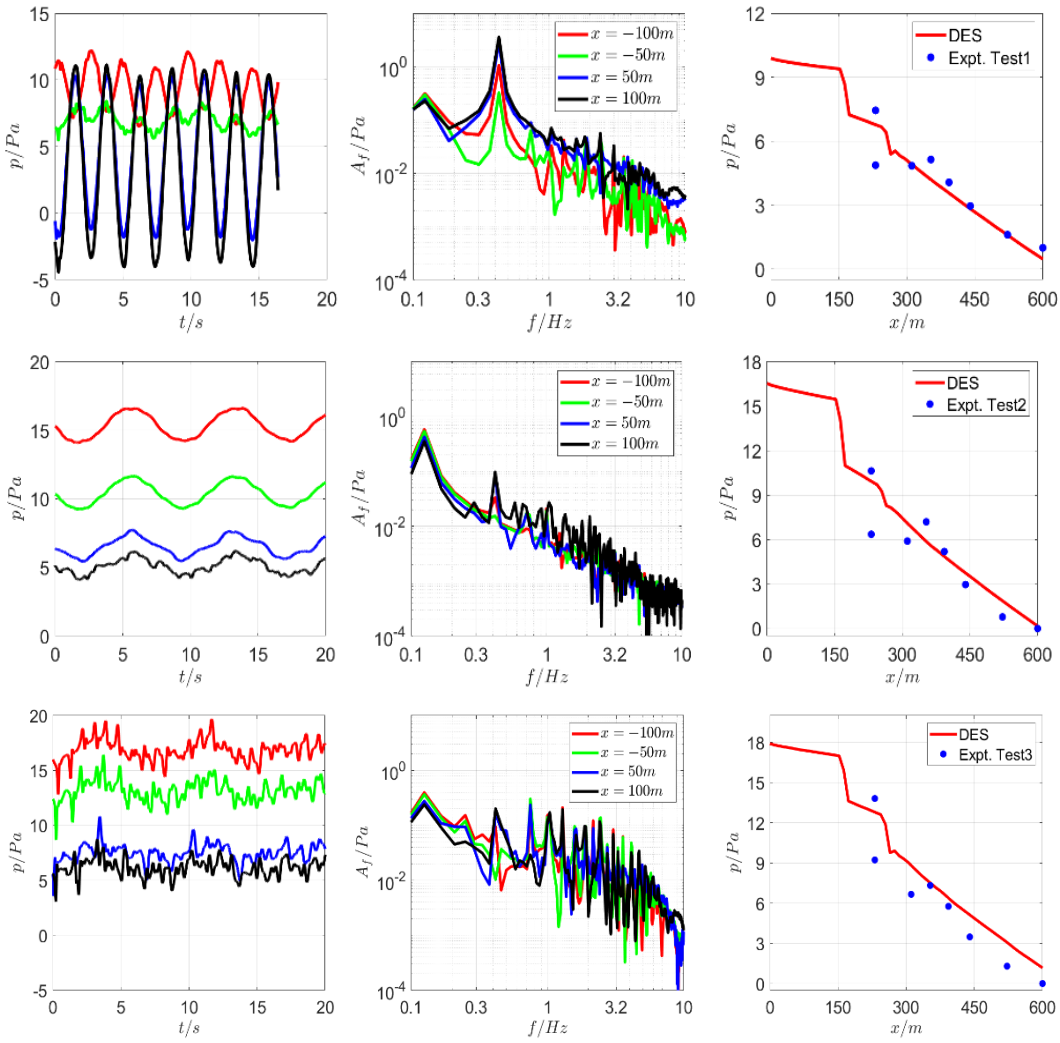

Figure 129: The pressure solutions at four points along the tunnel (left plot), the Fourier transform of pressure solution (canter plot) and averaged pressure solution along planes (right plot) is depicted for three different testcases using DES.

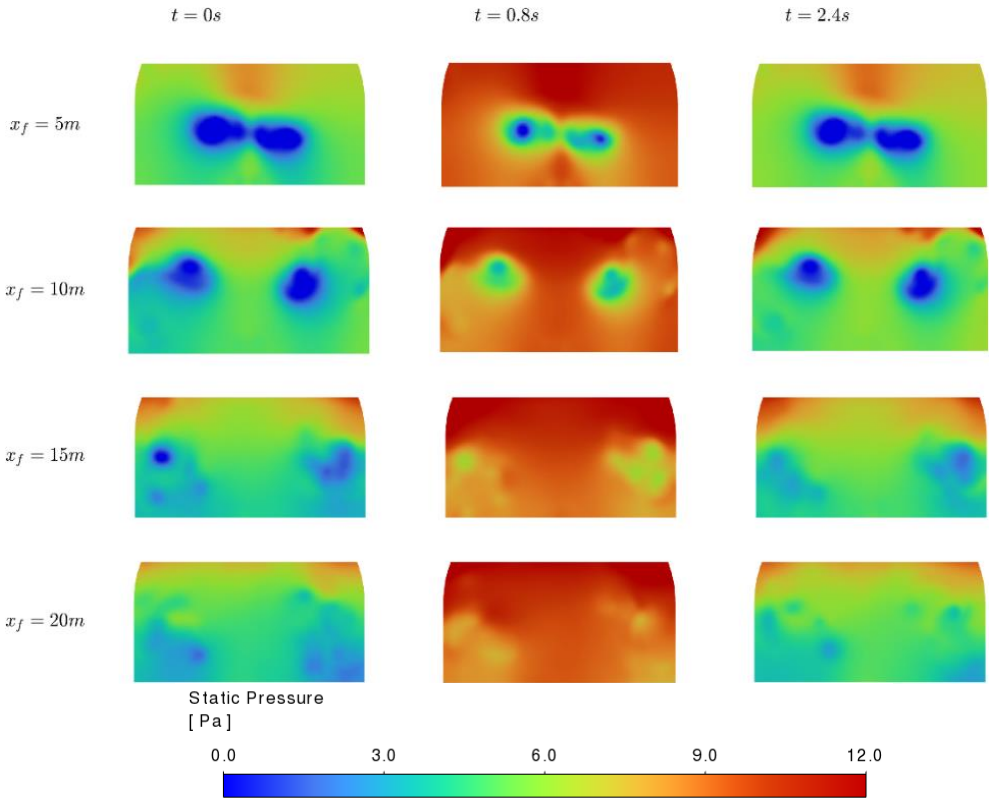

Figure 130: Pressure on cross-section at locations 5,10,15 and 20m downstream of heat source and three different time instances for testcase Test1.

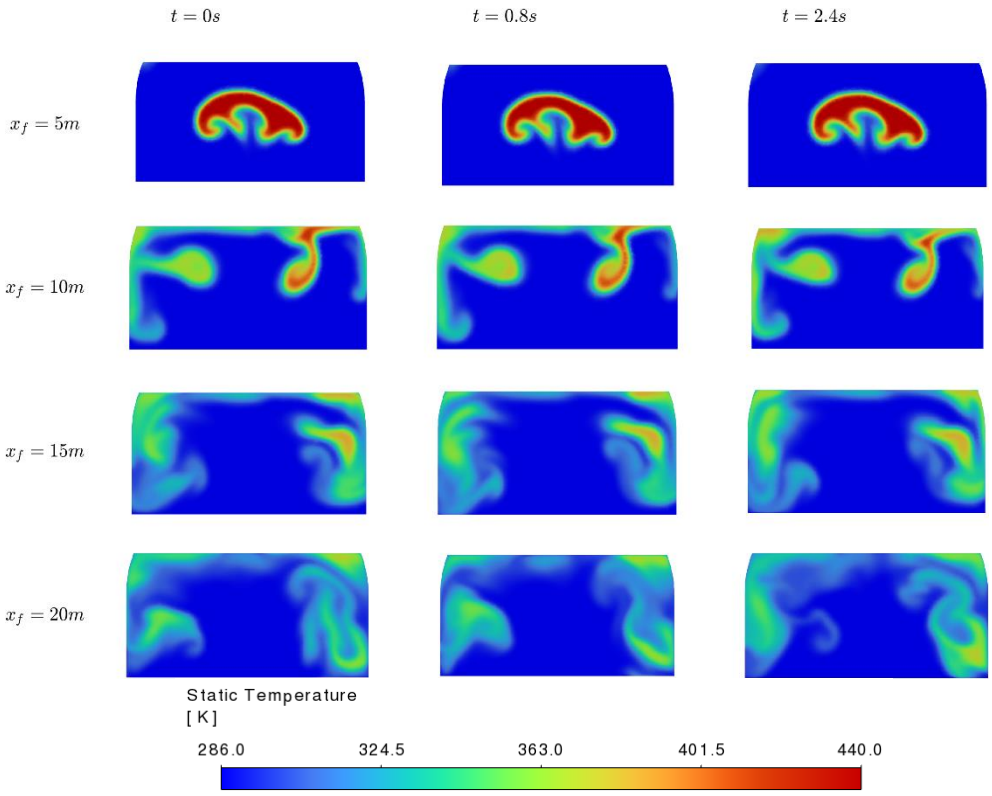

Figure 131: Temperature on cross-section at locations 5,10,15 and 20m downstream of heat source and three different time instances for testcase Test1.

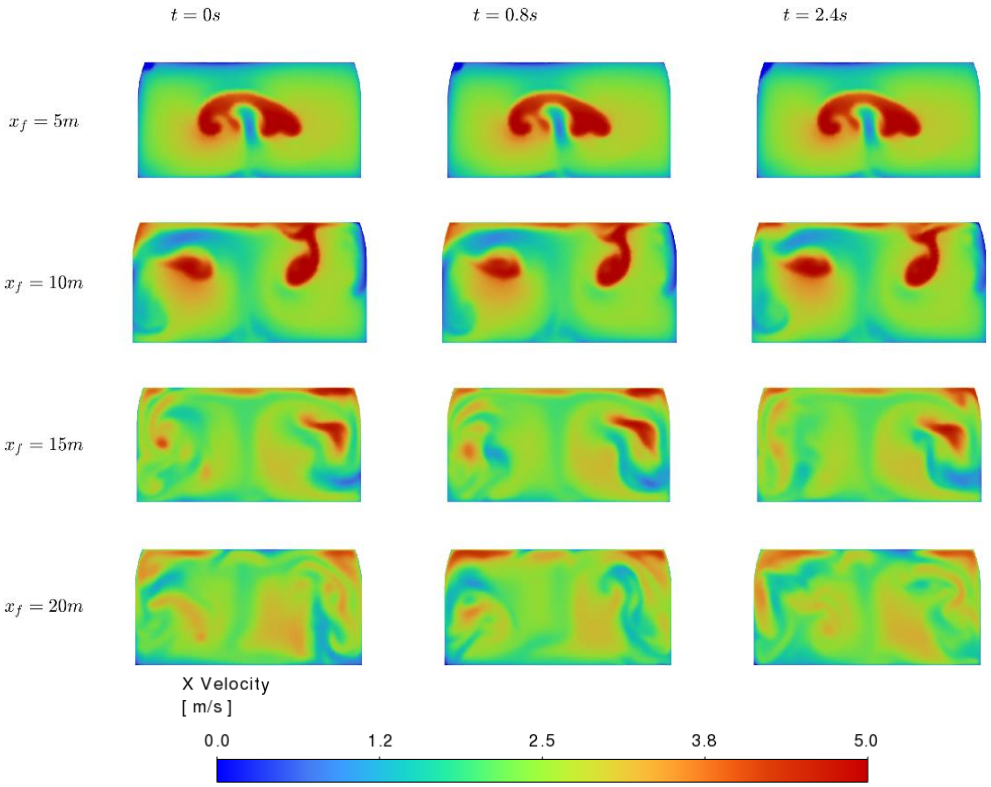

Figure 132: Fluid speed along tunnel axis on cross-section at locations 5, 10, 15 and 20m downstream of heat source and three different time instances for testcase Test1.

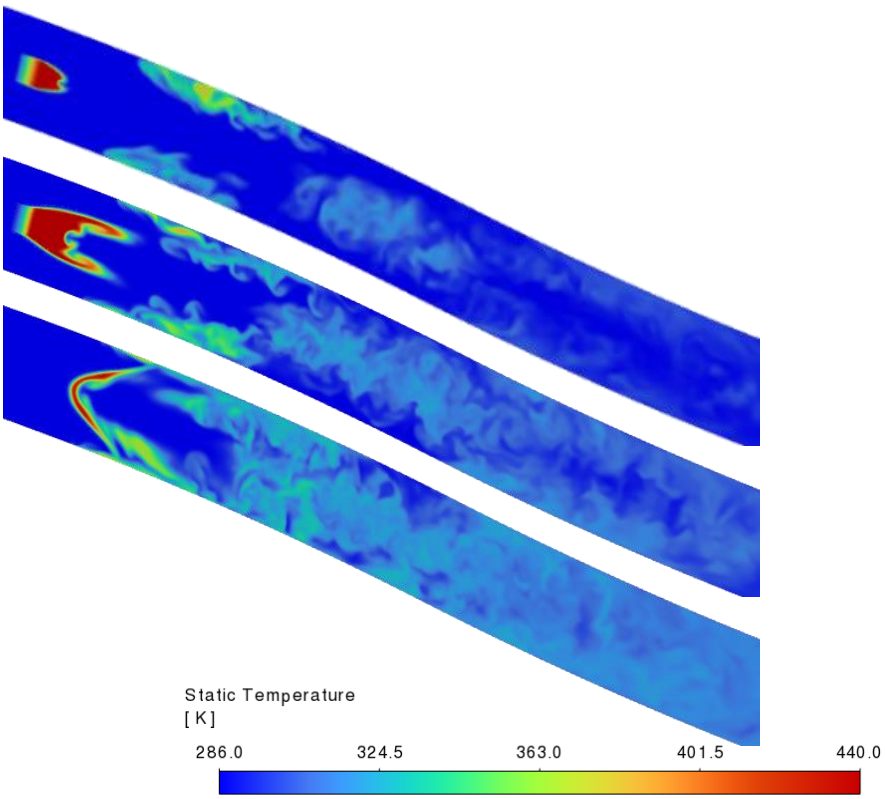

Figure 133: Temperature solutions at three different tunnel height of 1m, 2.5m and 4m for testcase Test1.

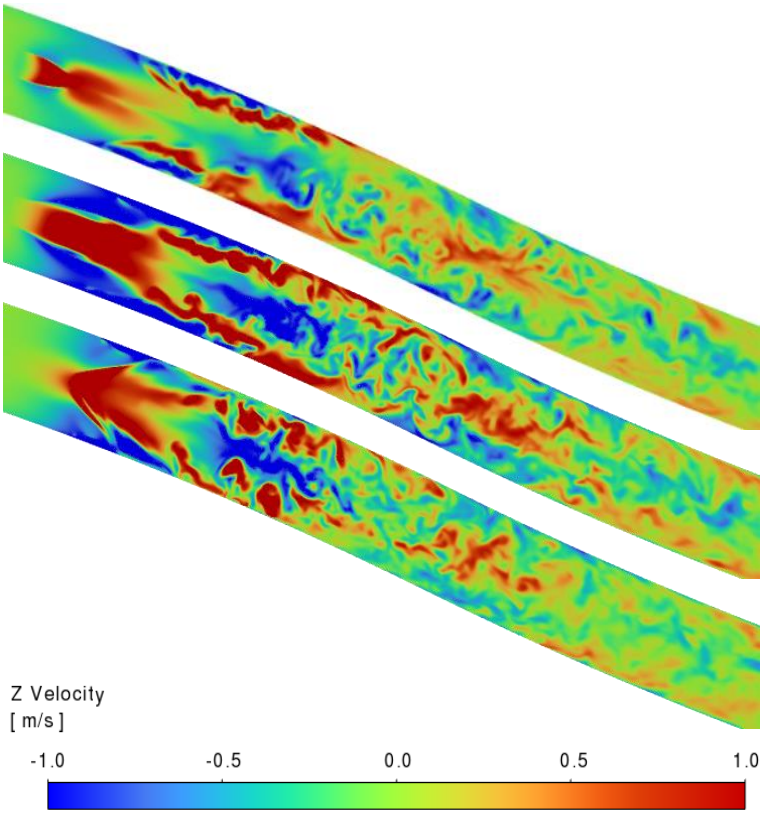

Figure 134: Fluid speed along the tunnel height at three different tunnel height of 1m, 2.5m and 4m for testcase Test1.

Figure 135 compares the fluid temperature for three test cases (Test1 at the top, followed by Test2 at the centre and Test3 at the bottom figure). Although, Test1 and Test2 corresponds to a low heat source term (4MW for Test1, 4.22MW for Test2). the inflow fluid speed at the tunnel entry is lower in Test1 as compared to Test2 (2.59m/s for Test1 and 3.7m/s for Test2). Therefore, Test1 observes more chaotic flow behaviour in the fire downstream and earlier breakdown of counter-rotating vortices due to earlier interaction with the wall. Due to high heat source and low jet fan strength which leads to low tunnel inlet flow speed, the Test3 reflects similar behaviour as of Test1 with higher temperature. Figure 136 obtains the flow speed along tunnel axis and Figure 137 obtains the flow speed along tunnel height for all three testcases. Here also it is clearly observed that Test2 observes more smoother transition to high-speed condition compared to Test1 and Test3.

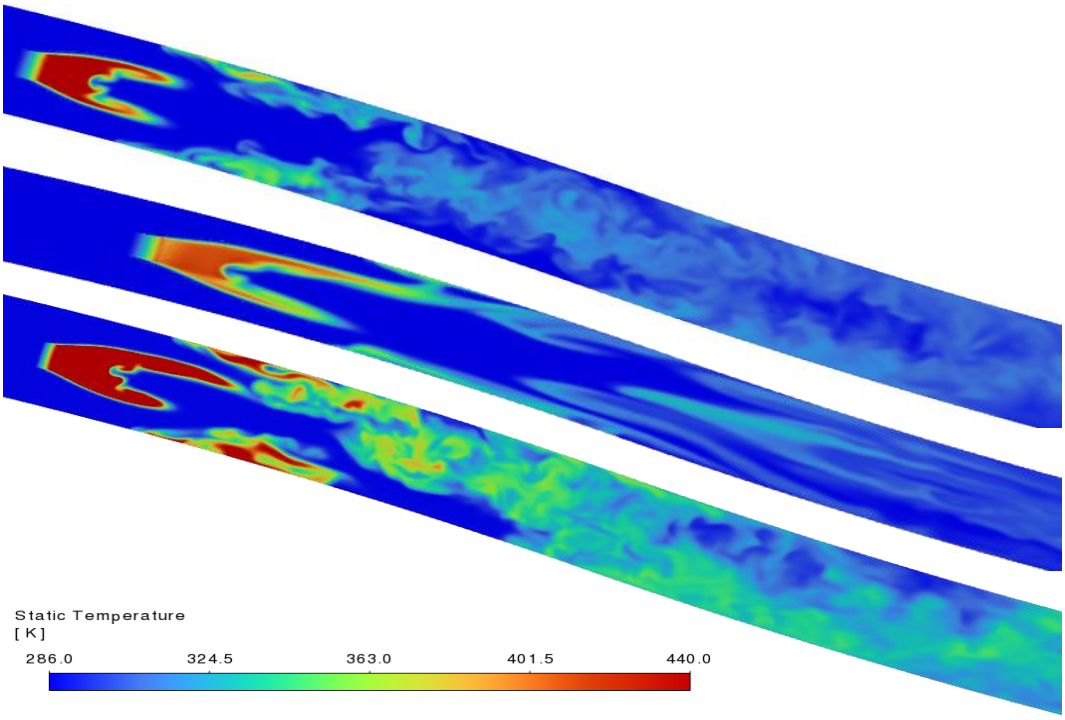

Figure 135: Temperature of the fluid at tunnel height of 2.5m for testcases Test1, 2, 3

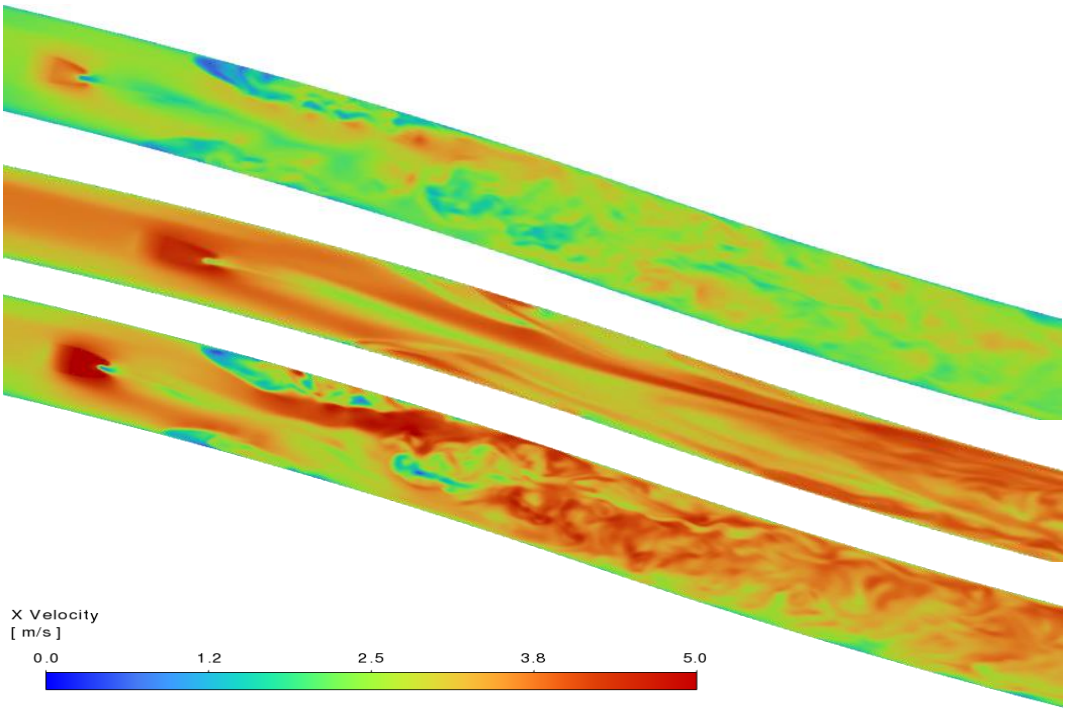

Figure 136: Fluid speed along the x-direction at tunnel height of 2.5m for testcases Test1, 2, 3

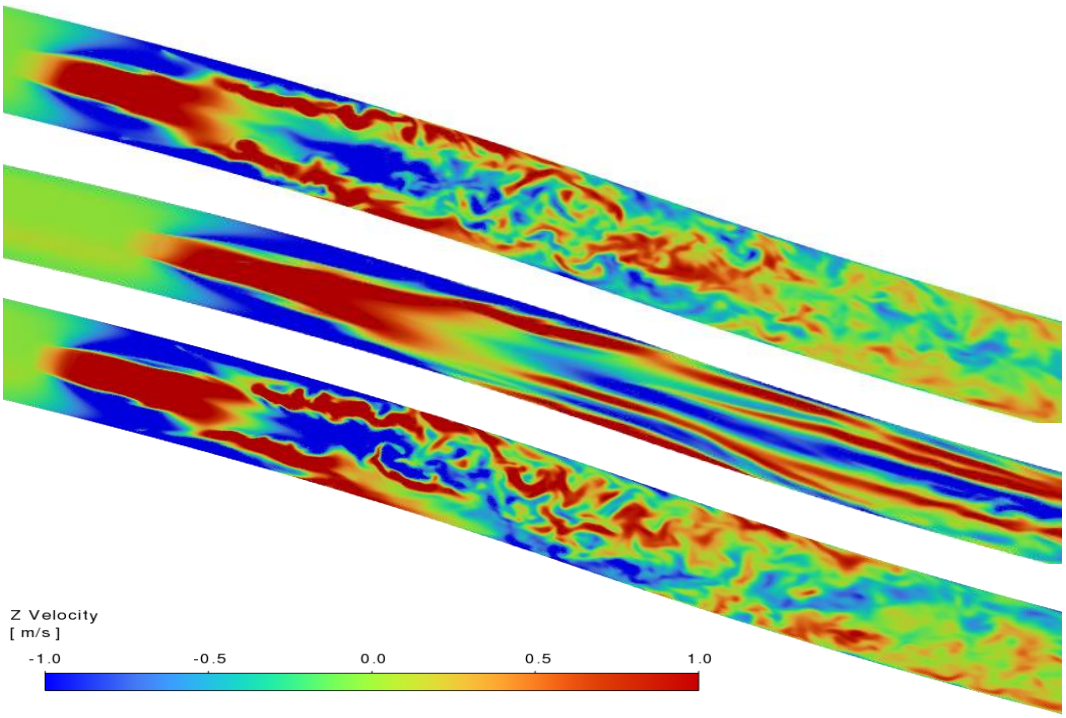

Figure 137: Vertical fluid speed along at tunnel height of 2.5m for testcases Test1, 2, 3.

Additional Scenarios for the Long Tunnel

This section includes pressure profiles along the tunnel for additional fire scenarios to the ones presented in section 6.1 of this report. The graphs demonstrate the influence of a variation of the heat release rate.

As observed in Figure 138 to Figure 141, the pressure drop across the fire increases with increasing heat release rate for same inlet flow speed of 3m/s. These results are obtained for the case of one percent slope against the flow along the 900m long tunnel. The variation in pressure drop for the rectangular cases is minor in RANS simulation. The arched type of tunnel shows slightly higher pressure drop but recovers back to values corresponding to rectangular cases in small distance (10m) aways from the fire. The overall pressure drop decrease in the case of VLES as compared to RANS simulations, whereas 1-D results observe intermediate values for pressure drop between the two different turbulence modelling approach. Further, the differences between RANS and VLES results increases with increase in heat release rate. The differences between the three models is significantly larger than the difference due to the shape of the tunnel cross-section.

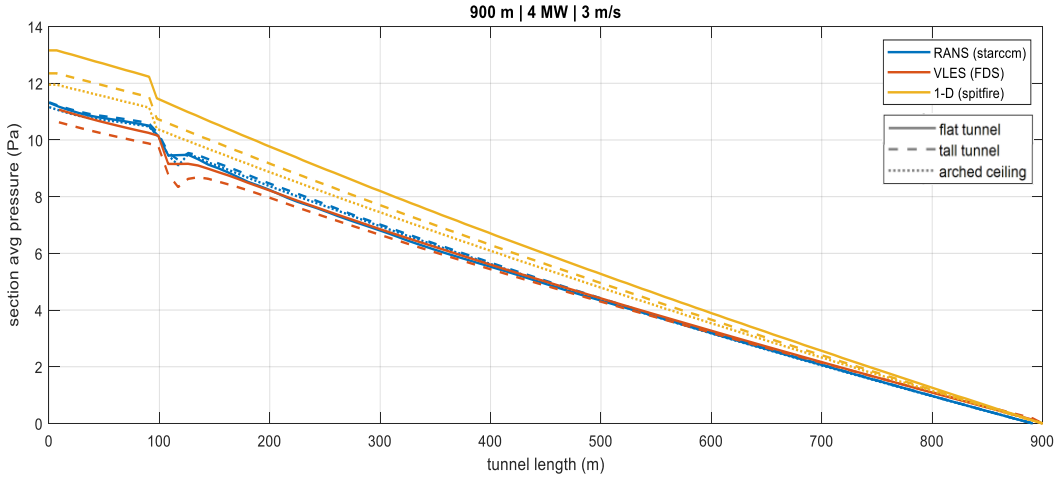

Figure 138: The average pressure along the tunnel for a 4MW fire

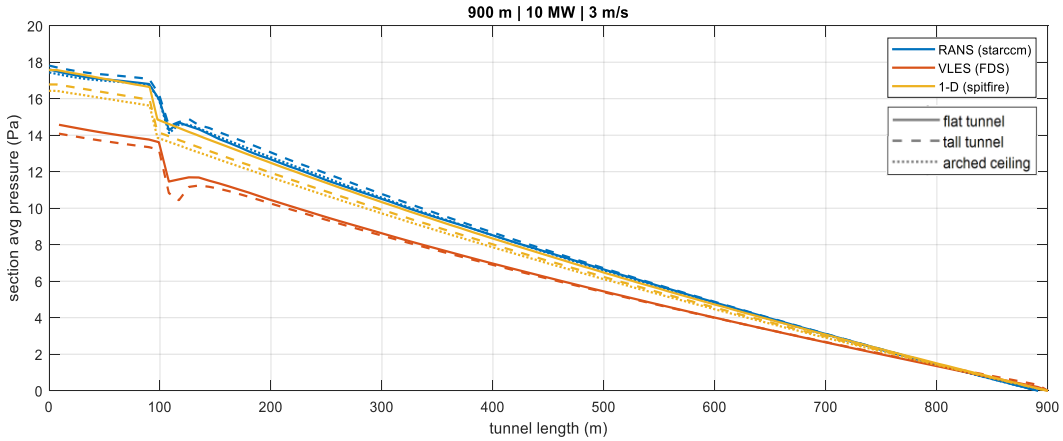

Figure 139: The average pressure along the tunnel for a 10MW fire

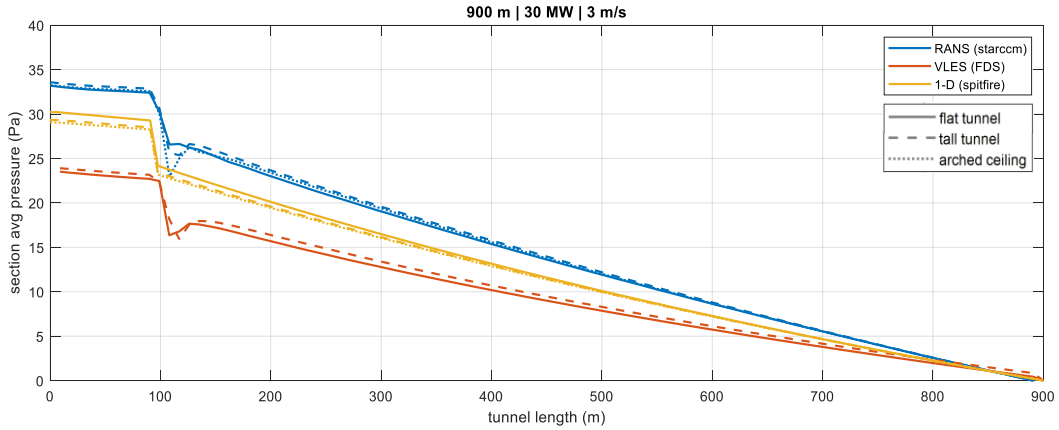

Figure 140: The average pressure along the tunnel for a 30MW fire

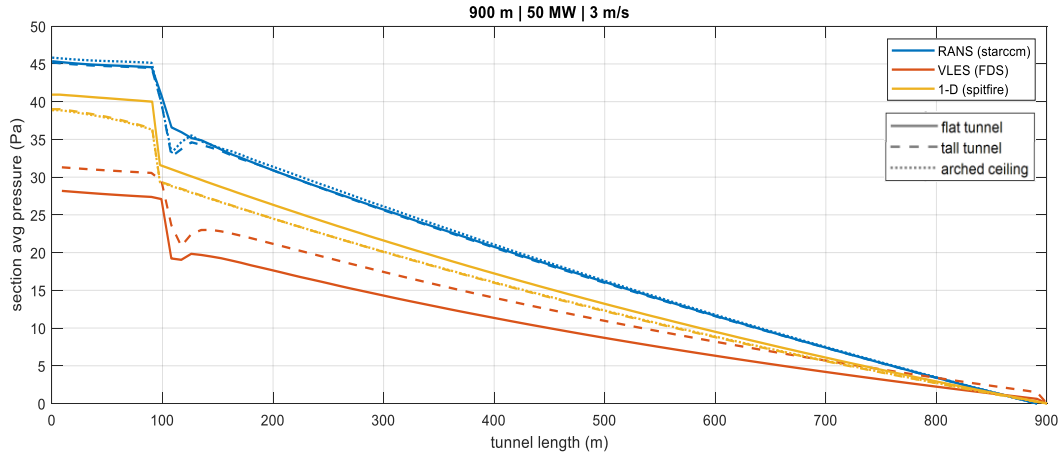

Figure 141: The average pressure along the tunnel for a 50MW fire

Figure 142 to Figure 145 obtain the pressure drop using no slope along the tunnel and the VLES simulation with FDS 6.9.1. As expected, the absolute pressure drop reduces for the case of no slope for all the four heat release rate values. However, the pressure drop obtained using FDS results with version 6.9.1 is observed to be much larger compared to FDS 6.8.0 version for the case of comparison of 50MW fire case, see Figure 115. This, therefore, provides the uncertainty using VLES modelling and FDS software to estimate the pressure drop in the case of higher value of heat source terms. It appears mute to validate a CFD code further that shows these significant changes between new versions.

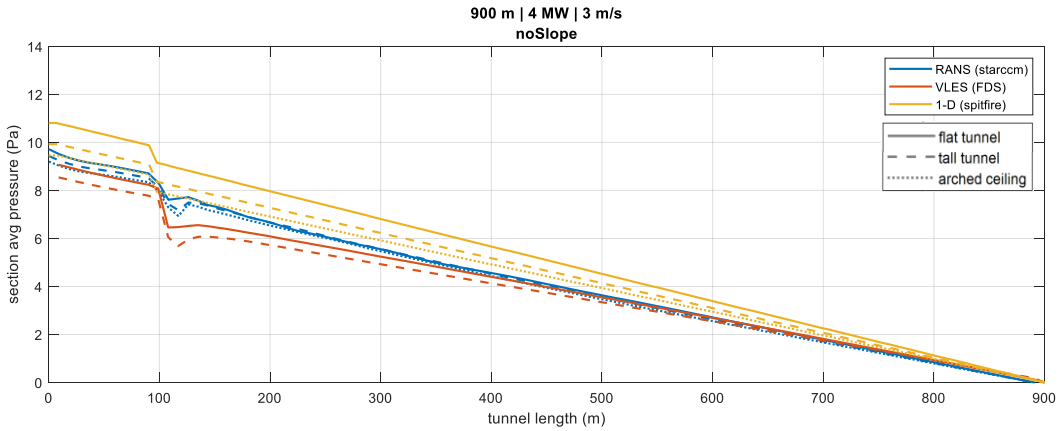

Figure 142: The average pressure along the tunnel using 10MW tunnel fire strength and no slope of the tunnel and FDS 6.9.1

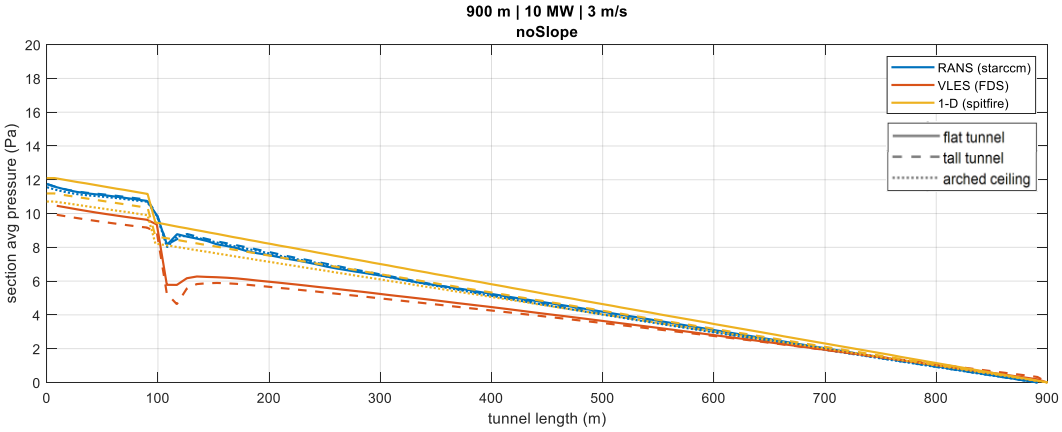

Figure 143: The average pressure along the tunnel using 10MW tunnel fire strength and no slope of the tunnel and FDS 6.9.1

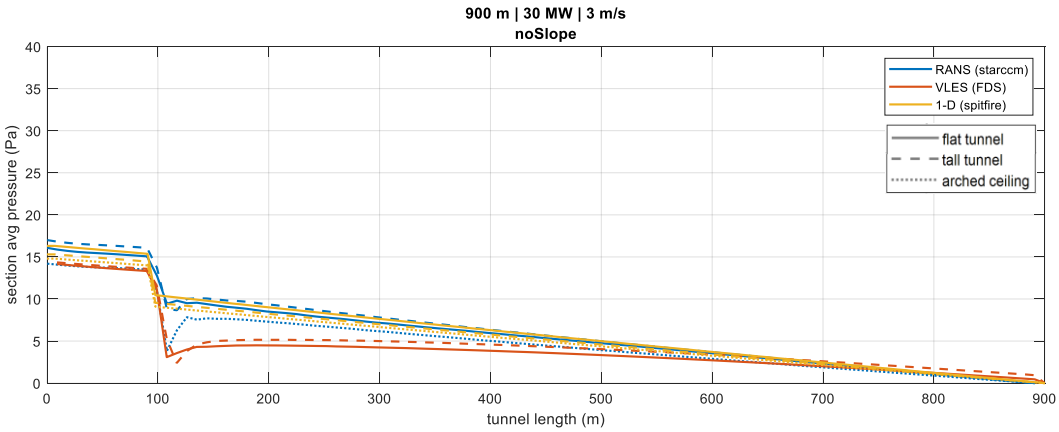

Figure 144: The average pressure along the tunnel using 30MW tunnel fire strength and no slope of the tunnel and FDS 6.9.1

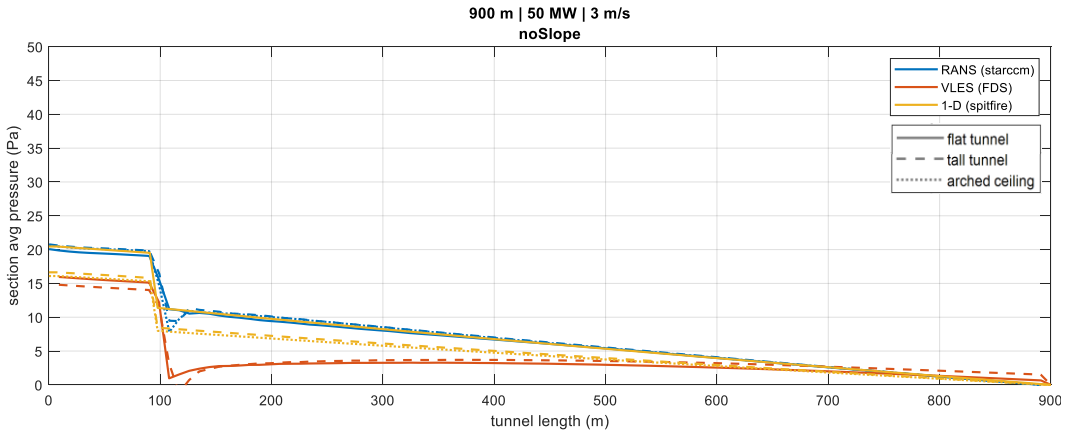

Figure 145: The average pressure along the tunnel using 50MW tunnel fire strength and no slope of the tunnel and FDS 6.9.1

Project conclusion

Schweizerische Eidgenossenschaft
Confédération suisse
Confederazione Svizzera
Confederaziun svizra

Eidgenössisches Departement für
Umwelt, Verkehr, Energie und Kommunikation UVEK
Bundesamt für Strassen ASTRA

FORSCHUNG IM STRASSENWESEN DES UVEK

Version vom 09.10.2013

Formular Nr. 3: Projektabschluss

erstellt / geändert am: 18.12.2025

Grunddaten

Projekt-Nr.:	BGT_20_00A_01
Projekttitel:	Flow Resistance of Fires in Road Tunnels - Validation
Enddatum:	31.03.2026

Texte

Zusammenfassung der Projektresultate:

The objective of the project was to experimentally validate the flow resistance caused by fires in road tunnels with longitudinal ventilation, as previously postulated in theoretical and CFD-based studies. In particular, the project aimed to assess whether CFD and existing 1-D models realistically represent the additional pressure losses induced by tunnel fires and whether these models are suitable for ventilation design purposes.

Large-scale fire tests with heat release rates between 4 and 10 MW were conducted in a 600 m long test tunnel with a geometry representative of real road tunnels. Measurements included differential pressure along the tunnel, airflow velocities, temperature distributions, and the heat release rate of the fires.

In parallel with the experiments, 1-D models and 3-D CFD simulations (RANS, VLES, and DES) were applied. The simulations were used both for test preparation and for validation and extrapolation of the measurement results to other tunnel geometries and higher fire heat release rates.

The large-scale fire tests showed that the additional flow resistance caused by tunnel fires is measurable but significantly lower than previously assumed in the study "Strömungswiderstand von Bränden in Strassentunneln" (Report 1679 Project AGT 2017/005). In particular, an additional pressure loss attributed to thermal stratification could not be confirmed experimentally and was identified as an artefact of the choosen CFD modelling approache. A good agreement was observed between measured data and simulated results for time-averaged pressure and temperature distributions along the tunnel. RANS in combination with k-ω SST turbulence modelling proved suitable for predicting the mean flow resistance with reasonable computational effort. LES is computationally intensive, but a combined model such as DES offers a good compromise between computational effort and the capture of turbulent behavior in the tunnel. The differences between the models increase with the heat release rate. This is partly due to the heat transfer model, i.e. the buoyancy in the inclined tunnel. Simulations with FDS versions v6.8.0, v6.9.1, and v6.10.0 showed significant differences between them, so these versions cannot be considered validated models for this application.

Parametric studies indicated that the tunnel cross-sectional shape has only a minor effect on pressure losses. In contrast, heat transfer processes, buoyancy effects in inclined tunnels, and turbulence modelling play a decisive role. Although high-frequency pressure fluctuations increased with rising fire power, their influence on the time-averaged pressure loss relevant for ventilation design remained limited. Application of the validated models to ventilation design according to ASTRA Guideline 13001 showed that existing implicit safety margins are generally sufficient to accommodate the additional fire-induced flow resistance. Therefore, no immediate need for retrofitting existing tunnels was identified, while explicit consideration of fire-related flow resistance is recommended for new tunnel projects and major refurbishments.

Schweizerische Eidgenossenschaft
Confédération suisse
Confederazione Svizzera
Confederaziun svizra

Eidgenössisches Departement für
Umwelt, Verkehr, Energie und Kommunikation UVEK
Bundesamt für Strassen ASTRA

Zielerreichung:

Large-scale fire tests were successfully conducted under realistic tunnel and ventilation conditions at heat release rates between 4 and 10 MW, determining the pressure distribution along the tunnel as well as the cross-sectional profiles of flow velocity and temperature downstream of the fire.
Comparisons between measured data , existing 1-D models and 3-D CFD simulations (RANS, VLES, and DES) showed good agreement for time-averaged pressure and temperature distributions, confirming the general applicability of CFD for this purpose within defined limits.

Folgerungen und Empfehlungen:

The fire tests in this study at «San Pedro des Anes» were limited to heat release rates of up to 10 MW due to the downstream tunnel length and limited protection in zone 1, while zone 2 can accommodate larger fires up to 200 MW. CFD models were validated for small fires 4-10 MW, showing good agreement, but scaling to 20-50 MW revealed significant discrepancies, indicating the need for further validation at higher intensities. The test facility at «San Pedro des Anes», featuring a service gallery, allows convenient differential pressure measurements. High-frequency pressure sensors are recommended to capture turbulence and acoustic effects and reduce dependence on tunnel operations. The setup is also suitable for studying smoke back-layering, critical ventilation velocity, and for validating updated NFPA502 formulations, supporting improved tunnel fire safety design.

Publikationen:

- Deb R., Weber A., Riess I. (2024), "Numerical investigation of flow resistance of fires in road tunnels, 20th International Symposium on Aerodynamics", Ventilation and Fires in Tunnels (ISAVFT), Copenhagen
- Riess I., Deb R., Friedl M., Weber A. (2026), "Flow Resistance of Fires in Road Tunnels - Validation", Final report Research project BGT 20_00A_01 at the request of Arbeitsgruppe Brücken, Geotechnik und Tunnel of Bundesamt für Strassen (Astra)

submitted, but not yet published:
- Deb R., Weber A., Riess I. (2025), "Numerical modeling and experimental investigation of flow resistance of fire to longitudinal ventilation along a tunnel", Journal of Wind Engineering and Industrial Aerodynamics
- Riess I., Deb R., Weber A. (2026), "On the flow resistance of tunnel fires - Validation by full-scale fire tests", 14th International Conference 'Tunnel Safety and Ventilation' 2026, Graz

Der Projektleiter/die Projektleiterin:

Name: Friedl Vorname: Markus

Amt, Firma, Institut: OST - Ostschweizer Fachhochschule, IET Institut für Energietechnik

Unterschrift des Projektleiters/der Projektleiterin:

Schweizerische Eidgenossenschaft
Confédération suisse
Confederazione Svizzera
Confederaziun svizra

Eidgenössisches Departement für
Umwelt, Verkehr, Energie und Kommunikation UVEK
Bundesamt für Strassen ASTRA

FORSCHUNG IM STRASSENWESEN DES UVEK
Formular Nr. 3: Projektabschluss

Beurteilung der Begleitkommission:

Beurteilung:

This research project aimed to analyze, both experimentally and through simulations, the additional pressure loss created locally by the effects of a tunnel fire. It was carried out in several phases: i) preparation of the experimental phase using 1D and 3D simulations; ii) fire tests and measurements of the phenomena; iii) calibration of the simulation models based on the measurement results; and iv) extrapolation using the calibrated models.

The project was conducted in accordance with the research group's initial proposal. The resources (simulation tools), the analytical work performed, and the final report are of high quality.

Umsetzung:

The following points should be noted:
- The instrumentation actually installed in the test tunnel did not fully meet the applicant's specifications, which may have limited the scope of the measurements and their interpretation.
- During the tests, the recreated fire power (HRR) was in the range of 5 to 10 MW, which corresponds to a light vehicle or van fire and is relatively low compared to the expected power during a heavy vehicle fire (>30 MW). The measured resistance effects are therefore likely lower than those expected during the design fire of the tunnel ventilation systems.

weitergehender Forschungsbedarf:

As indicated in research report, the additional flow resistance caused by tunnel fires in the rage of 10 to 20 MW were measurable but significantly lower than previously assumed. Furthermore CFD parametric studies have shown that the tunnel cross section shape has only minor effect on this specific pressure losses. Extrapolation to higher HRR (30 MW and more) could necessitate further research.

Einfluss auf Normenwerk:

OFROU to assess on the necessity to explicitely consider the additional fire resistance in the 13001 Guidelines.

Der Präsident/die Präsidentin der Begleitkommission:

Name: Guigas Vorname: François Xavier

Amt, Firma, Institut: WSP Consulting Engineers Ltd.

Unterschrift des Präsidenten/der Präsidentin der Begleitkommission: